



AD-A233 027

## REPORT DOCUMENTATION PAGE

1a. REPORT SECURITY CLASSIFICATION Unclassified			1b. RESTRICTIVE MARKINGS													
2a. SECURITY CLASSIFICATION AUTHORITY			3. DISTRIBUTION/AVAILABILITY OF REPORT Approved for public release; distribution is unlimited.													
2b. DECLASSIFICATION/DOWNGRADING SCHEDULE			5. MONITORING ORGANIZATION REPORT NUMBER(S) AFOSR-TR- 91 0047													
4. PERFORMING ORGANIZATION REPORT NUMBER(S)			7a. NAME OF MONITORING ORGANIZATION Air Force Office of Scientific Research													
6a. NAME OF PERFORMING ORGANIZATION University of Illinois at Chicago		6b. OFFICE SYMBOL (If applicable)	7b. ADDRESS (City, State and ZIP Code) Electronic and Material Sciences Bk1 410 Bolling Air Force Base, DC 20332-6448													
6c. ADDRESS (City, State and ZIP Code) P.O. Box 4348 M/C 273 Chicago, IL 60680		7c. ADDRESS (City, State and ZIP Code) Electronic and Material Sciences Bk1 410 Bolling Air Force Base, DC 20332-6448														
8a. NAME OF FUNDING/SPONSORING ORGANIZATION Air Force Office of Scientific Research		8b. OFFICE SYMBOL (If applicable)	9. PROCUREMENT INSTRUMENT IDENTIFICATION NUMBER #F49620-87-C0021													
8c. ADDRESS (City, State and ZIP Code) Electronic and Material Sciences Bk1 410 Bolling Air Force Base, DC 20332-6448		10. SOURCE OF FUNDING NOS. <table border="1"><thead><tr><th>PROGRAM ELEMENT NO.</th><th>PROJECT NO.</th><th>TASK NO.</th><th>WORK UNIT NO.</th></tr></thead><tbody><tr><td>62301E</td><td>5940</td><td></td><td></td></tr></tbody></table>			PROGRAM ELEMENT NO.	PROJECT NO.	TASK NO.	WORK UNIT NO.	62301E	5940						
PROGRAM ELEMENT NO.	PROJECT NO.	TASK NO.	WORK UNIT NO.													
62301E	5940															
11. TITLE (Include Security Classification) Unclassified "MBE growth, characterization.."																
12. PERSONAL AUTHOR(S) Dr. Jean-Pierre Faurie																
13a. TYPE OF REPORT Final		13b. TIME COVERED FROM 11/13/86 TO 11/12/89		14. DATE OF REPORT (Yr., Mo., Day)												
15. PAGE COUNT 66		16. SUPPLEMENTARY NOTATION														
17. COSATI CODES <table border="1"><thead><tr><th>FIELD</th><th>GROUP</th><th>SUB. GR.</th></tr></thead><tbody><tr><td></td><td></td><td></td></tr><tr><td></td><td></td><td></td></tr><tr><td></td><td></td><td></td></tr></tbody></table>		FIELD	GROUP	SUB. GR.										18. SUBJECT TERMS (Continue on reverse if necessary and identify by block number)		
FIELD	GROUP	SUB. GR.														
19. ABSTRACT (Continue on reverse if necessary and identify by block number)  (SEE ATTACHED)  <b>DTIC ELECTE</b> <b>S D D</b> <b>MAR 12 1991</b>																
20. DISTRIBUTION/AVAILABILITY OF ABSTRACT UNCLASSIFIED/UNLIMITED <input checked="" type="checkbox"/> SAME AS RPT. <input type="checkbox"/> DTIC USERS <input type="checkbox"/>		21. ABSTRACT SECURITY CLASSIFICATION <b>UNCLASSIFIED</b>														
22a. NAME OF RESPONSIBLE INDIVIDUAL Major Gernot Pomrenke		22b. TELEPHONE NUMBER (Include Area Code) (202) 767-4931		22c. OFFICE SYMBOL NE												

Here we report on the growth by molecular beam epitaxy of twin-free CdTe(111)B and HgCdTe(111)B epitaxial layers.

HgCdTe(111)B twin-free layers exhibit very different structural and electrical properties than twinned layers.

HgCdTe(211)B layers grown under the stringent growth control required for twin-free growth in (111)B exhibit outstanding properties.

Twin-free CdTe(111)B have been grown on slightly misoriented GaAs(100) substrate. FWHM of 60 arcsec have been obtained.

CdTe(111)B, CdTe(100) and HgCdTe(111)B have been successfully grown on Si(100) substrates.

Composition uniformity of 0.7% has been achieved on a 2-inch diameter  $\text{Hg}_{1-x}\text{Cd}_x\text{Te}$  ( $x = 0.22$ ) grown by MBE on a GaAs(100) substrate.

The crystallographic orientation has been found to have an influence in the sticking coefficient of mercury and on the intrinsic, as well as, the extrinsic doping.

The incorporation of indium which has been found to be an excellent donor incorporates very differently in (111)B and (100) orientation.

A low energy ion technique has been developed in the Microphysics Laboratory in order to fabricate p-n junction. This technique which has been found to be inexpensive, fast and reliable provides infrared diodes with similar performances than ion implanted diodes.

HgTe-CdTe valence band discontinuity has shown no temperature dependence from 300K and 50K when investigated by XPS and UPS. Most of the results including magneto-optics data are now consistent with a large value of 0.35eV.

Stimulated emission from Hg-based layers and heterostructures has been observed in the 2-3 $\mu\text{m}$  range. The threshold input optical power for the lasing action is lower than in equivalent III-V compounds laser heterostructures.

Preliminary results obtained in the new multiwafer machine are very promising. CdTe epilayers grown either on GaAs(100) or Si(100) are more uniform and of much better quality than layers grown under the same conditions in a conventional MBE machine.

MOLECULAR BEAM EPITAXIAL GROWTH,  
 CHARACTERIZATION AND ELECTRONIC DEVICE PROCESSING  
 OF HgCdTe, HgZnTe, RELATED HETEROJUNCTIONS  
 AND HgCdTe-CdTe SUPERLATTICES  
 NOV. 14, 1986 - NOV. 13, 1989

ADVANCED MOLECULAR BEAM EPITAXY  
 (MBE) PROTOTYPE FOR Hg BASED II-VI SEMICONDUCTING  
 ALLOYS AND HETEROSTRUCTURES  
 OCT. 1, 1987 - SEPT. 30, 1989

DARPA CONTRACT MONITORED BY AFOSR  
 #F49620-87-C-0021

FINAL REPORT

Jean-Pierre Faurie  
 Microphysics Laboratory  
 University of Illinois at Chicago *Civild*

Accession For	
NTIS CRA&I	<input checked="" type="checkbox"/>
DTIC TAB	<input type="checkbox"/>
Unannounced	<input type="checkbox"/>
Justification	
By	
Distribution /	
Availability Codes	
Dist	Avail & or Special
<b>A-1</b>	

The goals to be reached during this contract period were:

1. The growth and characterization of high quality HgCdTe with good lateral uniformity on large area CdTe, CdZnTe and GaAs substrate.
2. The understanding and the control of the doping in HgCdTe alloys by stoichiometry adjustment and/or by active impurities.
3. The growth and characterization of homojunctions and heterojunctions made in situ.
4. Photodiode device processing.
5. Surface and interface studies.
6. 1st add-on on the current contract. Design and installation of a multiwafer prototype MBE machine called OPUS 45
7. Preliminary experiments on the OPUS 45 (This work was supposed to be supported by a second add-on which has never been awarded to the Microphysics Laboratory)

## I INTRODUCTION

The research program on the growth by Molecular Beam Epitaxy of Hg-based alloys and heterostructures carried out in the Microphysics Laboratory at the University of Illinois at Chicago and supported by this contract has been extremely successful. Tremendous progress has been achieved towards the improvement of HgCdTe and related heterostructures in terms of structural, electrical and optical properties. A very important step has been passed through in the control of the twinning process during the growth in the (111)B orientation. Furthermore, it has been clearly established for the first time that twins or related dislocations are acting as acceptors in HgCdTe and are detrimental for diode performance, what was suspected but never proved until our conclusive experiments.

In 1988 it appears very clearly that microstructural defects present in HgCdTe layers grown in the (111)B orientation have an adverse effect on diode performance and have a determining influence on structural and electrical properties as well as on the intrinsic and extrinsic doping of HgCdTe.

The decision taken, after such a conclusion, was to overcome the twinning problem in the (111)B orientation and not to turn the problem by growing in a different crystallographic orientation. It will be explained in part II-1 why facing the twinning problem in (111)B was so important. In 1988 and 1989 understanding and solving the twinning problem in CdTe grown either on CdTe, GaAs and recently on Si and, above all, in HgCdTe has been one of the driving forces in the Microphysics Laboratory.

It is important to point out that most of the layers or heterostructures which have been tested during this contract period are (111)B twinned structures and therefore are not representative of the state-of-the-art of the Microphysics Laboratory at the end of the contract period i.e. November 1989. This should be kept in mind while reading this report.

The last year especially has been extremely rich in terms of achievements since in addition to the understanding and control of the twinning, the direct growth of CdTe and HgCdTe on Si(100) has been obtained, the stimulated emission in HgCdTe single layer and double heterostructures has been observed for the first time in MBE grown HgCdTe and the role of the crystallographic orientation on the intrinsic and extrinsic doping using Indium has been discovered. In addition, a new approach using low energy ion has been taken in order to fabricate photodiodes.

This approach is inexpensive, fast and reliable. High performance photodiodes have already been fabricated. These results attest to the high quality of HgCdTe epilayers grown by MBE and also give us a strong confidence in our photodiode technology.

In July 1989 a new MBE machine, OPUS 45, which is a prototype MBE equipment for mass-production has been installed in the Microphysics Laboratory. This Gallium-free multiwafer machine which has the capability of handling a 5-inch diameter substrate or any other combination should be fully tested during the next contract period. Our future goal is to demonstrate, with the help of this machine, that high quality HgCdTe suitable for high performance photodiodes and FPAs can be grown on large area substrates by MBE at a lower price than by LPE or by OMCVD.

The machine has been tested and acceptance tests have been performed. In addition, CdTe epilayers have been grown on 2-inch GaAs(100) and Si(100) substrates. Electron and X-ray diffraction both indicate that the structural quality of these epilayers is higher than the one observed for CdTe epilayers grown in the 2300 RIBER machine. This last part of the work was supposed to be supported by a second add-on to the current contract (the first add-on has been awarded to pay for OPUS 45) but the money was never received by the Microphysics Laboratory.

This research activity has been materialized by 59 papers published in refereed journals, 13 invited conferences and 62 contributed papers mostly presented at international meetings.

## II GROWTH OF $\text{Hg}_{1-x}\text{Cd}_x\text{Te}$ ON $\text{CdTe}(111)\text{B}$ BY MBE

### II-1 TWIN FORMATION

In terms of growth achievement about 700 epilayers of  $\text{HgCdTe}$  have been grown during this contract. Half of them have been grown on  $\text{CdTe}$  and  $\text{CdZnTe}$  substrate and the rest primarily on  $\text{GaAs}$  substrates. One of the major problems encountered in the growth of  $\text{HgCdTe}$  when a vapor phase technique such as MBE is used is the formation of twins. From the current work of different laboratories involved in the fabrication of IR photodiodes it appears that the presence of twins is highly deleterious for photodiode performances. Actually it is thought that what is detrimental to diode is the existence of dislocations associated with the twins. An Etch Pit Density (EPD) count of  $1 \times 10^6 \text{cm}^2$  or less is considered to be necessary to achieve good photodiodes. The  $(111)\text{B}$  orientation is particularly vulnerable to the twin formation but the other orientations such as  $(211)\text{B}$  and  $(311)\text{B}$  are also sensible to twinning. In addition, we think that hillock formation observed during the growth in the  $(100)$  orientation, which is highly detrimental to MIS structure, is also twin related. Therefore, identifying and solving the twinning problem was one of our major concern during the current contract.

The  $(111)\text{B}$  orientation despite its easiness to form twins is a very important orientation because the mercury consumption is lower than in the  $(100)$  orientation,<sup>(1)</sup> surfaces and interfaces usually are very smooth in the  $(111)\text{B}$  plane,  $\text{CdTe}$  and  $\text{CdZnTe}$  substrates are obtained in high yield in this orientation and it is so far the most favorable orientation to grow on  $\text{GaAs}(100)$  substrates.

Detailed investigations involving electron microscopy, cathodoluminescence (CL) chemical etching, x-ray diffraction as well as electron channeling pattern (ECP) have revealed the presence of twins in  $\text{CdTe}$  and  $\text{HgCdTe}$  epilayers grown in the  $(111)\text{B}$  orientation.

In zinc-blende structure the twinning illustrated in Fig. 1 is very often observed. It is a "rotation" type of twin corresponding to a  $180^\circ$  rotation about the  $[111]$  normal direction. The stacking of  $(111)$  plane in the fcc structure changes from abc type I configuration to acb type II configuration. The two stackings are equivalent, the changes require very low formation energy since  $\text{Cd}(\text{Hg}) - \text{Te}$  bonds are preserved. This change can therefore occur several times during the growth. This kind of twinning is sometimes called lamellar twinning.

During the first step of epitaxial growth, islands can be formed which will grow and coalesce to form the epitaxial film. These islands may be of type I or type II configuration since they are energetically almost equivalent (Fig. 2). Therefore, twin boundaries will exist after island coalescence and twin domains will grow in a columnar form. This kind of twinning which is also of a rotation type is sometimes called double positioning twinning.

These two kinds of rotation twins can coexist in the crystal but one or both can disappear during the growth. It is difficult to observe rotation twins during the MBE growth by electron diffraction because the streaked (2D) patterns of type I and type II configuration are identical to twin-free streaked patterns and sometimes roughening of the surface, which allows 3D diffraction, is not large enough. The twinned domains present in the crystal are visible on the surface of the crystal under scanning electron microscopy or cathodoluminescence investigations on the form of close loops as illustrated in Fig. 3 for a CdTe layer.

Electron channelling pattern can also help in the discovery of twins Fig. 4a,b shown two simulated ECP of a twin-free and a twinned crystal. The (113) plane family has a 3-fold symmetry illustrated in a form of a regular triangle in a twin-free configuration whereas in a twinned configuration a second inverted triangle is revealed. Fig. 4c shows the ECP pattern of a twinned CdTe layer similar to the one illustrated in Fig. 4b

These two kinds of twinning can occur in both CdTe and HgCdTe. In HgCdTe however due to the high mercury flux used during the growth we think that a third kind of twinning illustrated in Fig. 5 can occur. This reflection type twin is formed by a mirror reflection with respect to the (111) twin plane. This produces a change in the polarity of the face by creating an anti-phase boundary. As shown in Fig. 5 Hg-Hg bonds which usually require high formation energy occur at the plane of the reflection twin when the Hg flux is too high. This twinning does not occur across the entire area of the wafer therefore the growing surface exhibits (111)B and (111)A orientation simultaneously. The growth rate of (111)B and (111)A faces being different<sup>(1)</sup> a surface roughening allowing the observation of extra dots in the RHEED pattern is associated with this kind of twinning.

During the growth of HgCdTe in the (111)B orientation the presence of extra dots due to twinning are observed when the Hg flux is too high for a selected substrate temperature. A decrease in the Hg flux or an increase in the substrate temperature produce rapidly a change in the RHEED pattern, extra dots are

disappearing and the spotty pattern is transformed into a streaky one. This is expected since a (111)A face is a Hg terminated unstable face requiring a high Hg flux. A new antiphase boundary with Te-Te bond is created reversing the (111)A to a (111)B face.

Fig. 6 is a TEM picture of a HgCdTe (111)B layer grown on a CdTe(111)B/GaAs(100) substrate. It can be seen that the CdTe layer grown on GaAs is full of lamellar twins. At the initiation of HgCdTe growth twins were visible on the RHEED pattern. The growth conditions were kept the same for a while and then the substrate temperature was increased by 5°C. Almost instantaneously the RHEED changes for a twin free related electron diffraction pattern. The TEM micrograph confirms our in situ observation since a twin is visible in the HgCdTe layer and the position where the twin has disappeared corresponds very precisely to the change in the substrate temperature and the RHEED pattern. High resolution transmission electron microscopy (HRTEM) has not been able to confirm yet the "reflection" nature of the twin since it is extremely difficult to reveal fine details of atomic structure. However, it is highly probable that this kind of twinning occurs when the Hg flux is too high.

#### REFERENCES:

S. Sivananthan, X. Chu, J. Reno and J.P. Faurie, J. Appl. Phys. 60, 1359 (1986)

#### FIGURE CAPTIONS:

- Fig. 1      Lamellar or stacking fault twin formed by a 180° rotation about the [111] direction
- Fig. 2      Double positioning twin formed by a 180° rotation about the [111] direction
- Fig. 3      Cathodoluminescence image of a twinned CdTe(111)B epilayer
- Fig. 4      Electron channeling pattern simulation of a CdTe crystal along the (111) axis (a) twin free crystal; (b) twinned crystal; (c) ECP pattern of a twinned CdTe crystal
- Fig. 5      Reflection twin formed by a mirror reflection with respect to the (111) plane
- Fig. 6      Transmission electron microscopy of a HgCdTe(111)B/GaAs(100) substrate. Only CdTe epilayer exhibiting numerous lamellar twins and HgCdTe epilayer are visible.

Fig. 1

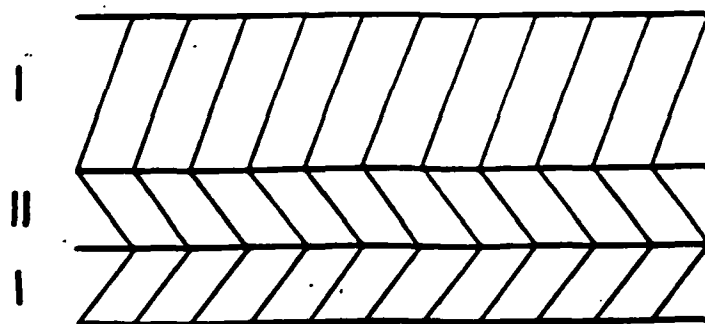
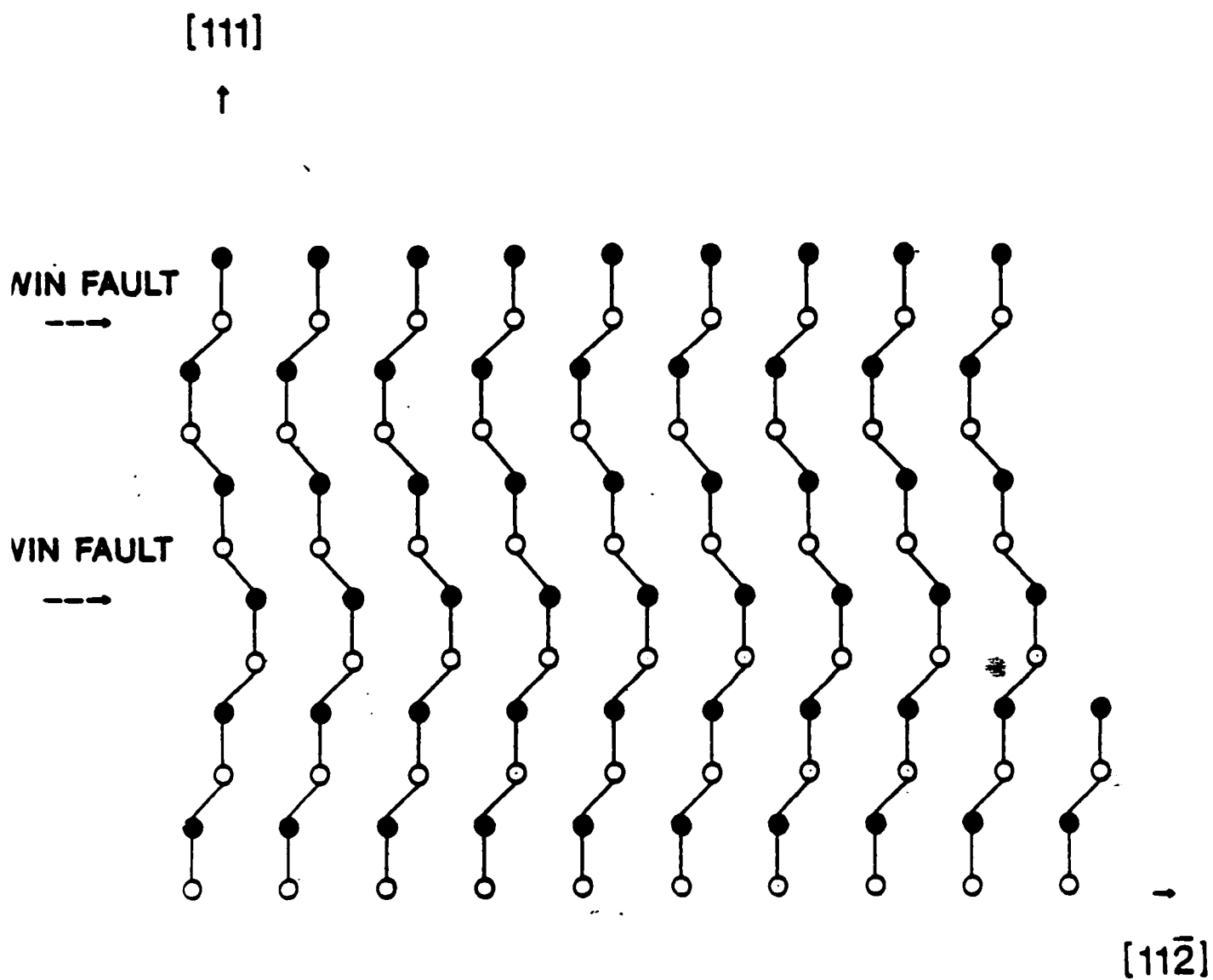


**Fig. 2**

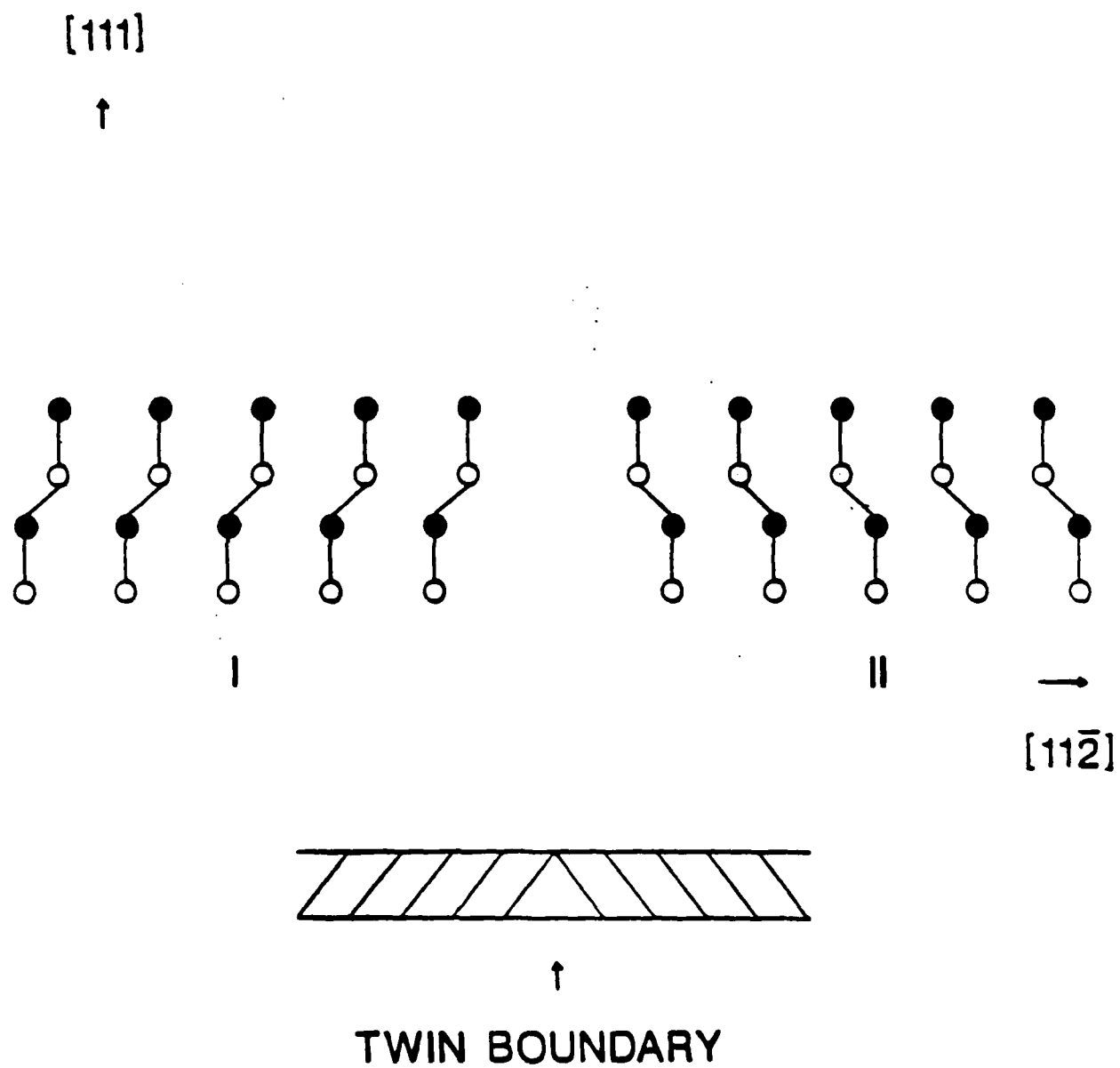
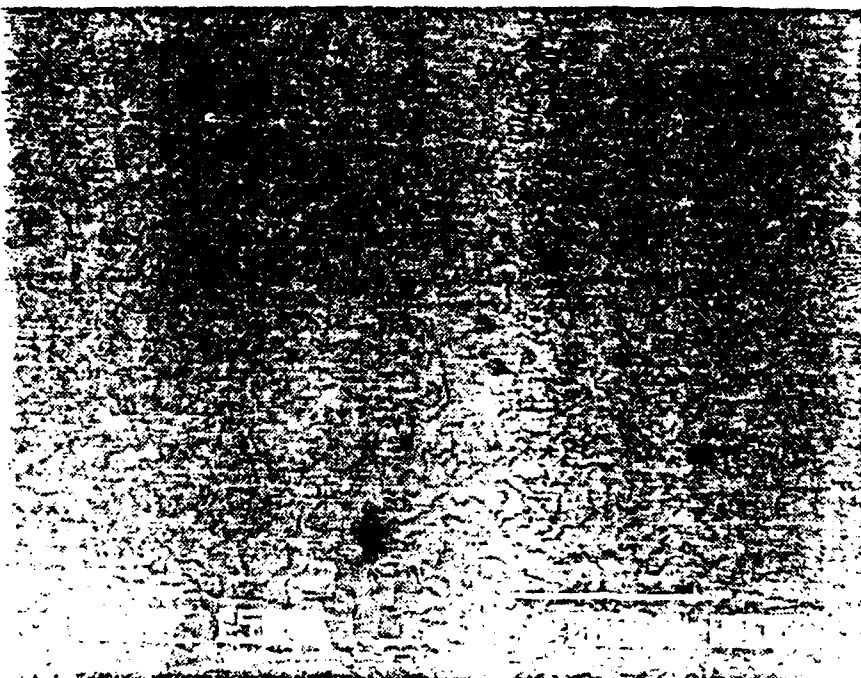
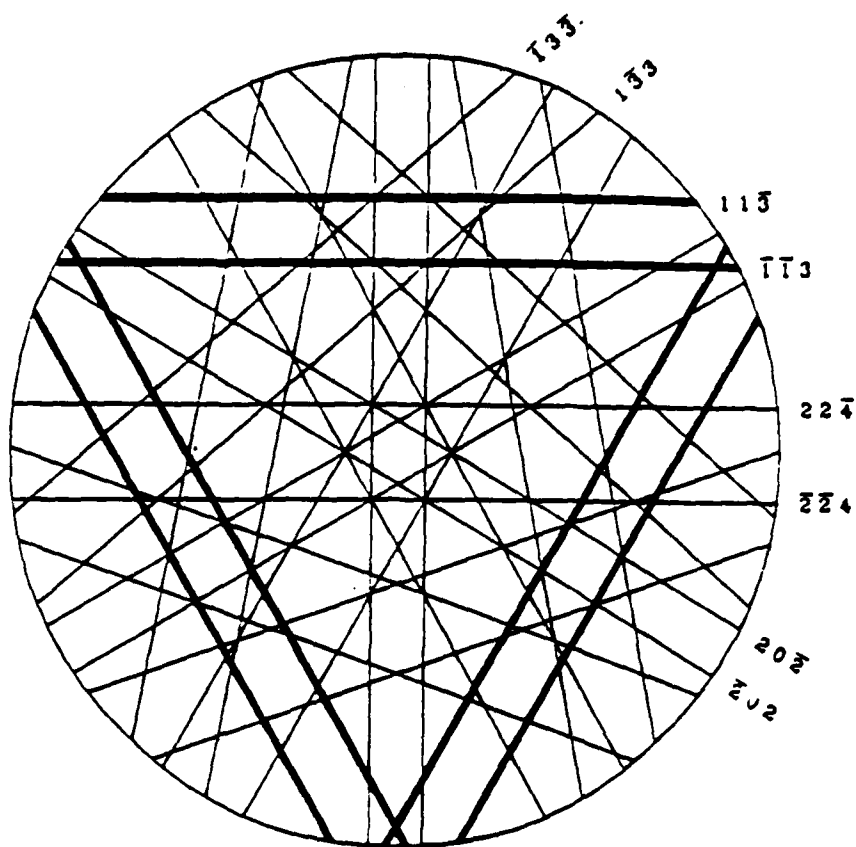


Fig. 3



2

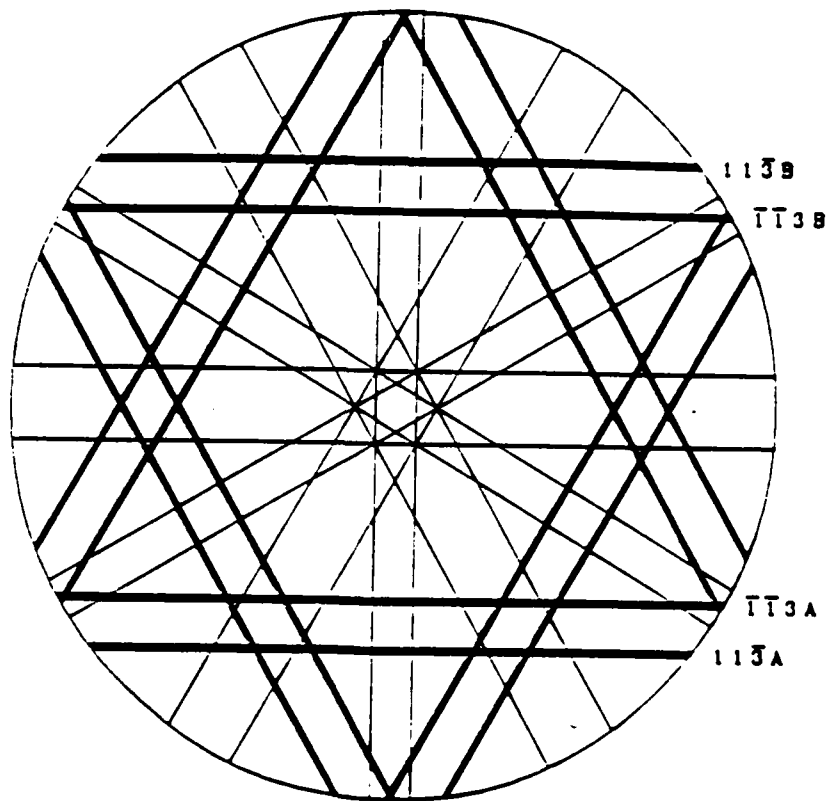
FCC lattice  
a=6.481 Å



10° —————

Fig. 4a

TWINNED FCC lattice  
 $a=6.481 \text{ \AA}$



$10^\circ$  —————

Fig. 4b

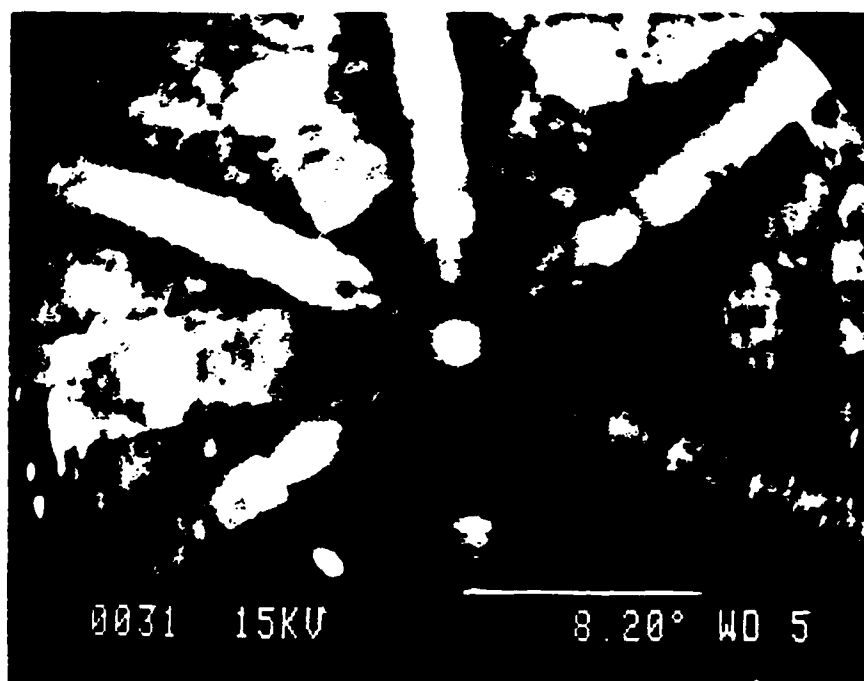


Fig. 4c

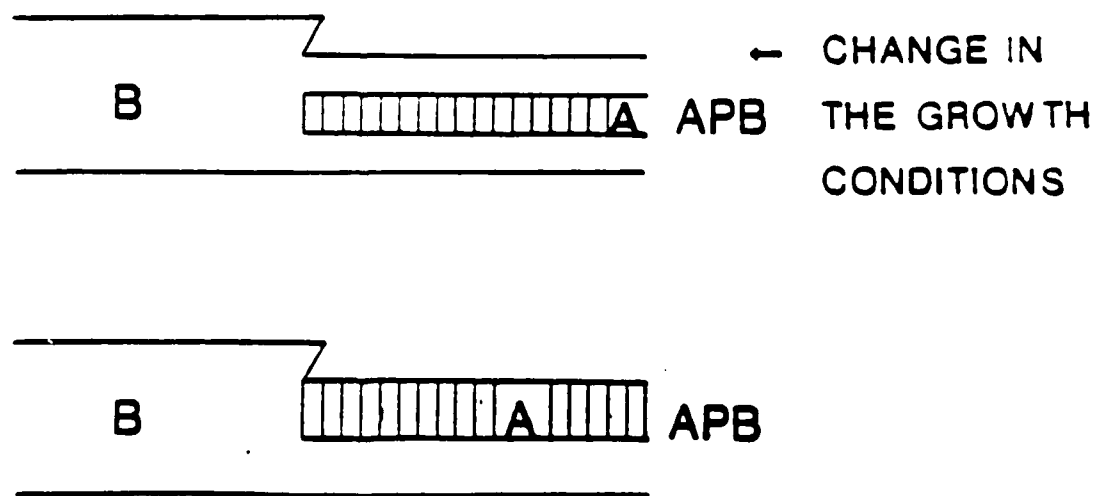
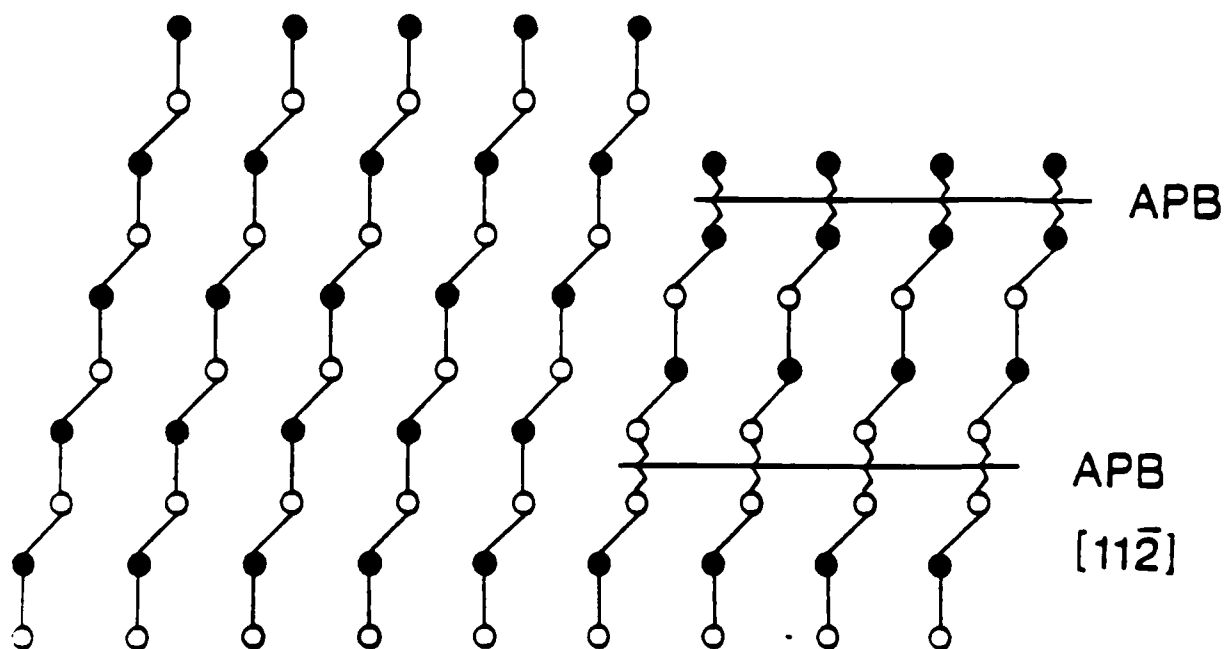


Fig. 6



## II-2 CdTe(111)B TWIN-FREE EPILAYERS

### II-2-1 CdTe(111)B/CdTe(111)B

The growth conditions for the homoepitaxial MBE growth of CdTe onto CdTe(111)B have been investigated thoroughly. The details are given in the attached paper.

Surface cleaning and growth parameters have been thoroughly investigated in order to prevent the twinning. Concerning CdTe, "reflection" type twin is very unlikely to occur when using a single effusion source which deliver a highly constant Cd/Te flux ratio. Therefore in CdTe case only the formation of the two kinds of "rotation" type twins has to be prevented. Double positioning twin which starts at the substrate epilayer interface seems to be substrate surface preparation related. Regarding lamellar twins, which form during the growth we have not yet precisely identified which parameter is triggering their formation. Concerning CdTe (111)B homoepitaxial growth, it has been found that twinning does not occur when the growth temperature is around 335°C but also if a pre-cleaning at 335° of the CdTe substrate has been done prior to a growth at 250°C.

#### ATTACHED PAPER: .

1. "Study of CdTe(111)B epilayers grown by Molecular Beam Epitaxy"

# Study of CdTe(111)*B* epilayers grown by molecular-beam epitaxy

G. Monfroy, S. Sivananthan, and J. P. Faurie

Department of Physics, University of Illinois at Chicago, Chicago, Illinois 60680

J. L. Reno

Sandia National Laboratories, Albuquerque, New Mexico 87185

(Received 11 October 1988; accepted 2 November 1988)

The growth of high-quality  $\text{Hg}_{1-x}\text{Cd}_x\text{Te}(111)\text{B}$  epitaxial layers involves the growth of a CdTe(111)*B* buffer layer, whether the growth is performed onto related or foreign substrates. CdTe(111)*B* layers have been investigated using the x-ray double-crystal rocking curve and the cathodoluminescence imaging techniques. The optimization of the growth conditions for CdTe(111)*B* layers is presented for a high-quality homoepitaxy. The heteroepitaxy of CdTe(111)*B* on GaAs(100) substrates is then discussed, in the case of GaAs substrates oriented (100), misoriented by  $2^\circ$  towards [110], and misoriented by  $5^\circ$  towards [111]. The results indicate that a  $2^\circ$  misorientation leads to CdTe(333) peaks with full width at half-maximum up to four times narrower than either of the other orientations tested. Furthermore, only threading dislocations were visible on this orientation by cathodoluminescence imaging.

## I. INTRODUCTION

The growth by molecular-beam epitaxy (MBE) of CdTe(111)*B* buffer layer is very important for the growth of high-quality  $\text{Hg}_{1-x}\text{Cd}_x\text{Te}$  (MCT) epilayers. Whether the MCT is grown on related substrates [i.e., CdTe(111)] or foreign substrates [i.e., GaAs(100)], there is need for a CdTe(111) buffer layer to minimize the defect density in the active MCT. Therefore, the quality of this buffer layer should be such that it does not limit the performances of the active HgCdTe.

Recently, Oron *et al.*<sup>1</sup> studied the homoepitaxy of CdTe grown by metalorganic chemical vapor deposition, reporting x-ray double-crystal rocking curves (DCRC's) peaks with full width at half-maximum (FWHM) between 400 and 800 arc s. The growth of CdTe(111)*B* by MBE leads to different results, and, in particular, to narrower FWHM. In this paper, the influence of the growth conditions on the quality of the CdTe(111)*B* buffer layer will be presented, together with cathodoluminescence (CL) imaging results indicating that the presence of twins is very likely to be responsible for our observations.

In spite of the significant improvements in the quality of the CdTe substrates in the last few years, they are still not as good as GaAs substrates. Also, these latter are available with large surface area and are cheaper than CdTe substrates. For these reasons, the growth of CdTe on GaAs has been widely studied. Recently, the possibility of growing highly uniform HgCdTe layers on a full 2-in. GaAs wafer has also been demonstrated.<sup>2</sup> Several types of buffer layers have been investigated, among which graded  $\text{Cd}_{1-x}\text{Zn}_x\text{Te}$  alloys,<sup>3</sup> for example. However, segregation problems have been encountered in the growth of such alloys by MBE,<sup>4</sup> inducing structural defects in the buffer layer itself. CdTe(111)*B* is another candidate as a buffer layer. Up until recently, no attempts had been reported on the growth of CdTe(111)*B* on misoriented GaAs(100) substrates.<sup>5</sup> It has been demonstrated for the growth of GaAs and AlGaAs on GaAs<sup>6</sup> and GaAs on Si<sup>7</sup> that misorienting the substrate could improve

the quality and the morphology of the epitaxial layers. Three substrate orientations were used in this study: GaAs(100)  $\pm 0.25^\circ$ ,  $2^\circ$  off towards [110], and  $5^\circ$  off towards [111]. X-ray DCRC and CL results along with tilt measurements between the substrate and the epilayers are reported in this paper.

## II. EXPERIMENTAL DETAILS

The layers grown on CdTe(111)*B* substrates have been fabricated in the Microphysics Laboratory at the University of Illinois at Chicago using a Riber 2300 MBE machine with a single CdTe effusion cell. All the substrates were from Galtech Semiconductors, Inc. and were etched in a bromine-methanol solution before being loaded in the ultrahigh vacuum chamber. They were then *in situ* thermally cleaned by annealing at  $300^\circ\text{C}$  for 5 min prior to CdTe growth. The substrate temperature was varied from 200 to  $335^\circ\text{C}$  and the growth rates from 0.5 to  $4.2 \text{ \AA/s}$ . Most of the layer thicknesses were kept  $\sim 3 \mu\text{m}$ , which corresponds to enough matter to observe a well-shaped diffraction peak for the epilayer and still allows for the substrate reflection to be diffracted through with enough intensity.

The layers grown on GaAs substrates were fabricated at Sandia National Laboratories. The substrates were cleaned using the standard procedure of etching in  $\text{H}_2\text{SO}_4$ ,  $\text{H}_2\text{O}_2$ : $\text{H}_2\text{O}$  (5:1:1) and HCl. All three orientations were mounted on the same molybdenum block and loaded into ultrahigh vacuum. The samples were then heated to  $600^\circ\text{C}$  to remove the oxide and then cooled to  $300^\circ\text{C}$  before the growth of CdTe. Typically, two growth rates were used: 1 and  $2 \text{ \AA/s}$ . The CdTe layer thicknesses were also varied from 2.5 to  $15.5 \mu\text{m}$  to determine the effect of these parameters on the layer quality.

X-ray double-crystal rocking curves of the CdTe(333) and GaAs(400) reflections were recorded using a copper anode (wavelength:  $1.540 \text{ \AA}$ ) and Si(331) and Ge(100) reference crystals, respectively. In order to check the homogeneity of the samples, several points were measured on each

sample using a broad incident beam ( $4 \text{ mm}^2$ ). The average FWHM and their corresponding standard deviations were calculated.

"Full rotation" double-crystal rocking curve analysis<sup>8</sup> was performed on the same diffractometer from Blake Industries, Inc. The Si(331) reference crystal was used for samples grown on CdTe substrates and Ge(100) for the samples grown on GaAs. This technique consists in following the evolution of the angular spacing between the substrate and the epilayer reflections while rotating the sample about its normal and keeping the x-ray beam position fixed (Fig. 1).

The cathodoluminescence images were acquired in a JEOL JXA 840 scanning electron microscope, using a 15-kV incident beam emitted from a tungsten filament and a probe current of  $\sim 10^{-7} \text{ A}$ . The working distance was set at 15 mm. The CL signal was detected by a photomultiplier fitted with an infrared filter. The detection range is from 700 to 1200 nm.

### III. RESULTS AND DISCUSSION

#### A. Growth on CdTe(111)*B* substrates

Due to its closeness in lattice parameter ( $< 0.3\%$  mismatch), CdTe is an obvious choice for substrate material to grow HgCdTe. To initiate the MCT growth, a thin CdTe buffer layer is grown, using a single CdTe effusion cell. Though such a homoepitaxy should be straightforward, it is very important to optimize the growth conditions, as will be discussed in the course of this paper. Indeed, x-ray double-crystal diffraction patterns exhibit two peaks, a sharp one attributed to the substrate and a second peak, much broader, shifted towards higher  $d$  spacings, attributed to the epilayer reflection (Fig. 2). The evolution of the spectrum has been studied as a function of the growth parameters. Table I lists the characteristics of the samples which have been studied by x-ray diffraction. The average FWHM and their corresponding standard deviations calculated for each sample and for both peaks, are also reported in Table I, along with

the average angular spacing between peaks and its standard deviation.

Inspection of the FWHM of the peaks attributed to the epilayer indicates a narrowing of the reflection when the substrate temperature is increased from 200 to 335 °C. In addition, the angular spacing between peaks is also decreased when the growth temperature is raised.

Another important observation concerns the width of the peak attributed to the substrate. The substrates have been carefully investigated prior to growth, in order to compare the width of the reflection before and after growth. Before growth, a typical FWHM for the substrates was between 20 and 25 arc s. There is, indeed, a broadening of this reflection. The magnitude of this broadening decreases when the growth temperature is increased.

Several causes which could be responsible for these observations have been investigated. A possible tilt between the substrate and the epilayer (111) planes was investigated by full rotation DCRC analysis. The results indicate that, within the accuracy of our measurements ( $< 50 \text{ arc s}$ ), there is no tilt.

The fact that the two peaks are brought closer together when the substrate temperature is increased suggests a possible stoichiometry deviation problem in the substrate and/or the epilayer. As a matter of fact, an increase in  $T$ , brings the growth conditions of the MBE layer closer to that of the bulk CdTe. The angular spacing corresponds to a mismatch of  $\sim 0.15\%$  which seems large. However, variations in the lattice parameters of CdTe grown from melt solutions have been reported in the literature indicating mismatches of the same order:  $6.480 \text{ \AA}$  for a Cd-rich to  $6.488 \text{ \AA}$  for a Te-rich melt.<sup>9</sup> To test this assumption, CdTe MBE layers have been grown under an excess Te flux and an excess Cd flux provided by the adjunction of extra cells of pure Te and pure Cd. The excess Cd induces a broadening of the reflection along with a decrease in the angular spacing between peaks. The excess Te leaves the angular spacing nearly unchanged, but narrows the reflection widths. In view of these observations, it seems unlikely that the stoichiometry deviation is responsible for the noncoherent growth of CdTe(111)*B*.

The fact that the excess Te flux narrows the reflection widths is important and is currently under investigation. It can be seen from Table I that the excess Te leads to an improvement of the structural quality of the layers for a given temperature. The layer quality obtained at 250 °C with an excess Te is equivalent to that of samples grown at 300 °C using a CdTe effusion cell only. It has been demonstrated<sup>10</sup> that the growth on CdTe(111)*B* faces at 300 °C under Te flux led to an increase in the growth rate from  $0.5 \mu\text{m/h}$  (no excess Te) to  $0.64 \mu\text{m/h}$  (excess Te). Such a growth rate corresponds to what has been observed for a growth at 200 °C using a single CdTe effusion cell. It is also reported<sup>11</sup> that when the growth is performed on a (111)Te face, it is controlled by the Te. If the growth rate increases under an excess Te flux, it indicates that, with a single CdTe cell only, the growth is carried out under active atomic Te-deficient conditions. For these reasons, we believe that it is very important to investigate the growth of CdTe(111)*B* under excess Te flux. This could lead to an improvement in the crys-

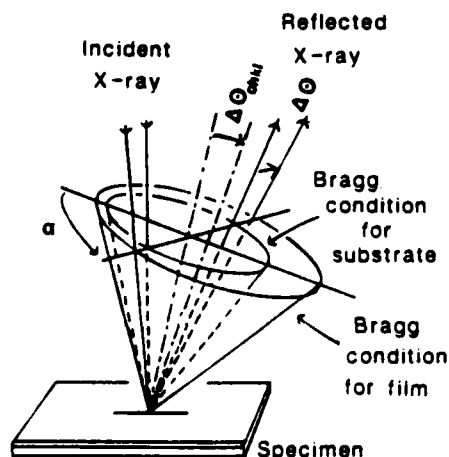


FIG. 1. Full rotation double-crystal rocking curve analysis. Schematic diagram of Bragg reflection from film and substrate.

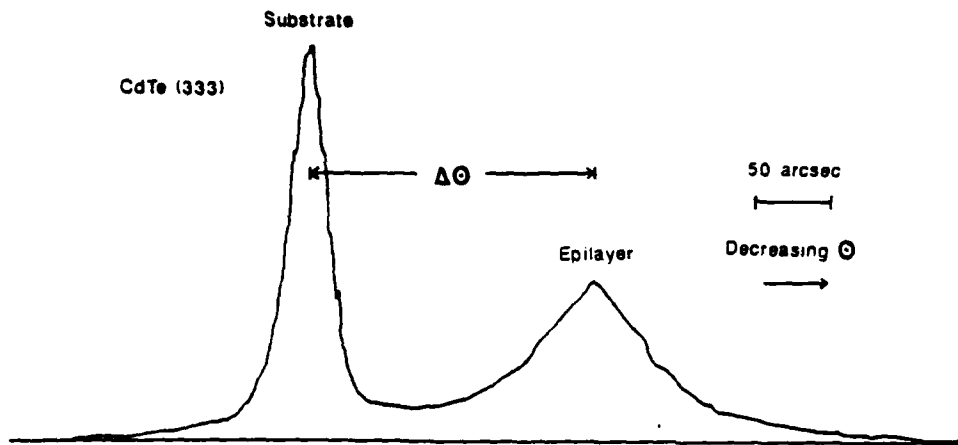


FIG. 2. CdTe(111)*B* epilayer grown on CdTe(111)*B* substrate CdTe(333) reflection using Cu  $K_{\alpha 1}$  ( $\lambda = 1.540 \text{ \AA}$ ) and Si(331) as a reference crystal. Part of the CdTe grows coherently with the substrate while the twinned orientation gives rise to a second peak.

talline quality and a lowering of the growth temperature. However, the possible occurrence of Te inclusions will then have to be considered.

There have been several reports in the literature about the twinning occurring in the crystals having a zinc-blende structure, and, in particular, in the CdTe system.<sup>11</sup> One of the consequences of twinning on an x-ray diffraction spectrum is a broadening of the reflection together with a slight shift of its angular position.<sup>12</sup> In view of these results, our observations could be interpreted as follows. The CdTe crystal is growing partially coherently with the substrate, which accounts for the broadening of the peak attributed to the substrate. The second peak, which is broader and shifted, would be the reflection from the twinned orientation. If the growth conditions are not optimized, both the matrix and the twinned orientations coexist in the samples. This inter-

pretation is corroborated by three important results. First, CL images exhibit a collection of dark closed loops [Fig. 3(a)] surrounding microdomains, whose size and density decrease when the substrate temperature is raised. These microdomains, which are currently under investigation, are assumed to be microtwins. The second important result is the fact that, on sample 62A whose CdTe thickness is  $5 \mu\text{m}$ , two peaks are still observable. In addition, the peak in position of the substrate is still more intense than the peak in position of the epilayer. This confirms the fact that two orientations are growing. It also indicates that the twinned crystal is slightly misoriented with respect to the matrix in order to give rise to

TABLE I. Characteristics of CdTe(111)*B* samples grown on CdTe(111)*B* substrates.  $T_s$  is the substrate temperature; G. R., the growth rate; FWHM:SD, the average full width at half-maximum of the reflection and its standard deviation;  $\Delta\theta$ :SD, the angular spacing between the substrate and the epilayer peaks and its standard deviation.

Sample no.	$T_s$ (°C)	G. R. (Å/s)	$t$ (μm)	FWHM:SD (arc s)				Delta $\theta$ :SD (arc s)	
				Epilayer		Substrate			
49	200	1.5	3.8	471	76	36	3	292	12
44	250	0.5	3.0	210	25	...	...	234	15
46	250	0.9	2.2	144	23	41	6	222	40
62A	250	1.3	5.0	237	7	57	12	318	13
50	250	1.7	4.4	352	16	53	6	232	26
43	250	1.8	2.9	263	25	36	3	196	8
45	250	3.3	3.2	318	25	54	1	237	42
48	250	4.2	3.0	205	13	33	2	322	10
51	300	1.1	2.9	169	7	...	...	182	3
52	335	1.4	7.5	49	7	...	...	...	...
53	335	3.0	7.5	116	23	...	...	...	...
60A + Te	250	1.4	2.5	155	4	25	3	225	8
63A + Cd	250	1.4	< 5.0	very broad		...	...	...	...

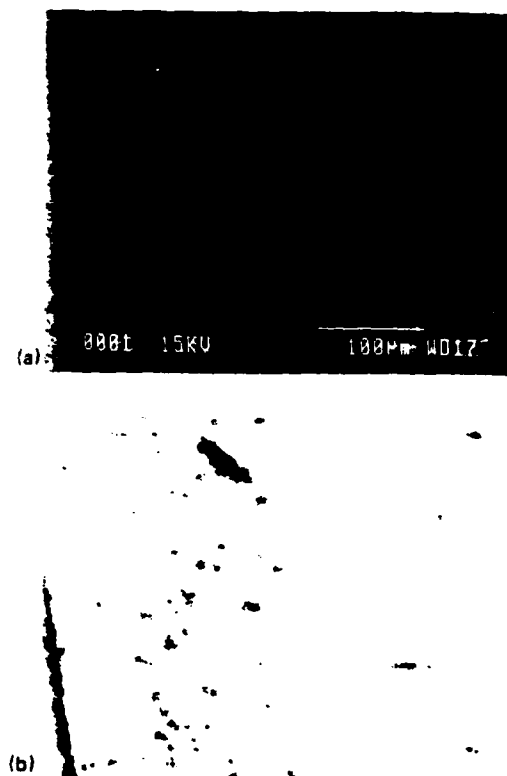


FIG. 3. Typical cathodoluminescence images: (a) CdTe(111)*B* on GaAs(100) [similar pictures were observed for CdTe(111)*B* on CdTe(111)*B*] and (b) CdTe(111)*B* on GaAs(100) off 2° towards [111] (similar images were observed for CdTe on GaAs(100) off 5° towards [111]).

a second diffraction peak in the DCRC spectrum. Finally, the third important result comes from the x-ray diffraction and CL observations made on samples grown at 335 °C. CL images of these samples exhibit very few microdomains, and of very small sizes. In addition, single peaks were recorded with FWHM as low as 40 arc s. Furthermore, layer 52 was etched step by step and the DCRC spectra exhibited a single diffraction peak all the way down to the substrate.

From inspection of Table I, it seems that the FWHM of both reflections decrease when the growth rate increases. However, the growth rate seems to have no influence on the angular spacing between the two peaks.

For these reasons, we believe that the optimization of the growth conditions are very important for the homoepitaxy of CdTe(111)B layers, in particular, the substrate temperature. If the substrate temperature is too low, twins are initiated which propagate throughout the crystal, limiting its crystalline quality. As a consequence, these results are also very important in order to limit the twinning during the growth of HgCdTe(111)B.

### B. Growth on GaAs substrates

Because of the large mismatch between GaAs and HgCdTe (~14.6%), it is necessary to first grow a buffer layer on the GaAs.

CdTe buffer layers have been grown simultaneously on three GaAs substrate orientations: GaAs(100), GaAs(100) off 2° towards [110], and GaAs off 5° towards [111]A. These layers have been investigated by double-crystal x-ray diffraction. Table II lists the characteristics of the studied layers along with their FWHM and standard deviations.

DCRC recorded on the CdTe(333) reflections exhibit consistently lower FWHM on substrates misoriented by 2° than on the other tested orientations. Though the standard

deviations indicate that the samples may not be as homogeneous as those grown on oriented GaAs(100) substrates, FWHM's a factor of 1.5 to 4 times narrower demonstrate the higher crystalline quality of the layers grown on substrates misoriented by 2°. Large variations in the FWHM averages and large standard deviations observed on CdTe(333) reflections from layers grown on substrates misoriented by 5° attest to the difficulties in growing crystal with a consistent quality on this orientation. It can also be seen from Table II that the growth rate appears to have no significant influence on the FWHM. The effect of the thickness has also almost no influence. Only slightly narrower reflections were recorded for film thicknesses > 2.5 µm.

It is worth noting that the underlying GaAs substrates have also been characterized after growth. All substrates appeared to have a high, homogeneous quality and therefore are not responsible for the variations observed in the FWHM of the CdTe reflections.

Two types of cathodoluminescence images are observed. On oriented substrates, the images consist of a collection of dark closed loops as has been observed for CdTe(111)B on CdTe(111)B substrates. We believe that, as for the case of the homoepitaxy of CdTe(111)B, these loops are twins, since the presence of twins in such systems has already been reported.<sup>13</sup> On both of the misoriented substrates, CL images exhibit dark dots and short line segments (Fig. 3). This indicates the presence of threading dislocations. The importance of this result resides in the fact that threading dislocations can be blocked by the insertion of an appropriate superlattice. It has already been reported<sup>14</sup> that a HgZnTe-CdTe superlattice could block the dislocations which propagate from a GaAs substrate. The density of dislocations was then reduced by a factor of 10 to 100.

Dislocation densities have been calculated using the model of Gay *et al.*<sup>15</sup>:

$$N_D = (F^2 - f^2)/(9b^2),$$

where  $E$  is the FWHM, in radians, of the crystal under investigation,  $f$  is the FWHM, in radians, of the monochromator crystal, and  $b$  is the magnitude of the Burgers vector. For the Si(331) reflection which was used,  $f$  was < 3 arc s. Since the direction of the Burgers vector is not known, the smallest Burgers vector possible in a face-centered-cubic crystal is chosen, i.e.,  $b = a/2^{1/2}$ .<sup>16</sup> Therefore, the dislocation densities presented in Table II are upper limits.

On the substrates misoriented by 2°, all the  $N_D$  are in the  $10^7 \text{ cm}^{-2}$  range. This means that reduction of  $N_D$  by a factor 10 to 1000 brings the density of dislocations in the  $10^5 \text{ cm}^{-2}$  range, corresponding to a quality suitable for device applications.

For these reasons, the growth of CdTe can be greatly improved by using substrates misoriented by 2°. It is worth noting that these results were corroborated by photoluminescence microscopy.<sup>5</sup>

Further investigations are currently being carried out on CdTe(111)B grown on this orientation. In particular, full rotation DCRC analysis indicates that part of the large mismatch between CdTe and GaAs is released by a tilt of ~0.75° between the epilayer and the substrate planes.

TABLE II. Characteristics of the CdTe(111)B samples grown on the three orientation for GaAs.  $t$  is the thickness of the CdTe layer; G. R., the growth rate; FWHM:SD, the average full width at half-maximum of the CdTe(333) reflection and its standard deviation;  $N_D$ , the density of dislocations calculated using Ref. 14.

Sample	Misorientation	$t$ ( $\mu\text{m}$ )	G. R. ( $\text{\AA}/\text{s}$ )	FWHM:SD (arc s)		$N_D \times 10^7$ ( $\text{cm}^{-2}$ )
17A	0°	2.5	1	252	6	8
17B	2°	2.5	1	158	18	3
17C	5°	2.5	1	285	33	10
5A	0°	5.0	1	219	4	6
5B	2°	5.0	1	108	10	1
5C	5°	5.0	1	165	18	3
18A	0°	2.5	2	266	49	9
18B	2°	2.5	2	135	10	2
18C	5°	2.5	2	262	...	9
8A	0°	5.0	2	269	14	9
8B	2°	5.0	2	82	6	1
8C	5°	5.0	2	168	28	4
10A	0°	7.5	2	334	14	14
10B	2°	7.5	2	84	20	1
10C	5°	7.5	2	...	...	...
7A	0°	15.5	2	356	11	16
7B	2°	15.5	2	99	20	1
7C	5°	15.5	2	67	7	1

#### IV. CONCLUSION

We have demonstrated that the optimization of the growth conditions are very important for the homoepitaxy of CdTe(111)B. If the substrate temperature is too low, twins are initiated that develop throughout the entire layer. This leads to the observation of two diffracted peaks: a narrow one which is matched with the substrate peak and a broad peak which corresponds to the twinned orientation. A substrate temperature of 335 °C, and a growth rate of  $\sim 1.5$  Å/s gave a layer with a FWHM  $< 50$  arc s, showing the optimization of the growth conditions, as well as the preparation of the substrate before growth.

The advantages of growing CdTe(111)B layer on GaAs(100) misoriented by 2° have also been demonstrated for two important reasons. The first one is the fact that the FWHM are narrower on this orientation. The second is the presence of threading dislocations which can be blocked by the insertion of an appropriate superlattice.

Transmission electron microscopy experiments are currently being carried out to confirm the fact that the microdomains observed on CL images are microtwins. Further experiments will include x-ray precession investigations to evidence if the twinning was completely avoided or not by optimizing the growth conditions.

#### ACKNOWLEDGMENTS

The authors would like to acknowledge Galtech Semiconductors, Inc. for supplying high-quality CdTe(111)B substrates. They would also like to acknowledge the technical assistance provided by S. Burns and L. L. Stephenson in preparing the samples. The work at the University of Illinois

was supported by SDIO/IST and monitored by NRL N00014-86K-2023 and by DARPA and monitored by AFOSR No. 49620-87-C-0021. The work at Sandia was supported by the U.S. Department of Energy under Contract No. DE-AC04-76DP00789.

- <sup>1</sup>M. Oron, A. Raizman, H. Shtrickman, and G. Cinader, *Appl. Phys. Lett.* **52**, 1059 (1988).
- <sup>2</sup>M. D. Lange, S. Sivananthan, X. Chu, and J. P. Faurie, *Appl. Phys. Lett.* **52**, 978 (1988).
- <sup>3</sup>A. Million, L. Di Cioccio, J. P. Gaillard, and J. Piagnet, *J. Vac. Sci. Technol. A* **6**, 2813 (1988).
- <sup>4</sup>R. D. Feldman, R. F. Austin, P. H. Fuoss, A. H. Dayem, E. H. Westerwick *et al.*, *J. Vac. Sci. Technol. B* **5**, 690 (1987).
- <sup>5</sup>J. L. Reno, P. L. Gourley, G. Monfroy, and J. P. Faurie, *Appl. Phys. Lett.* **53**, 1747 (1988).
- <sup>6</sup>R. K. Tsui, J. A. Curless, G. D. Kramer, M. S. Peffley, and D. L. Rode, *J. Appl. Phys.* **58**, 2570 (1985).
- <sup>7</sup>P. L. Gourley, M. Longerbone, S. L. Zhang, and H. Morkoc, *Appl. Phys. Lett.* **51**, 599 (1987).
- <sup>8</sup>R. M. Park, J. Kleinman, and H. Mar, *SPIE* **796**, 86 (1987).
- <sup>9</sup>K. Zanio, in *Semiconductors and Semimetals* (Academic, New York, 1978), Vol. 13, p. 54.
- <sup>10</sup>S. Sivananthan, X. Chu, J. Reno, and J. P. Faurie, *J. Appl. Phys.* **60**, 1359 (1986).
- <sup>11</sup>For example, C. Ghezzi and C. Paorici, *J. Cryst. Growth* **20**, 58 (1974).
- <sup>12</sup>B. E. Warren, *X-ray Diffraction* (Addison-Wesley, Reading, MA, 1969), Chap. 13.
- <sup>13</sup>R. D. Horning and J. L. Staudenmann, *Appl. Phys. Lett.* **49**, 1590 (1986).
- <sup>14</sup>J. P. Faurie, X. Chu, J. Petruzzello, and D. J. Olego, presented at DARPA IR Focal Plane Array Materials and Processing Review, Washington, DC, 1988 (unpublished results).
- <sup>15</sup>P. Gay, P. B. Hirsch, and A. Kelly, *Acta Metall.* **1**, 315 (1953).
- <sup>16</sup>J. Weertman, *Elementary Dislocation Theory* (MacMillan, New York, 1964), Chap. 4, p. 90.

## II-2-2 CdTe/GaAs(100)

It has been previously reported that the growth of CdTe onto GaAs(100) can occur in two different orientations i.e. (100) or (111) depending on the substrate thermal treatment. It is believed that (100)//(100) is achieved over an As rich GaAs(100) surface whereas (111)B//(100) is observed on a Ga rich GaAs(100). In the (100)//(100) case a 14.5% lattice mismatch is experienced in all crystallographic directions whereas in the (111)//(100) case there is only 0.7% mismatch between  $\langle 211 \rangle$  CdTe axis and  $\langle 011 \rangle$  GaAs axis (14.5% mismatch still exists between  $\langle 110 \rangle$  CdTe axis and  $\langle 110 \rangle$  GaAs axis). It appeared that (111)//(100) is the most favorable case.

Therefore the problem of twinning had to be investigated. This was done in the MPLab and in collaboration with J. Reno, a former student who is currently a scientist at Sandia National Laboratory. By growing on GaAs(100) misoriented substrates both an improvement in CdTe crystal quality and the elimination of the twinning have been observed as illustrated in Fig.1. During this investigation twin-free CdTe(111)B epitaxial layers exhibiting a FWHM of about 1 arc min have been grown on GaAs 2° off(100) towards [110] and 5° off(100) towards [111]Ga (see Fig. 2).

These layers display the best characteristics ever reported for CdTe epilayers grown on GaAs. Even though they are still not as good as CdTe bulk crystal they are already suitable as an alternate substrate for the growth of HgCdTe. Three years ago it was difficult to find commercially available CdTe substrates with a uniform FWHM better than 60 arc sec with no multiple peak in the x-ray diffraction pattern. HgCdTe epilayers grown on CdTe(111)/GaAs(100) alternate substrate have electrical properties as good as those obtained on CdTe or CdZnTe substrates as reported in the attached paper #2.

The details of the experiments as well as the results are given in the attached publication #1.

### FIGURE CAPTIONS:

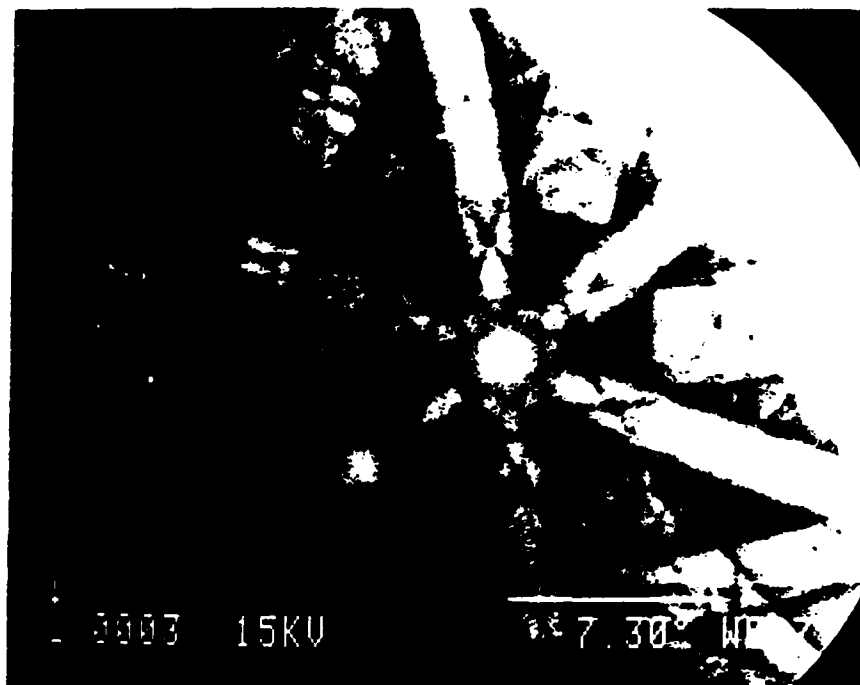
Fig. 1      Electron channeling pattern of a twin-free CdTe(111)B layers grown on GaAs(100) 2° off towards  $\langle 110 \rangle$

Fig. 2      X-ray double crystal rocking curve of a 7.5 $\mu$ m CdTe(111)B grown on GaAs(100) 2° off towards  $\langle 110 \rangle$

**ATTACHED PAPERS:**

1. "Effects of substrate misorientation on the structural properties of CdTe(111) grown by MBE on GaAs(100)"
2. "New achievements in  $\text{Hg}_{1-x}\text{Cd}_x\text{Te}$  grown by molecular beam epitaxy"

Fig. 1



Electron channelling pattern obtained  
on a 2.3 $\mu$ m thick CdTe layer  
on GaAs(100) 2° off towards  $\langle 110 \rangle$ .

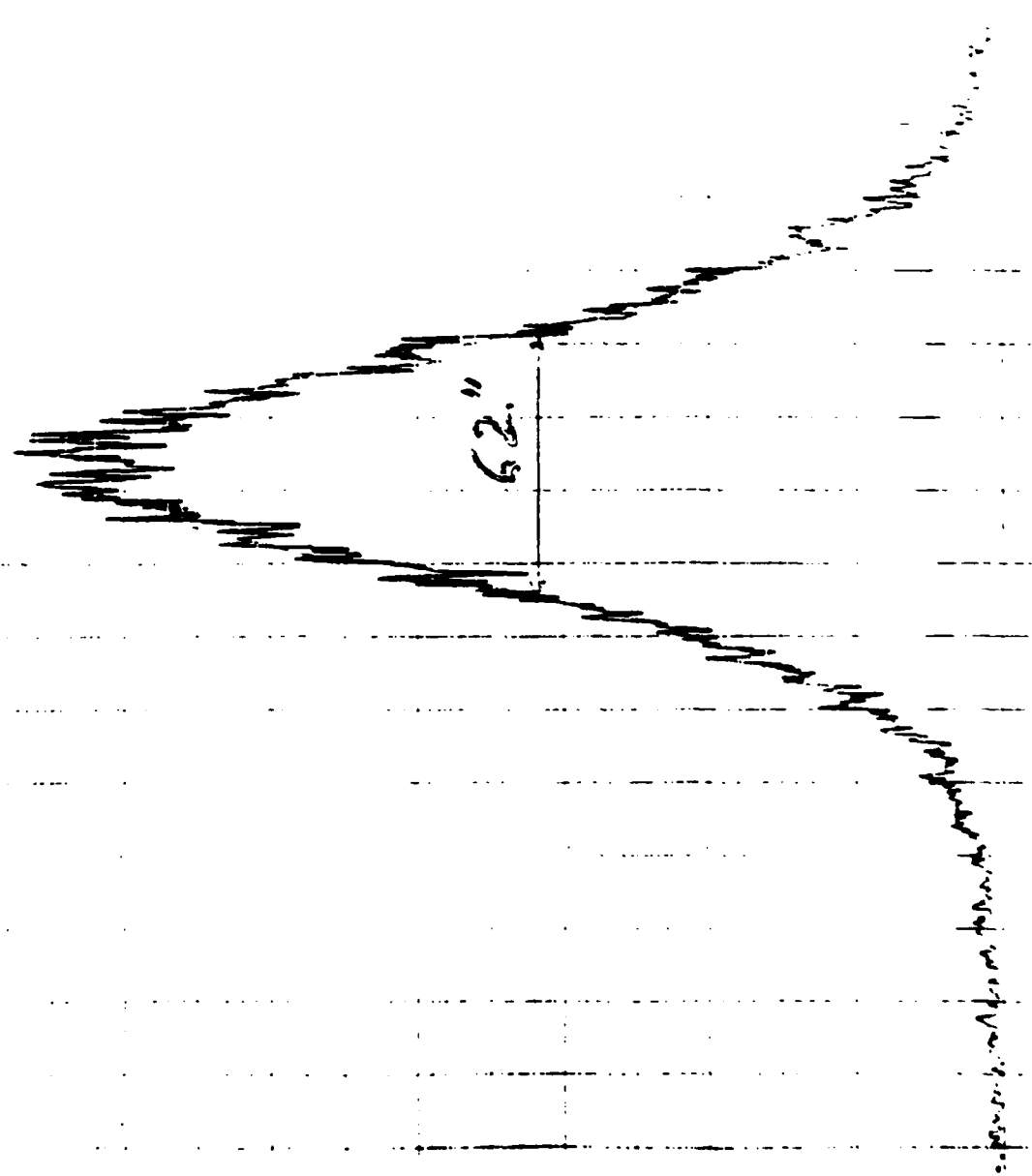
Fig. 2

XRAY DOUBLE CRYSTAL ROCKING CURVE  
CdTe (111)B // GaAs (100) 2° off towards [110]

CdTe (333)

Thickness 7.5  $\mu$ m

Growth Rate 2 A/s



# Effects of substrate misorientation on the structural properties of CdTe(111) grown by molecular beam epitaxy on GaAs(100)

J. L. Reno and P. L. Gourley

Sandia National Laboratory, Albuquerque, New Mexico 87185

G. Monfroy and J. P. Faurie

Department of Physics, University of Illinois at Chicago, Chicago, Illinois 60680

(Received 11 July 1988; accepted for publication 29 August 1988)

CdTe (111) layers were grown by molecular beam epitaxy on oriented and misoriented GaAs (100) substrates. The layers were characterized by x-ray diffraction and photoluminescence microscopy. The results indicate that the CdTe layers grown on GaAs (100) misoriented  $2^\circ$  towards the [110] direction had peaks with full width at half-maximum up to four times narrower than either of the other orientations tested. Only threading dislocations were visible on this orientation by photoluminescence microscopy. These results indicate that the structural quality of CdTe grown on GaAs can be significantly improved by the use of an appropriately misoriented substrate.

The growth of high quality epitaxial layers of  $\text{Hg}_{1-x}\text{Cd}_x\text{Te}$  is limited by the substrate quality. Due to its closeness in lattice parameter, CdTe is one of the obvious choices for substrate material. In spite of significant improvements in CdTe substrates in the last few years, they are still not as good as GaAs substrates. Also CdTe is considerably more expensive than GaAs and not available with as large a surface area. It has recently been demonstrated that it is possible to grow  $\text{HgCdTe}$  with excellent uniformity on a full 2 in. GaAs wafer.<sup>1</sup> Because of the large lattice mismatch between GaAs and  $\text{HgCdTe}$  ( $\sim 14.6\%$ ), it is necessary to first grow a CdTe buffer layer on the GaAs substrate. The quality of the active  $\text{HgCdTe}$  is then limited by the quality of the CdTe buffer layer. Thus it is of great importance to improve the quality of CdTe grown on GaAs.

It has been demonstrated for the growth of GaAs and AlGaAs on GaAs that misorienting the substrate can improve the quality and morphology of the epitaxial layers.<sup>2</sup> Improvement has also been observed for the mismatched growth of GaAs on Si.<sup>3</sup> In order to test this effect on II-VI semiconductors, we have grown CdTe(111) on oriented and misoriented GaAs(100) substrates. Three orientations were used. The orientations included  $(100) \pm 0.25^\circ$ ,  $2^\circ$  off (100) towards [110], and  $5^\circ$  off (100) towards [111]Ga. These orientations were chosen due to their common use in the growth of GaAs and AlGaAs on GaAs and of GaAs on Si.

The GaAs substrates were cleaned using the standard procedures of etching in  $\text{H}_2\text{SO}_4:\text{H}_2\text{O}_2:\text{H}_2\text{O}$  (5:1:1) and HCl. All three orientations were then mounted on the same molybdenum block and loaded into the growth chamber. The samples were then heated to  $600^\circ\text{C}$  to remove the oxide and cooled to  $300^\circ\text{C}$  before growth of the CdTe was begun. This preparation led to the growth of CdTe in the (111) orientation.<sup>4</sup> Growth rates of 1 and  $2 \text{ \AA/s}$  were used. The total thickness was also varied so that the effect of growth rate and total thickness could be determined, in addition to the effect of the orientation. After growth the samples were removed from the growth chamber and characterized by x-ray diffraction and photoluminescence microscopy.

X-ray double crystal rocking curves (DCRC's) of the CdTe (333) reflection were recorded using a copper anode

and a Si (331) reference crystal. In order to check the homogeneity of the samples, several points were measured using a broad incident beam ( $4 \text{ mm}^2$ ). The average full widths at half-maximum (FWHM) and their corresponding standard deviations were calculated. The results are presented in Table I, along with the substrate orientation, thickness, and the growth rate of each of the investigated samples.

The CdTe grown on GaAs (100) substrates misoriented by  $2^\circ$  towards the [110] direction exhibited consistently lower FWHM than the other orientations. Inspection of the standard deviations indicated that these samples may not be quite as homogeneous as those grown on GaAs substrates cut as close as possible to the (100) orientation. However, FWHM 1.5 to 4 times larger were recorded on the oriented samples, thus demonstrating their poorer crystalline quality. DCRC's measured on CdTe grown on GaAs (100) substrates misoriented by  $5^\circ$  towards the [111] direction attest to the difficulties in growing samples of consistent crystalline quality of this type of substrate. Large variations in the average FWHM as well as large standard deviations and sometimes asymmetric peaks were observed.

Also from Table I it can be seen that the growth rate appears to have no significant influence on the FWHM. It does appear that there is a slight improvement in the FWHM for thicknesses greater than  $2.5 \mu\text{m}$ .

It is worth noting that the underlying GaAs substrates have also been characterized after growth by x-ray diffraction, with the exception of the substrates having a  $15.5\text{-}\mu\text{m}$ -thick CdTe overlayer. The (400) reflection of a Ge crystal was used as a reference. FWHM recorded from the GaAs substrates, at the approximate same location as for the CdTe scans, indicated the high quality as well as the homogeneity of the substrates. Therefore, the quality of the GaAs substrates was not responsible for the variations observed in the FWHM of the CdTe diffraction peaks.

Dislocation densities  $N_D$  were evaluated using the model developed by Gay *et al.*<sup>5,6</sup>

$$N_D = (F^2 - f^2)/9b^2,$$

where  $F$  is the FWHM, in radians, of the crystal under investigation,  $f$  is the FWHM, in radians, of the monochromator

**TABLE I.** Growth characteristics of CdTe (111) samples grown on GaAs (100) substrates along their average FWHM measured on the CdTe (333) reflections using the Cu  $K_{\alpha 1}$  ( $\lambda = 1.540\,562\text{ \AA}$ ) radiation and a Si (331) reference crystal. The GaAs substrates are either oriented (100), misoriented  $2^\circ$  towards the [110] direction, or misoriented  $5^\circ$  towards the [111] direction.  $N_D$  is the dislocation density calculated from the model of Gay *et al.*

Sample	Misorientation	Thickness ( $\mu\text{m}$ )	Growth rate ( $\text{\AA/s}$ )	(FWHM) $\pm \sigma$ (arcsecond)	$N_D \times 10^7$ ( $\text{cm}^{-2}$ )
17A	$0^\circ$	2.5	1	$252 \pm 6$	8
17B	$2^\circ$	2.5	1	$158 \pm 18$	3
17C	$5^\circ$	2.5	1	$285 \pm 33$	10
5A	$0^\circ$	5.0	1	$219 \pm 4$	6
5B	$2^\circ$	5.0	1	$108 \pm 10$	1
5C	$5^\circ$	5.0	1	$165 \pm 18$	3
18A	$0^\circ$	2.5	2	$266 \pm 49$	9
18B	$2^\circ$	2.5	2	$135 \pm 10$	2
18C	$5^\circ$	2.5	2	262	9
8A	$0^\circ$	5.0	2	$269 \pm 14$	9
8B	$2^\circ$	5.0	2	$82 \pm 6$	1
8C	$5^\circ$	5.0	2	$168 \pm 28$	4
10A	$0^\circ$	7.5	2	$334 \pm 14$	14
10B	$2^\circ$	7.5	2	$84 \pm 20$	1
10C	$5^\circ$	7.5	2	...	...
7A	$0^\circ$	15.5	2	$356 \pm 11$	16
7B	$2^\circ$	15.5	2	$99 \pm 20$	1
7C	$5^\circ$	15.5	2	$67 \pm 7$	1

crystal, and  $b$  is the magnitude of the Burgers vector. For the Si (331) reflection which was used,  $f$  was equal to 8 arcseconds. Since the direction of the Burgers vector was not known, the smallest Burgers vector possible in a face-centered cubic crystal was chosen, i.e.,  $b = a/\sqrt{2}$ .<sup>7</sup> Therefore, the densities of dislocations presented in Table I are an upper limit. The calculated values are in the  $10^7/\text{cm}^2$  range. As expected from the FWHM, they are not significantly influenced by either the epilayer thickness or the growth rate.

For the photoluminescence microscopy (PLM), the sample was photoexcited at room temperature with  $\sim 10^3\text{ W/cm}^2$  of 7525 Å laser light. This light penetrates the sample to a depth of approximately  $0.5\text{ }\mu\text{m}$ . The resulting near-band-gap CdTe luminescence at 8200 Å was imaged onto a CCD TV camera with  $\sim 600\times$  magnification. Compared to the near-band-gap luminescence of the CdTe, the scattered laser light was reduced by two orders of magnitude with a long pass filter (7800 Å cutoff). It has been previously demonstrated that this technique is able to image dislocations which serve as nonradiative recombination sites for the photoexcited electron-hole pairs.<sup>8,9</sup> These defects thus appear as dark areas on the PLM micrograph. The PLM technique is useful for simultaneously assessing the dislocation content and the photoluminescence intensity. Photoluminescence from all samples was sufficiently intense so that the PLM micrographs could be recorded at room temperature.

On both of the misoriented substrates, PLM micrographs exhibited dark dots and short line segments (see Fig. 1). This indicates the presence of threading dislocations. A lower limit on the dislocation density was about  $10^7/\text{cm}^2$ . This is in good agreement with the upper limit on the dislocation density calculated from the x-ray data. The CdTe grown on the oriented GaAs exhibited strikingly different PLM images. They consisted of a collection of dark closed loops with diameters of  $20\text{--}40\text{ }\mu\text{m}$  (see Fig. 1). Within the loops the photoluminescence intensity was the same as out-

side the loops. The loops were located about  $40\text{ }\mu\text{m}$  apart. We believe that the dark loops are due to nonradiative recombination at boundaries of microcrystallites and that the microcrystallites are probably twins of the main material. Investigations to identify these structures are in progress.

The effect of the thickness of the layer could also be seen by this technique. The thinnest layers ( $2.5\text{ }\mu\text{m}$  thick) exhib-

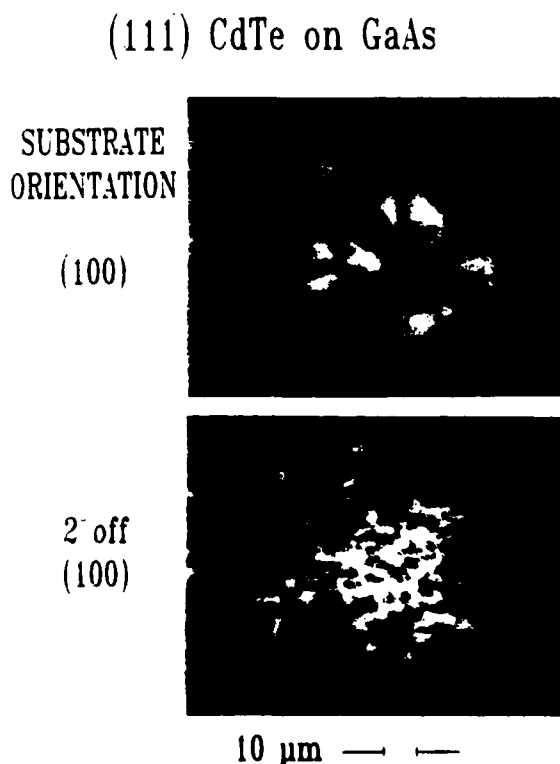


**FIG. 1.** Photoluminescence micrographs of CdTe(111) grown on oriented GaAs(100) and misoriented  $2^\circ$  towards the [110]. The micrographs were taken at room temperature using 7525 Å laser light.

ited the highest dislocation density and the lowest photoluminescence intensity. This indicates a lower quality of the material if only  $2.5\text{ }\mu\text{m}$  is grown. There was no significant difference between layers  $5.0\text{ }\mu\text{m}$  and thicker. Also there was no apparent dependence on the growth rate.

In conclusion, we have grown CdTe (111) on oriented and misoriented GaAs (100) and have characterized the layers by x-ray diffraction and photoluminescence microscopy. The FWHM's of the CdTe grown on GaAs (100) misoriented  $2^\circ$  towards the [110] were found to be significantly better than for either other orientation tested. Photoluminescence microscopy showed a totally different type of defect structure for the oriented substrate than for the misoriented substrates. The CdTe grown on the misoriented substrates exhibited only threading dislocations. For these reasons we believe that the growth of CdTe on GaAs can be greatly improved by the use of substrates that are misoriented  $2^\circ$  towards the [110]. Not only is the FWHM significantly smaller than for the oriented samples, but only threading dislocations are present which can be blocked by the inclusion of an appropriate superlattice. This has already been demonstrated for (100) CdTe on GaAs(100) using a HgZnTe-CdTe superlattice.<sup>10</sup> Since this is a difficult superlattice to grow, work on the design of a simpler superlattice is presently under way.

The authors would like to acknowledge the technical assistance provided by L. L. Stephenson in preparing the

samples and A. E. McDonald in obtaining the PLM micrographs. The work at Sandia was supported by the U. S. Department of Energy under contract number DE-AC04-76DP00789. The work at the University of Illinois at Chicago was supported by Defense Advanced Research Projects Agency (DARPA) under contract No. F49620-87-C-0021 monitored by the Air Force Office for Scientific Research.

<sup>1</sup>M. D. Lange, S. Sivananthan, X. Chu, and J. P. Faurie, *Appl. Phys. Lett.* **52**, 978 (1988).

<sup>2</sup>R. K. Tsui, J. A. Curless, G. D. Kramer, M. S. Peffley, and D. L. Rode, *J. Appl. Phys.* **58**, 2570 (1985).

<sup>3</sup>P. L. Gourley, M. Longerbone, S. L. Zhang, and H. Morkoç, *Appl. Phys. Lett.* **51**, 599 (1987).

<sup>4</sup>J. P. Faurie, C. Hsu, S. Sivananthan, and X. Chu, *Surf. Sci.* **168**, 473 (1986).

<sup>5</sup>P. Gay, P. B. Hirsch, and A. Kelly, *Acta Metall.* **1**, 315 (1953).

<sup>6</sup>J. Auleytner, *X-ray Methods in the Study of Single Crystals* (PWN-Polish Scientific Publishers, Warszawa, 1967), Chap. 2, p. 152.

<sup>7</sup>J. Weertman, *Elementary Dislocation Theory* (MacMillan, New York, 1964) Chap. 4, p. 90.

<sup>8</sup>P. L. Gourley, R. M. Biefeld, and L. R. Dawson, *Appl. Phys. Lett.* **47**, 482 (1985).

<sup>9</sup>P. L. Gourley, R. M. Biefeld, and L. R. Dawson, *Mater. Res. Soc. Symp. Proc.* **56**, 229 (1986).

<sup>10</sup>J. P. Faurie, X. Chu, J. Petruzzello, and D. J. Olego, presented at DARPA IR Focal Plane Array Materials and Processing Review, Washington, DC, April 1988 (unpublished results).

# New achievements in $\text{Hg}_{1-x}\text{Cd}_x\text{Te}$ grown by molecular-beam epitaxy

S. Sivananthan, M. D. Lange, G. Monfroy, and J. P. Faurie  
*University of Illinois at Chicago, Department of Physics, Chicago, Illinois 60680*

(Received 5 September 1987; accepted 14 December 1987)

A review of our recent achievements in the growth of  $\text{Hg}_{1-x}\text{Cd}_x\text{Te}$  by molecular-beam epitaxy is presented here. The influences of the substrate temperature, the crystallographic orientation, and the nature of the substrate on the properties of  $\text{Hg}_{1-x}\text{Cd}_x\text{Te}$  are discussed in detail. We show that to grow high-quality material with good uniformity in terms of the alloy composition and the doping by crystal stoichiometry deviation, the substrate temperature should be between 180 °C and  $T_{\text{max}}$ . We report mobilities as high as  $5.0 \times 10^5 \text{ cm}^2 \text{ V}^{-1} \text{ s}^{-1}$  for *n*-type layers and  $1.2 \times 10^3 \text{ cm}^2 \text{ V}^{-1} \text{ s}^{-1}$  for *p*-type layers, achieved by precisely controlling the growth parameters. We illustrate that the Hg condensation coefficient is influenced by the crystallographic orientation. Our results show that for  $\text{Hg}_{1-x}\text{Cd}_x\text{Te}$  grown on both the (111)*B* and the (100) faces of CdTe or GaAs the Hall mobilities are very high and comparable. We report our important achievement of the successful growth of 2-in.-diam  $\text{Hg}_{1-x}\text{Cd}_x\text{Te}$  films on GaAs(100), with  $\Delta x/\bar{x}$  as low as 0.7% for  $\bar{x} = 0.218$  ( $\Delta x$  is the standard deviation and  $\bar{x}$  is the mean value),  $\Delta t/\bar{t}$  as low as 0.6% for the layer thickness, excellent uniformity in the doping, and high electron or hole mobility. This illustrates the excellent control that our group has achieved toward the growth of this material by molecular-beam epitaxy.

## I. INTRODUCTION

Since 1981, important progress has been achieved toward the growth of  $\text{Hg}_{1-x}\text{Cd}_x\text{Te}$  by molecular-beam epitaxy (MBE). The growth of high-quality epitaxial single layers and heterostructures is of vital interest for device technology.  $\text{Hg}_{1-x}\text{Cd}_x\text{Te}$  is already the most important material for infrared technology, and is now appearing as a promising material for optical telecommunication systems.<sup>1</sup> The crystal quality along with the electrical performances of  $\text{Hg}_{1-x}\text{Cd}_x\text{Te}$  epilayers grown by MBE have been greatly improved by careful control of the growth parameters. In terms of quality and electrical performance, MBE layers of  $\text{Hg}_{1-x}\text{Cd}_x\text{Te}$  can now be compared with the best  $\text{Hg}_{1-x}\text{Cd}_x\text{Te}$  grown by any other technique.

In this paper, we present a concise account of our recent achievements in the growth of  $\text{Hg}_{1-x}\text{Cd}_x\text{Te}$  by MBE. The influence of various parameters such as the substrate temperature, the Hg flux, the crystallographic orientation and the nature of the substrate are discussed. The growth on 2-in.-diam GaAs substrates of  $\text{Hg}_{1-x}\text{Cd}_x\text{Te}$  epilayers that are highly uniform in terms of alloy composition, mobility, and carrier concentration from doping by crystal stoichiometry deviation represents the best achievement ever reported for this material on such a large surface area and illustrates the excellent level of control that our group has reached in this difficult procedure. A brief summary of the results will be given here.

## II. GROWTH ON $\text{CdTe}(111)\text{B}$ SUBSTRATES

MBE compositional control is difficult to achieve for  $\text{Hg}_{1-x}\text{Cd}_x\text{Te}$  due to the noncongruent reevaporation of this compound.<sup>2</sup> We have previously reported that reflected high-energy electron diffraction (RHEED) can be used to monitor the suitable Hg flux.<sup>3</sup> For a given Hg flux, a high-quality monocrystalline  $\text{Hg}_{1-x}\text{Cd}_x\text{Te}$  film can be grown in the (111)*B* orientation within a narrow substrate tempera-

ture range ( $T_{\text{max}} - T_{\text{min}}$ ) of about 10 to 15 °C when the substrate temperature ( $T_s$ ) is in the 180–190 °C temperature range. When  $T_s$  is below  $T_{\text{min}}$  the excess Hg desorbs, however, twins, which are detrimental for electrical performance, are observed. When growth occurs close to  $T_{\text{min}}$ , these growth defects might still exist on a longer periodicity range of 100 Å or more and consequently would not be easily detected by RHEED.<sup>4</sup> These defects are detrimental to the quality of the layer. When  $T_s$  is above  $T_{\text{max}}$  two possibilities exist. (1) If  $T_s$  is below 190 °C the excess Te leads to a polycrystalline material. (2) If  $T_s$  is above 195 °C the excess Te is reevaporated and the film still grows monocrystalline, but a change in composition is observed. Therefore, to grow high-quality  $\text{Hg}_{1-x}\text{Cd}_x\text{Te}$  by MBE it is very important to control the Hg flux and the substrate temperature accurately and reproducibly from run to run, and uniformly over the sample. It should be pointed out that these parameters also play an important role in the doping of the film by crystal stoichiometry deviation. The growth rate, which has not yet been fully investigated, is also playing an important role in terms of crystal quality. A growth rate of about  $4 \text{ Å s}^{-1}$ , which represents the best compromise between the crystal characteristics and the growth duration of 10- to 15-μm-thick epilayers, is currently used.

Hg tends to evaporate preferentially from a  $\text{Hg}_{1-x}\text{Cd}_x\text{Te}$  surface. It has been experimentally shown that the condensation coefficient for Hg is on the order of  $10^{-3}$  for *n*-type  $\text{Hg}_{1-x}\text{Cd}_x\text{Te}$  ( $x \approx 0.22$ ) grown in the (111)*B* orientation at a temperature 190 °C.<sup>5</sup> The condensation coefficient for a given element is defined as the ratio of the number of atoms incorporated in the layer to the number of atoms impinging the surface. As was pointed out already in 1982,<sup>6</sup> a temperature of 180 °C or more is required to grow high-quality  $\text{Hg}_{1-x}\text{Cd}_x\text{Te}$  films by MBE along the (111)*B* direction. Therefore, a very high Hg flux is necessary to maintain epitaxial growth. To grow *p*-type  $\text{Hg}_{1-x}\text{Cd}_x\text{Te}$  ( $x \approx 0.22$ ) with a growth rate of about  $4 \text{ Å/s}$  and a substrate temperature of

195 °C, about 1.5  $\text{cm}^3$  of Hg per micron layer is necessary in our system. This means that if a regular cell is used at a constant temperature, the Hg level would continuously change and would cause changes in the Hg flux which are unacceptable. This problem is solved by a continuous-feed Hg cell, such as the one we are currently using.

It has been previously reported that the composition ( $x$ ) is primarily controlled by the Cd to Te flux ratio. This is correct when the Hg flux is roughly constant from one growth to the next and the substrate temperature is in the 180–190 °C range. We have investigated the influence of substrate temperature on the composition.  $\text{Hg}_{1-x}\text{Cd}_x\text{Te}$  layers that were grown at different substrate temperatures, but with the same fluxes. The thicknesses and the compositions are obtained by infrared transmission spectroscopy at room temperature. For each, the cutoff wavelength is defined as that for which the absorption coefficient ( $\alpha$ ) is equal to 500  $\text{cm}^{-1}$ . The formula for the absorption coefficient is  $\alpha = -\ln(\text{transmittance})/\text{thickness}$ . This method has been proven to provide band gap measurements which are in good agreement with those determined from the temperature dependence of the  $R_0A$  products of diodes.<sup>7</sup> The thicknesses of the layers are calculated from the interference peak spacings on the infrared transmission spectra. A large change in the transmission spectrum was observed between the layers grown at 205 and 213 °C, while a smaller but not negligible change was observed between those grown at 200 and 205 °C (Fig. 1). In a different experiment carried out at temperatures 185 and 200 °C no changes in the growth rate, and consequently composition were observed between 185 and 195 °C (Table I). Due to the large change in the condensation coefficient of Hg with temperature, it is impossible to carry out one set of experiments for the entire temperature range. Comparing changes in the composition and the growth rate, one can see that these are both caused by a change in the growth rate of HgTe, but not of CdTe (Table I). The composition remains constant for substrate temperatures between 185 and 195 °C showing that the condensation coefficient of Te is constant for the given Hg flux. When the substrate temperature is above 204 °C, which is the maximum substrate temperature for given Hg flux, the rapid re-

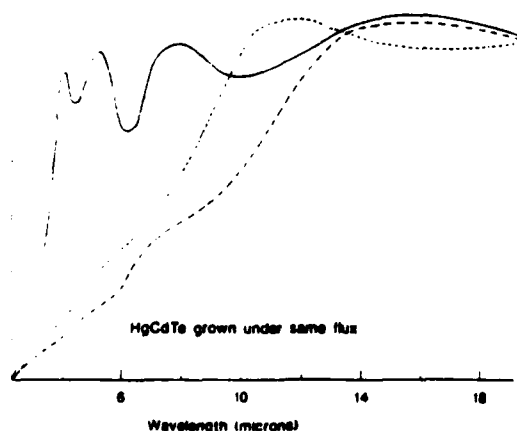


FIG. 1. Infrared transmission spectroscopic measurements of  $\text{Hg}_{1-x}\text{Cd}_x\text{Te}$  grown with the same fluxes, but at different temperatures. — = 210 °C; --- = 205 °C; - - - = 200 °C.

TABLE I. Comparison of growth rates and the  $x$  values for layers grown with the same fluxes but different substrate temperatures.

Substrate temperature (°C)	Composition ( $x$ )	Growth rate ( $\text{\AA}/\text{s}$ )	Relative growth rate of CdTe ( $\text{\AA}/\text{s}$ )	Relative growth rate of HgTe ( $\text{\AA}/\text{s}$ )
185 <sup>a</sup>	...	...	...	4.39
195 <sup>a</sup>	...	...	...	4.40
200	0.17	5.17	0.88	4.29
205	0.19	4.67	0.89	3.78
213	0.31	2.78	0.86	1.92

<sup>a</sup> Extrapolated from a separate experiment.

vaporation of Hg leaves free Te which is also reevaporated and the film still grows monocrystalline. But an increase in the  $x$  value of 1.5% to 2% for each 1 °C increase in the substrate temperature is observed, along with a large change in the growth rate. This problem could be partially solved by increasing the Hg flux.

It is important to recall that a change in  $x$  of only  $\Delta x = \pm 0.0015$  is the objective to reach for infrared detection devices operating at a cutoff wavelength of 10  $\mu\text{m}$  at 77 K. It is obvious that such a requirement cannot be achieved if part of the substrate temperature is above  $T_{\text{max}}$ . Now if the substrate temperature is between  $T_{\text{max}}$  and  $T_{\text{min}}$  (incidentally the  $T_{\text{max}}$  and  $T_{\text{min}}$  values are changing over the substrate since the Hg flux distribution is not constant) the epilayers will still experience a change in the doping level and even in the conduction type.

Stability in the temperature, with variations much less than  $\pm 0.5$  °C during the growth can be achieved. But, uniformity in the temperature with variations  $< \pm 0.5$  °C over large surface areas has not yet been demonstrated. Consequently, taking into consideration the need of high-quality material with excellent uniformity in the composition, the substrate temperatures used should be between 180 °C and  $T_{\text{max}}$ . Also, to grow  $\text{Hg}_{1-x}\text{Cd}_x\text{Te}$  with good uniformity in the composition and the carrier concentration over the substrate, it is important to achieve a very low temperature gradient and to control precisely the substrate temperature in the 180 °C– $T_{\text{max}}$  range. In addition, a reproducibility of the substrate temperature within 1 °C should be achieved in order to produce both the composition and the carrier concentration desired from run to run.

Such control will be fruitless if the Hg, Cd, and Te fluxes are not very constant. The Cd and Te fluxes are precisely controlled through the temperatures of the effusion cells which are stable within 0.2 °C. The Hg flux, which has lesser importance than the Cd and Te fluxes in controlling of the composition, is monitored by an ion gauge and kept constant within a range of fluctuation of  $< 10\%$ . This represents cell temperature fluctuations of  $< 0.5$  °C.

Gradients in the substrate temperature and the fluxes (the latter due to the cosine distributions of the fluxes) increase with the size of the substrate. Therefore, it becomes obvious that MBE growth of  $\text{Hg}_{1-x}\text{Cd}_x\text{Te}$  on large area 2-in. diameter or greater substrates, uniform both in composition and carrier concentration, represents a real challenge. The need

for rotation of the substrate becomes unavoidable because the alternative of using cell-to-substrate distances of about one meter is unacceptable in terms of Hg consumption. Rotation of the substrate, however, hinders proper mechanical contact between the thermocouple and the substrate holder. (Such use of a thermocouple is normally a convenient way to control the temperature of the surface, although not reliably accurate in case of sudden change of the surface temperature.) Therefore a pyrometer must be used.

### III. THE INFLUENCE OF THE CRYSTALLOGRAPHIC ORIENTATION

In MBE a nonequilibrium situation is intentionally introduced to drive the system to form a solid from the vapor phase by adjusting the substrate temperature and the partial pressures of the molecular fluxes. The formation of epitaxial layers is highly influenced by the mass transport and the crystal surface. Therefore the crystallographic orientation can play a major role in the growth and properties of  $\text{Hg}_{1-x}\text{Cd}_x\text{Te}$  grown by MBE.

The influence of the crystallographic orientation on condensation coefficients has been compared among the (111)*A*, (111)*B*, and (100) orientations. In each case the  $\text{Hg}_{1-x}\text{Cd}_x\text{Te}$  growth was closely followed by RHEED. The minimum amount of Hg necessary to maintain the growth was determined by slowly decreasing the Hg flux until difficulties in maintaining monocrystalline growth were observed. As we have reported<sup>8</sup> before, with all the other conditions including the composition kept constant, the minimum amount of Hg necessary to maintain epitaxial growth of  $\text{Hg}_{1-x}\text{Cd}_x\text{Te}$  at 185°C is almost an order of magnitude higher for the (111)*A* orientation than for the (111)*B* orientation. The minimum amount of Hg necessary to maintain epitaxial growth along the (100) orientation falls in between that for the (111)*A* and the (111)*B* orientations. These results can be explained in terms of the bonding of surface atoms. Hg atoms are more well protected from reevaporation in the (111)*B* orientation than the (100) orientation, and have the least protection in the (111)*A* orientation. A similar but less dramatic tendency is observed for Cd.

Results regarding the growth parameters for different orientations provide an important means for ascertaining the best orientation for growth. From a Hg consumption point of view, one could conclude that the (111)*B* orientation is the best. But it is important that other parameters, such as the quality of the layer and the ease of control of the doping by stoichiometry deviation, are taken into consideration before coming to a conclusion. For the (111)*A* orientation, growth by MBE of a high-quality CdTe buffer layer with a low-defect density is very difficult. Moreover, the amount of Hg needed to maintain the epitaxial growth of  $\text{Hg}_{1-x}\text{Cd}_x\text{Te}$  for the (111)*A* orientation is about ten times that for the (111)*B* orientation. This huge amount of Hg needed for the (111)*A* orientation growth creates a major problem for the ultrahigh vacuum (UHV) of the MBE system. Therefore, the (111)*A* orientation is not suitable for MBE growth of  $\text{Hg}_{1-x}\text{Cd}_x\text{Te}$ . For this reason we have investigated only the (111)*B* and the (100) orientations.

On the other hand the (111)*B* orientation has a major disadvantage for the control of the growth of high-quality layer. That is stacking faults, which are often observed on the (111)*B* face. When the Hg flux is too high, twinning effects which are caused by antiphase domains are observed. This implies that the twinning process occurs very easily along this direction. This problem is in fact often observed for zinc-blende crystals grown in the (111) orientation, but the growth of pyramids has been observed when the growth conditions are not well controlled.<sup>4</sup> No such phenomenon is observed for the (100) orientation. Samples for which twins are observed by RHEED during growth exhibit high-carrier concentration and low mobility. Also, electroreflectance measurements carried out on some (111)*B* orientation  $\text{Hg}_{1-x}\text{Cd}_x\text{Te}$  layers have shown an increase in the line width ( $\Gamma$ ) on such films.<sup>10</sup> For the (100) orientation, even though more Hg is necessary to grow  $\text{Hg}_{1-x}\text{Cd}_x\text{Te}$  no such defects are observed. Thus the growth seems to be more easy to control in the (100) orientation than in the (111)*B* orientation. It should be pointed out that *n*-type  $\text{Hg}_{1-x}\text{Cd}_x\text{Te}$  can easily be grown along the (100) orientation even for  $x > 0.30$ , while *p*-type  $\text{Hg}_{1-x}\text{Cd}_x\text{Te}$  is easily grown in the (111)*B* orientation for  $x > 0.19$ . This experimental result is difficult to understand if one considers that the *p*-type characteristic is associated with Hg vacancies because then (100) layers should be more *p*-type than (111)*B* layers since the Hg condensation coefficient is lower on the (100) face. We are currently investigating this problem.

Table II shows a comparison of the best Hall data of *n*-type samples grown either in the (100) or the (111)*B* surface. These values indicate that the mobilities are very much comparable for the two crystallographic orientations. The electron mobility of  $5.0 \times 10^3 \text{ cm}^2 \text{ V}^{-1} \text{ s}^{-1}$  for  $\text{Hg}_{1-x}\text{Cd}_x\text{Te}$  grown on the (111)*B* face, is close to the theoretical limit of the electron mobility in  $\text{HgCdTe}$  with this Cd concentration. Often,  $\text{Hg}_{1-x}\text{Cd}_x\text{Te}$  grown on the (100) surface has a higher electron mobility than that on the (111)*B* surface. This shows that the control of the growth parameters for  $\text{Hg}_{1-x}\text{Cd}_x\text{Te}$  grown by MBE is more critical for the (111)*B* orientation than the (100) orientation.

Table III compares the hole mobility of  $\text{Hg}_{1-x}\text{Cd}_x\text{Te}$  grown on the (100) and the (111)*B* surfaces. It is important to point out that these high-hole mobilities have been obtained for epilayers which have no small  $\text{HgTe}$  layer at the interface with the substrate (we have shown that the presence of  $\text{HgTe}$  at that interface can enhance hole mobility).<sup>10</sup> The hole mobility of  $1.2 \times 10^3 \text{ cm}^2 \text{ V}^{-1} \text{ s}^{-1}$  observed in a (111)*B* orientation is higher than the best *p*-type mobility of  $5.1 \times 10^2 \text{ cm}^2 \text{ V}^{-1} \text{ s}^{-1}$  for layers grown on the (100) surface. It should be pointed out that we do not have as much data for *p*-type  $\text{Hg}_{1-x}\text{Cd}_x\text{Te}$  grown on the (100) surface. Therefore, it would be premature to draw a final conclusion for hole mobilities.

Since the (100) surface requires more Hg than the (111)*B* surface, then from both the UHV and the economic points of view, the (111)*B* orientation is the best. As for the growth point of view, we suggest that high-quality *n*-type  $\text{Hg}_{1-x}\text{Cd}_x\text{Te}$  layers are more easily grown along the (100) orientation [more has to be understood about the *n*-type

TABLE II. Electrical characteristics of *n*-type  $\text{HgCdTe}$  grown by MBE between 180 and 190 °C.

Sample	Composition $x$	Thickness	Orientation	Carrier conc.	Mobility	$T$	Carrier conc.	Mobility
				$N_D - N_A (\text{cm}^{-3})$ at 300 K	$\mu_H (\text{cm}^2 \text{V}^{-1} \text{s}^{-1})$		$N_D - N_A (\text{cm}^{-3})$	$\mu_H (\text{cm}^2 \text{V}^{-1} \text{s}^{-1})$
CdTe substrate								
241-600	0.18	8.0 $\mu\text{m}$	(100)	$1.3 \times 10^{17}$	$3.0 \times 10^4$	20 K	$4.2 \times 10^{15}$	$3.7 \times 10^5$
214-526	0.19	11.7 $\mu\text{m}$	(111) $B$	$4.6 \times 10^{16}$	$1.6 \times 10^4$	20 K	$2.5 \times 10^{14}$	$3.1 \times 10^5$
7-233(82)	0.20	6.0 $\mu\text{m}$	(111) $B$	$4.0 \times 10^{16}$	$1.7 \times 10^4$	77 K	$2.0 \times 10^{15}$	$1.9 \times 10^5$
162-431	0.22	2.0 $\mu\text{m}$	(100)	$2.0 \times 10^{16}$	$2.0 \times 10^4$	77 K	$6.0 \times 10^{15}$	$1.6 \times 10^5$
CdZnTe substrate								
32-598	0.18	8.6 $\mu\text{m}$	(111) $B$	$1.1 \times 10^{17}$	$1.0 \times 10^4$	20 K	$9.9 \times 10^{14}$	$2.1 \times 10^5$
19-405	0.20	9.0 $\mu\text{m}$	(111) $B$	$3.1 \times 10^{16}$	$1.4 \times 10^4$	77 K	$2.0 \times 10^{15}$	$1.2 \times 10^5$
GaAs substrate								
576-396	0.18	2.7 $\mu\text{m}$	(111) $B$	$1.0 \times 10^{17}$	$1.9 \times 10^4$	30 K	$1.5 \times 10^{15}$	$5.0 \times 10^5$
12- 17	0.19	6.2 $\mu\text{m}$	(100)	$1.0 \times 10^{17}$	$2.4 \times 10^4$	30 K	$1.0 \times 10^{16}$	$2.4 \times 10^5$
403-250	0.20	1.0 $\mu\text{m}$	(100)	$5.0 \times 10^{16}$	$1.5 \times 10^4$	40 K	$1.0 \times 10^{16}$	$3.0 \times 10^5$
191-102	0.22	1.0 $\mu\text{m}$	(111) $B$	$2.0 \times 10^{16}$	$1.1 \times 10^4$	50 K	$4.0 \times 10^{15}$	$1.0 \times 10^5$

doping in (100)], while high-quality *p*-type  $\text{Hg}_{1-x}\text{Cd}_x\text{Te}$  layers are more easily obtained by growing along the (111)*B* orientation. Therefore provided that a good control of the growth parameters is achieved, what actually can be done, (111)*B* seems to be the best orientation.

#### IV. GROWTH ON GaAs(100) SUBSTRATES

The growth of high-quality epitaxial films is limited by the substrate quality. CdTe, because of its closeness in lattice parameter and its metallurgical compatibility with  $\text{Hg}_{1-x}\text{Cd}_x\text{Te}$ , is a natural choice for the substrate material. However, the lack of availability of high-structural perfection CdTe substrates has stimulated interest in growth of

$\text{Hg}_{1-x}\text{Cd}_x\text{Te}$  by MBE on other substrates. X-ray rocking curves measured on samples grown on CdTe, and CdZnTe substrates indicate that comparable crystalline qualities can be reached, but the nonhomogeneity of the substrates appears to be the primary limiting factor. Large dispersions in full widths at half-maximum (FWHM) are currently observed on commercially available CdTe or CdZnTe substrates. Nevertheless, it is important to point out that when the growth conditions are under good control and the substrates of high quality,  $\text{HgCdTe}$  epilayers can almost duplicate the crystal quality of substrates. As an illustration, FWHM as low as 17 and 18 arcsec (Fig. 2) were recorded on samples grown on CdTe and CdZnTe. Nevertheless when

TABLE III. Electrical characteristics of *p*-type  $\text{HgCdTe}$  grown by MBE between 190 and 200 °C (no HgTe layer at the interface).

Sample	Substrate	Composition $x$	Thickness	Carrier conc.	Mobility	$T$	Carrier conc.	Mobility
				$N_D - N_A (\text{cm}^{-3})$ at 300 K	$\mu_H (\text{cm}^2 \text{V}^{-1} \text{s}^{-1})$		$N_A - N_D (\text{cm}^{-3})$	$\mu_H (\text{cm}^2 \text{V}^{-1} \text{s}^{-1})$
(111) $\beta$ orientation								
196-481	CdTe	0.20	4.8 $\mu\text{m}$	$1.6 \times 10^{16}$	$9.0 \times 10^3$	30 K	$6.0 \times 10^{15}$	$1.1 \times 10^5$
198-484	CdTe	0.21	4.3 $\mu\text{m}$	$2.9 \times 10^{16}$	$8.5 \times 10^3$	30 K	$5.1 \times 10^{15}$	$1.0 \times 10^5$
242-602	CdTe	0.22	11.9 $\mu\text{m}$	$2.1 \times 10^{16}$	$8.4 \times 10^3$	23 K	$2.0 \times 10^{15}$	$1.1 \times 10^5$
215-527	CdTe	0.25	11.9 $\mu\text{m}$	$5.8 \times 10^{15}$	$7.5 \times 10^3$	30 K	$6.2 \times 10^{15}$	$9.7 \times 10^4$
205-516	CdTe	0.29	15.6 $\mu\text{m}$	$3.0 \times 10^{15}$	$4.5 \times 10^3$	30 K	$7.5 \times 10^{15}$	$9.7 \times 10^4$
216-528	CdTe	0.34	12.1 $\mu\text{m}$	$1.6 \times 10^{16}$	$1.5 \times 10^3$	77 K	$3.6 \times 10^{15}$	$8.0 \times 10^4$
667-532	GaAs	0.20	2.1 $\mu\text{m}$	$2.4 \times 10^{16}$	$1.0 \times 10^4$	23 K	$4.1 \times 10^{15}$	$1.2 \times 10^5$
681-540	GaAs	0.21	3.7 $\mu\text{m}$	$2.4 \times 10^{16}$	$1.0 \times 10^4$	23 K	$3.6 \times 10^{15}$	$1.1 \times 10^5$
583-453	GaAs	0.22	5.4 $\mu\text{m}$	$1.8 \times 10^{16}$	$6.7 \times 10^3$	30 K	$1.4 \times 10^{15}$	$8.7 \times 10^4$
654-508	GaAs	0.25	3.8 $\mu\text{m}$	$6.2 \times 10^{15}$	$4.5 \times 10^3$	30 K	$1.1 \times 10^{16}$	$7.3 \times 10^4$
393-244	GaAs	0.28	1.3 $\mu\text{m}$	$1.3 \times 10^{16}$	$1.3 \times 10^3$	40 K	$2.8 \times 10^{15}$	$5.2 \times 10^4$
500-308	GaAs	0.31	2.3 $\mu\text{m}$	$2.6 \times 10^{15}$	$2.4 \times 10^3$	30 K	$1.1 \times 10^{15}$	$4.5 \times 10^4$
4-319	CdTeSe	0.31	7.6 $\mu\text{m}$	$3.1 \times 10^{15}$	$3.2 \times 10^3$	30 K	$2.4 \times 10^{15}$	$9.4 \times 10^4$
2-310	CdTeSe	0.32	9.4 $\mu\text{m}$	$2.1 \times 10^{15}$	$1.9 \times 10^3$	30 K	$1.2 \times 10^{15}$	$6.7 \times 10^4$
34-605	CdZnTe	0.24	9.2 $\mu\text{m}$	$8.6 \times 10^{15}$	$5.7 \times 10^3$	23 K	$1.4 \times 10^{15}$	$8.0 \times 10^4$
(100) orientation								
673-534	GaAs	0.21	4.2 $\mu\text{m}$	$2.0 \times 10^{16}$	$4.6 \times 10^3$	23 K	$3.4 \times 10^{15}$	$5.1 \times 10^4$
125-304	CdTe	0.24	3.0 $\mu\text{m}$	$4.1 \times 10^{15}$	$3.6 \times 10^3$	77 K	$2.0 \times 10^{16}$	$2.5 \times 10^4$
127-306	CdTe	0.29	2.7 $\mu\text{m}$	$4.1 \times 10^{15}$	$2.9 \times 10^3$	77 K	$1.5 \times 10^{16}$	$1.2 \times 10^4$

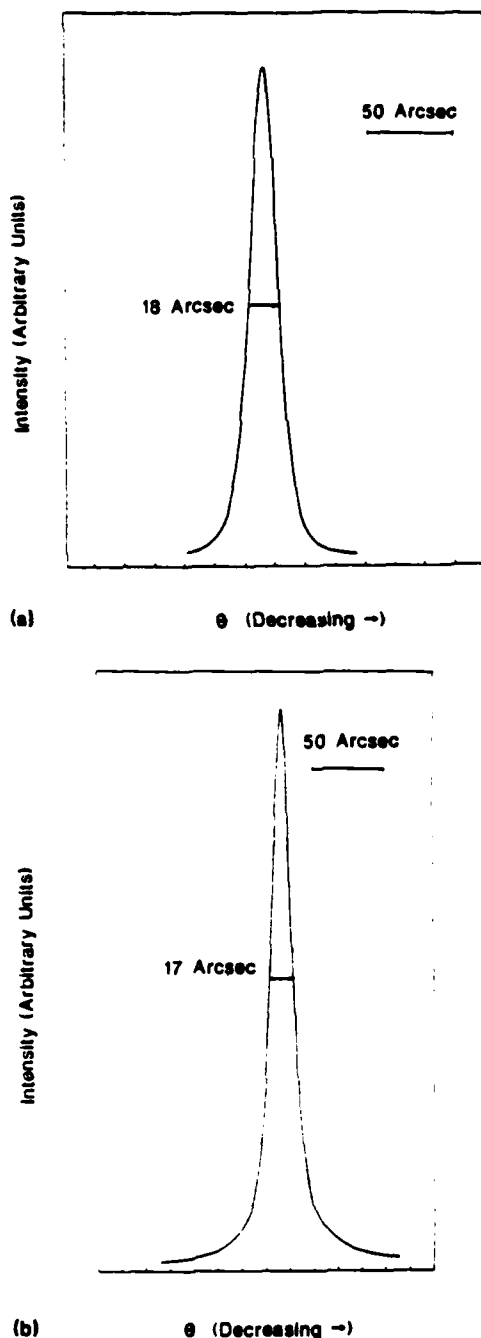


FIG. 2. X-ray rocking curve recorded along the (333) direction, using the  $\text{Cu-K}_\alpha$  line ( $\lambda = 1.540562 \text{ \AA}$ ). (a)  $\text{HgCdTe}$  on  $\text{CdTe}$  substrate. Sample #242602, reflection (333). (b)  $\text{HgCdTe}$  on  $\text{CdZnTe}$  substrate. Sample #38617, reflection (333).

the x-ray probe was moved the half-width deteriorated due to the lack of uniformity of the substrates. The lack of availability of tellurium-based substrates makes GaAs very attractive. The interest in growing  $\text{Hg}_{1-x}\text{Cd}_x\text{Te}$  on GaAs still exists, despite the important progress made in the improvement of  $\text{CdTe}$  crystal quality during this last year, because  $\text{CdTe}$  and related materials are much more expensive than GaAs and not available in 2- and 3-in.-diam sizes. Thus it is interesting to update constantly the data obtained for epilayers grown on these different substrates. Electron and hole mobility, and carrier concentration are chosen for such com-

parison because such characterization is closely related to device characteristics.

Much discussion has occurred regarding the epitaxy of  $\text{CdTe}$  on  $\text{GaAs}(100)$  since both (111) $B$  and (100) oriented  $\text{CdTe}$  can be grown on  $\text{GaAs}(100)$ .<sup>11-15</sup> It has been recently shown that (111) $B$  orientation and (100) orientation  $\text{CdTe}$  grown on  $\text{GaAs}(100)$  are of high quality, but also that the quality of the (100)  $\text{CdTe}$  improves when the oxide is totally desorbed prior to growth. In order to completely desorb the oxide the  $\text{GaAs}$  should be preheated to  $580^\circ\text{C}$ . However, this creates an As deficient surface. Therefore, to grow (100)  $\text{CdTe}$ , either the substrate should be preheated to  $580^\circ\text{C}$  under As or Te flux, or first  $\text{Cd}_{1-x}\text{Zn}_x\text{Te}$  with  $x > 0.15$  should be grown after preheating to  $580^\circ\text{C}$ . The growth of  $\text{Hg}_{1-x}\text{Cd}_x\text{Te}$  on  $\text{CdTe}/\text{GaAs}(100)$  substrate has been previously reported.<sup>16</sup> Electron diffraction patterns obtained during such growth attest to the high quality of these films. The observation of an electron mobility as high as  $5.0 \times 10^5 \text{ cm}^2 \text{ V}^{-1} \text{ s}^{-1}$  for  $\text{Hg}_{1-x}\text{Cd}_x\text{Te}$  (111) $B$  grown on  $\text{GaAs}$  indeed indicates that the quality of such layers is excellent. Tables II and III display and compare electrical characteristics of  $n$ -type and  $p$ -type  $\text{Hg}_{1-x}\text{Cd}_x\text{Te}$  epilayers grown on various substrates. Using mobility as a tool to compare the quality of these layers, one could conclude that  $\text{Hg}_{1-x}\text{Cd}_x\text{Te}$  grown on  $\text{GaAs}(100)$  substrates is of high quality, comparable to that grown on  $\text{CdTe}$ ,  $\text{CdZnTe}$ , and  $\text{CdTeSe}$ . Of course finally the comparison of IR devices made from  $\text{Hg}_{1-x}\text{Cd}_x\text{Te}$  layers grown on different substrates will provide the ultimate test.

## V. GROWTH ON 2-IN.-DIAM $\text{GaAs}(100)$ SUBSTRATES

As discussed above, the growth of  $\text{Hg}_{1-x}\text{Cd}_x\text{Te}$  on 2-in.-diam  $\text{GaAs}(100)$  substrates represents a real challenge since all the growth parameters must be extremely well controlled. But certainly success in this endeavor will be an important achievement for  $\text{Hg}_{1-x}\text{Cd}_x\text{Te}$  detector technology. Several 2-in.-diam  $\text{Hg}_{1-x}\text{Cd}_x\text{Te}$  layers have been grown on  $\text{GaAs}(100)$ . All of them exhibit uniform mirrorlike surfaces. The details of the growth and characterization are given elsewhere.<sup>17</sup> In order to determine the uniformity in thickness composition, infrared transmission measurements have been performed at several positions on the samples. A standard deviation ( $\Delta x/x$ ) as low as 0.7% of the mean composition ( $\bar{x}$ ) and likewise a measurement for  $\Delta t/t$  of 0.6% for the thickness have been observed for 5- $\mu\text{m}$ -thick layers with composition around 0.22.

For a  $p$ -type film grown on the (111) $B$  surface the carrier concentration ( $N_a - N_d$ ) increased by a factor of 2 from  $3.6 \times 10^{15} \text{ cm}^{-3}$  at the center to  $7.2 \times 10^{15} \text{ cm}^{-3}$  at the edge of the film, while the hole mobility increased from  $5.7 \times 10^2 \text{ cm}^2 \text{ V}^{-1} \text{ s}^{-1}$  at the center to  $6.2 \times 10^2 \text{ cm}^2 \text{ V}^{-1} \text{ s}^{-1}$  at the edge. A 2-in.-diam  $n$ -type  $\text{Hg}_{1-x}\text{Cd}_x\text{Te}$  film was grown on the (100) surface. For this film mobility varied between  $1.3 \times 10^5 \text{ cm}^2 \text{ V}^{-1} \text{ s}^{-1}$  and  $1.8 \times 10^5 \text{ cm}^2 \text{ V}^{-1} \text{ s}^{-1}$  indicating a layer of good quality. Also for this  $n$ -type layer the carrier concentration ( $N_d - N_a$ ) ranged only from  $4.0 \times 10^{15}$  to  $4.4 \times 10^{15} \text{ cm}^{-3}$ , exhibiting extreme uniformity.

## VI. CONCLUSION

In this paper we have presented recent achievements in the growth of  $\text{Hg}_{1-x}\text{Cd}_x\text{Te}$ . We have shown that in order to grow high quality, homogeneous, thick  $\text{Hg}_{1-x}\text{Cd}_x\text{Te}$  epilayers of large area the substrate temperature should not be lower than 180 °C or higher than  $T_{\text{max}}$ . We have discussed the role of the crystallographic orientation in terms of the Hg condensation coefficient and the control of the conduction type [*n*-type  $\text{Hg}_{1-x}\text{Cd}_x\text{Te}$  films can easily be grown in the (100) orientation, whereas *p*-type  $\text{Hg}_{1-x}\text{Cd}_x\text{Te}$  layers are easily grown in the (111)*B* orientation]. Electrical measurements show that when the growth parameters are well controlled, the quality of  $\text{Hg}_{1-x}\text{Cd}_x\text{Te}$  grown in both the (111)*B* and the (100) orientations is comparable, thus giving the advantage to the (111)*B* growth direction which requires less mercury. We confirm that  $\text{Hg}_{1-x}\text{Cd}_x\text{Te}$  layers grown on GaAs substrates are electrically as good as those grown on CdTe, CdZnTe or CdTeSe substrates. We have shown that high-quality  $\text{Hg}_{1-x}\text{Cd}_x\text{Te}$  films of 2-in.-diam can be grown. High-Hall mobilities, uniform thicknesses, and very uniform compositions have been achieved already in these films. Further improvements in the temperature uniformity of the samples, along with increased uniformity of the Hg flux on the samples is expected to improve the uniformity of  $\text{Hg}_{1-x}\text{Cd}_x\text{Te}$  layers with even larger surface areas. These results represent important achievements toward the use of  $\text{Hg}_{1-x}\text{Cd}_x\text{Te}$  layers grown by MBE for infrared detector technology.

## ACKNOWLEDGMENTS

The authors would like to thank P. S. Wijewarnasuriya, I. K. Sou, X. Chu, and M. Boukerche for their assistance, and

S. Farook and Z. Ali for the technical assistance. This work was supported by DARPA and monitored by Air Force Office of Scientific Research under Contract No. F49620-87-C-0021.

- <sup>1</sup>C. Verie, F. Raymond, and G. Neu, *J. Vac. Sci. Technol. B* **4** (1986).
- <sup>2</sup>R. F. C. Farrow, C. R. Jones, G. M. Williams, P. W. Sullivan, W. J. O. Boyle, and J. T. M. Wotherspoon, *J. Phys. D* **12**, L117 (1979).
- <sup>3</sup>J. P. Faurie, J. Reno, S. Sivananthan, I. K. Sou, X. Chu, M. Boukerche, and P. S. Wijewarnasuriya, *J. Vac. Sci. Technol. B* **4**, 585 (1986).
- <sup>4</sup>R. D. Horning and J. L. Stauderman, *Appl. Phys. Lett.* **49**, 1590 (1986).
- <sup>5</sup>J. P. Faurie and A. Million, *J. Cryst. Growth* **54**, 582 (1981).
- <sup>6</sup>J. P. Faurie and A. Million, *Appl. Phys. Lett.* **41**, 264 (1982).
- <sup>7</sup>J. P. Faurie, S. Sivananthan, M. Lange, R. F. Dewames, A. M. B. Vandewyck, G. M. Williams, Dan Yamini, and E. Yao, *Appl. Phys. Lett.* (submitted).
- <sup>8</sup>S. Sivananthan, X. Chu, J. Reno, and J. P. Faurie, *J. Appl. Phys.* **60**, 1359 (1986).
- <sup>9</sup>P. M. Raccach, J. W. Garland, Z. Zhang, A. H. M. Chu, J. Reno, I. K. Sou, M. Boukerche, and J. P. Faurie, *J. Vac. Sci. Technol. A* **4**, 2077 (1986).
- <sup>10</sup>J. P. Faurie, I. K. Sou, D. Rafol, and K. C. Woo, *Phys. Rev. B* **34**, 6000 (1986).
- <sup>11</sup>J. P. Faurie, C. Hsu, S. Sivananthan, and X. Chu, *Surf. Sci.* **168**, 473 (1986).
- <sup>12</sup>J. M. Ballingall, M. L. Wroge, and D. J. Leopold, *Appl. Phys. Lett.* **48**, 1273 (1986).
- <sup>13</sup>L. A. Kolodziecki, R. L. Gunshor, N. Otsuka, X. C. Zhang, S. K. Chang, and A. V. Nurmikko, *Appl. Phys. Lett.* **47**, 882 (1985).
- <sup>14</sup>R. N. Bickness, R. Y. Yanka, N. C. Giles, J. F. Schetzina, T. Z. Nagee, C. Leung, and H. Hawayoshi, *Appl. Phys. Lett.* **44**, 363 (1984).
- <sup>15</sup>P. P. Chow, L. A. Greenlaw, and D. Johnson, *J. Vac. Sci. Technol. A* **1**, 562 (1983).
- <sup>16</sup>J. P. Faurie, S. Sivananthan, M. Boukerche, and J. Reno, *Appl. Phys. Lett.* **45**, 1307 (1984).
- <sup>17</sup>M. D. Lange, S. Sivananthan, X. Chu, and J. P. Faurie, *Appl. Phys. Lett.* (to be published).

## II-2-3 CdTe/Si(100)

The direct growth of CdTe-HgCdTe on Silicon substrates is especially attractive in view of producing large area monolithic IR focal-plane arrays, combining HgCdTe IR detectors with Si integrated circuits for signal processing. Si substrates are commercially available in large area and are inexpensive compared to CdTe or even GaAs. Therefore Si would be an ideal candidate as an alternative substrate if 19% of difference between CdTe and Si lattices did not exist.

Despite the enormous interest in a IR monolithic approach based on Si-based growth technology only few attempts to grow CdTe directly on Silicon have been published. The MPLab has reported the first successful growth of (111)B CdTe on Silicon by MBE. CdTe(100) has also been obtained when an intermediate layer of ZnTe is grown first. The (111)B oriented layers are made of two twinned domains which are rotated by 90°. It has been shown that using a 8°off Si(100) substrate a single twin-free domain is observed. CdTe layers have been characterized by high energy electron diffraction, photoluminescence spectroscopy, scanning electron microscopy and x-ray diffraction. The detail of this very exciting work has been published in the attached paper.

During this study it was found that the cleaning of Si substrate is extremely critical. The thermal treatment at 850°C is very important step as well as the background pressure during the treatment. The temperature should be very uniform across the entire wafer. In the current machine silicon wafers are held on the substrate holder with indium. During the thermal cleaning procedure indium tends to form islands which leads to temperature uniformity regarding the surface of Si. This is one of the major problems encountered here.

From this preliminary study it is concluded that the new prototype MBE machine OPUS 45 is much more suitable since Si substrates are held without Indium or Gallium and a better temperature uniformity is expected. In addition this machine can handle a 5-inch Si substrate taking full advantage of Si substrate.

### ATTACHED PAPER:

1. "Molecular beam epitaxial growth of CdTe and HgCdTe on Si(100)."

## II-3 HgCdTe(111)B TWIN-FREE EPILAYERS

### II-3-1 CONTROL OF THE GROWTH

The improvement of HgCdTe MBE grown epilayers in terms of structural, transport and optical properties has been a constant concern over these past years in the MPLab. It is of extreme importance to control carefully each step of the growth process. The surface of the substrate as discussed in part II-2-1 should be prepared under very clean conditions and within the proper temperature range. The growth of the CdTe buffer layer has also to be grown under optimized growth conditions in order to obtain the highest crystal quality. CdTe buffer layer grown either on CdTe, CdZnTe, GaAs or Si should be twin-free and should exhibit a low dislocation density.

As discussed in part II-2-2 the growth of CdTe on GaAs has been improved drastically during the contract period but still does not compare with the best CdTe grown on CdTe or CdZnTe. The growth of HgCdTe as reported previously and discussed in the paper "New achievements in  $\text{Hg}_{1-x}\text{Cd}_x\text{Te}$  grown by MBE" demands very stringent requirements in terms of flux and temperature stability and reproducibility.

The growth of twin free (111)B HgCdTe represents a real challenge. In addition to rotation type twins, reflection type twins have been observed as discussed in part II-1. First of all the substrate or the buffer layer should be twin free. Therefore great care has to be taken during substrate preparation and buffer layer growth as discussed before. The same precautions have to be observed during the first steps of the HgCdTe growth in order to prevent double positioning twin formation. During the growth we have seen that an increase in the Hg flux or a decrease in the substrate temperature can trigger the formation of an antiphase boundary.

The control of the Hg flux is achieved though the use of a constant level Hg cell. During the growth and from run-to-run the Hg flux monitored by an ion gauge is kept within less than 5% fluctuation. The control of the substrate temperature  $T_S$  is the most difficult task because what has to be controlled is, in fact, the temperature of the surface  $T_{SS}$ . We have verified that the temperature indicated by the thermocouple located in the back of the substrate which rotates

- 1) does not give an accurate reading of the substrate temperature
- 2) does not account quickly for surface temperature change

The use of an IR pyrometer does not represent either an ideal solution. When  $T_{SS}$  is kept constant at 190°C, by using a front thermocouple, at the initiation of HgCdTe growth a jump of approximately 25°C (in our MBE configuration) occurs in the pyrometer reading  $T_P$  due to scattered IR radiation primarily from the hot CdTe cell as illustrated in Fig. 1. Immediately  $T_P$  falls steeply due to both the rapid decrease in reflectance of the block and the fall toward the first minimum in the interference pattern related to the presence of a thin HgCdTe layer. Once the first minimum is reached  $T_P$  rises toward the next maximum. Several more oscillations of decreasing amplitude follow. After about 1.5  $\mu\text{m}$  of growth, the oscillations are almost completely gone. At this point  $T_P$  is approximately 15°C higher than the reading before growth. This increase is primarily due to emitted radiation since emittance increases as cadmium composition decreases.

During this time the back thermocouple  $T_B$  reading has increased by 15–20°C. In other words if  $T_B$  is kept constant,  $T_{SS}$  will decrease. Then the Hg flux kept constant will become too high since the Hg sticking coefficient changes drastically with temperature and reflection twin visible on the RHEED pattern will be formed. From these experiments it appears that the control of the surface substrate temperature  $T_{SS}$  which is a key parameter and should be kept constant within 1°C is an extremely difficult task. The Microphysics Laboratory has devoted a lot of time in order to achieve the best control of  $T_{SS}$ .

Since a front thermocouple cannot be left during conventional growth using rotation, a double control involving a back thermocouple and an IR pyrometer along with the knowledge based on tedious experiments identical to the one describe before, is currently utilized in the Microphysics Laboratory. It is very important to point out that if these observations are certainly valid for MBE growth of HgCdTe carried out in any MBE machine and using a substrate stuck with Gallium on a Molybdenum block, the magnitude of relative changes between  $T_B$ ,  $T_P$  and  $T_{SS}$  will depend strongly on the substrate heater technology and effusion cell geometry. These investigations have resulted in a better control of the surface preparation, the stability, and reproducibility of all the fluxes and the surface substrate temperature. This improvement has been confirmed by the growth of twin-free HgCdTe(111)B illustrated in the ECP of Fig. 2 and excellent results for epilayers grown in (211)B orientation presented in part II-3-3

## FIGURE CAPTIONS:

- Fig. 1      Plot of the temperature pyrometer reading  $T_p$  vs  $t$  for  $\text{Hg}_{1-x}\text{Cd}_x\text{Te}$  ( $x = 0.26$ ) grown on  $\text{CdTe}(111)\text{B}$ . During the experiment the surface temperature of the substrate  $T_{ss}$  is kept constant at  $190^\circ\text{C}$ .
- Fig. 2      Electron channeling pattern along the  $(111)$  axis of a twin free  $\text{HgCdTe}(111)\text{B}$  layer grown on  $\text{CdZnTe}(111)\text{B}$  substrate.

# Molecular beam epitaxial growth of CdTe and HgCdTe on Si (100)

R. Sporken, S. Sivananthan, K. K. Mahavadi, G. Monfroy, M. Boukerche, and J. P. Faurie

*Microphysics Laboratory, Department of Physics, University of Illinois at Chicago, Chicago, Illinois 60680*

(Received 17 July 1989; accepted for publication 24 August 1989)

CdTe has been grown on Si(100) by molecular beam epitaxy. Two orientations can be obtained: (111)*B* CdTe when the CdTe is deposited directly on the Si(100) substrates, and (100)CdTe when an intermediate layer of ZnTe is grown first. The (111)*B* oriented layers are made of two domains which are rotated by 90°. A layer with only one domain can be grown on Si(100) misoriented by 8°, but the best misorientation for this purpose still needs to be found. These layers were characterized by reflection high-energy electron diffraction, photoluminescence spectroscopy, scanning electron microscopy, and x-ray diffraction. Hg<sub>1-x</sub>Cd<sub>x</sub>Te has also been grown by molecular beam epitaxy on (111)*B* CdTe on Si(100).

The narrow band-gap semiconductor mercury cadmium telluride (Hg<sub>1-x</sub>Cd<sub>x</sub>Te) is actively studied by several groups because of its high-technology application in infrared (IR) detection and, possibly, telecommunication. Over the past several years, significant progress has been achieved in the growth of epitaxial layers of this semiconductor. More specifically, molecular beam epitaxy (MBE) has now reached a state where layers with sufficient quality for photovoltaic detectors can be produced.<sup>1-4</sup>

CdTe and CdZnTe are the most widely used substrates for epitaxial growth of Hg<sub>1-x</sub>Cd<sub>x</sub>Te. Unfortunately, it is difficult to produce good single crystals of these materials on a large area, and these substrates are very expensive. Silicon is an attractive candidate as an alternative substrate for Hg<sub>1-x</sub>Cd<sub>x</sub>Te. High quality Si wafers are commercially available in large areas and they are inexpensive compared to CdTe or even GaAs. The main advantage of growing CdTe or Hg<sub>1-x</sub>Cd<sub>x</sub>Te directly on silicon is that it could eventually become possible to fabricate large-area monolithic IR focal plane arrays taking advantage of the well-developed Si integrated circuit technology. However, one severe problem with this heteroepitaxy is the very large (19%) lattice mismatch between CdTe and Si.

So far, only few attempts to grow CdTe directly on silicon have been published.<sup>5-7</sup> Although the orientation of the CdTe is not specified in some cases, it seems that (100)CdTe was obtained by both MBE<sup>5</sup> and low-pressure metalorganic chemical vapor deposition.<sup>6,7</sup> One group reports the growth of (111)*B* CdTe on Si(111) by MBE, but they use a (Ca,Ba)F<sub>2</sub> buffer layer.<sup>8</sup>

In this letter we report our first successful growth of (111)*B* CdTe and (100)CdTe on silicon by MBE. The (111)*B* orientation was obtained by growing CdTe directly on Si(100), whereas an intermediate layer of ZnTe was used to obtain the (100)CdTe orientation. We have also grown Hg<sub>1-x</sub>Cd<sub>x</sub>Te by MBE on (111)*B* CdTe grown on Si(100). The CdTe films were characterized by reflection high-energy electron diffraction (RHEED), scanning electron microscopy (SEM), photoluminescence (PL) spectroscopy, and x-ray diffraction measurements.

Si(100) wafers, both oriented and misoriented by 8° towards (011), were used for this experiment. They were cleaned using a procedure developed by Ishizaka and Shiraki.<sup>9</sup> This method is a wet chemical etching, which leaves the

silicon surface with a thin protective oxide. The sample is then outgassed in vacuum at 500 °C for several hours before the oxide is removed in the growth chamber by heating at 850 °C. On such a surface, no sign of contamination could be detected by x-ray induced photoelectron spectroscopy (XPS) or Auger electron spectroscopy (AES).

Figure 1 shows RHEED patterns obtained during the growth of CdTe directly on Si(100). The CdTe grows in the (111) orientation, and two domains rotated by 90° are observed. For this epitaxial relationship, the  $[\bar{2}11]$  CdTe axis is parallel to either the  $[0\bar{1}1]$  or the  $[011]$  Si axis. In this direction, the lattice mismatch is reduced to only 3.4%. After 1 μm of CdTe, some roughness is still seen in the  $[0\bar{1}1]$  CdTe direction, whereas the streaked pattern corresponding to the

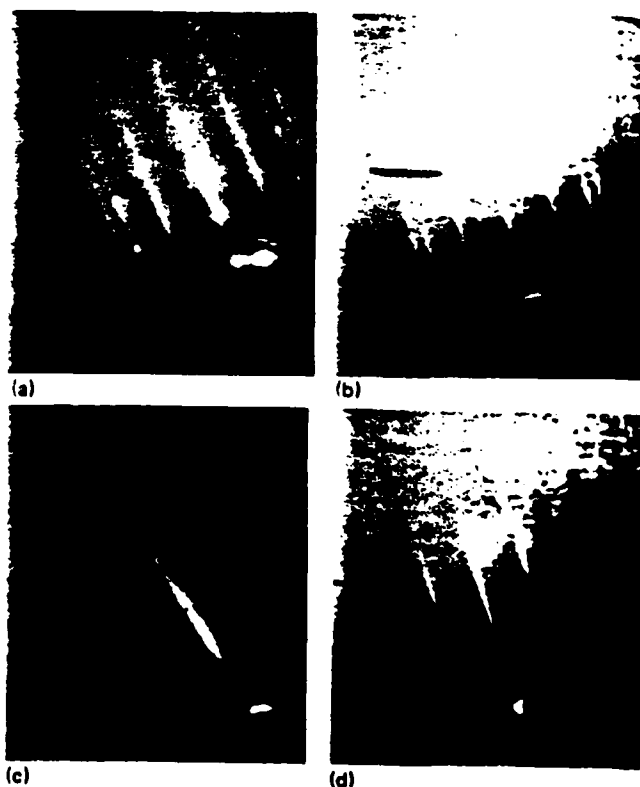


FIG. 1. RHEED patterns obtained during the growth of CdTe on Si(100), e-beam along Si $[011]$ . (a) 1 μm CdTe, (b) 20 μm CdTe, (c) 13 μm CdTe on Si(100) cut 8° off axis and, (d) same as (c) but 4 μm Hg<sub>0.2</sub>Cd<sub>0.8</sub>Te.  $E_e = 40$  keV.

$[211]$  CdTe azimuth shows that the surface of the domains is smooth in this direction. The diffraction patterns eventually become streaked in both directions, and very weak higher order streaks are sometimes observed. Because of the superposition of the two domains and because the higher order streaks are too weak, we could not yet identify the reconstruction. It is clear, however, that the  $(2 \times 2)$  reconstruction which is always observed on a  $(111)A$  CdTe face grown by MBE is not observed here. We conclude that a  $(111)B$  face is obtained on Si(100) in our experiment. This fact will be confirmed later based on the growth of  $Hg_{1-x}Cd_xTe$  on these CdTe layers.

We have grown up to 20- $\mu$ m-thick layers of CdTe on Si(100) at a growth rate of  $2.6 \text{ \AA s}^{-1}$ . These layers are quite smooth, as is seen from the RHEED pattern in Fig. 1(b). Figure 2 shows a SEM image of the surface of a 20- $\mu$ m-thick CdTe layer on Si(100). This surface shows some weak roughness on a micron scale, associated with the growth of hexagonal columns. In the case of GaAs on Si, film cracking during the cooling has sometimes been reported when the layer thickness exceeds several microns.<sup>10</sup> We did not observe such problems for CdTe on Si(100).

Low-temperature (12 K) PL spectra were measured on CdTe epitaxial layers to investigate the quality of these layers. The 514.5 nm line of a 50 mW Ar-ion laser was used here. A PL spectrum measured on an 8- $\mu$ m-thick layer of  $(111)B$  CdTe grown on Si(100) is shown in Fig. 3. The narrower peak at 1.592 eV is attributed to bound exciton (BE) recombinations and perhaps some band-to-band transitions from near-band-edge states. The broader feature (around 1.55 eV) is due to band-to-acceptor radiative transitions.<sup>11</sup> It is generally accepted that this band is related to some kind of defects or impurities in CdTe, but no information on the microscopic origin of these transitions is available. An identification of the nature of the defects or impurities involved is beyond the scope of this letter. Also a detailed study of the influence of the parameters used for the MBE growth still needs to be done.

The photoluminescence full width at half maximum (FWHM) and the intensity of the BE band can be used to judge the quality of the CdTe layers. In the spectrum of Fig. 3, the higher energy BE peak has a FWHM of 7.5 meV, and a shoulder due to a poorly resolved peak is even distinguished at the right-hand side of the band. We have measured



FIG. 2. SEM micrograph of the surface structure near a cleaved edge of CdTe on Si(100).

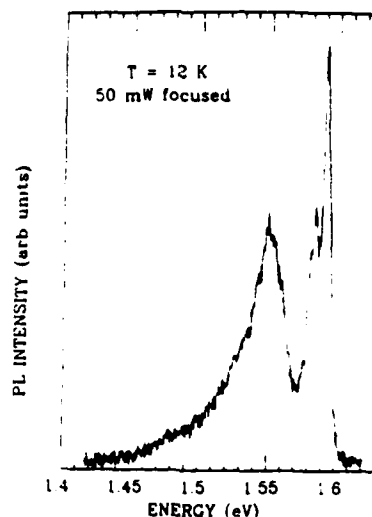


FIG. 3. 12 K photoluminescence spectrum of CdTe on Si(100) excited with a 50 mW Ar-ion laser at 514.5 nm wavelength.

FWHMs as low as 5.6 meV on some samples, which compare very well with the value of 5 meV reported for high quality CdTe grown on GaAs.<sup>11</sup> The intensity ratio  $I_{1.592\text{ eV}}/I_{1.55\text{ eV}}$  is 0.5 for the spectrum shown in Fig. 3. Although it is difficult quantitatively to compare this intensity ratio with other published values because it depends on experimental parameters such as the laser power, these results give direct evidence of the successful growth of the epitaxial layers of CdTe on Si(100) and are very encouraging for future use of these substrates for the growth of CdTe and HgCdTe by MBE. However, the natural FWHM of the CdTe(333) x-ray diffraction line determined from double-crystal rocking curves is still very large (16–20 arcmin), which means that the structural quality of these layers needs to be significantly improved. This should be possible if the substrate cleaning procedure can be optimized. More specifically, the vacuum requirements appear to be much more stringent for silicon than for CdTe, and a different mounting procedure should also be used. These points are now being investigated.

$(111)B$  CdTe can also be grown on Si(100) tilted  $8^\circ$  towards  $(011)$ . The RHEED pattern corresponding to a 23- $\mu$ m-thick layer of CdTe show that these films have a single domain structure (Fig. 1(c)). We suggest that this is due to the reconstruction of the Si surface itself. It has been shown that a double domain  $(2 \times 2)$  reconstruction is obtained on Si(100) whereas a single domain  $(2 \times 2)$  is obtained when the Si(100) is cut off axis by  $4^\circ$ .

Although the  $8^\circ$  tilt changes the double-domain structure into a single-domain one, it does not reduce the FWHM of the x-ray diffraction rocking curves. This could be due to two reasons. First, even though the substrate tilt helps to suppress the double-domain structure, the best value of the tilt angle still needs to be found. Initially, a tilt angle of  $8^\circ$  was chosen because it is expected to produce enough atomic steps to generate dislocations in order to accommodate the 19% lattice mismatch between  $(100)$  CdTe and Si(100). However, since the  $(111)$  orientation is obtained when CdTe is grown directly on Si(100) by MBE, this mismatch is reduced to 3.4% in the  $[211]$  CdTe direction. In

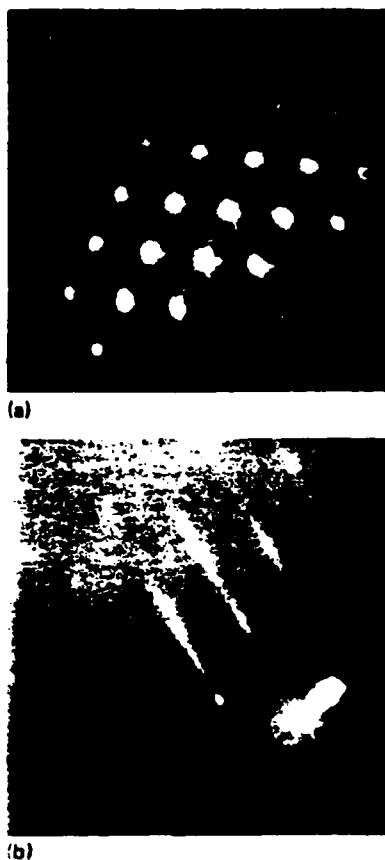


FIG. 4 RHEED patterns obtained during the growth of (100)CdTe on Si(100) with an intermediate layer of ZnTe. (a) 500 Å of ZnTe. (b) Sum of CdTe.  $E_e = 40$  keV,  $\psi$ -beam along Si[011].

this case a smaller tilt angle can probably be used.

Second, the cleaning of these tilted substrates is even more difficult than for regular Si(100), since even very low surface impurity concentrations seem to create faceting in some cases. Since the cleaning of the Si substrate is the most critical step in these experiments, particular care needs to be taken during the preparation of tilted Si(100) substrates prior to the growth of CdTe by MBE.

The growth of (100)CdTe is obtained when a layer of ZnTe is first deposited on Si(100). This is illustrated in Fig. 4, which shows RHEED patterns obtained at two representative stages of the growth. It can be seen that the ZnTe grows via a three-dimensional mechanism and that the films are still rough after 500 Å. When the growth of the CdTe is started, this roughness is reduced and eventually the RHEED pattern of a smooth (100)CdTe surface is obtained. This result is similar to the one reported for the growth of CdTe on GaAs(100) by MBE,<sup>14</sup> where the growth of a Cd<sub>1-x</sub>Zn<sub>x</sub>Te layer at the interface can control whether the CdTe grows in the (100) or the (111)B orientation, depending on the composition of the CdZnTe layer.

Finally, a first attempt has been made to grow Hg<sub>1-x</sub>Cd<sub>x</sub>Te on CdTe grown on Si(100). The CdTe layer

was 20 μm thick and a 7 μm-thick layer of Hg<sub>1-x</sub>Cd<sub>x</sub>Te was grown at 190 °C. Figure 1(d) shows that a smooth surface is obtained and that the two domains in the CdTe layer are present throughout the HgCdTe layer. The composition  $x$  and the thickness were measured by Fourier transform infrared transmission spectroscopy. The values obtained are  $x = 0.22$  and  $d = 4$  μm. The same thickness is also deduced from a SEM observation of a cleaved edge of the sample. The Hg flux used for this growth was the same as what is usually needed for the growth of Hg<sub>1-x</sub>Cd<sub>x</sub>Te on (111)B CdTe at 190 °C. Since the Hg flux for the growth on (111)A CdTe would be about ten times higher,<sup>14</sup> this confirms that the (111)B orientation is obtained on Si(100).

In summary, we have grown (111)B CdTe and (100)CdTe on Si(100) by MBE despite the lattice mismatch of 19%. The (111)B orientation is obtained directly on Si(100), whereas a layer of ZnTe is grown at the interface in order to obtain the (100) orientation. HgCdTe has also been grown by MBE on top of the (111)B CdTe layers on Si(100). Tilting the Si(100) surface helps to suppress a double-domain structure in the (111) layers, but the best tilt angle still needs to be found. Photoluminescence data obtained on these layers are encouraging for the future use of Si as alternative substrates for the growth of CdTe and HgCdTe.

We would like to thank Z. Ali and S. Farook for their help and J. Kubby (Xerox) and J. Griffith (AT&T Bell Laboratories) for providing some of the Si substrates. This work is supported by Defense Advanced Research Projects Agency and monitored by Air Force Scientific Office for Research under contract No. F48620-87-C-0021. One of us (R.S.) is grateful to the Belgian National Foundation for Scientific Research (Fonds National de la Recherche Scientifique (FNRS)) for financial support.

1. P. Faurie, A. Million, R. Boich, and J. L. Tissot, *J. Vac. Sci. Technol.* **A** *1*, 1593 (1983).
2. P. Faurie, S. Sivananthan, M. Lange, R. E. Dewames, A. M. G. Vandewyck, G. M. Williams, D. Yamani, and E. Tao, *Appl. Phys. Lett.* **52**, 2151 (1988).
3. S. Yoo, M. Boukerche, M. DeSouza, and J. P. Faurie, *SPIE Proc.* **100**, 15 (1989).
4. J. M. Anas, S. H. Shin, J. G. Pasko, R. E. Dewames, and E. R. Gertner, *J. Appl. Phys.* **65**, 1747 (1989).
5. Y. Lu, R. N. Bicknell, T. H. Myers, J. F. Schetzina, and H. H. Stadelmeier, *J. Appl. Phys.* **54**, 4228 (1983).
6. R. L. Chou, M. S. Lin, and K. S. Chou, *Appl. Phys. Lett.* **48**, 1211 (1986).
7. M. S. Lin, R. L. Chou, and K. S. Chou, *J. Cryst. Growth* **77**, 125 (1986).
8. H. Zogg and S. Blumier, *Appl. Phys. Lett.* **49**, 1531 (1986).
9. A. Ishizuka and Y. Shiraki, *J. Electrochem. Soc.* **133**, 666 (1986).
10. R. M. Lum, J. K. Klingert, R. B. Bylma, A. M. Glass, A. T. Macrander, T. D. Harris, and M. G. Lamont, *J. Appl. Phys.* **64**, 6727 (1988).
11. D. J. Olego, J. P. Faurie, S. Sivananthan, and P. M. Raccan, *Appl. Phys. Lett.* **47**, 1172 (1985).
12. G. V. Hansson and R. I. G. Uhrberg, *Surf. Sci. Rep.* **9**, 225 (1988).
13. J. P. Faurie, C. Hsu, S. Sivananthan, and X. Chu, *Surf. Sci.* **168**, 471 (1986).
14. S. Sivananthan, X. Chu, J. Reno, and J. P. Faurie, *J. Appl. Phys.* **60**, 150 (1986).

$T_{SS}$  is kept constant at 190°C, by using a front thermocouple, at the initiation of HgCdTe growth a jump of approximately 25°C (in our MBE configuration) occurs in the pyrometer reading  $T_p$  due to scattered IR radiation primarily from the hot CdTe cell as illustrated in Fig. 1. Immediately  $T_p$  falls steeply due to both the rapid decrease in reflectance of the block and the fall toward the first minimum in the interference pattern related to the presence of a thin HgCdTe layer. Once the first minimum is reached  $T_p$  rises toward the next maximum. Several more oscillations of decreasing amplitude follow. After about 1.5 $\mu$ m of growth, the oscillations are almost completely gone. At this point  $T_p$  is approximately 15°C higher than the reading before growth. This increase is primarily due to emitted radiation since emittance increases as cadmium composition decreases.

During this time the back thermocouple  $T_B$  reading has increased by 15–20°C. In other words if  $T_B$  is kept constant,  $T_{SS}$  will decrease. Then the Hg flux kept constant will become too high since the Hg sticking coefficient changes drastically with temperature and reflection twin visible on the RHEED pattern will be formed. From these experiments it appears that the control of the surface substrate temperature  $T_{SS}$  which is a key parameter and should be kept constant within 1°C is an extremely difficult task. The Microphysics Laboratory has devoted a lot of time in order to achieve the best control of  $T_{SS}$ .

Since a front thermocouple cannot be left during conventional growth using rotation, a double control involving a back thermocouple and an IR pyrometer along with the knowledge based on tedious experiments identical to the one describe before, is currently utilized in the Microphysics Laboratory. It is very important to point out that if these observations are certainly valid for MBE growth of HgCdTe carried out in any MBE machine and using a substrate stuck with Gallium on a Molybdenum block, the magnitude of relative changes between  $T_B$ ,  $T_p$  and  $T_{SS}$  will depend strongly on the substrate heater technology and effusion cell geometry. These investigations have resulted in a better control of the surface preparation, the stability, and reproducibility of all the fluxes and the surface substrate temperature. This improvement has been confirmed by the growth of twin-free HgCdTe(111)B illustrated in the ECP of Fig. 2 and excellent results for epilayers grown in (211)B orientation presented in part II-3-3

#### FIGURE CAPTIONS:

Fig. 1 Plot of the temperature pyrometer reading  $T_p$  vs  $t$  for  $Hg_{1-x}Cd_xTe$

( $x = 0.26$ ) grown on CdTe(111)B. During the experiment the surface temperature of the substrate  $T_{ss}$  is kept constant at 190°C.

Fig. 2 Electron channeling pattern along the (111) axis of a twin free HgCdTe (111)B layer grown on CdZnTe(111)B substrate.

Fig. 1

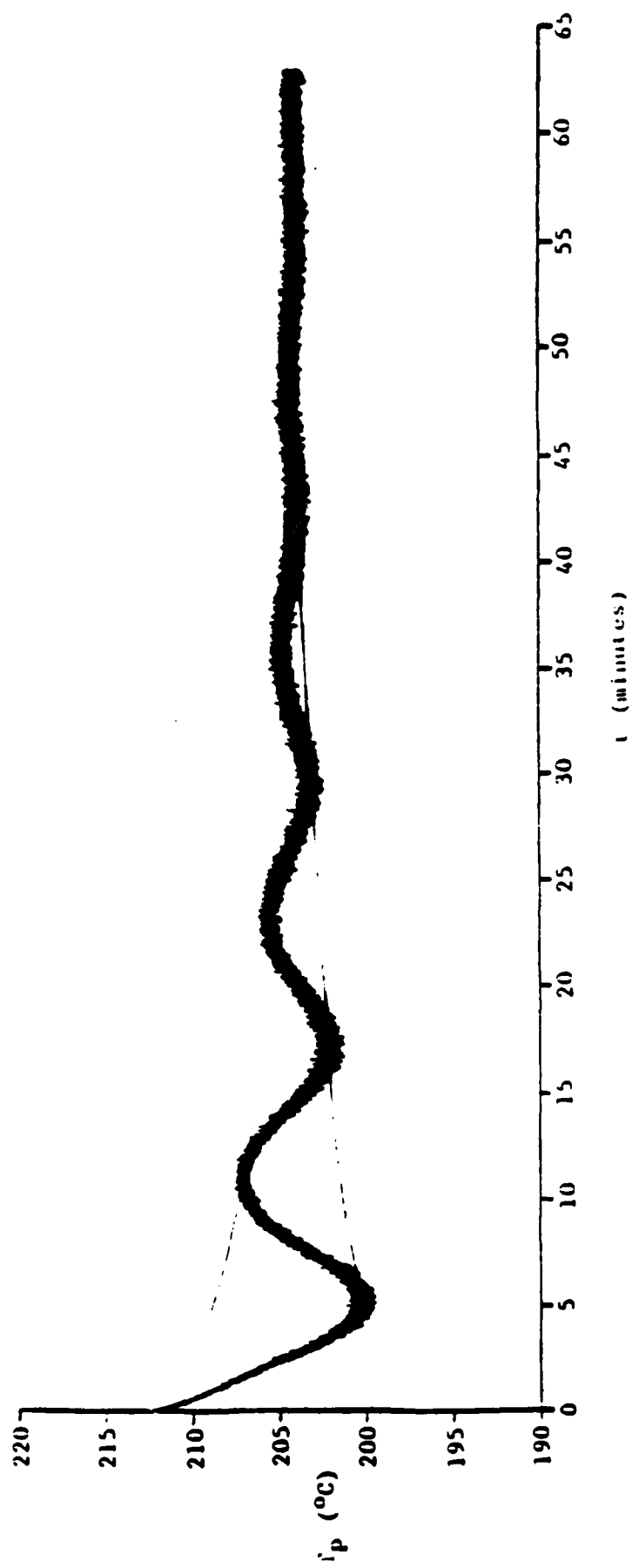
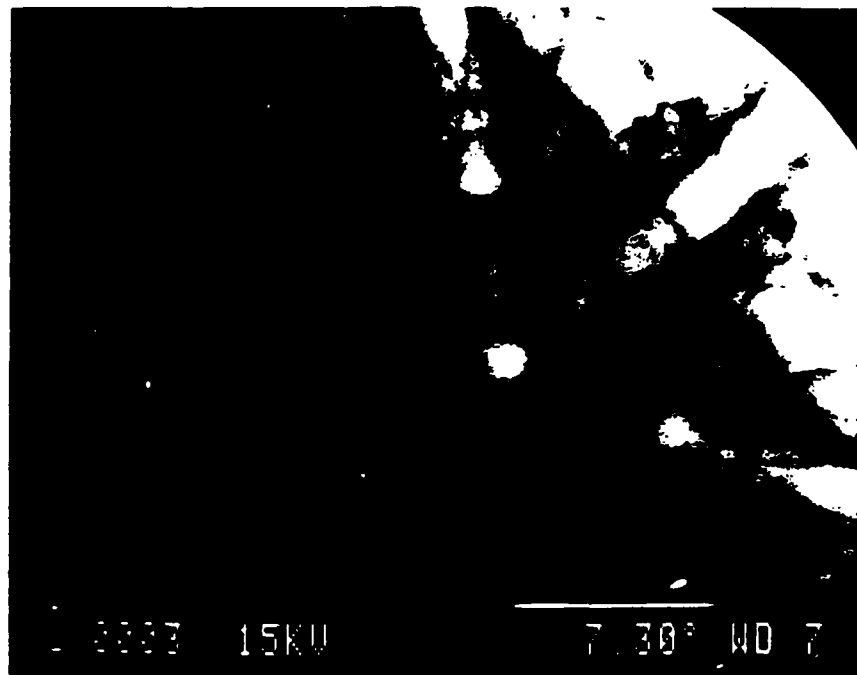


Fig. 2



### II-3-2 HgCdTe (111)B-COMPARISON BETWEEN TWINNED AND TWIN-FREE LAYERS

Hg<sub>1-x</sub>Cd<sub>x</sub>Te twinned layers grown by the Microphysics Laboratory in the (111)B orientation usually exhibit a p-type character with hole mobility approaching or even exceeding  $10^3 \text{cm}^2 \text{v}^{-1} \text{s}^{-1}$ <sup>(1)</sup> and excess carrier lifetime in the  $20\text{--}100 \times 10^{-9} \text{s}$ .<sup>(2)</sup> An excellent electrical mobility is often considered to be associated with an excellent crystal quality. It turns out that it is not precisely the case here.

All the layers exhibiting  $10^3 \text{cm}^2 \text{v}^{-1} \text{s}^{-1}$  have been investigated using x-ray diffraction. X-ray rocking curve recorded for the (422) reflection have shown for all of them 6 peaks while rotating the sample about the  $\langle 111 \rangle$  axis while only three peaks should be observed in a twin-free epilayer. These findings were confirmed by ECP experiments. The first thought was that the presence of twins does not degrade the hole mobility. In order to confirm this, two HgCdTe epilayers ( $x = 0.25$ ) have been grown under the same growth condition except that the Hg flux was increased several times for several minutes during the growth of layer A whereas for layer B the twin-free growth conditions have been applied. X-ray diffraction confirmed that layer B is twin-free and layer A is twinned. Both layers have a p-type character, however, whereas layer A exhibits a hole mobility of  $900 \text{cm}^2 \text{v}^{-1} \text{s}^{-1}$  layer B has only a hole mobility of  $300 \text{cm}^2 \text{v}^{-1} \text{s}^{-1}$  at 23K. All the twin-free p-type layers grown so far have a hole mobility not exceeding  $500 \text{cm}^2 \text{v}^{-1} \text{s}^{-1}$ .

In addition the carrier concentration  $N_A - N_D$  for p-type twinned layers has been consistently found to be in the  $1\text{--}5 \times 10^{16} \text{cm}^{-3}$  and from the Hall data curve fitting  $N_A$  has been calculated to be in the  $5\text{--}8 \times 10^{16} \text{cm}^{-3}$  range as reported before.<sup>(3)</sup> P-type twin-free layer displays a much lower carrier concentration:  $N_A - N_D$  is in the low  $10^{15} \text{cm}^{-3}$  range. The decrease in  $N_A - N_D$  is so drastic in twin-free layers that many of them turned to be n-type. Anyway the lower hole mobility in twin-free layers cannot be explained by an increase in scattering due to a larger acceptor concentration since it is the opposite. Therefore it is concluded that:

- 1) electrically active acceptors are associated with the presence of twins in HgCdTe
- 2) a relationship exists between the high hole mobility and the presence of twins in HgCdTe.

Hg<sub>1-x</sub>Cd<sub>x</sub>Te grown at 200°C under Te-rich conditions, such as MBE but under

thermal equilibrium conditions, unlike MBE, should produce an intrinsic hole concentration due to Hg vacancy close to  $1 \times 10^{16} \text{cm}^{-3}$ .<sup>(4,5)</sup> Hence it appears that in the (111)B orientation twinned layers have a p-type doping level exceeding the one expected from growth under thermodynamical equilibrium at the same temperature. In addition the fact that fast low temperature isothermal (mercury-rich) anneals make the (111)B materials even more p-type leads us to believe that extended defects are mostly responsible for the electronic activity in the as-grown material. The increase in the acceptor level could be explained by the presence of numerous (111)A planes in the twin boundaries and antiphase boundaries. As reported before<sup>(6)</sup> a (111)A plane which is Hg terminated is very unstable and thus should have a Hg-vacancy density higher than the one thermodynamically calculated for a bulk crystal.

Concerning the high hole mobility no clear explanation has yet been found. However it is possible that with the excess of mercury, which triggers the formation of Hg-rich antiphase boundaries, Hg-rich alloy zones are formed in the crystal. Therefore numerous Type III (semimetal-semiconductor) interfaces exist within the crystal. It has been discovered and explained<sup>(7,8)</sup> that a high hole mobility due to light-heavy hole effective mass is associated with Type III interface. Hence the measured Hall mobility in these non-homogenous crystals would average the high hole mobility associated with the Type III interface holes and the low hole mobility of the bulk.

Indium diffusion experiments which have been carried out in doped Quantum well (111)B structures<sup>(9)</sup> have shown that several In diffusion coefficients are required to explain the observed secondary ion mass spectrometry data. A fraction of the indium has been found to be fast diffusing through a defect related matrix.

Another important difference related to etch-pit density (EPD) and reported in Table I has been found between twinned and twin-free layers in good agreement with ref. 10. EPD count which is related to dislocation density, is determined using defect chemical etching solution suitable for the investigated crystallographic orientation. The percentage of twin has been qualitatively determined from x-ray diffraction by comparing the intensities of twin-related peaks with crystal lattice peaks.

TABLE I

Hg <sub>1-x</sub> Cd <sub>x</sub> Te Samples	x	Twin	EPD(cm <sup>-2</sup> )
935	0.24	50%	8x10 <sup>6</sup>
933	0.33	10%	5x10 <sup>5</sup>
932	0.21	0	8x10 <sup>4</sup>

One can see that by eliminating twins EPD can drop tremendously indicating a drastic improvement in the crystal quality unexpectedly associated with a decrease in the hole mobility measured by Hall in p-type layers.

Very long isothermal annealings have been performed on twinned and twin-free (111)B HgCdTe layers and very similar residual doping level have been found. The material is n-type with a background level in the  $5 \times 10^{15} - 2 \times 10^{16} \text{cm}^{-3}$  range. This background does not seem to be controlled by residual impurities. SIMS analysis indicates that MBE layers are very clean. Although all the complex relationships between growth parameters and intrinsic doping are not fully understood it is currently postulated that the residual donor doping level in MBE grown HgCdTe layers is due to tellurium atoms in antisite position i.e. replacing Hg atoms.<sup>(11)</sup>

We have also found evidence from dopant diffusion such as indium and junction formation experiment using our low ion energy sputtering technique that one diffusion component is very fast. We believe that this fast component is related to the twin boundaries. We have not yet been able to establish a formal proof of it.

Table II provides a brief summary of the main differences between (111)B twinned and twin-free layers grown by MBE.

TABLE II

	Twinned Layer	Twin-Free Layer
Conduction Type	p-type	p-type - n-type
p-type layers		
$N_A - N_D$	$2-5 \times 10^{16} \text{cm}^{-3}$	$1-2 \times 10^{15} \text{cm}^{-3}$
Hole mobility	$800-1600 \text{cm}^2/\text{vsec}$	$300-500 \text{cm}^2/\text{vsec}$
EPD	$10^6-10^7 \text{cm}^{-2}$	$10^4-10^5 \text{cm}^{-2}$
Residual doping level after isothermal annealing	$5 \times 10^{15}-2 \times 10^{16} \text{cm}^{-3}$	

## REFERENCES:

1. S. Sivananthan, M.D. Lange, G. Monfroy and J.P. Faurie, J. VAc. Sci. Technol. B6, 788 (1988)
2. M.E. de Souza, M. Boukerche and J.P. Faurie, J. Appl. Phys. (Nov. 15, 1990)
3. M. Boukerche, S. Sivananthan, P.S. Wijewarnasuriya, I.K. Sou and J.P. Faurie, J. Vac. Sci. Technol. A7, 311 (1989)
4. G.L. Destefanis, J. Cryst. Growth, 86, 700 (1988)
5. H.R. Vydyanath and C.H. Hiner, J. Appl. Phys. 65, 3080 (1989)
6. S. Sivananthan, X. Chu, J. Reno and J.P. Faurie, J. Appl. Phys. 60, 1359 (1986)
7. J.P. Faurie, M. Boukerche, S. Sivanthan, J. Reno, and C. Hsu, Superlattices and Microstructures, 1, 237 (1985)
8. J.R. Meyer, C.A. Hoffman, F.J. Bartoli, J.W. Han, J.W. Cook, Jr., J.F. Schetzina, X. Chu, J.P. Faurie, J.N. Schulman, Phys. Rev. B 38, 2204 (1988)
9. I.K. Sou and J.P. Faurie (unpublished)
10. K.A. Harris, T.H. Meyers, R.W. Yanka, L.M. Mohnkern, R.W. Green and N. Otsuka, 1989 MCT Workshop
11. J.P. Faurie, HgCdTe MBE Workshop DARPA-CNVEO, Washington 1987 (unpublished results)

### II-3-3 GROWTH IN (211)B ORIENTATION

The progress accomplished in the growth in the (111)B orientation has been used to control in a better way the growth in different orientations. We have devoted our recent efforts in the growth along the  $\langle 211 \rangle$  azimuth where the twinning problem does not appear as severe as in the (111)B. The layers grown in the (211)B orientation under the stringent growth control previously discussed exhibit excellent properties. As an example the layer #1008 has the following characteristics:

x	=	0.18
thickness:		16.2 $\mu$ m
$N_d - N_a$ :		$1.9 \times 10^{14} \text{cm}^{-3}$ at 15K
electron mobility:		$1.1 \times 10^6 \text{cm}^2 \text{v}^{-1} \text{s}^{-1}$ at 15K
lifetime:		$9 \times 10^{-6} \text{sec}$ at 250K
		$2.2 \times 10^{-6} \text{sec}$ at 77K

This result reflects the state-of-the-art of the growth of HgCdTe alloys in the Microphysics Laboratory. These results are at least as good as the best results ever reported for HgCdTe grown by any technique for this composition. Diodes fabricated on twin-free (211)B layers showed improved operational yields.<sup>(1)</sup>

#### REFERENCES:

1. S.S. Yoo, M. Boukerche and J.P. Faurie (unpublished results)

II-4 MBE GROWTH AND CHARACTERIZATION OF TWO-INCH DIAMETER P- AND N-TYPE  $\text{Hg}_{1-x}\text{Cd}_x\text{Te}$  FILMS ON GaAs(100) SUBSTRATE

The growth of p-type and n-type layers have been successfully achieved on two-inch GaAs(100) substrates. Their surfaces were shiny and mirror-like from center to edge. Their thicknesses were uniform within 0.6%. Their Cd concentrations (x) were very uniform, exhibiting standard deviations  $\Delta x/x$  as low as 0.7%. These films were completely uniform in their conduction types, that is, the n-type films were entirely n-type, and likewise for the p-type films. The Hall mobilities of these films show them to be of high quality, with values as high as  $6.7 \times 10^2 \text{ cm}^2 \text{ s}^{-1}$  for p-type ( $x=0.22$ ), and  $1.8 \times 10^5 \text{ cm}^2 \text{ V}^{-1} \text{ s}^{-1}$  for the n-type films ( $x=0.21$ ). These results represent an important achievement towards the future of infrared detector technology. For more details see the attached paper. In summary composition uniformity on a 2-inch wafer matches the requirements in terms of wavelength cutoff dispersion for an IR detector.

ATTACHED PAPER:

1. "Molecular beam epitaxial growth and characterization of two-inch diameter  $\text{Hg}_{1-x}\text{Cd}_x\text{Te}$  films on GaAs(100) substrates."

# Molecular beam epitaxial growth and characterization of 2-in.-diam $\text{Hg}_{1-x}\text{Cd}_x\text{Te}$ films on GaAs (100) substrates

M. D. Lange, S. Sivananthan, X. Chu, and J. P. Faurie

University of Illinois at Chicago, Department of Physics, P. O. Box 4348, Chicago, Illinois 60680

(Received 21 October 1987; accepted for publication 25 January 1988)

$\text{Hg}_{1-x}\text{Cd}_x\text{Te}$  films with 2 in. diameters have been grown by molecular beam epitaxy on GaAs (100) substrates. These films were grown in both the (100) and  $(\bar{1}\bar{1}\bar{1})B$  crystallographic orientations and in both conduction types. They were characterized by *in situ* electron diffraction, infrared absorption, and van der Pauw dc Hall measurements. Their surfaces were shiny and mirrorlike from center to edge. The Cd concentrations ( $x$ ) of these films were very uniform, exhibiting standard deviations ( $\Delta x$ ) as low as 0.7% of the mean ( $\bar{x}$ ). Their thicknesses also were uniform within 0.6%. These films were completely uniform in their conduction types; that is, the  $n$ -type films were entirely  $n$  type, and likewise for the  $p$ -type films. The Hall mobilities of these films show them to be of high quality, with values as high as  $6.7 \times 10^2 \text{ cm}^2 \text{ V}^{-1} \text{ s}^{-1}$  for the  $p$ -type ( $x = 0.22$ ) and  $1.8 \times 10^5 \text{ cm}^2 \text{ V}^{-1} \text{ s}^{-1}$  for the  $n$ -type films ( $x = 0.21$ ). These results represent an important achievement toward the future of infrared detector technology.

$\text{Hg}_{1-x}\text{Cd}_x\text{Te}$  is the most important material for infrared detectors and imaging arrays, and has promise for applications in fiber-optic telecommunication systems. This is primarily due to the fact that the band gap for  $\text{Hg}_{1-x}\text{Cd}_x\text{Te}$  is a function of the Cd concentration ( $x$ ) as well as the ambient temperature ( $T$ ). There are two main windows in the atmosphere of the earth with wavelengths in the 3–5  $\mu\text{m}$  and 8–14  $\mu\text{m}$  regions, while fiber-optic telecommunication systems currently operate in the 1.3–1.6  $\mu\text{m}$  range. Control of the  $x$  value during growth of  $\text{Hg}_{1-x}\text{Cd}_x\text{Te}$  tailors the band gap to fall into the energy ranges for all these wavelength regions.

As the molecular beam epitaxial (MBE) growth technique has continued to improve for  $\text{Hg}_{1-x}\text{Cd}_x\text{Te}$  epilayers, the prospects for films of larger area have begun to be explored. These larger area films are important for imaging arrays and will be especially vital in the future for the efficient production of  $\text{Hg}_{1-x}\text{Cd}_x\text{Te}$  material. The growth by MBE of a uniform  $\text{Hg}_{1-x}\text{Cd}_x\text{Te}$  film on a large substrate is very difficult to achieve because of the nonuniform distribution of the fluxes and nonuniform temperature of the substrate. The cosine distribution of the fluxes is usually encountered in the MBE growth of III-V compounds, and its consequences are (1) thickness variation over the wafer, (2) change in composition for an alloy with more than two elements, and (3) change in the doping level when an electrically active impurity is evaporated at the same time (the doping in III-V compounds is not controlled by stoichiometry deviation). In the case of  $\text{Hg}_{1-x}\text{Cd}_x\text{Te}$  a simple cosine distribution is expected for the Cd and Te fluxes, but due to the high effusion rate required for Hg the expected Hg flux distribution has the behavior of  $\cos^{3/2} \theta$ , where  $\theta$  is measured from the axis of the Hg effusion cell<sup>1</sup>. Therefore, with this more forward directional Hg flux the nonuniformity in thickness and composition currently observed in the growth by MBE of semiconducting alloys should be worse in the case of  $\text{Hg}_{1-x}\text{Cd}_x\text{Te}$ . In addition to that, since the conduction type and the carrier concentration can be controlled by stoichiometry deviation during the growth of  $\text{Hg}_{1-x}\text{Cd}_x\text{Te}$  by

MBE, these spatial flux variations will also have an effect on the electrical properties of the layers.

Above all however, there is the problem due to the exponential change of the Hg condensation coefficient with temperature. We have shown that for a given Hg flux, a high-quality monocrystalline  $\text{Hg}_{1-x}\text{Cd}_x\text{Te}$  film can be grown in the  $(\bar{1}\bar{1}\bar{1})B$  orientation within a narrow substrate temperature range ( $T_{\text{max}} - T_{\text{min}}$ ) of about 10–15 °C when the substrate temperature ( $T_s$ ) is in the 180–190 °C temperature range.<sup>2</sup> When  $T_s$  is below  $T_{\text{min}}$  the excess Hg desorbs, but twins, which are detrimental for electrical performance, are observed. When  $T_s$  is above  $T_{\text{max}}$  two possibilities exist. (1) If  $T_s$  is below 190 °C the excess Te leads to a polycrystalline material. (2) If  $T_s$  is above 195 °C the excess Te is reevaporated and the film still grows monocrystalline, but an increase in the  $x$  value of 1.5–2% for each 1 °C increase in the substrate temperature is observed, along with a large change in the growth rate.<sup>3</sup>

It is important to recall that a change in  $x$  of only  $\Delta x = \pm 0.001$  is the goal to reach for infrared detection devices operating at a cutoff wavelength of 10  $\mu\text{m}$  at 77 K. It is obvious that such a requirement cannot be achieved if part of the substrate temperature is above  $T_{\text{max}}$ . Now if the substrate temperature is between  $T_{\text{max}}$  and  $T_{\text{min}}$  (incidentally the  $T_{\text{max}}$  and  $T_{\text{min}}$  values are changing over the substrate since the Hg flux distribution is not constant) the epilayers will still experience a change in the doping level and even in the conduction type.

To minimize these temperature variations the substrate must be rotated during the growth, but this also hinders the precise temperature measurement of the substrate by a thermocouple. In order to have adequate control of the temperature during the growth, the use of an infrared pyrometer, which can give reproducible results, has been employed.

The combination of flux distribution and substrate temperature variation makes the growth by MBE of large high-quality uniform  $\text{Hg}_{1-x}\text{Cd}_x\text{Te}$  films a real challenge.<sup>4</sup> For the first time we report here 2-in.-diam  $\text{Hg}_{1-x}\text{Cd}_x\text{Te}$  films, both  $p$ -type and  $n$ -type, grown by MBE, which exhibit uni-

The 2-in.-diam  $\text{Hg}_{1-x}\text{Cd}_x\text{Te}$  films were grown in the ultrahigh vacuum of a Riber 2300 MBE machine modified to handle Hg. In this machine the substrate is situated to face an array of effusion cells containing CdTe, Te, and Hg. The temperatures of these cells and the substrate are precisely controlled to achieve proper growth conditions. The sample manipulator is designed to allow for rotation of the sample in the plane of its surface. This feature was exploited for the growth of the 2-in.-diam  $\text{Hg}_{1-x}\text{Cd}_x\text{Te}$  films to achieve higher uniformity.

Several 2-in.-diam  $\text{Hg}_{1-x}\text{Cd}_x\text{Te}$  films of each conduction type were grown in both the (100) and the  $(\bar{1}\bar{1}\bar{1})B$  orientations. In an earlier article<sup>7</sup> it was shown that the minimum Hg flux required for successful growth differs for these two orientations. Growth in the (100) orientation requires a higher flux than that in the  $(\bar{1}\bar{1}\bar{1})B$  orientation. The Hg flux in combination with the substrate temperature used for the growth of  $\text{Hg}_{1-x}\text{Cd}_x\text{Te}$  determines the crystal stoichiometry deviation, and thus the conduction type. The substrate temperatures chosen for the growth of the films reported here were 190°C for the *p*-type and 185°C for the *n*-type film, and the Hg flux used for the *n*-type film was higher than that used for the *p*-type film. We report here the data from one representative film of each conduction type.

The *p*-type film reported here was grown in the (111)*B* orientation, while the orientation for the reported *n*-type film was (100). The films exhibited uniform mirrorlike surfaces, as illustrated by the photograph in Fig. 1. In order to ascertain the uniformity of each  $\text{Hg}_{1-x}\text{Cd}_x\text{Te}$  film over its 2-in.-diam surface area, infrared transmission and van der

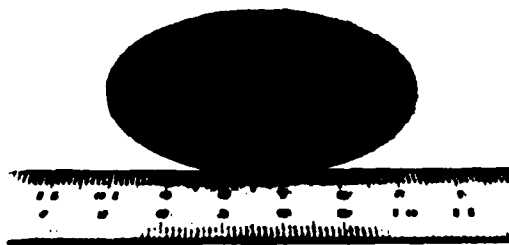
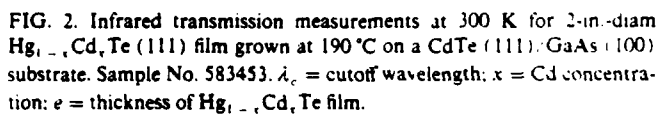


**FIG. 1. Two-in. Hg<sub>1-x</sub>Cd<sub>x</sub>Te film, grown by MBE on a CdTe/GaAs substrate.**



For the *p*-type film reported here the uniformity of the *x* value proved to be excellent, as illustrated in Fig. 2. The average value of *x* (denoted by  $\bar{x}$ ) was 0.22, while the standard deviation  $\{\Delta x = [\Sigma(x - \bar{x})^2/n - 1]^{1/2}\}$  was 0.0015, giving as a measure of the composition uniformity  $\Delta x/\bar{x} = 0.7\%$ . This is an excellent result since the goal required for infrared detectors in terms of composition uniformity is

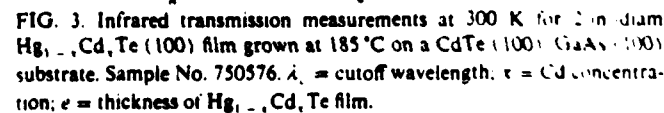


TABLE I. Hall measurements at  $B = 0.2$  T for 2-in.-diam  $\text{Hg}_{1-x}\text{Cd}_x\text{Te}$  (111) film grown at 190 °C on  $\text{CdTe}$  (111)/GaAs (100) substrate. Sample No. 583453.  $x = 0$ ,  $y = 0$  is at the center of the sample.

$x$ (mm)	$y$ (mm)	Cond. type	300 K $N_d - N_a$ ( $\text{cm}^{-3}$ )	$\mu_H$ ( $\text{cm}^2 \text{V}^{-1} \text{s}^{-1}$ )	$T$ (K) when $R_H = 0$	Cond. type	40 K $N_d - N_a$ ( $\text{cm}^{-3}$ )	$\mu_H$ ( $\text{cm}^2 \text{V}^{-1} \text{s}^{-1}$ )
0	0	$n$	$2.1 \times 10^{16}$	$6.4 \times 10^3$	90	$p$	$3.6 \times 10^{15}$	$5.7 \times 10^2$
4	0	$n$	$2.0 \times 10^{16}$	$5.0 \times 10^3$	90	$p$	$3.0 \times 10^{15}$	$5.2 \times 10^2$
7	0	$n$	$2.1 \times 10^{16}$	$6.3 \times 10^3$	90	$p$	$4.7 \times 10^{15}$	$5.5 \times 10^2$
11	0	$n$	$1.9 \times 10^{16}$	$6.2 \times 10^3$	90	$p$	$5.1 \times 10^{15}$	$5.7 \times 10^2$
15	0	$n$	$1.9 \times 10^{16}$	$6.8 \times 10^3$	90	$p$	$5.6 \times 10^{15}$	$6.5 \times 10^2$
18	0	$n$	$1.8 \times 10^{16}$	$6.8 \times 10^3$	90	$p$	$7.2 \times 10^{15}$	$6.2 \times 10^2$
0	7	$n$	$1.9 \times 10^{16}$	$6.6 \times 10^3$	90	$p$	$4.9 \times 10^{15}$	$6.0 \times 10^2$
0	15	$n$	$1.8 \times 10^{16}$	$6.8 \times 10^3$	90	$p$	$6.1 \times 10^{15}$	$6.7 \times 10^2$

TABLE II. Hall measurements at  $B = 0.2$  T for 2-in.-diam  $\text{Hg}_{1-x}\text{Cd}_x\text{Te}$  (100) film grown at 185 °C on  $\text{CdTe}$  (100)/GaAs (100) substrate. Sample No. 750576.  $x = 0$ ,  $y = 0$  is at the center of the sample.

$x$ (mm)	$y$ (mm)	Cond. type	300 K $N_d - N_a$ ( $\text{cm}^{-3}$ )	$\mu_H$ ( $\text{cm}^2 \text{V}^{-1} \text{s}^{-1}$ )	Cond. type	23 K $N_d - N_a$ ( $\text{cm}^{-3}$ )	$\mu_H$ ( $\text{cm}^2 \text{V}^{-1} \text{s}^{-1}$ )
0	0	$n$	$3.6 \times 10^{16}$	$1.2 \times 10^4$	$n$	$4.2 \times 10^{15}$	$1.3 \times 10^5$
11	0	$n$	$4.0 \times 10^{16}$	$1.0 \times 10^4$	$n$	$4.0 \times 10^{15}$	$1.3 \times 10^5$
11	3	$n$	$4.5 \times 10^{16}$	$1.1 \times 10^4$	$n$	$4.2 \times 10^{15}$	$1.5 \times 10^5$
0	6	$n$	$3.9 \times 10^{16}$	$1.1 \times 10^4$	$n$	$4.2 \times 10^{15}$	$1.4 \times 10^5$
0	9	$n$	$4.0 \times 10^{16}$	$9.8 \times 10^3$	$n$	$4.2 \times 10^{15}$	$1.3 \times 10^5$
0	13	$n$	$6.2 \times 10^{16}$	$9.2 \times 10^3$	$n$	$4.4 \times 10^{15}$	$1.3 \times 10^5$
0	20	$n$	$6.3 \times 10^{16}$	$1.1 \times 10^4$	$n$	$4.3 \times 10^{15}$	$1.8 \times 10^5$

almost achieved on 2-in.-diam  $\text{Hg}_{1-x}\text{Cd}_x\text{Te}$  films. For the reported  $n$ -type film the uniformity of  $x$  was almost as good with  $\Delta x/\bar{x} = 1.4\%$ , as shown in Fig. 3. For this  $n$ -type film the thickness ( $e$ ) was very uniform with  $\Delta e/\bar{e} = 0.6\%$ .

Each 2-in.-diam  $\text{Hg}_{1-x}\text{Cd}_x\text{Te}$  film also showed complete uniformity over its surface in the conduction type exhibited. That is,  $p$ -type films were entirely  $p$  type, and  $n$ -type films were entirely  $n$  type. The carrier concentrations ( $N_d - N_a$  or  $N_a - N_d$ ) and the Hall mobilities ( $\mu_H$ ), however, showed some variation as may be seen in Tables I and II. It should be pointed out that both the electron and the hole mobilities are high for this cadmium concentration and attest to the high quality of the material grown here. The carrier concentrations are also in a range suitable for photo-voltaic devices.

For both the  $p$ -type and  $n$ -type films reported here, non-uniformities in the carrier concentrations or the  $x$  values indicate variations in the sample temperature and Hg flux over the surface of the samples. Other hypotheses which have not been considered here, such as the role of the crystallographic orientation, could also contribute to the structural and electrical parameters observed. In order to grow  $\text{Hg}_{1-x}\text{Cd}_x\text{Te}$  epilayers on even larger substrates, more uniform sample temperatures (which ideally must be constant within 1 °C) and a more uniform Hg flux are required.

In summary, it has been demonstrated here that high-quality  $\text{Hg}_{1-x}\text{Cd}_x\text{Te}$  films of 2-in. diameter can be grown by MBE. High Hall mobilities, low carrier concentrations, uniform thicknesses, and very uniform Cd concentrations have been achieved already in these films which make them suitable for infrared device applications. These uniformities are much better than those currently achieved using the organometallic vapor phase epitaxy (OMVPE) growth method ( $\Delta x = \pm 0.004$  for a 1-in. square CdTe substrate<sup>9</sup> and

$\Delta x = \pm 0.005$  for a  $1 \times 2 \text{ cm}^2$  CdTeSe substrate<sup>10</sup>). This achievement represents a major step toward the future of infrared detector technology which demands ever greater uniformity over ever larger surface areas. We have demonstrated here that MBE is a prominent growth technique which can fulfill this requirement. Further improvements in the temperature uniformity of the sample, along with increased uniformity of the Hg flux on the sample, are expected to produce  $\text{Hg}_{1-x}\text{Cd}_x\text{Te}$  films of even better uniformity on larger surface areas.

The authors would like to thank P. S. Wijewarnasuriya for performing the Hall measurements and the Defense Advanced Research Projects Agency for its financial support under contract F49620-87-C-0021, monitored by the Air Force Office for Scientific Research.

- <sup>1</sup>S. C. Jackson, B. N. Baron, R. E. Rocheleau, and T. W. F. Russell, *J. Vac. Sci. Technol. A* **3**, 1916 (1985).
- <sup>2</sup>J. P. Faurie, J. Reno, S. Sivananthan, I. K. Sou, X. Chu, M. Brucher, and P. S. Wijewarnasuriya, *J. Vac. Sci. Technol. B* **4**, 585 (1986).
- <sup>3</sup>S. Sivananthan, M. D. Lange, X. Chu, and J. P. Faurie, *J. Vac. Sci. Technol.* (to be published).
- <sup>4</sup>R. F. C. Farrow, *J. Vac. Sci. Technol. A* **3**, 60 (1985).
- <sup>5</sup>N. Otsuka, L. A. Kolodziejski, R. L. Gunshor, S. Datta, R. W. H. H. H. and J. F. Schetzina, Proceedings of the Materials Research Society Meeting, Boston, Nov. 1984.
- <sup>6</sup>J. P. Faurie, C. Hsu, S. Sivananthan, and X. Chu, *Surf. Sci.* **168**, 47 (1986) and references therein.
- <sup>7</sup>S. Sivananthan, X. Chu, J. Reno, and J. P. Faurie, *J. Appl. Phys.* **60**, 45 (1986).
- <sup>8</sup>G. L. Hansen, J. L. Schmit, and T. N. Casselman, *J. Appl. Phys.* **53**, 700 (1982).
- <sup>9</sup>S. J. C. Irvine, J. S. Gough, J. Giess, J. B. Mullin, and G. Crines, 1987 Workshop on the Physics and Chemistry of HCT, Oct. 1987 (unpublished result).
- <sup>10</sup>I. B. Bhat, H. Fardi, S. K. Ghandhi, and C. J. Johnson, 1987 U.S. Workshop on the Physics and Chemistry of Mercury Cadmium Telluride, New Orleans, Oct. 1987, Extended Abstracts, p. VII-9.

### III DOPING

#### III-1 DOPING BY STOICHIOMETRY DEVIATION

It is well established that  $\text{Hg}_{1-x}\text{Cd}_x\text{Te}$  should be written  $(\text{Hg}_{1-x}\text{Cd})_y\text{Te}_{1-y}$  to take into account the stoichiometry deviation. The maximum concentration of electrically active centers due to stoichiometry deviation  $\delta y$  is about  $10^{-5}$ . This means that doping level up to  $10^{17}\text{cm}^{-3}$  can be reached by acting on the stoichiometry. A metal-rich material (or Te-deficient) will exhibit a n-type conduction whereas a metal-deficient (or Te-rich) will show a p-type conduction, if there is no other electrically active impurity or defect.

In early MBE experiments it has been shown that the conduction type of (111)B HgCdTe layer could be controlled, within a certain limit and for a narrow range in composition (0.20–0.25), during the growth process itself. N-type to p-type conversion was achieved either by lowering the Hg flux or by raising the substrate temperature. The observation was consistent with the Hg vacancy model. However, the work carried out in the MPLab these last years has shown that into account the influence of the crystallographic orientation, the evidence of an electrical activity associated with the twins and the presence of antisite Te atoms, the doping problem is much more complex than that.

One of the major discoveries of the laboratory is related to the role of the crystallographic orientation during the growth by MBE. In a first step we have observed that the sticking coefficient for Hg, cd and Te changes with the crystallographic orientation. In the case of mercury the effect is quite dramatic since a (111)A face requires almost 10 times more mercury than a (111)B face at  $190^\circ\text{C}$ . These results have been confirmed since then and the summary is presented in the following table:

Substrate orientation	(211)B	(111)B	(100)	(111)A
Hg flux (arbitrary units)	1	1.25	5.5	11.25

TABLE: Minimum amount of Hg (in arbitrary units) needed to

maintain the monocrystalline growth of HgCdTe

These results are of fundamental importance since a classical thermodynamic approach using the mass action law and neglecting surface kinetics cannot describe the MBE growth of HgCdTe. In addition, it is obvious that such a difference in the sticking coefficient has an incidence on the Hg vacancy formation i.e. on the intrinsic and extrinsic doping of HgCdTe and very likely also on CdTe and other wide gap materials, since Cd and Te sticking coefficients are also orientation dependent. We found that (111)B HgCdTe layers are usually p-type whereas (100) films are n-type. It is the opposite of what is expected since Hg vacancies should be more easily formed in the (100) orientation than in (111)B because the sticking coefficient for mercury is lower. To explain this, the hypothesis of Te antisite formation in (100) orientation has been proposed. In this hypothesis Te is acting as a donor which could explain the n-type character of the material.<sup>(1)</sup> SIMS measurements cannot explain the donor character in HgCdTe MBE grown layer.

In addition with the elimination of the twins in the (111)B orientation a residual n-type character does now appear, such as in the (100) orientation. In (211)B n-type layers are often grown but it seems that p-type layers with a high residual n-type character can be grown at high temperature i.e. when Hg vacancies can dominate the transport properties.

Isothermal annealings have been performed on many layers (111)B layers and on some (100) and (211)B layers. The residual n-type doping in (111)B has been found to be in the  $5 \times 10^{15} - 2 \times 10^{16} \text{cm}^{-3}$  range which does confirm the Hall data analysis (see enclosed papers). The results obtained in (100) are unclear, more work is needed.

In the (211)B direction the residual n-type doping has been found ranging from  $2 \times 10^{15} - 1 \times 10^{16} \text{cm}^{-3}$  range. Unfortunately these films have different compositions and different growth parameters have been used therefore it has not been possible to determine yet, a clear relationship between Hg flux and residual doping.

The MPLab has devoted a great deal of time to understand and to control the intrinsic doping. Even though all the complex relationships between growth parameters and intrinsic doping are not fully understood appreciable progress has been made. It is now very likely that the residual donor doping level in MBE layers is due to the tellurium in antisite. This very important information has been proposed for the first time by the MPLab.

**REFERENCES:**

1. J.P. Faurie, DARPA IR Focal Plane Array Materials and Processing, April 1989 (unpublished)

**ATTACHED PAPERS:**

1. "The doping of mercury cadmium telluride by molecular beam epitaxy"
2. "Electrical properties of intrinsic p-type shallow levels in HgCdTe grown by molecular beam epitaxy in the (111)B orientation"
3. "High-quality p-type MCT grown by molecular beam epitaxy"

# The doping of mercury cadmium telluride grown by molecular-beam epitaxy

M. Boukerche, P. S. Wijewarnasuriya, S. Sivananthan, I. K. Sou, Y. J. Kim,  
K. K. Mahavadi, and J. P. Faurie

*Department of Physics, University of Illinois at Chicago, Chicago, Illinois 60680*

(Received 9 December 1987; accepted 29 February 1988)

The electrical properties of the mercury cadmium telluride semiconductor material grown by the molecular-beam epitaxy are reviewed. The doping effects linked to the growth conditions, as well as the influence of indium or lithium incorporation are discussed. The results on doping by silicon, arsenic, and antimony are presented. It will be shown that all the impurities studied interact primarily with the metal site. It will confirm that the growth occurs under very rich tellurium conditions.

## I. INTRODUCTION

The growth of mercury cadmium telluride (MCT) by the molecular-beam epitaxy (MBE) technique has become the subject of an important research effort recently. This flexible technique can be monitored during the growth by high-energy electron diffraction (HEED). The substrate temperature is low (190 °C), and control along the growth axis can be in the order of atomic scale distances. The epitaxy of this important infrared material on cadmium telluride by MBE was first reported in 1981.<sup>1</sup> Since then very important improvements in the growth control and understanding have been made.<sup>2</sup> The as-grown majority carrier and crystallographic properties of the best MBE materials are comparable to the ones made by the other techniques using postannealing procedures. MCT epitaxial layers highly uniform in carrier concentration and cadmium composition were recently obtained on 2-in. GaAs substrates.<sup>3</sup>

The control and understanding of the doping properties of this new material as grown is obviously of primordial importance for *in situ* junction formation which has already been demonstrated.<sup>4</sup> To our knowledge, no direct studies of deep levels or minority carriers have been reported yet. We will review the few doping studies made by majority carrier measurements and present the latest results on the work made in our laboratory.

## II. DOPING BY STOICHIOMETRY DEVIATION DURING GROWTH

Residual intrinsic doping by stoichiometry deviation is unavoidable in II-VI materials. It should be controlled during growth before any attempt of low-level *in situ* extrinsic doping is made. This technological challenge has to be faced even if stoichiometric doping alone is not in general recommended for device application due to stability considerations. It also frequently generates deep recombination centers. A few degrees change in substrate or mercury cell temperature can switch the electrical type of the material being grown. If the drift is sufficiently large, the annealing properties of the layer will be unpredictable.

The best compromise between the growth requirements of HgTe and CdTe sets the substrate temperature ( $T_s$ ) between 185 and 195 °C.<sup>2</sup> For fixed growth rates and cadmium compositions, high-quality epitaxy can only be achieved within narrow ranges of Hg pressures and substrate

temperatures. Within these limits, when the Hg flux is decreased, or  $T_s$  is increased, the layers tend to become  $p$  type. These effects are consistent with a low Hg sticking coefficient highly dependent on temperature and the known electrical properties of Hg vacancies in MCT. Further decrease in Hg flux or increase in  $T_s$  will create rings on the HEED screen. This is attributed to tellurium precipitation. For the (111) orientation, an excessive increase of the Hg pressure or decrease of  $T_s$  will induce twin dots along the diffraction lines of the HEED. This was shown to degrade the electric properties of the film.<sup>5</sup> These defects may be related to anti-phase domains occurring along the growth direction and very often lead to  $n$ -type conduction. Such material behaves abnormally after postgrowth isothermal annealing.<sup>6</sup> However, we should point out that, because of Hg overpressure, the same electrical type is obtained before the defects are visible. It has also been shown that the minimum necessary Hg flux to maintain monocrystalline growth was an order of magnitude higher for the (111) $A$  face than for the (111) $B$  face.<sup>7</sup> The (100) orientation was found to be an intermediate case. As we will see later, the electrical properties of the layers made with the (100) and (111) $B$  orientations are also very different. This proves that the intrinsic properties of the material are directly linked to the growth mechanisms.

The growth along the (100) orientation leads to  $n$ -type material when the Cd composition is  $< 0.35$ .  $p$ -type material was only reported for substrate temperatures exceeding 200 °C.<sup>2,6</sup> The range of suitable Hg fluxes is wider than for the (111) orientation since no twinning is observed. The growth along this direction can produce high-quality  $n$ - or  $p$ -type material. The Hall data on  $n$ -type layers show a fully ionized behavior with quasilocal resonant states merged inside the conduction band. The intrinsic region of the curves matches perfectly the expected variation of the intrinsic carrier concentration versus temperature.<sup>8</sup> The doping level does not exceed the low- $10^{16}$  range. We should also mention that faceting during growth in the (100) direction resulting in pyramidal voids has been reported recently.<sup>9</sup> We did observe the same effect in some cases. Whether these defects are a serious limitation for this orientation, or are predominantly linked to the growth control, is still opened to debate.

Even though more difficult to achieve than on (100), the growth along the (111) $B$  face (Te face) has been studied most. This is mainly due to the lower Hg pressure requirements, which were a serious concern in the early MCT MBE

systems. This orientation will probably remain the most important one for future industrial applications since the price of high-purity mercury will have to be included in the operating cost. In addition to the effects of  $T$ , and the Hg flux previously mentioned, an increase in cadmium composition tends to produce  $p$ -type material.<sup>10</sup> Good layers can only be grown  $p$  type for Cd compositions  $x$  more than 0.3, and  $n$  type for  $x < 0.2$ .<sup>2</sup> The doping level for  $p$ -type material can reach the mid- $10^{17}$  cm<sup>-3</sup> range. Analysis of the Hall data with a model including nonparabolicity effects and assuming a single doping level showed good agreement between the carrier concentrations calculated and measured in the intrinsic and transition regions, for a Cd composition very close to the one measured. The donor compensation was estimated to be in the low- $10^{17}$  cm<sup>-3</sup> range for these particular samples. The shallow doping level was separated from the valence-band edge by not more than 8 meV for  $x < 0.38$ . The level merges into the valence band to form resonant states for Na-Nd  $> 10^{17}$  cm<sup>-3</sup>. More recently the best Hall mobilities reached consistently 1100 cm<sup>2</sup>/V s without two-dimensional effects due to HgTe interfaces.<sup>11</sup> Excess carrier lifetimes measured on several samples with  $x > 0.3$  reached 800 ns. Nearly Auger limited operation down to liquid-nitrogen temperature was also seen in some of these samples.<sup>12</sup> High-performance photovoltaic detectors made without annealing by ion implantation have recently been demonstrated on such materials.<sup>13</sup>

High-mobility  $n$ -type layers can also be achieved by intrinsic doping, but the concentration never exceeds the low- $10^{16}$  range. When  $x$  is  $< 0.2$ , the carrier concentration can be higher than the intrinsic value expected at room temperature, and can decrease more slowly with temperature. Such a behavior cannot be fitted by a two-band model with a single impurity level, and might be related to impurity bands occurring inside the band gap. If the  $n$ -type character would be linked to a native point defect, its doping concentration should not be limited to the low- $10^{16}$  range. Further investigation is needed in this case.

The different Hg pressure requirements for the (111) $B$  and (111) $A$  faces were previously interpreted as a screening effect of the Te surface front limiting the mercury (and cadmium) reevaporation during the growth along the (111) $B$  orientation.<sup>7</sup> We think that Te is also responsible for the very different doping properties between (100) and (111) $B$  materials. The  $p$ -type character for the (111) orientation is probably mainly controlled by excess Te dissolved in the layers, either interstitial or at the antiphase boundaries when they are detected on the low Hg flux side. We suggest that the  $n$ -type character for the (100) orientation is due to substitutional Te on the metal site.<sup>14</sup> This is consistent with the fact that a substrate temperature in excess of 200 °C is necessary to produce (100)  $p$ -type material since Te reevaporation then becomes substantial.

### III. INDIUM DOPING

Indium was found to behave as an  $n$ -type dopant when evaporated during growth on (111)CdTe/(100)GaAs

combination substrates.<sup>15</sup> The doping level was increasing with the In effusion cell temperature. The maximum level obtained reached  $2 \times 10^{18}$  cm<sup>-3</sup>, which is two orders of magnitude more than what stoichiometry deviation can achieve on the same orientation. Secondary ion mass spectrometry (SIMS), calibrated with implanted reference samples, was used to evaluate the impurity atomic concentration. The apparent doping efficiency (defined as the ratio of the carrier concentration measured at low temperatures by the Hall technique divided by the In atomic concentration measured by SIMS), reached 70% for a doping level close to  $1 \times 10^{18}$  cm<sup>-3</sup>. This quantity obviously includes the intrinsic compensating acceptors. More recently we did measure apparent doping efficiencies close to 100% for doping level in the high- $10^{17}$  cm<sup>-3</sup> range. The set of samples used for this study had Cd compositions varying from 0.2 to 0.31 and were grown to produce native  $p$ -type material if In had not been introduced. Uncertainties apparent in the experimental relation between the doping efficiency and the doping level were then anticipated. Absolute concentration measurements are also known to be difficult to achieve by the SIMS technique. Nevertheless, a clear trend was detected, with a maximum around  $10^{18}$  cm<sup>-3</sup> and a sharp falloff below this value. We concluded that the In incorporation mechanism was not a steep function of the Cd composition in this narrow-band-gap range. The experimental observation could be successfully modeled assuming that a fraction of the In atoms was singly ionized, while the rest was precipitating in the crystal to form In<sub>2</sub>Te<sub>3</sub>. A fixed  $3 \times 10^{17}$  cm<sup>-3</sup> acceptor compensation was also assumed for this set of samples. These results are in agreement with a previous study of In doping by diffusion in bulk material.<sup>16</sup> The electrical efficiency reported here is higher probably because of the lower MBE growth temperature minimizing the In<sub>2</sub>Te<sub>3</sub> precipitation. The presence of this constituent in the crystal should actually not be considered as a defect since In<sub>2</sub>Te<sub>3</sub> has been shown to form a solid solution with HgTe preserving its sphalerite structure for a composition range of 0 to 0.2.<sup>17</sup> The fact that the compensation could be assumed constant means that the interaction between In and the Hg vacancies could be neglected.

The SIMS profiling of the doped layers showed In transitions at the buffer interface as sharp as the Cd and Hg on layers as thick as 5  $\mu$ m, equivalent to 3-h growth time. We conclude that the In diffusion was less than the resolution of the instrument, i.e., 2000 Å. The electron mobilities obtained looked promising in view of the Cd compositions and doping levels involved. Unlike stoichiometry deviation doping, a high Cd composition layer with  $x = 0.55$  could be doped in the  $10^{18}$  cm<sup>-3</sup> range.

We discovered that when several In doped layers are grown, the subsequent unintentionally doped MBE materials produced are  $n$  type. SIMS measurements showed that In was still present in the crystals. This is obviously a very serious limitation for device application, but since it seems to be a technological growth related problem, rather than a fundamental physical one, this effect should be investigated further. We think that the unique properties of In doping during MBE growth will deserve such an additional effort.

#### IV. LITHIUM DOPING

Li is a column I element and was considered first as a prospective *p*-type dopant for the (100) orientation, since this electrical type is difficult to achieve by stoichiometry control. Hole conduction was indeed observed.<sup>18</sup> The doping level increased monotonically with the Li effusion cell temperature and could reach as much as  $8 \times 10^{18} \text{ cm}^{-3}$ . Since a calibrated sample implanted with Li was not available, the amount of Li incorporated in the layers was estimated from the effusion cell temperature and the growth rate, assuming a sticking coefficient equal to unity. Since very good agreement was obtained with the doping levels measured by Hall above  $5 \times 10^{17} \text{ cm}^{-3}$ , we can conclude that nearly all the Li is incorporated and is electrically active. The impurity is singly ionized and no evidence of precipitation is detected. The evidence of a compensating donor becomes clear for Li concentrations in the low- $10^{17} \text{ cm}^{-3}$  range. Hole freezeout from a shallow acceptor level was only seen once for a doping level of  $10^{16} \text{ cm}^{-3}$ . For doping levels above  $4 \times 10^{16} \text{ cm}^{-3}$ , the acceptors are completely ionized (flat curve after the transition region). Above  $2 \times 10^{18} \text{ cm}^{-3}$ , the carrier concentration begins again to decrease slightly with temperature along a curved shape, showing the onset of a degenerate quasimetallic behavior. The hole mobilities measured are all in the 300–400  $\text{cm}^2/\text{Vs}$  range at low temperatures. Simple impurity scattering calculations similar to the ones used by Ref. 19 were made. They agree reasonably well with the measured values for the high doping levels in the  $10^{17} \text{ cm}^{-3}$  range or higher when, the lattice mobility (mobility without lithium) is assumed to be 500  $\text{cm}^2/\text{Vs}$ , and the Li is singly ionized.

The same element has also been incorporated successfully as a *p*-type dopant during the growth along the (111)*B* face, even for cadmium compositions  $< 0.16$  where intrinsic doping alone would produce *n*-type material. Thus Li appears to be a very efficient *p*-type dopant probably substituting with the metal site in the crystal. Unfortunately, we discovered by SIMS profiling that it diffuses uniformly in unintentionally doped layers grown under or above Li doped regions. Isothermal annealings also demonstrated that Li can diffuse out of the crystals since they became *n* type. We also noticed that when the layers with low Li doping levels are stored at room temperature, their electrical properties can evolve slowly with time. Because of its small atomic mass and radius, the Li atom is highly mobile in the MCT material.

#### V. DOPING WITH OTHER ELEMENTS

The doping properties of silicon during the (111)*B* growth were also investigated. It was found to produce *n*-type material. The highest level obtained reached  $1.7 \times 10^{17} \text{ cm}^{-3}$  for an effusion cell temperature of 1000 °C. We did not observe a systematic memory effect like in the indium case, but the reproducibility of the doping levels was more difficult to achieve. This might be due to the lower levels investigated or to a more intimate interaction between Si and the native growth conditions due to its potential amphoteric character demonstrated in the III–V materials. We should mention that Si was reported to dope the MCT material *n*

type before.<sup>20</sup> A fully ionized behavior with a carrier concentration independent of temperature was seen, even in the  $10^{15} \text{ cm}^{-3}$  range. But an important ion scattering linked to acceptor compensation was obvious in this case. The SIMS profilings resolved  $< 1000 \text{ Å}$  doping transitions on layers 3  $\mu\text{m}$  thick. This element was successfully used to produce the first *in situ* homojunction.<sup>4</sup> It was suspected in this study that the doping close to the junction interface was not uniform.

The column V elements arsenic and antimony act as *n*-type dopants in MCT when they are incorporated during the MBE process. The doping concentration remains in the low- $10^{16} \text{ cm}^{-3}$  range or lower. The effect is obvious for Cd compositions  $> 0.3$ , since the native material would be *p* type. It is also true for low-*x* material, since the carrier concentration remains independent of temperature in the extrinsic region of the Hall curves. After isothermal annealing at temperatures between 200 and 250 °C the samples remained *n* type showing that the doping mechanism during growth was stable. This experiment was undertaken since As has been shown to be a *p*-type dopant by diffusion.<sup>20</sup> We conclude that these impurities interact preferentially with the metal site. We also think that they are self-compensated, since the doping concentrations remain low, and the Hall measurements show evidence of a strong impurity scattering limiting the mobility at low temperature. Arsenic was previously found to be amphoteric when incorporated during liquid phase epitaxial growth of MCT from Te rich solutions.<sup>21</sup> Illumination of the substrate during MBE MCT growth by ultraviolet light or a green Nd:Yag laser pulsed at 10-kHz repetition rate did not increase substantially the carrier concentration and left the material *n* type. The details of this study will be published elsewhere.

#### VI. DISCUSSION AND CONCLUSION

We showed that all the extrinsic impurities studied interact primarily with the metal site. Indium, a column III element, mostly substitutes to dope *n* type. The rest of it bonds isoelectrically with Te. Lithium, a column I element substitutes the same atoms to dope the material *p* type. Silver is also found to dope the material *p* type.<sup>22</sup> The other elements investigated from columns IV (Si) and V (As, Sb) have a more complex amphoteric or self-compensating behavior, but still dope the material *n* type. We see a clear degradation of the doping quality when going from group III to group V.

For the (111)*B* face the growth could be schematically represented by a Te saturated surface front evolving under a very high local pressure of Hg. This medium is acting as a screen between the vacuum and the underlying growing crystal. The presence of impinging Cd atoms condensating on the surface might decrease the probability of incorporation of the weakly attracted heavy Hg atoms. Some excess Te atoms will be incorporated. No chalcogenide site could be available for impurity substitution since they are all saturated by Te, and it would disrupt the growth itself in the (111)*B* orientation. In the (100) case, some Te atoms will substitute on the metal site to create *n*-type material.

## ACKNOWLEDGMENTS

We want to thank M. De Souza for the electro-optical measurements and A. Jakimavicius for the final preparation of the manuscript. The continuous technical support of Z. Ali and S. Farook was greatly appreciated. This work was funded by DARPA under Contract No. F49620-87-C-0021.

- <sup>1</sup>J. P. Faurie and A. Millon, *J. Cryst. Growth* **54**, 582 (1981).
- <sup>2</sup>S. Sivananthan, M. D. Lange, X. Chu, and J. P. Faurie, *J. Vac. Sci. Technol.* (to be published).
- <sup>3</sup>M. D. Lange, S. Sivananthan, X. Chu, and J. P. Faurie, *Appl. Phys. Lett.* **52**, 978 (1988).
- <sup>4</sup>M. Boukerche, S. Yoo, I. K. Sou, M. De Souza and J. P. Faurie, *J. Vac. Sci. Technol. A* **6**, 2623 (1988) (these proceedings).
- <sup>5</sup>J. P. Faurie, J. Reno, S. Sivananthan, I. K. Sou, X. Chu, M. Boukerche, and P. S. Wijewarnasuriya, *J. Vac. Sci. Technol. B* **4**, 585 (1986).
- <sup>6</sup>J. M. Arias, S. H. Shin, J. T. Cheung, J. S. Chen, S. Sivananthan, J. Reno, and J. P. Faurie, *J. Vac. Sci. Technol. A* **5**, 3133 (1987).
- <sup>7</sup>S. Sivananthan, X. Chu, J. Reno, and J. P. Faurie, *J. Appl. Phys.* **60**, 1359 (1986).
- <sup>8</sup>G. L. Hansen and J. L. Schmit, *J. Appl. Phys.* **54**, 1639 (1983).
- <sup>9</sup>R. J. Koestner and H. F. Schaake, *J. Vac. Sci. Technol. A* **6**, 2834 (1988) (these proceedings).
- <sup>10</sup>M. Boukerche, P. S. Wijewarnasuriya, J. Reno, I. K. Sou, and J. P. Faurie, *J. Vac. Sci. Technol. A* **4**, 2072 (1986).
- <sup>11</sup>J. P. Faurie, I. K. Sou, P. S. Wijewarnasuriya, S. Rafol, and K. C. Woo, *Phys. Rev. B* **34**, 6000 (1986).
- <sup>12</sup>M. De Souza, M. Boukerche, and J. P. Faurie (unpublished results).
- <sup>13</sup>J. P. Faurie, S. Sivananthan, M. Lange, R. E. Dewames, A. M. B. Vandewyck, G. M. Williams, D. Yamini, and E. Yao, *J. Appl. Phys.* (to be published).
- <sup>14</sup>J. P. Faurie, HgCdTe MBE Workshop, DARPA-CNVEO, Washington, 1987 (unpublished results).
- <sup>15</sup>M. Boukerche, J. Reno, I. K. Sou, C. Hsu, and J. P. Faurie, *Appl. Phys. Lett.* **48**, 1733 (1986).
- <sup>16</sup>H. R. Vydyanath, *J. Electrochem. Soc.* **128**, 2619 (1981).
- <sup>17</sup>P. M. Spencer, *Br. J. Appl. Phys.* **15**, 625 (1964).
- <sup>18</sup>P. S. Wijewarnasuriya, I. K. Sou, Y. J. Kim, K. K. Mahavadi, S. Sivananthan, M. Boukerche, and J. P. Faurie, *Appl. Phys. Lett.* **51**, 2025 (1987).
- <sup>19</sup>H. R. Vydyanath, *J. Electrochem. Soc.* **128**, 2609 (1981).
- <sup>20</sup>E. S. Johnson and J. C. Schmit, *J. Electron. Mater.* **6**, 25 (1977).
- <sup>21</sup>H. R. Vydyanath, S. R. Hampton, P. B. Ward, L. Fishman, J. Slawinski, and T. Krueger, paper presented at the 1986 IRS Detector Specialty Group Meeting, NASA AMES Research Center, Moffet Field, CA.
- <sup>22</sup>M. L. Wroge, D. J. Peterman, B. J. Morris, D. J. Leopold, J. G. Broerman, and B. J. Feldman, *J. Vac. Sci. Technol. A* **6**, 2826 (1988) (these proceedings).

# Electrical properties of intrinsic *p*-type shallow levels in HgCdTe grown by molecular-beam epitaxy in the (111)*B* orientation

M. Boukerche, S. Sivananthan, P. S. Wijewarnasuriya, I. K. Sou, and J. P. Faurie  
*Department of Physics, The University of Illinois at Chicago, Chicago, Illinois 60680*

(Received 11 October 1988; accepted 9 November 1988)

The electrical properties of the unintentionally doped *p*-type HgCdTe material as grown in the (111)*B* orientation by molecular-beam epitaxy are revised. The analysis of the Hall coefficient in the whole temperature range with a model based on the two-band nonparabolic Kane model, a fully ionized compensating donor concentration, and two independent discrete acceptor levels is presented. The donor compensation is found to be much lower than before, in agreement with the latest study of extrinsic doping by indium. A defect level with an energy of 30 to 50 meV is found necessary to explain properly some of the crystals' data. The results of a three-carrier band modeling of the Hall constant versus field are also presented for one sample and are in very good agreement with the expected band structure of the material. These results show that important improvements have been made recently in the control of stoichiometry during growth.

## I. INTRODUCTION

Mercury cadmium telluride (MCT) material as grown is not suitable for infrared applications when grown by conventional techniques. Like for other II-VI materials, the residual doping by native defects (intrinsic doping) is unavoidable due to the large stoichiometry deviation range ( $\delta y < 10^{-5}$ ). The necessary electronic properties are usually achieved through postgrowth annealing procedures. However, high-quality as-grown MCT has been achieved by the molecular-beam epitaxy (MBE) technique.<sup>1</sup> A direct study of the doping mechanisms in the as-grown material can then be performed and correlated with the growth conditions. Previous studies showed that the (111)*B* MBE-MCT material is in general *p*-type in the usual growth temperature range (180–200 °C) except for low cadmium compositions (*x*) and high mercury conditions.<sup>2</sup> By investigating the effects of several extrinsic dopants it was concluded that the growth occurred under tellurium rich conditions in this temperature range.<sup>3</sup> We will present our latest results and compare them with the previously published studies for MCT material grown by MBE as well as by other growth techniques using annealing. We will mainly concentrate on the analysis of (111)*B* unintentionally doped *p*-type material for Cd compositions between 0.2 and 0.3, as grown, and measured by the Hall technique.

## II. EXPERIMENTAL

The technique used to grow the samples has been previously described.<sup>1</sup> The sample temperature was precisely controlled within the range 190–200 °C for the *p*-type layers. Most of them were grown on CdTe substrates with 2000-Å CdTe buffer layers. Some of the samples were grown CdTe(111)*B*/GaAs(100), CdZnTe(111), or CdSnTe(111) substrates. In the following course of this paper, we will point out the nature of the substrate if it is different from CdTe(111)*B*. The classical Hall measurement technique systematically performed on all the crystals has also been previously described<sup>2</sup> and uses the Van der Pauw geometry except for the field-dependent measurements

where the Hall bar design was selected. The magnetic field was varied from 0.2 to 1 T for the temperature-dependent measurements, the lowest field being used for the data to be fitted theoretically. The field-dependent measurements covered the range 0.01–1 T. The temperature was varied from 300 K down to 20 K. The few unusual samples detected with doping inhomogeneities or surface inversion will not be considered.

## III. RESULTS

The model previously used to analyze the *p*-type MCT Hall data included the two-band nonparabolic Kane model, a single acceptor level, a fully ionized compensating donor concentration, and a semiempirical approximation of the carrier mobility ratio at high temperature.<sup>2</sup> A heavy-hole effective mass equal to 0.64 and a well-known empirical approximation of the band gap versus cadmium composition and temperature<sup>4</sup> are also used in the calculation. It is well known that such a fitting technique is difficult to achieve. It can only have physical significance if the quality of the fit is nearly perfect, if the uncertainty associated with the data points is very small, and if the temperature range is wide enough. The influence of the compensation density alone, for example, with every other parameter being kept optimized, is to barely change the curvature of the freeze-out region. It also affects the shape of the curve just after the transition region, especially at high *x*, and the precision of the doping level determination. Nevertheless with the previous model the study of the samples grown on CdTe(111)/GaAs(100) showed that while the doping level was in the  $10^{16} \text{ cm}^{-3}$  range, a high compensating donor concentration was necessary to achieve a very good fitting of the experimental data.

Since then several hundred layers have been grown in our laboratory. Doping levels in the  $10^{15} \text{ cm}^{-3}$  range have been achieved. A careful analysis with the same model including only one acceptor level distinguished two groups of samples. The first group could be fitted with compensation levels in the low  $10^{16} \text{ cm}^{-3}$  range (Fig. 1). We should emphasize this

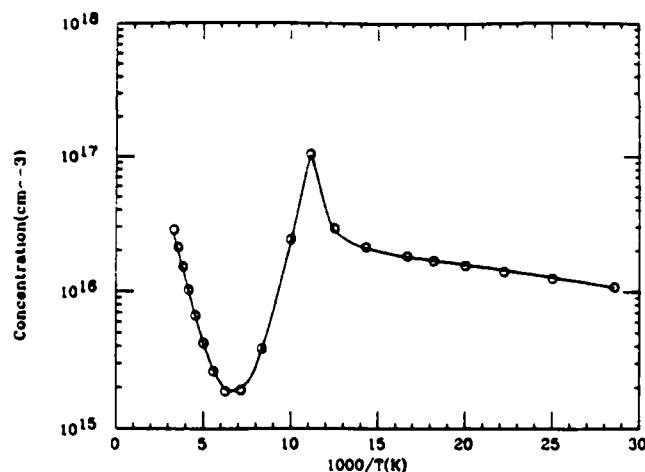


FIG. 1. Experimental (O) and theoretical (—) curves of the carrier concentration vs reciprocal temperature deduced from the inverse of the Hall constant for sample 571. Parameters used in the calculation: fully ionized donor concentration ( $N_d$ ) =  $1.3 \times 10^{16} \text{ cm}^{-3}$ , shallow acceptor concentration ( $N_a$ ) =  $3.8 \times 10^{16} \text{ cm}^{-3}$ , acceptor energy level ( $E_a$ ) = 4.3 meV, and cadmium composition ( $x$ ) = 0.199.

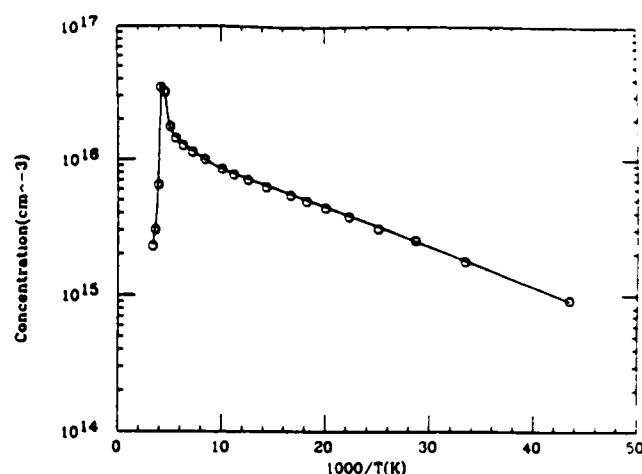


FIG. 2. Experimental (O) and theoretical (—) curves of the carrier concentration vs reciprocal temperature deduced from the inverse of the Hall constant for sample 612. Parameters used in the calculation: fully ionized donor concentration ( $N_d$ ) =  $5.6 \times 10^{16} \text{ cm}^{-3}$ , shallow acceptor concentration ( $N_{a1}$ ) =  $6.58 \times 10^{16} \text{ cm}^{-3}$ , shallow acceptor energy level ( $E_{a1}$ ) = 3.9 meV, deep acceptor concentration ( $N_{a2}$ ) =  $7.1 \times 10^{15} \text{ cm}^{-3}$ , deep acceptor energy level ( $E_{a2}$ ) = 50 meV, and cadmium composition ( $x$ ) = 0.311.

fact because it is probably related to important improvements in the growth conditions since the previous study. The second group either could not be fitted with any certainty, or required high compensation levels as before. We could notice that in this case the doping level was in general lower than  $2 \times 10^{16} \text{ cm}^{-3}$ . A small persistent disagreement also remained between the calculated curve and the data points just after the transition region, when the Fermi level is still relatively deep in the band gap. We thus added a second independent acceptor level in the model. An example of such a calculation is shown in Fig. 2. The values of the extracted parameters for several crystals are presented in Table I. The quantity  $\chi^2$  is a measure of the quality of the fit. We can see that the compensation level is in the  $10^{16} \text{ cm}^{-3}$  range for the other group of crystals. A concentration of deeper acceptors (30–50 meV) in the  $10^{15} \text{ cm}^{-3}$  range is also required.

The fact that the data are very well modeled in the whole temperature domain including the transition region, and with cadmium compositions consistently very close to their actual values measured by Fourier transform infrared transmission measurements (FTIR), gives credit to the reliability of the deep level. So far it seems that there is no clear correla-

tion between the deep and the shallow levels. The deep level would remain in the same carrier concentration range, and would be hidden by high doping levels. We suspect that the two levels have different origins. At the present time we cannot relate them to physical defects with any certainty. For the MCT material grown by the conventional techniques, it is now generally accepted that the intrinsic *p*-type doping is mainly created by mercury vacancies having two shallow ionization states varying between 3 and 15 meV depending on the doping level, the composition, and the compensation used.<sup>5,6</sup> Since in this study, the deep-level energy cannot be < 30 meV without noticeable discrepancies between the data and the calculated values, we think that this energy level is specific to the MBE-MCT (111)*B* material.

The previous results are in agreement with our latest study of extrinsic indium doping. Thanks to improvements in the stoichiometry control of the growth, carrier concentrations in the low  $10^{16} \text{ cm}^{-3}$  range can now be obtained routinely for indium doped MCT with Cd compositions  $x = 0.2$ – $0.3$ . This represents a major improvement compared to what was reported before<sup>7</sup> and shows that the memory effect linked to this material can be greatly reduced. The indium electrical

TABLE I. Summary of the fitted parameters for the *p*-type (111)*B* layers studied.

Sub	No.	$N_d$ ( $\text{cm}^{-3}$ )	$N_{a1}$ ( $\text{cm}^{-3}$ )	$E_{a1}$ (meV)	$N_{a2}$ ( $\text{cm}^{-3}$ )	$E_{a2}$ (meV)	$\mu_n/\mu_p$ 300K	$x$	$\chi^2$ $\log^2(\text{cm}^{-3})$
CT	827	$5.3 \times 10^{16}$	$5.8 \times 10^{16}$	5.5	$5.2 \times 10^{15}$	43	38	27.1	$5.0 \times 10^{-4}$
GA	571	$1.3 \times 10^{16}$	$3.8 \times 10^{16}$	4.3	...	...	31	19.9	$3.8 \times 10^{-4}$
CT	612	$5.6 \times 10^{16}$	$6.6 \times 10^{16}$	3.9	$7.1 \times 10^{15}$	50	34	31.1	$5.7 \times 10^{-4}$
CT	561	$6.4 \times 10^{16}$	$8.2 \times 10^{16}$	5.0	$5.1 \times 10^{15}$	48	38	32.5	$5.7 \times 10^{-4}$
CT	523	$2.9 \times 10^{16}$	$6.0 \times 10^{16}$	3.0	...	...	42	25.9	$7.7 \times 10^{-4}$
CTS	309	$3.2 \times 10^{16}$	$5.4 \times 10^{16}$	6.8	$8.0 \times 10^{15}$	33	36	28.6	$1.7 \times 10^{-4}$
CZT	605	$5.2 \times 10^{16}$	$6.6 \times 10^{16}$	3.4	$4.3 \times 10^{15}$	40	41	24.4	$5.0 \times 10^{-4}$
CT	166	$2.7 \times 10^{16}$	$8.5 \times 10^{16}$	1.5	...	...	36	27.6	$3.3 \times 10^{-4}$

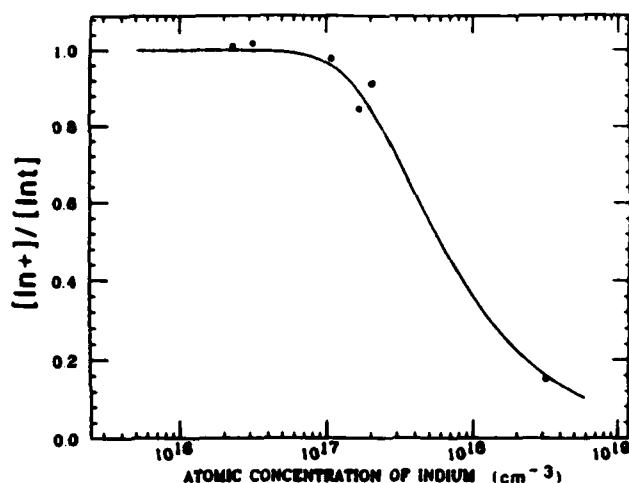


FIG. 3. Experimental (O) and theoretical (—) curves showing the relation between the ratio of ionized to total indium concentrations and the total indium concentration. The experimental data were determined by calibrated secondary ions mass spectrometry measurements and the theoretical data used an acceptor compensation level in the  $10^{15}$  range, the model being the same as in Ref. 7.

efficiency is now close to 100% even for doping levels in the  $10^{17}$   $\text{cm}^{-3}$  range (Fig. 3). This fact is consistent with intrinsic acceptor (or donor) ionized impurities concentrations in the low  $10^{16}$   $\text{cm}^{-3}$  range for the (111) $B$  orientation.

Some of these  $p$ -type MBE layers have been studied versus magnetic field assuming that the electronic transport occurs in three carrier bands. The technique models the variation of the Hall constant versus magnetic field and is similar to Ref. 8. An example of carrier concentrations calculated in each band is shown in Fig. 4 for crystal 571 that was already

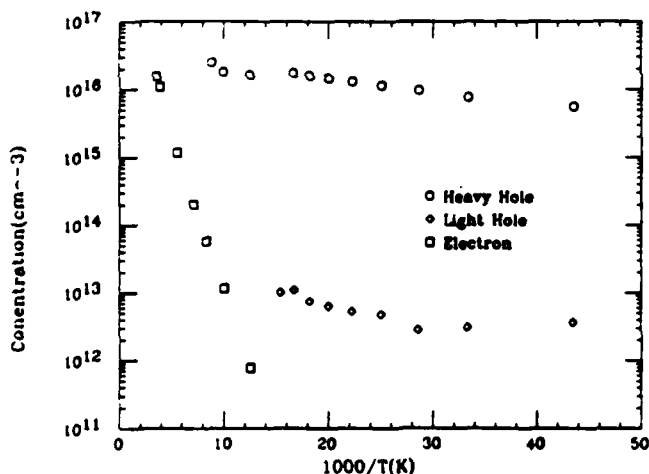


FIG. 4. Variation with reciprocal temperature of the carrier concentrations deduced from magnetic field analysis at each temperature assuming a three-band model.

shown in Fig. 1 as an example of fitting versus temperature. The electron concentration is resolved down to the  $10^{11}$   $\text{cm}^{-3}$  range. We can clearly see the freeze-out of the two hole bands. When both the electrons and the heavy holes are resolved, the product of their concentrations is in good agreement with the expected intrinsic carrier concentration.<sup>9</sup> The mobility ratio at 80 K between these two carriers (last electron concentration resolved) is close to 140 which seems reasonable for this composition. We conclude that gross defects like substantial concentration of metallic inclusions are not present in the crystal.

#### IV. CONCLUSION

We have described an improved Hall fitting technique which allows us to model nearly all of the well-behaved samples in the whole temperature range. It was used to show that important improvements in the growth control were made recently. The intrinsic doping level can now be set in the  $10^{15}$   $\text{cm}^{-3}$  range. The donor compensation level is in the low  $10^{16}$   $\text{cm}^{-3}$  range in agreement with the latest results on indium doping. A deep level with an energy of 30 to 50 meV is sometimes necessary to model the Hall data, particularly when the doping level is lower than  $2 \times 10^{16}$   $\text{cm}^{-3}$ . We think that it is probably specific to the MBE (111) $B$  material. The multi-band transport analysis confirmed the expected band structure of the material with one electron and two holes. The freeze-out of the two-hole bands could be detected and the concentrations of electrons and heavy holes agreed with the accepted intrinsic carrier concentrations.

These powerful tools will help us in the future to perform the needed correlations between the defect structure of the MBE material and the growth conditions.

#### ACKNOWLEDGMENTS

The work at the University of Illinois at Chicago is supported by the U.S. Defense Advanced Research Projects Agency and monitored by the U.S. Air Force Office of Scientific Research under Contract No. F 4920-87-C-0021

<sup>1</sup>S. Sivananthan, M. D. Lange, G. Monfroy, and J. P. Faure, *J. Vac. Sci. Technol. B* 6, 788 (1988).

<sup>2</sup>M. Boukerche, P. S. Wijewarnasuriya, J. Reno, I. K. Sou, and J. P. Faure, *J. Vac. Sci. Technol. A* 4, 2072 (1986).

<sup>3</sup>M. Boukerche, P. S. Wijewarnasuriya, S. Sivananthan, I. K. Sou, Y. J. Kim et al., *J. Vac. Sci. Technol. A* 6, 2830 (1988).

<sup>4</sup>G. L. Hansen, J. L. Schmit, and T. N. Casselman, *J. Appl. Phys.* 53, 7099 (1983).

<sup>5</sup>W. Scott, E. L. Stelzer, and R. J. Hager, *J. Appl. Phys.* 67, 1408 (1976).

<sup>6</sup>E. Finkman and Y. Nemirovsky, *J. Appl. Phys.* 59, 1205 (1986).

<sup>7</sup>M. Boukerche, J. Reno, I. K. Sou, C. Hsu, and J. P. Faure, *Appl. Phys. Lett.* 48, 1733 (1986).

<sup>8</sup>G. Fisher, *Helv. Phys. Acta* 33, 463 (1960).

<sup>9</sup>G. L. Hansen and J. L. Schmit, *J. Appl. Phys.* 54, 1639 (1983).

# High-quality *p*-type HgCdTe grown by molecular beam epitaxy

P. S. Wijewarnasuriya, M. Boukerche, and J. P. Faurie

Department of Physics, University of Illinois at Chicago, Chicago, Illinois 60680

(Received 14 December 1988; accepted for publication 28 September 1989)

The galvanomagnetic transport in (111)B HgCdTe *p*-type layers, grown by molecular beam epitaxy, was studied as a function of temperature and magnetic field strength. Experimental data on the Hall coefficient and conductivity tensor versus magnetic field have been analyzed with the assumption of three charge carriers involved in the conduction mechanism: one carrier coming from the conduction band and the other two from the complex nature of the valence band. Indeed, two kinds of positive charge carriers with completely different mobilities in the extrinsic region are seen. The extracted parameters are in very good agreement with the intrinsic concentration over a wide temperature range.

## I. INTRODUCTION

HgCdTe is currently the most important semiconductor material for the IR detection technology. Different growth techniques are used to produce HgCdTe, but the achievement of high-quality material is still the object of intensive efforts. Among other techniques, molecular beam epitaxy (MBE) is one of the most promising due to its versatility. Furthermore, the growth is carried out at a low temperature which limits the interdiffusion process. HgCdTe was grown for the first time by MBE in 1981 on CdTe substrates.<sup>1</sup> Since then, this technique has produced *n*- and *p*-type HgCdTe layers exhibiting structural and electrical properties comparable to or even better than layers grown by conventional techniques.<sup>2</sup> In order to optimize the growth conditions to prepare high-quality epitaxial layers suitable for infrared photodetectors or other devices, the understanding of the electrical properties of the epilayers is essential. The understanding of the transport properties of HgCdTe is rather difficult, especially for *p*-type HgCdTe epilayers<sup>3-5</sup> because of the complex nature of the valence band and the high electron-to-heavy-hole mobility ratio. Measurements taken at constant field are not sufficient to understand this complex valence-band structure. The electrical conduction versus magnetic field has been described in the literature in two ways: the Hall coefficient ( $R_h$ ) and resistivity ( $\rho$ )<sup>5-8,10</sup> or the conductivity tensor components  $\sigma_{xx}$  and  $\sigma_{xy}$ .<sup>9</sup> In all these cases, more than two charge carriers were necessary to explain the conduction mechanism. For *n*-type HgCdTe it has also been proposed that more than one kind of electron is

necessary to explain the results.<sup>10</sup> To the best of our knowledge such an analysis has not yet been performed on MBE-grown HgCdTe layers. In this paper we will analyze the Hall coefficient  $R_h$  and the conductivity tensor  $\sigma_{xy}$  for MBE-grown *p*-type HgCdTe epilayers to study the galvanomagnetic properties versus magnetic fields up to 1.0 T.

## II. EXPERIMENT AND THEORY

The (111)B HgCdTe layers were grown on CdTe(111)B, CdZnTe(111)B, and GaAs(100) substrates in a Riber 2300 MBE machine designed to handle mercury. In the case of GaAs substrates, 2–3  $\mu\text{m}$  CdTe buffer layers were grown prior to the HgCdTe. The Cd composition for each layer was determined at room temperature by infrared transmission measurements. The Hall coefficient and the resistivity of the layers measured by the van der Pauw technique<sup>11</sup> for temperatures ranging from 300 to 20 K and magnetic fields up to 1.0 T.

Assuming the existence of three charge carriers,  $R_h$  can be expressed as a function of magnetic field<sup>6</sup>

$$R_h = \frac{A_1 + A_2x + A_3x^2}{q \times (1 + A_4x + A_5x^2)}, \quad (1)$$

where  $q$  is the electronic charge in coulombs and  $x = (10^{-8}B)^2$ ;  $B$  is the magnetic field strength in Gauss, and  $A_1, A_2, A_3, A_4$ , and  $A_5$  are the nonlinear coefficients of the mobility ( $\mu_i$ ) and the concentration ( $n_i$ ) of the three charge carriers involved in the conduction mechanism. These coefficients are given by

$$A_1 = \frac{n_1\mu_1^2 + n_2\mu_2^2 + n_3\mu_3^2}{A^2},$$

$$A_2 = \frac{n_1\mu_1^2(\mu_2^2 + \mu_3^2) + n_2\mu_2^2(\mu_1^2 + \mu_3^2) + n_3\mu_3^2(\mu_1^2 + \mu_2^2)}{A^2},$$

$$A_3 = \frac{(n_1 + n_2 + n_3)\mu_1^2\mu_2^2\mu_3^2}{A^2},$$

$$A_4 = \frac{(n_1 + n_2)^2\mu_1^2\mu_2^2 + (n_1 + n_3)^2\mu_1^2\mu_3^2 + (n_2 + n_3)^2\mu_2^2\mu_3^2 + 2n_1n_2\mu_1\mu_2\mu_3^2 + 2n_1n_3\mu_1\mu_3\mu_2^2 + 2n_2n_3\mu_2\mu_3\mu_1^2}{A^2},$$

$$A_5 = \frac{(n_1 + n_2 + n_3)^2\mu_1^2\mu_2^2\mu_3^2}{A^2}, \quad (2)$$

where

$$A = \frac{1.0}{q\rho(0)}$$

The experimental  $R_h$  data for various magnetic fields can be fitted according to Eq. (1) using the standard nonlinear procedure. From the values of  $A_1, A_2, A_3, A_4$ , and  $A_5$  obtained by fitting the Hall coefficient and the resistivity at zero field, the carrier concentration and the mobility in each band can be calculated using Eqs. (2).

The conductivity tensor components ( $\sigma_{xx}, \sigma_{xy}$ ) are given by<sup>10</sup>

$$\sigma_{xx} = \frac{\rho}{\rho^2 + R_h^2 B^2} \approx \sum_{i=1}^3 \frac{n_i q \mu_i}{1 + \mu_i^2 B^2}$$

(3)

and

$$\sigma_{xy} = \frac{R_h B}{\rho^2 + R_h^2 B^2} \approx \sum_{i=1}^3 \frac{n_i q \mu_i^2 B}{1 + \mu_i^2 B^2}$$

Here the concentrations and mobilities of the charge carriers are directly obtained from the fitting parameters of the conductivity tensor.

### III. RESULTS AND DISCUSSION

Figure 1 shows the magnetic field dependence of  $R_h$  and  $\sigma_{xy}$  for sample No. 571 at 85 K. It can be seen that the dependence of  $R_h$  on the magnetic field is significant and at high fields it approaches a constant value. For  $\sigma_{xy}$ , as the magnetic field increases  $\sigma_{xy}$  starts from zero, decreases, and goes through a minimum. It then behaves as a linear function of the magnetic field. In this limit  $\mu_p B \ll 1$  and the contribution from heavy holes to the conductivity tensor  $\sigma_{xy}$  is reduced to approximately  $q\mu_p^2 B$ . This condition is justified for the low mobility holes up to the maximum magnetic field used in this investigation.

It is more convenient to calculate the carrier parameters

from  $\sigma_{xy}$  than  $R_h$ . To use  $R_h$ , after the fitting is done, we have to go through a cumbersome technique to predict the carrier parameters. Since  $\sigma_{xy}$  is decomposed [see Eqs. (3)] according to the three charge carriers involved in the conduction, it is more illustrative to study  $\sigma_{xy}$  versus magnetic field than to study  $R_h$  versus magnetic field.

All the analyzed samples showed evidence of three kinds of charge carriers participating in the conduction mechanism. We observe two positive carriers, identified as light and heavy holes coming from the complex nature of the valence band of HgCdTe. Hence, the light-hole contribution cannot be neglected in HgCdTe narrow-gap semiconductors. Accounting for these light holes in the transport measurements produces significant effects at weak magnetic fields. We took great care recording the experimental data in this limit. Table I shows the extracted parameters for light and heavy holes for MBE-grown HgCdTe epilayers in the extrinsic temperature region. From now on, we will consider the behavior of sample No. 571, which presents the general trends of the MBE layers studied in this paper.

Figures 2 and 3 show the extracted mobilities and carrier concentrations involved in the conduction mechanism. The carrier parameters deduced from both the  $R_h$  and  $\sigma_{xy}$  models are in very good agreement. We can see that both types of holes show carrier freezeout at low temperatures. At intermediate temperatures (60–100 K), the heavy-hole concentration is nearly constant indicating an exhaustion plateau that is not apparent in the carrier concentration deduced simply from the reciprocal of the Hall constant (Fig. 4). As the temperature increases, the heavy-hole concentration begins to increase due to the intrinsic conduction.

For the electrons, their concentration falls off drastically as the temperature decreases. However, down to 80 K, the data show evidence of intrinsic electrons. The electron population cannot be determined accurately with either technique as the temperature goes further down. However, the

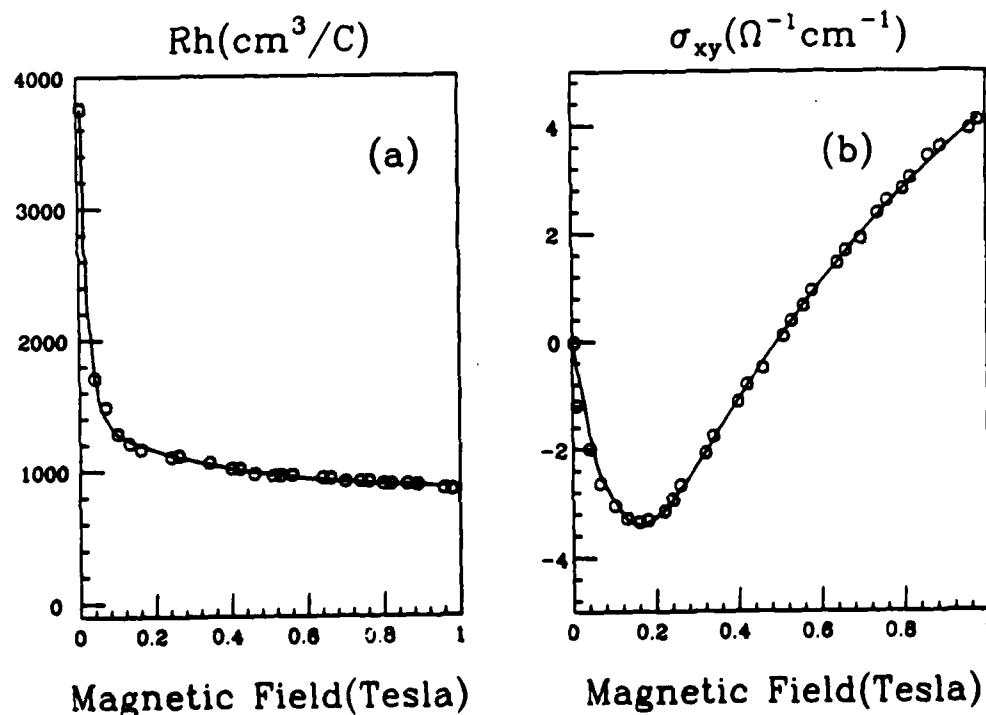


FIG. 1. Magnetic field dependence of Hall coefficient  $R_h$  (a) and conductivity tensor  $\sigma_{xy}$  (b) measured on sample No. 571 at 85 K. The solid lines show the fit according to the three-band model.

TABLE I. Parameters extracted from the  $R_h$  technique for light and heavy holes for  $p$ -type MBE-grown HgCdTe epilayers at different temperatures.

$x$ (%)	Sample (No.)	$T$ (K)	Light Holes		Heavy holes	
			Mobility ( $\text{cm}^2/\text{V s} \times 10^4$ )	Conc. ( $\text{cm}^{-3} \times 10^{11}$ )	Mobility ( $\text{cm}^2/\text{V s} \times 10^3$ )	Conc. ( $\text{cm}^{-3} \times 10^{15}$ )
21.0	601	60	1.70	67.50	0.84	9.17
		20	3.38	22.70	1.68	1.47
28.0	780	90	2.72	5.98	0.30	17.00
22.0	602	90	2.63	30.50	0.62	11.10
		30	2.26	56.60	1.40	2.78
20.5	571	60	1.55	111.00	0.54	17.50
		23	1.89	36.40	0.61	5.60

electron population can be resolved down to the  $10^{11} \text{ cm}^{-3}$  range [Fig. (2)].

In Fig. 5 we have compared the intrinsic carrier concentration of Hansen and Schmit<sup>12</sup> with the one deduced from  $R_h$ . The circles represent the values of  $n_i = (np)^{1/2}$  calculated from our data. There is a good agreement between the two intrinsic concentrations. This gives credibility to the band parameters extracted from the Hall coefficient versus magnetic field measurements. It also demonstrates that no additional electrons are detected in the material down to very low concentrations in the extrinsic region. We conclude that there is no inversion layer at the interfaces, and gross defects like metallic clusters are not present.

On one hand, at temperatures below 70 K the samples exhibit mixed conduction as is seen from both the high-mobility holes and the low-mobility carriers. Since the electron population is less than  $10^{11} \text{ cm}^{-3}$  in this temperature range the electron mobility and concentration cannot be determined with reliability. On the other hand at high temperatures (above 75 K), the  $R_h$  technique does not give realistic parameters for the light holes. Therefore, in Figs. 2 and 3 the parameters for only two major bands, electrons and heavy holes, are shown from the  $R_h$  technique in this temperature

limit. With the  $\sigma_{xy}$  fitting all the assumed three bands are visible except at low temperatures when the electron population is less than  $10^{11} \text{ cm}^{-3}$ . The mobility ratio  $\mu_e/\mu_p$  can be calculated from the values of the electron and heavy hole mobilities. This is shown in Table II. There is no clear temperature dependence of the mobility ratio, but the values are greater than  $10^2$  in the temperature range between 140 and 75 K. This is expected for such a cadmium composition.

As mentioned above, Fig. 4 shows the measured Hall carrier concentration versus reciprocal temperature at 0.2 T. In the analysis of this set of data versus temperature, we used the technique described in Ref. 13. We assumed a nonparabolic Kane model, a single acceptor level, and a fully ionized compensating donor level. The solid line in Fig. 4 is the best fit according to this model. The extracted doping level,  $2.5 \times 10^{16} \text{ cm}^{-3}$ , is higher than that obtained from the magnetic field analysis. This is expected, since at 0.2 T, the electrons contribute to the data around 80 K even though the Hall constant is positive. The slope of the heavy-hole concentration versus reciprocal temperature is closely related to the acceptor energy  $E_A$ . From Fig. 2,  $E_A \approx 4.4 \text{ meV}$ . This is in good agreement with the fitted acceptor level,  $E_A = 4.3 \text{ meV}$  in Fig. 4. The consistency of both analyses implies that

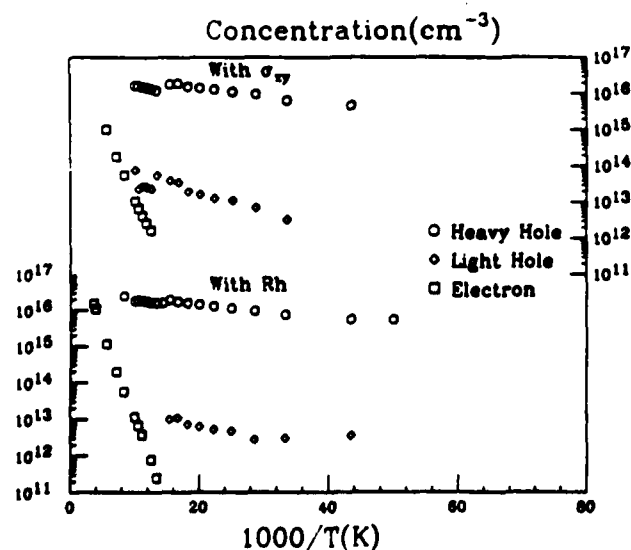


FIG. 2. Carrier concentrations extracted from the three-band model vs reciprocal temperature for sample No. 571.

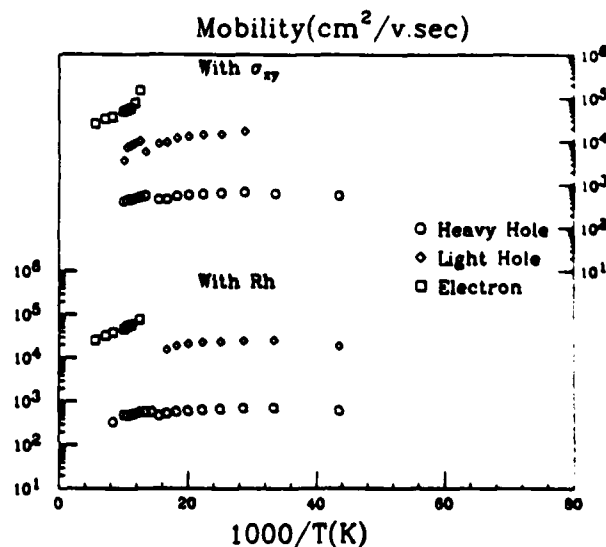


FIG. 3. Mobilities extracted from the three-band model vs reciprocal temperatures of sample No. 571.

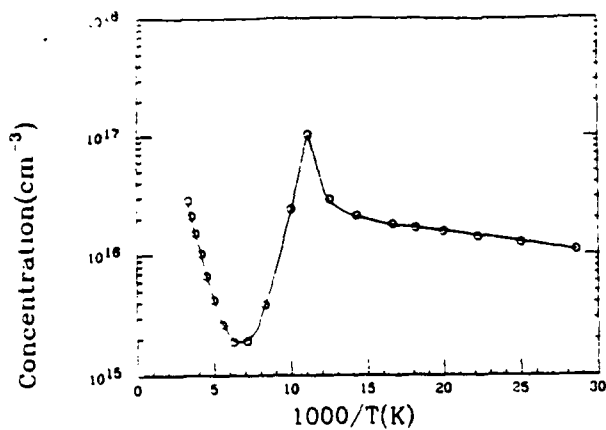


FIG. 4. Curve fitting of the carrier concentration deduced from the Hall measurements vs reciprocal temperature for sample No. 571. Parameters used:  $x = 19.9\%$ ,  $N_a - N_d = 2.5 \times 10^{16} \text{ cm}^{-3}$ ,  $N_d = 1.3 \times 10^{16} \text{ cm}^{-3}$ , and  $E_a = 4.3 \text{ meV}$ .

the sample under investigation has a good doping uniformity along the growth direction, and is free of other additional dominant charges in the conduction mechanism.

#### IV. CONCLUSION

We have studied the band parameters of MBE-grown  $p$ -type HgCdTe by analyzing the Hall coefficient  $R_h$  and the conductivity tensor  $\sigma_{xy}$  versus magnetic field at different temperatures. We resolve two kinds of positive charge carriers in the extrinsic region. With the technique described it was possible to determine the carrier mobility and the concentration versus temperature for each band, including those of the minority carriers. The extracted parameters are in good agreement with the ones expected from the intrinsic concentration. The two types of analyses were consistent with each other. Our data show that the conductivity tensor technique is more useful than the technique using  $R_h$  at some temperatures. On the other hand, with the  $\sigma_{xy}$  technique it is impossible, especially for  $p$ -type epilayers, to reach the high field limit  $\mu_p B > 1$  with the magnetic fields that we have

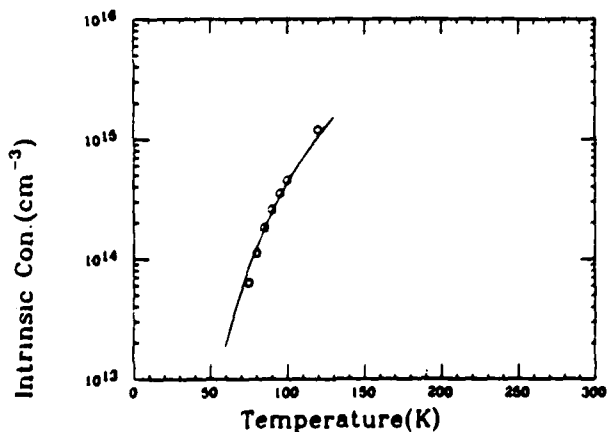


FIG. 5. Temperature dependence of  $(np)^{1/2}$  for sample No. 571. The solid line shows  $n$ , calculated from Hansen and Schmit (Ref. 12).

TABLE II. Temperature dependence of the ratio of the electron to the heavy-hole mobilities for sample No. 571.

$T$ (K)	$\mu_e/\mu_h$ (with $R_h$ )	$\mu_e/\mu_h$ (with $\sigma_{xy}$ )
140	135	136
120	115	104
100	93	120
95	112	120
90	116	128
85	123	135
80	137	147
75	259	296

used. Hence, initial guesses for the parameters in the curve fitting with  $\sigma_{xy}$  are difficult to determine. Any values for the initial parameters might give a good fit since, for the investigated magnetic field limit,  $\sigma_{xy}$  is a linear function of the fitting parameters.

This multiband transport analysis confirms the expected band structure of MBE-grown HgCdTe with one electron and two holes. This study confirms that MBE HgCdTe layers can be grown with a good doping uniformity and free of gross metallic defects and inversion layers. From Fig. 1, it is seen that the magnetic field strength is essential when one specifies the measured quantities, such as  $R_h$  and, therefore, the Hall mobility. The information on the minority carriers can also help to improve the control of the growth parameters to obtain high-quality HgCdTe epilayers.

#### ACKNOWLEDGMENTS

We wish to thank Dr. K. C. Woo for giving helpful suggestions, and Z. Ali and A. Farook for their technical assistance. This work was funded by the Defense Advanced Research Project Agency and monitored by the Air Force Office for Scientific Research under Contract No. F 49620-87-C-0021.

<sup>1</sup>J. P. Faurie and A. Million, *J. Cryst. Growth* **54**, 582 (1981).

<sup>2</sup>S. Sivanathan, M. D. Lange, G. Monfroy, and J. P. Faurie, *J. Vac. Sci. Technol. B* **6**, 788 (1988).

<sup>3</sup>R. Dornhaus and G. Nimtze, *Narrow Gap Semiconductors*, Vol. 98 in *Springer Tracts in Modern Physics* (Springer, Berlin, 1983), pp. 202-221.

<sup>4</sup>C. T. Scott and R. J. Hager, *J. Appl. Phys.* **42**, 803 (1971).

<sup>5</sup>C. T. Elliott, I. Melngailis, T. C. Harman, and A. G. Foyt, *J. Phys. Chem. Solids* **33**, 1527 (1972).

<sup>6</sup>G. Fisher, *Helv. Phys. Acta* **33**, 463 (1960).

<sup>7</sup>T. C. Harman, J. M. Honig, and P. Trent, *J. Phys. Chem. Solids* **28**, 1995 (1967).

<sup>8</sup>M. C. Gold and D. A. Nelson, *J. Vac. Sci. Technol. A* **4**, 2040 (1986).

<sup>9</sup>D. L. Leslie-Pelecky, D. G. Seiler, M. R. Loloee, and C. L. Littler, *Appl. Phys. Lett.* **51**, 1916 (1987).

<sup>10</sup>E. Finkman and Y. Nemirovsky, *J. Appl. Phys.* **53**, 1052 (1982).

<sup>11</sup>L. J. van der Pauw, *Philips Tech. Rev.* **20**, 220 (1958).

<sup>12</sup>G. L. Hansen and J. L. Schmit, *J. Appl. Phys.* **54**, 1639 (1983).

<sup>13</sup>M. Boukerche, P. S. Wijewarnasuriya, J. Reno, I. K. Sou, and J. P. Faurie, *J. Vac. Sci. Technol. A* **4**, 2072 (1986).

### III-2 EXTRINSIC DOPING

#### III-2-1 N-TYPE DOPING: INDIUM

In the final report of DARPA contract MDA 903-85K-0330 entitled, "MBE growth of mercury cadmium telluride and superlattices." the properties of In doped HgCdTe MBE layers have been discussed. It appeared that In is a very good n-type dopant but also that it presents a serious memory effect problem as illustrated by Table III. A layer grown after a In-doped one was always n-type even though a p-type conduction was expected.

Therefore we have worked on this question and by changing the position of the cells and also the way that part of the growth is carried out we have solved most of this problem. Now a layer grown after a In-doped layer exhibits a p-type character (see quarterly report dated March 15, 1988). However it is unclear whether or not a low In contamination still exists in those p-type layers.

SIMS measurements have been performed on In-doped HgCdTe layers and have shown that a doping level as low as  $2.0 \times 10^{16} \text{ cm}^{-3}$  controlled by the In level has been achieved. This represents a major improvement compared to our results published previously (Applied Physics Letters 48, 1733, 1986). This means that we have a much better control of the stoichiometry. It is also confirmed that In is 100% active in HgCdTe MBE grown layer since the  $N_D - N_A$  value determined by Hall measurements is identical to [In] measured by SIMS using a calibrated sample.

The third observation concerns the abruptness of the In profile. It is confirmed that junctions grown by MBE using In can be very abrupt, which is excellent for in situ device technology. Details are given in the attached paper #1. Thanks to its exceptional electrical properties this element is now established as the best n-type dopant of MBE grown HgCdTe.

Concerning the crystallographic orientation we have also found that it does play also a role in the incorporation of impurity, such as, Indium. Indium has been incorporated as a donor during MBE growth of MCT in the (100) orientation. As compared to the (111)B orientation, Hall and SIMS measurements have shown that Indium in the (100) MCT layers is at least doubly ionized. This is true at least for  $N_{In}$  below  $1 \times 10^{17} \text{ cm}^{-3}$ . We believe that most of the In atoms are triply ionized and incorporated interstitially in MCT. The other In atoms could be single ionized in substitution on the metal site vacancies not already filled by the Te atoms like in the (111)B direction. Such an incorporation mechanism of

indium supports a Te antisite model for explaining the favorable n-type behavior on (100) MCT grown by MBE. It also agrees with the growth in the (100) direction occurring under Te-rich conditions like in the (111)B direction. These results imply that foreign dopants, in general, should be incorporated interstitially at least to some significant extent in the (100) orientation. We think that interstitial doping by MBE in the (100) orientation might present serious limitation for its future electronic applications. These results are extremely important for the fabrication of MCT devices involving doping application in general, since it indicates that the orientation might play a very important role. For more details, see the attached paper #2.

**ATTACHED PAPERS:**

1. "The intrinsic and extrinsic doping of mercury cadmium telluride grown by molecular beam epitaxy"
2. "Role of the crystallographic orientation on the incorporation of Indium in HgCdTe epilayers grown by molecular beam epitaxy"

## **The intrinsic and extrinsic doping of mercury cadmium telluride grown by molecular beam epitaxy**

M. Boukerche and J.P. Faurie

University of Illinois, Dept of Physics, Chicago, Illinois 60680

**ABSTRACT:** The electrical properties of the mercury cadmium telluride semiconducting alloy grown by the molecular beam epitaxy technique are reviewed. The intrinsic doping produced by stoichiometry deviation during growth, as well as the extrinsic doping resulting from incorporation of indium, lithium, silicon, arsenic and antimony are described. The element from column I (Li) is a p-type dopant whereas the others dope the material n-type. We will show that these impurities mostly substitute in the metal site. We will conclude that the growth occurs under tellurium rich conditions.

### **1. INTRODUCTION**

The mercury cadmium telluride material (MCT) is recognized as the most important infrared material for detector applications in the 8-12 $\mu$ m and 3-5 $\mu$ m wavelength atmospheric transparency windows. Since its direct bandgap can be tuned by adjusting its cadmium composition, it was also suggested as a candidate for photonic applications in a much wider energy range. The molecular-beam epitaxy (MBE) technique is now established as a possible technique to grow high quality MCT epitaxial layers.

Very important improvements have been made in the growth control and understanding (Sivananthan et al 1988) since it was first reported seven years ago (Faurie and Millon 1981). The best as-grown MBE material compares with the best post-annealed material produced by the other techniques. Highly uniform hetero-epitaxial MCT-MBE layers have been demonstrated on two-inch GaAs substrates (Lange et al 1988). Characterizations of heterojunctions and homojunctions made in-situ have already been reported (Boukerche et al 1988a). High performance photovoltaic operation has also been shown recently on homojunction diodes made ex-situ by ion implantation on unannealed MBE material (Faurie et al 1988, Arias et al 1988).

The highly flexible MBE growth technique is an ideally versatile tool to study the correlations between the growth conditions and the electrical properties of the layers. It is also being considered for industrial applications. We will review the few studies published on the doping of the MBE-MCT material, and will present the latest results obtained in our laboratory.

### **2. INTRINSIC DOPING**

Like for the other techniques, the MBE technique is facing all the difficulties associated with the ionicity of this II-VI pseudo-random alloy. The large

stoichiometry deviation range ( $\delta y \leq 10^{-5}$ ) can generate intrinsic dopings in the  $10^{17} \text{ cm}^{-3}$  range. We can see that the growth control is even more critical than for the III-V materials. A few degrees change in substrate or Hg cell temperature can change substantially the doping concentration of the material being grown. The precision of the growth controls will determine the minimum extrinsic doping level achievable with reproducibility.

The best compromise between the growth requirements of CdTe and HgTe sets the substrate temperature ( $T_s$ ) around 190°C (Sivananthan et al 1988) for Cd compositions ( $X$ ) close to 0.2-0.3. Monitoring the growth by high energy electron diffraction (HEED) and establishing correlations with Hall measurements showed that high quality epitaxy can only be achieved within narrow ranges of Hg pressures and substrate temperatures for fixed  $X$  and growth rates in the (111)B orientation. If the Hg flux is too low or  $T_s$  too high the p-type character of the layer increases. When rings become detectable on the HEED screen, which is attributed to tellurium precipitation, the Hall mobility decreases to  $100 \text{ cm}^2/\text{V}\cdot\text{s}$  or less and the doping level is p-type in the low  $10^{17} \text{ cm}^{-3}$  range for  $X=0.2-0.3$  and growth along the (111)B orientation. In the same crystallographic orientation, if the mercury pressure is too high or  $T_s$  is too low, twin dots appear along the diffraction lines of the HEED screen, and the electrical properties of the layers degrade rapidly (Faurie et al 1986a). They usually show n-type conduction. We think that the related defects are twins. Abnormal behaviors were reported for such layers after isothermal anneals under mercury pressure (Arias et al 1987). The fact that excess Hg produces n-type material even before twins are visible is consistent with the well recognized properties of Hg in MCT (Vydyanath 1981a).

The growth requirements vary with the growth orientation. These differences will also be reflected in their respective electrical properties. The minimum Hg pressure found necessary to maintain a monocrystalline growth was found to be an order of magnitude higher for the (111)A cadmium face than for the (111)B tellurium face (Sivananthan et al 1986). The same results were also reported for the (112)Cd and Te faces (Koestner and Schaske 1988). The case of the (100) face lies somewhere in between. This is one of the reasons why the (111)B orientation was studied first since high vacuum conditions were difficult to sustain in non specifically designed MBE systems. The price of high purity mercury is also to be taken into consideration for industrial applications.

In addition to the effects of the Hg flux and  $T_s$  previously mentioned, an increase in Cd composition tends to produce p-type material (Boukerche et al 1986). In the (111)B orientation good quality layers can only be grown p-type for Cd compositions more than .2, and n-type for  $X$  less than 0.2 (Sivananthan et al 1988). The p-type intrinsic doping level can reach the mid- $10^{17} \text{ cm}^{-3}$  range (Boukerche et al 1986). Fittings of the Hall data with a model based on two band Kane theory and a single shallow doping level singly ionized were performed. Very good agreements could be obtained between the carrier concentrations measured and calculated in the hole temperature range, as well as for the Cd compositions measured by Fourier transform infrared spectroscopy (FTIR) at room temperature and the ones fitted. The donor compensation was estimated to be in the low  $10^{17} \text{ cm}^{-3}$  range for this particular set of samples. Automatic fittings made with the same model on crystals grown more recently gave compensation levels in the mid- $10^{16} \text{ cm}^{-3}$  range (Fig. 1). Interestingly, a two level model with a doubly ionized state was not required to reach such lower compensation magnitudes. The non-uniform or suspicious layers were obviously not considered in this analysis. We should point out that surface inversion in as-grown p-type

MBE layers is very unusual, even for doping levels of  $1 \times 10^{16} \text{ cm}^{-3}$ . The best p-type Hall mobilities reached consistently  $1100 \text{ cm}^2/\text{V.s}$  or more (Table I) without two dimensional confinement effects due to HgTe interfaces (Faurie et al 1986b). They compare favorably with published data for the other growth techniques (Gold and Nelson 1986, Meyer et al 1987). Doping levels in the  $10^{15} \text{ cm}^{-3}$  range were also observed. Excess carriers lifetimes were measured on these materials being illuminated by a solid state laser. The photosignal was always checked for exponentiality. The electron lifetime in some of these p-type layers could exceed 700ns at 220K (Fig. 2) and was very well fitted with a Shockley-Read model including a recombination level near mid-gap (DeSouza et al 1988). The analysis of such material versus magnetic field with a three band model confirmed the expected band structure with one light electron, one light hole and one heavy hole bands (Wijewarnasuriya et al 1988).

High mobility n-type layers can also be achieved in the (111) direction by stoichiometry adjustment. However, the carrier concentration determined by the Hall measurement monotonically decreases with temperature and never exceeds the low  $10^{16} \text{ cm}^{-3}$

range at low temperatures (Boukerche et al 1986a). When the Cd composition is less than .2, the carrier concentration at high temperatures can be higher than the expected intrinsic carrier concentration. Such layers were confirmed to be n-type by capacitance measurements on MIS structures (Yoo et al 1988) and thermoelectric probing at cryogenic temperatures. Such a behavior looks similar to bandgap narrowing due to the formation of an impurity band. We suggest that it could also be related to a self-compensated native defects together with a low electron to hole mobility ratio. This subject is still being investigated.

MBE growth along the (100) orientation can also produce high quality n or p-type MCT material. However, the layers are n-type for Cd compositions less than .35. P-type material can be achieved only when the substrate temperature exceeds 200C (Arias et al 1987, Sivananthan et al 1988). No twinning is observed on the HEED screen during the growth. As previously

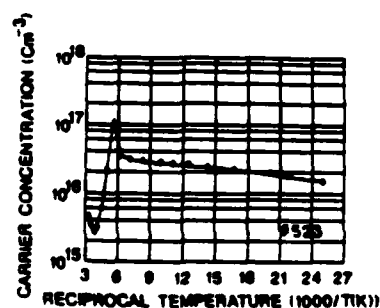


Fig. 1. Hall curve calculation for a p-type intrinsic layer parameters used:  $x = .259$ ,  $N_d = 2.9 \times 10^{16} \text{ cm}^{-3}$ ,  $N_A = 6 \times 10^{16} \text{ cm}^{-3}$ ,  $E_A = 3 \text{ meV}$ , the donors are assumed fully ionized.

SAMPLE	SUBSTRATE	x	THICKNESS $\mu\text{m}$	T	CARRIER CONC. $N_D - N_A (\text{cm}^{-3})$	MOBILITY $\mu (\text{cm}^2/\text{V.s})$
(111) ORIENTATION						
196 481	CdTe	0.20	4.8um	30K	$6.0 \times 10^{16}$	$1.1 \times 10^4$
198 484	CdTe	0.21	4.3um	30K	$5.1 \times 10^{16}$	$1.0 \times 10^4$
242 602	CdTe	0.22	11.9um	25K	$2.0 \times 10^{16}$	$1.1 \times 10^4$
213 527	CdTe	0.23	11.9um	30K	$6.2 \times 10^{16}$	$8.7 \times 10^3$
205 516	CdTe	0.29	13.6um	30K	$7.5 \times 10^{16}$	$8.7 \times 10^3$
216 528	CdTe	0.34	12.1um	77K	$3.6 \times 10^{16}$	$8.0 \times 10^3$
647 532	GdAs	0.20	2.1um	25K	$4.1 \times 10^{16}$	$1.2 \times 10^4$
681 540	GdAs	0.21	3.7um	25K	$3.6 \times 10^{16}$	$1.1 \times 10^4$
583 433	GdAs	0.22	5.4um	30K	$1.4 \times 10^{16}$	$8.7 \times 10^3$
634 508	GdAs	0.23	3.8um	30K	$1.1 \times 10^{16}$	$7.3 \times 10^3$
393 244	GdAs	0.28	1.3um	40K	$2.8 \times 10^{16}$	$5.2 \times 10^3$
500 308	GdAs	0.31	2.3um	30K	$1.1 \times 10^{16}$	$4.5 \times 10^3$
4 319	CdTeSe	0.31	7.6um	30K	$2.6 \times 10^{16}$	$8.4 \times 10^3$
2 310	CdTeSe	0.32	9.4um	30K	$1.2 \times 10^{16}$	$6.7 \times 10^3$
13 601	CdZnTe	0.21	12.1um	25K	$1.5 \times 10^{16}$	$1.6 \times 10^4$
34 603	CdZnTe	0.24	9.2um	25K	$1.5 \times 10^{16}$	$8.0 \times 10^3$
(100) ORIENTATION						
473 534	GdAs	0.21	4.2um	25K	$3.4 \times 10^{16}$	$5.1 \times 10^3$
125 306	CdTe	0.24	3.0um	77K	$2.0 \times 10^{16}$	$2.5 \times 10^3$
127 306	CdTe	0.29	2.7um	77K	$1.5 \times 10^{16}$	$1.2 \times 10^3$

TABLE 1: Electrical characteristics of p-type HgCdTe grown by MBE between 190-200°C (No HgTe layer at the interface).

mentioned the magnitude of the Hg flux necessary to maintain monocrystallinity is larger than in the (111)B case. The growth is actually easier to control since the suitable relative range of Hg flux is wider. As in the (111)B case, the n-type doping level is limited to the low  $10^{16} \text{ cm}^{-3}$  range. The carrier concentration and resistivity deduced from the Hall measurements follow the anticipated behaviors of the narrow bandgap n-type MCT material versus temperature (Hansen and Schmit 1983). The donor level is merged in the conduction band and is always fully ionized. The resistivity dips at the onset of extrinsic conduction. Faceting during growth along the (100) direction resulting in pyramidal voids present in the layers was reported recently (Million et al 1988). They were shown to originate at the CdTe interface. The density of these defects was function of the substrate used and the surface preparation. We did observe the same defects. Whether they will remain a serious limitation for the growth in the (100) orientation, or are linked to the quality of the growth control, is still to be determined.

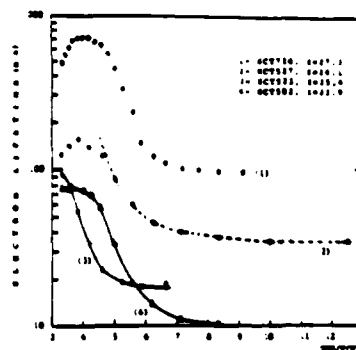


Fig. 2. Example of photodecay lifetime measurements on p-type intrinsic material. ---: calculation with the Shockley-Read theory,  $E_T/E_g = .49$ ,  $\tau_{no} = 35 \text{ ns}$ .

We see that the physical and electrical properties of the layers are totally dependent on the growth orientation. It was previously suggested that the Hg pressure requirements for the (111)Te face were smaller because the Te growing front was acting as a protective layer limiting the Hg (and Cd) reevaporation (Sivananthan et al 1986). We think that Te is responsible for the different intrinsic properties of the MCT-MBE material in the two directions described above. The (111)B growth seems to be intrinsically p-type. The negative sign of the Hall constant at low  $X$  is more linked to the narrow bandgap effects (electron to hole mobility and density of states ratios) than to the actual doping density. An opposite situation prevails in the (100) orientation since the layers are definitely doped n-type. This difference cannot be explained by a model based on the concentration of mercury vacancies since more Hg is required to grow the (100) direction. Furthermore the (100) growth orientation leads to p-type material only when the substrate temperature exceeds  $200^\circ\text{C}$ , which is known to induce substantial tellurium reevaporation (Sivananthan et al 1986). We conclude that Te is indeed responsible for the different doping properties of these two growth orientations. Substitutional Te atoms on the metal site might explain the (100) n-type (Faurie 1987). We will now see that it also controls its extrinsic doping properties.

### 3. DOPING WITH INDIUM

Controlled In evaporation during MBE growth was found to produce n-type layers on CdTe(111)//GaAs(100) combination substrates (Boukerche et al 1986b). The maximum electron concentration measured by Hall could reach  $2 \times 10^{18} \text{ cm}^{-3}$ , which is two orders of magnitude more than what can be achieved by stoichiometry deviation. The carrier concentration at low temperatures was compared to the atomic In concentration determined by secondary ion mass spectrometry (SIMS) calibrated with implanted reference samples. Even

though the Cd composition of the samples varied from .2 to .3 and some uncertainty was unavoidable, a clear trend was detected. The data measured could be very well fitted with a model assuming that part of the In concentration precipitated in the form of  $\text{In}_2\text{Te}_3$ , the rest of it being singly ionized. The formation of this compound should actually not be seen as a singular defect since it has been reported in solid solution in  $\text{HgTe}$  for compositions between 0 and 0.2 (Spencer 1964). The model also assumed a fixed concentration of compensating acceptors in the low  $10^{17}\text{cm}^{-3}$  range. This value was not surprising since the layers were intentionally grown with conditions adjusted to produce intrinsic p-type material without In. More recent results analyzed with the same model show that the In population is fully ionized for concentrations of  $10^{17}\text{cm}^{-3}$  or below (Sou et al 1988) as can be seen in Fig. 3. The compensating acceptor concentration will be precisely determined when more measurements will be available. At the present time it could only be estimated to be at least a decade lower than previously reported. The electrical efficiency of In in MCT made by MBE is larger than for other growth techniques (Vydyanath 1981b). This is probably related to the lower substrate temperature used during growth decreasing the rate of  $\text{In}_2\text{Te}_3$  precipitation. SIMS profiling of In junctions grown during two hours or more showed diffusion profiles around 2000Å wide probably limited by the instrument itself (Fig. 4). Uncorrected spreading resistance data measured at cryogenic temperature gave a transition width of 3000Å for a junction 2.5µm deep. A layer with a Cd composition 0.55 was doped with In and was measured having  $10^{15}\text{cm}^{-3}$  electrons. This could never be achieved by stoichiometry adjustment. In general the Hall mobilities of the In doped layers look promising in view of their doping levels and Cd compositions (Fig. 5). We discovered that the layers grown after In doping was used tend to be n-type. SIMS measurements proved that In was still present in the subsequently grown material. This limitation is obviously critical if junctions are to be realized. However we think that it is a technological rather than physical limitation linked to the high vapor pressure of In versus temperature. This problem has now nearly been solved since intrinsic p-type layers could be grown after In doped material. Thanks to its exceptional electrical properties, this element will most certainly

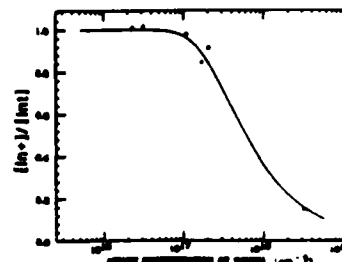


Fig. 3. Fraction of ionized indium atoms versus the atomic concentration of indium.

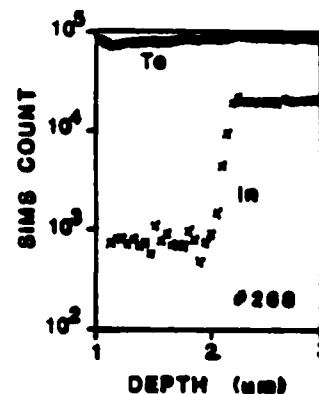


Fig. 4. SIMS profile of sharp In doping transition made during growth.

remain as a one of the major n-type dopants of MBE-MCT. We should also mention that it was demonstrated as an efficient n-type dopant in the  $10^{17}\text{cm}^{-3}$  range for CdTe grown by laser assisted MBE (Bicknell et al 1987).

#### 4. DOPING WITH LITHIUM

The need for a p-type dopant in MBE-MCT rises first for the growth in the (100) orientation since it usually produces intrinsic n-type material as mentioned above. Since Li is a column I element, it was expected to behave as a p-type dopant. Such was indeed the case (Wijewar-nasuriya et al 1987). Doping levels as high as  $8 \times 10^{18}\text{cm}^{-3}$  could be measured. The amount of Lithium incorporated in the MBE layers grown was estimated from the Li effusion cell temperature, the geometrical configuration of the system, and the growth rate, assuming a unity condensation coefficient. A very good agreement was found between these calculated values and the carrier concentration deduced from the Hall measurements above  $5 \times 10^{17}\text{cm}^{-3}$  (Fig. 6). We conclude that most of the Li atoms are indeed incorporated and singly ionized in the crystal. Hole freeze-out was only detected once for a doping level of  $10^{16}\text{cm}^{-3}$ . The carrier concentration remained independent of temperature in agreement with a shallow

doping level merged into the valence band for doping levels of  $4 \times 10^{16}\text{cm}^{-3}$  or more. Above  $2 \times 10^{18}\text{cm}^{-3}$  the carrier concentration started to decrease slightly along a curved shape with reciprocal temperature showing the onset of semi metallic impurity band conduction. Impurity scattering calculations similar to the ones made by Vydyanath (1981a) were attempted. When the mobility without  $\text{In}$  is assumed to be around  $500\text{cm}^2/\text{V.s}$ , the calculated and measured values, assuming that the donors are singly ionized at low temperatures, are in reasonable agreement (Fig. 7). Lithium was also found to dope the (111)B MBE grown material p-type, even for Cd compositions as low as 0.16. The Hall constant measured on such low X MBE material is always negative without lithium incorporation. It thus seems

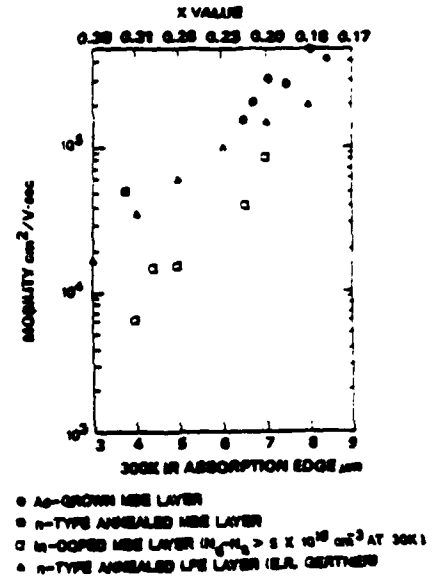


Fig. 5. Comparison of mobilities for MCT layers from different origins.

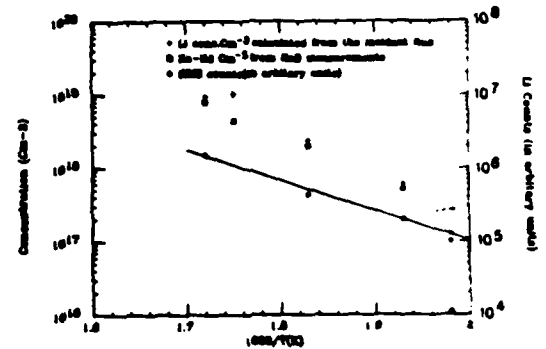


Fig. 6. Comparison of calculated Li incident flux with SIMS and electrical data.

that Li is a very efficient p-type dopant probably substituting in the metal site. Unfortunately we discovered that the MCT material grown above or below Li doped regions had basically the same Li content as detected by SIMS. Lithium is highly mobile in the MBE layers. It can also diffuse out of the material since some Li doped crystals were measured n-type after annealing. This result is not surprising since the Li atomic radius is small, and it obviously compromises any electronic device application.

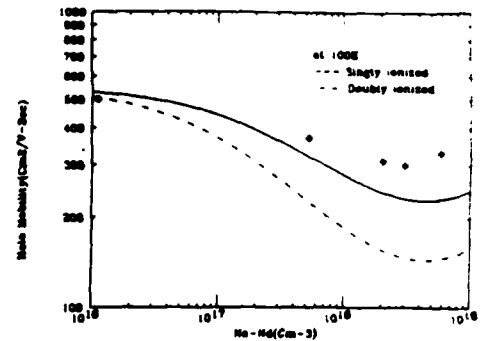


Fig. 7. Measured and calculated hole mobilities versus Li doping level.

##### 5. DOPING WITH OTHER ELEMENTS

Silicon, a column IV element, was found to behave as an n-type dopant when evaporated during MBE-MCT growth (Boukerche et al 1988b). The highest level achieved reached  $1.7 \times 10^{17} \text{ cm}^{-3}$ . Unlike for the case of indium, no memory effect was observed. The reproducibility of the doping level was more difficult to achieve, probably because of the more intimate interaction between this element and the native growth conditions. The amphoteric character of this element is recognized in the growth of III-V materials and it was previously shown to produce n-type MCT material before (Johnson and Schmit 1977). A fully ionized behavior independent of temperature was seen even for doping levels in the  $10^{15} \text{ cm}^{-3}$  range. A strong acceptor compensation was suspected since strong impurity scattering limited the mobility at low temperatures. SIMS profiles could resolve less than 1000 Å transitions on 3 μm thick junctions. Homostructures made on intrinsic p-material with this dopant were reported recently (Boukerche et al 1988a). The doping concentration was suspected to be non-uniform close by the junction. It was also concluded that the device operation was limited by generation-recombination.

The column V elements arsenic and antimony were also found to act as n-type dopants in MBE-MCT. The doping levels achieved never exceeded the  $10^{16} \text{ cm}^{-3}$  range. The carrier concentration was nearly independent of temperature in the extrinsic range. Unlike intrinsic doping it was also the case for low X material in the (111)B orientation. Strong impurity scattering was limiting the mobility at low temperature. Since the doping magnitude remained low, we think that these elements were highly self-compensated in the MBE material. Arsenic was previously reported to be amphoteric when incorporated during tellurium rich MCT growth by the liquid phase epitaxial technique (Vydyanath et al 1986). Illumination of the crystal during the growth by an Nd-Yag green laser pulsed at 10 KHz only slightly increased the Cd composition and the electron concentration in the material, but did not change its electrical type. Isothermal annealing at temperatures between 200 and 250°C also kept the samples n-type, showing that the doping mechanism was stable.

This is a very important result giving insights on the MBE growth mechanism since As was found to dope MCT p-type by diffusion (Johnson and Schmit 1977).

## CONCLUSION

We showed that lithium, a column I element, substitutes in the metal site to dope the material p-type. Silver, another element from column I, was also reported as doping the MBE material p-type (Wroge et al 1988). Indium, a column III element, was shown to dope efficiently the layers n-type, mostly substituting in the metal site, the rest precipitating isoelectrically in the form of  $\text{In}_2\text{Te}_3$ . When going to column IV (Si) and column V (As,Sb) the elements investigated still dope the material n-type, but the maximum doping levels achieved decrease sharply and the self-compensation increases. We conclude that none of the elements studied could substitute in the chalcogenide site. This proves that the MBE-MCT growth is occurring under very rich Te conditions so that no Te site is available for substitution. This analysis is consistent with the case of intrinsic doping discussed above since we already suggested that Te is responsible for the electrical properties of the layers.

## ACKNOWLEDGEMENTS

The authors would like to thank I.K.Sou, Y.J.Kim and S.Sivananthan for the growth of the samples, P.S.Wijewarnasuriya and S.Yoo for their electrical characterizations, K.K.Mahavadi for the SIMS measurements, Z.Ali and S.Farook for their technical support.

This work was funded by the Defense Advance Research Project Agency under contract No.F49620-87-C-0021.

- Arias J M, Shin S B, Cheung J T, Chen J S, Sivananthan S, Reno J and Faurie J P 1987 *J.Vac.Sci.Technol.* A5 3133  
 Arias J M, Shin S B, Pasko J G and Gertner E R 1988 *Appl.Phys.Lett.* 52 39  
 Bicknell R N, Giles N C and Schetzina J F 1987 *Appl.Phys.Lett.* 50 691  
 Boukerche M, Wijewarnasuriya P S, Reno J, Sou I K and Faurie J P 1986a *J.Vac.Sci. Technol.* A4 2072  
 Boukerche M, Reno J, Sou I K, Hsu C and Faurie J P 1986b *Appl.Phys.Lett.* 48 1733  
 Boukerche M, Yoo S, Sou I K, DeSouza M and Faurie J P 1988a *J.Vac.Sci. Technol.* A6 2623  
 Boukerche M, Wijewarnasuriya P S, Sivananthan S, Sou I K, Kim Y J, Mahavadi K K and Faurie J P 1988b *J.Vac.Sci.Technol.* A6 2830  
 DeSouza M, Boukerche M and Faurie J P 1988 (to be published)  
 Faurie J P and Millon A 1981 *J.Cryst.Growth* 54 582  
 Faurie J P, Reno J, Sivananthan S, Sou I K, Chu X, Boukerche M and Wijewarnasuriya P S 1986a *J.Vac.Sci.Technol.* B4 585  
 Faurie J P, Sou I K, Wijewarnasuriya P S, Rafol S and Woo K C 1986b *Phys. Rev.* 34 6000  
 Faurie J P 1987 HgCdTe MBE Workshop, DARPA-CNVEO, Washington (unpublished results)  
 Faurie J P, Sivananthan S, Lange M, DeWames R E, Vandewyck A M B, Williams G M, Yamini D, and Yao E 1988 *Appl.Phys.Lett.* 52 2151  
 Gold M C and Nelson D A 1986 *J.Vac.Sci.Technol.* A4 2040  
 Hansen G L and Schmit J L 1983 *J.Appl.Phys.* 54 1639  
 Johnson E S and Schmit J C 1977 *J.Electron.Mater.* 6 25  
 Koestner R J and Schaake H F 1988 *J.Vac.Sci.Technol.* A6 2834  
 Lange M D et al 1988 *Appl.Phys.Lett.* 52 978  
 Meyer J R, Bartoli F J and Hoffman C A 1987 *J.Vac.Sci.Technol.* A5 3035  
 Million A, DiCioccio L, Gaillard J P and Piaguet J 1988 *J.Vac.Sci.Technol.* A6 2813

- Sivananthan S, Chu X, Reno J and Faurie J P 1986 J.Appl.Phys. 60 1359  
Sivananthan S, Lange M D, Monfroy G and Faurie J P 1988 J.Vac.Sci.Technol. B6 788  
Sou I K, Boukerche M and Faurie J P 1988 (unpublished results)  
Spencer P M 1964 Br.J.Appl.Phys. 15 625  
Vydyanath H R 1981a J.Electrochem.Soc. 128 2609  
Vydyanath H R 1981b J.Electrochem.Soc. 128 2619  
Vydyanath H R, Hampton S R, Ward P B, Fishman L, Slawinski J and Krueger T 1986 paper presented at the IRS Detector Specialty Group Meeting, NASA AMES Research Center, Moffet Field, California  
Wijewarnasuriya P S, Sou I K, Kim Y J, Mahavadi K K, Sivananthan S, Boukerche M and Faurie J P 1987 Appl.Phys.Lett. 51 2025  
Wijewarnasuriya P S, Boukerche M and Faurie J P 1988 (to be published)  
Worge M L, Peterman D J, Morris B J, Leopold D J, Broerman J G and Feldman B J 1988 J.Vac.Sci.Technol. A6 2826  
Yoo S, Boukerche M and Faurie J P 1988 (unpublished results)

# Role of the crystallographic orientation on the incorporation of indium in HgCdTe epilayers grown by molecular beam epitaxy

I. K. Sou, P. S. Wijewarnasuriya, M. Boukerche, and J. P. Faurie  
University of Illinois at Chicago, Department of Physics, P.O. Box 4348, Chicago, Illinois 60680

(Received 27 January 1989; accepted for publication 23 June 1989)

In-doped HgCdTe films have been grown by molecular beam epitaxy (MBE) on CdTe substrates in the (100) crystallographic orientation. They were characterized by Hall and secondary-ion mass spectroscopy measurements. The results are compared with those of In-doped HgCdTe layers grown in the (111)*B* orientation. In the (111)*B* orientation indium is incorporated in the metal site whereas in the (100) orientation it appears that indium is mainly incorporated interstitially. The results agree with a Te antisite model as a possibility for explaining the electrical behavior of (100) HgCdTe grown by MBE.

The growth of the infrared material HgCdTe (MCT) by molecular beam epitaxy (MBE) has been studied since the beginning of this decade. Most of the reported results have been obtained in the (111)*B* and (100) orientations. It is well known that the conduction type (*p* or *n*) can be controlled stoichiometrically by varying the Hg flux (low or high) or the substrate temperature.<sup>1</sup> This principle is based on the assumption that Hg vacancies act as acceptors and Hg interstitials act as donors. Change in conduction type has been observed when the growth occurs in the (111)*B* orientation. In the (100) orientation, in spite of a much higher Hg flux requirement, which means that a higher tendency for Hg vacancy formation is expected, the MCT layers exhibit *n*-type conduction for a substrate temperature less than 200 °C. This happens even in the low Hg flux limit where polycrystalline growth begins to occur.

Hg vacancies and Hg interstitials are considered, respectively, to be the sources of *p*- and *n*-type doping in the (111)*B* orientation. Actually, *p*-type character was more often observed in this orientation. This is probably because the weak bonding between Te and Hg in MCT makes the formation of Hg vacancies easier than that of interstitials. Recently, Boukerche *et al.*<sup>2</sup> have suggested a different model in which the *p*-type character for the (111)*B* orientation is considered due to some excess Te dissolving in the layers interstitially.

Faurie has suggested that the *n*-type character observed for the (100) orientation is probably due to substitutional Te on the metal site.<sup>3</sup> Since this Te antisite model has been proposed, there has been neither direct nor indirect experimental results which could strongly support it so far.

Modern solid-state devices have had their most dramatic and extensive applications through doping by foreign impurities into the host semiconductor materials. In a previous letter<sup>4</sup> we have reported the electrical characterization and secondary-ion mass spectroscopy (SIMS) measurements on In-doped MCT grown by MBE in the (111)*B* orientation. The indium impurity was detected fully ionized. Its doping efficiency strongly depended on the indium atomic concentration when the concentration was above  $1 \times 10^{18} \text{ cm}^{-3}$ . Hall and SIMS data could be very well fitted with a model assuming that part of the indium concentration precipitates in the form of  $\text{In}_2\text{Te}_3$  (neutral molecular complexes), the

rest of it being singly ionized (probably filling the metal vacancy sites). These results agree with Vydyanath's model for In diffusion in bulk materials.<sup>5</sup> In the previous study a fixed concentration of compensating acceptors in the low  $10^{17} \text{ cm}^{-3}$  range was also assumed.

The same model has been used to fit In-doped (111)*B* layers recently grown in our laboratory.<sup>6</sup> The fitting gives a value around  $1 \times 10^{16} \text{ cm}^{-3}$  for the compensating acceptor concentration  $N_A$ . The precise value of  $N_A$  cannot be determined unless more experimental data become available. It is worthy to note that this new value of  $N_A$  is much lower than that reported earlier ( $3 \times 10^{17} \text{ cm}^{-3}$ ),<sup>4</sup> which indicates that a much lower compensation level has been achieved. This is attributed to recent improvements in the growth by MBE of HgCdTe related to a very precise control of the substrate temperature and fluxes during the growth.<sup>7</sup>

The purpose of this work is to study the incorporation of indium in MCT grown in the (100) orientation by MBE. As in the (111)*B* case, we expect that this study will give us further information about the intrinsic doping properties of MBE-grown MCT in the (100) orientation.

A Riber 2300 MBE machine modified to handle Hg was used for the crystal growth. All the layers were grown on CdTe (100) substrates. Before growth each CdTe substrate was cleaned in organic solvents, chemically etched in a  $\text{Br}_2$ -methanol solution, and finally rinsed in methanol and loaded in the growth chamber. A brief thermal cleaning was performed *in situ* at about 300 °C prior to the growth. The growth of In-doped crystals requires four effusion cells containing mercury, tellurium, cadmium telluride, and indium, respectively. Aside from the much higher Hg flux used, the fabrication of In-doped (100) MCT is similar to that described for the (111)*B* orientation.<sup>4</sup> The growth conditions were controlled such as to require only the minimum amount of Hg for single-crystal formation. The growth temperature was controlled through an infrared pyrometer and *in situ* quality monitoring was achieved through reflected high-energy electron diffraction (RHEED). The substrate temperature was kept at 190 °C for all the layers. By varying the In cell temperature, different doping concentrations were obtained.

Table I lists the transport properties of the layers which have been studied by Hall measurements. Sample No. 856 is

TABLE I. Hall and SIMS data of In-doped MCT layers grown by MBE (Hall data were at 23 K, except for sample 856, which was at  $T = 70$  K).

Sample	Orientation	Cd composition (%)	Hall mobility ( $\times 10^3 \text{ cm}^2 \text{ V}^{-1} \text{ s}^{-1}$ )	Carrier concentration ( $\times 10^{14} \text{ cm}^{-3}$ ) ( $N_D - N_A$ )	$N_{\text{In}}$ ( $\times 10^{14} \text{ cm}^{-3}$ )
856	(100)	20.5	110	8.8	...
875	(100)	23.0	70	43	2.5
876	(100)	25.0	3.7	110	4.2
859	(100)	24.5	48	290	12
860	(100)	26.5	33	550	23
861	(100)	25.5	41	1000	41
863	(100)	33.0	16	2100	78
714	(111) <i>B</i>	24.0	31	200	23
715	(111) <i>B</i>	26.5	18	290	32
697	(111) <i>B</i>	27.5	14	1000	110
716	(111) <i>B</i>	26.5	21	1400	170
705	(111) <i>B</i>	20.5	28	2400	270

an undoped MCT layer grown just prior to the In-doped layers. The fact that the electron mobility of this layer reaches  $1.1 \times 10^5 \text{ cm}^2 \text{ V}^{-1} \text{ s}^{-1}$  at 70 K demonstrates that the growth conditions used for this work were well controlled and thereby achieved good electrical quality. The meaning of the electron carrier concentration listed in Table I will be discussed in the following paragraph. For comparison, in Table I we also give the data of recently grown In-doped (111)*B* layers.

SIMS measurements were conducted using a Riber MQ 156 ion microprobe system. A 10 keV oxygen primary beam was focused on the target at  $30^\circ$  off the surface normal. A 10% beam blanking was used to exclude ions originating from the sloping sides of the sputtered crater. Sputtering rates were around 2 nm/s. The secondary-ion spectrum of  $^{115}\text{In}$  was normalized to the  $^{130}\text{Te}$  matrix ion. An In-implanted layer with known In atomic concentration was used as a reference sample. In order to have a meaningful comparison between the different growth orientations, we performed SIMS on some of the recently grown In-doped (111)*B* MCT layers along with the newly grown (100) layers under the same experimental conditions, calibrating with the same implanted reference sample. The In atomic concentrations of these layers measured by SIMS are also listed in Table I as  $N_{\text{In}}$ .

From inspection of Table I, the most remarkable point is that the In atomic concentrations measured by SIMS are less than half of the electron carrier concentrations derived from the Hall measurements in the (100) case. If we compare two layers having the same In content but grown in different directions (Nos. 860 and 714) we can see that the doping level in the (100) direction is 2.75 times higher than in the (111)*B* direction. The fact that the consistent factor of 2–3 difference is much larger than the total error (within  $\pm 40\%$ ) estimated for such a comparison implies that it is a real physical effect.

Upon examination of the SIMS profiles, no systematic difference on the sputtering rates and Te intensities was detected between the two orientations. We have also grown two layers on a CdTe (111)*B* and a CdTe(100) substrate, respectively, using the same indium cell temperature. SIMS measurements on these two layers gave basically the same

indium atomic concentrations. (The difference is less than 10%.) The above observations rule out the probability that the SIMS measurement on these two orientations have a significant orientation dependence.

The behavior described above undoubtedly indicates that the indium in (100) MCT is at least doubly ionized. This experimental observation suggests that indium might be incorporated interstitially in MCT crystals. Regarding the *n*-type behavior of MCT in the (100) orientation as pointed out before, we suggest the following model. We believe that Te atoms are filling enough metal vacancies to convert the MBE epilayer to *n* type. These antisite Te atoms are actually acting as donors, which explains the *n*-type behavior. Under this circumstance, the additional incoming In atoms have to take the interstitial sites. The smaller surface atomic density in the (100) direction, as compared to that in the (111)*B* direction, may enhance this trend. Since the distance between an interstitial atom and the neighboring lattice sites is shorter than that between a substitutional atom and the neighboring lattice sites, we should expect that the screening effect due to the electron clouds of neighboring lattice atoms is stronger for an interstitial atom.<sup>8</sup> The relatively weaker binding energy in the interstitial sites does allow the In atoms to be at least doubly ionized. Consequently, the electron carrier concentrations listed in Table I are greater than  $2N_{\text{In}}$ .

Another interesting point can be noted from further inspection of Table I. The electron Hall mobilities of the In-doped (100) layers are slightly higher than those of the (111)*B* layers, even though higher than singly ionized scattering centers should be expected in the former case. We believe that this discrepancy is mainly due to the scattering by twin defects which are often observed during the growth along the (111)*B* direction.

A typical SIMS profile of an In-doped (100) MCT layer grown by MBE is shown in Fig. 1. The MCT:In/CT interface is visible. The In transition at the interface is as sharp as those of Cd and Hg. A slight accumulation of indium atoms at the interface is also visible, which is not observed in the layers grown in the (111)*B* orientation (see Fig. 2). We speculate that this character is somehow related to the interstitial mechanism of indium incorporation in MCT grown in

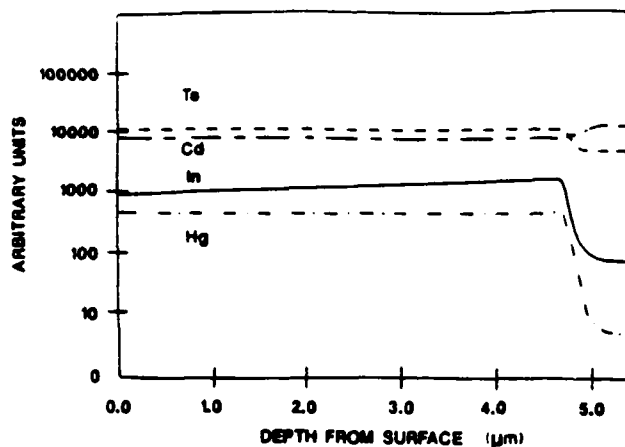


FIG. 1. SIMS profile of an In-doped (100) MCT grown by MBE.

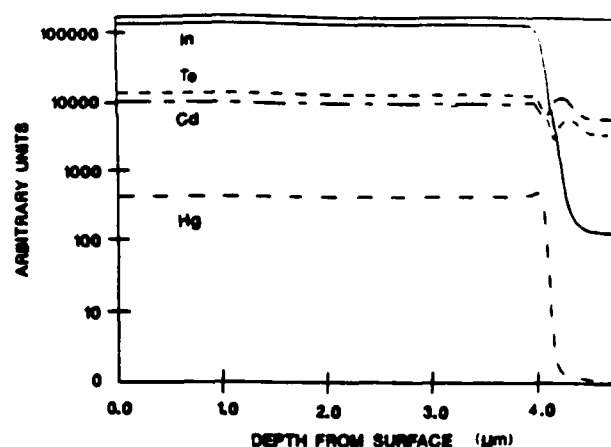


FIG. 2. SIMS profile of an In-doped (111)B MCT grown by MBE.

the (100) orientation. Indium diffusion experiments are currently under way. The preliminary results confirm that indium is incorporated differently in the (111)B and (100) orientations. We expect that further information about the orientation dependence of indium incorporation will be available through this study.

In conclusion, indium has been incorporated as a donor during MBE growth of MCT in the (100) orientation. As compared to the (111)B orientation, Hall and SIMS measurements have shown that indium in the (100) MCT layer is at least doubly ionized. This is true at least for  $N_{In}$  below  $1 \times 10^{17} \text{ cm}^{-3}$ . We believe that most of the In atoms are triply ionized and incorporated interstitially in MCT. The other In atoms could be singly ionized in substitution on the metal site vacancies not already filled by the Te atoms like in the (111)B direction. Such an incorporation mechanism of indium supports a Te antisite model for explaining the favorable  $n$ -type behavior on (100) MCT grown by MBE. It also agrees with the growth in the (100) direction occurring under Te-rich conditions like in the (111)B direction.<sup>2</sup> These results imply that foreign dopants, in general, should be incorporated interstitially at least to some significant extent in the (100) orientation. We think that interstitial doping by MBE in the (100) orientation might present serious limitation for its future electronic applications. These results are extremely important for the fabrication of MCT devices in-

volving doping application in general, since it indicates that the orientation might play a very important role.

The authors would like to thank Z. Ali and S. Farook for their technical assistance and the Defense Advanced Research Projects Agency for its financial support under contract F49620-87-C-0021 monitored by the Air Force Scientific Office for Research.

<sup>1</sup>J. P. Faurie, A. Million, R. Boch, and J. L. Tissot, *J. Vac. Sci. Technol. A* 1, 1593 (1983).

<sup>2</sup>M. Boukerche, P. S. Wijewarnasuriya, S. Sivananthan, I. K. Sou, Y. J. Kim, K. K. Mahavadi, and J. P. Faurie, *J. Vac. Sci. Technol. A* 6, 2830 (1988).

<sup>3</sup>J. P. Faurie, HgCdTe Molecular Beam Epitaxy Workshop, Defense Advanced Research Projects Agency, Center for Night Vision and Electro-Optics, Washington, 1987 (unpublished results).

<sup>4</sup>M. Boukerche, J. Reno, I. K. Sou, C. Hsu, and J. P. Faurie, *Appl. Phys. Lett.* 48, 1733 (1986).

<sup>5</sup>H. R. Vydyanath, *J. Electrochem. Soc.* 128, 2619 (1981).

<sup>6</sup>M. Boukerche, S. Sivananthan, P. S. Wijewarnasuriya, I. K. Sou, and J. P. Faurie, *J. Vac. Sci. Technol. A* 7, 311 (1989).

<sup>7</sup>M. D. Langa, S. Sivananthan, X. Chu, and J. P. Faurie, *Appl. Phys. Lett.* 52, 978 (1988).

<sup>8</sup>C. G. Morgan-Pond and R. Raghavan, *Phys. Rev. B* 31, 6616 (1985).

### III-2-2 P-TYPE DOPING

#### III-2-2-1 GROUP I ELEMENT: LITHIUM

Hg vacancies are easily formed in HgCdTe, therefore a Group I Element which should be a substitute to Hg should be appropriate as a p-type dopant. Lithium has been incorporated in MCT layers during MBE growth. We have demonstrated that Li behaves as a p-type dopant in MBE grown  $\text{Hg}_{1-x}\text{Cd}_x\text{Te}(100)$ . This represents the first successful attempt to incorporate electrically active acceptors during MBE growth. These Li-doped MCT layers have been estimated to have very shallow acceptor levels. The calculated activation energy was 8.3meV. Using Li as a p-type dopant, carrier concentrations up to  $8 \times 10^{18}\text{cm}^{-3}$  have been achieved. At low doping levels, layers show compensation due to the residual donors from stoichiometry deviation. The doping level in the samples can be controlled by varying the Li cell temperature. An incorporation coefficient of 1 and almost 100% electrical efficiency for Li in MBE grown MCT layers were observed.

In order to investigate the diffusivity of Li, a sample consisting of a nondoped MCT layer (0.93 $\mu\text{m}$  thick) on top of a Li-doped MCT layer (0.93 $\mu\text{m}$  thick) has been grown. From the SIMS profile of this sample, Li can be seen in the undoped layer in amounts comparable to that in the intentionally doped one. This indicates that Li is highly mobile in MCT layers grown by MBE. At this point, we have no evidence from SIMS data that Li is diffusing in CdTe buffer layer and substrate.

In addition, some layers tested by Hall several months after growth appeared to have been n-type converted which confirms the high diffusivity of Li even at room temperature. This obviously comprises any electronic device application.

#### ATTACHED PAPER:

1. "Electrical properties of Li-doped  $\text{Hg}_{1-x}\text{Cd}_x\text{Te}(100)$  by molecular beam epitaxy"

# Electrical properties of Li-doped $\text{Hg}_{1-x}\text{Cd}_x\text{Te}(100)$ by molecular beam epitaxy

P. S. Wijewarnasuriya, I. K. Sou, Y. J. Kim, K. K. Mahavadi, S. Sivananthan, M. Boukerche, and J. P. Faurie

Department of Physics, University of Illinois at Chicago, Chicago, Illinois 60680

(Received 1 July 1987; accepted for publication 12 October 1987)

*p*-type doping of  $\text{HgCdTe}(100)$  layers with lithium during growth by molecular beam epitaxy is reported. Hall measurements have been performed on these layers between 300 and 30 K. The Li concentration is found to increase with the Li cell temperature. Li-doped  $\text{HgCdTe}$  layers are estimated to have very shallow acceptor levels. Acceptor concentrations as high as  $8 \times 10^{18} \text{ cm}^{-3}$  have been achieved. At low doping levels, due to residual donors, layers show compensation. Incorporation coefficient of Li close to 1 and almost 100% electrical efficiency for Li in molecular beam epitaxy  $\text{HgCdTe}$  layers were observed. However, Li is found to diffuse rapidly in  $\text{HgCdTe}$  layers grown by molecular beam epitaxy.

Over the past ten years  $\text{Hg}_{1-x}\text{Cd}_x\text{Te}(\text{MCT})$  has emerged as an important material for infrared (IR) detector technology. MCT was grown by molecular beam epitaxy (MBE) on CdTe substrates for the first time in 1981.<sup>1</sup> Since then, this technique has produced MCT layers of either *n* or *p* type and of a quality comparable to the layers grown by other techniques. However, very little information exists on the incorporation of foreign elements in MBE grown epitaxial layers. Recently, successful *n*-type doping of MCT layers with indium during growth by MBE was reported.<sup>2</sup> Carrier concentrations of two orders of magnitude more than what can be achieved by stoichiometry deviation have been reached for MBE layers grown in the (111)*B* orientation. Antimony and arsenic (group V elements) act as *p*-type dopants in MCT using other growth techniques<sup>3</sup> such as liquid phase epitaxy. But in the case of MBE grown MCT layers, both Sb and As behave as *n*-type dopants.<sup>4</sup> In the case of (100) orientation only *n*-type MCT with doping levels ranging from  $10^{15}$  to mid- $10^{16} \text{ cm}^{-3}$  can easily be produced by stoichiometry deviation for  $x < 0.35$ . *p*-type (100) is difficult to achieve for  $x < 0.24$ .<sup>5</sup> Therefore, in order to obtain *p*-type MCT layers in the (100) orientation, incorporation of foreign elements in group I was studied. Li behaves as a *p*-type dopant, as expected. Here, we report results on Li, the first impurity successfully incorporated as an electrically active acceptor in MBE grown MCT layers.<sup>6</sup> In this letter, we present electrical properties of lithium-doped MCT(100) MBE layers studied by variable temperature Hall measurements.

MCT layers were grown in a Riber 2300 MBE machine which is designed to handle mercury. MCT layers were grown on 2–3  $\mu\text{m}$  thick CdTe buffer layers which were deposited on GaAs(100)-substrates. The growth was monitored by reflection high-energy electron diffraction (RHEED). The growth rate was 4–5  $\text{\AA}/\text{s}$ . Li was provided by a separated effusion cell loaded with pure Li. Since it is a very reactive material, great care has been taken when loading it into the growth chamber. This was done in an inert atmosphere. The Li cell temperature range was 205–280  $^{\circ}\text{C}$ . The Cd composition in the MCT layers was determined at room temperature by infrared transmission measurements and by energy dispersive spectroscopy measurements. The

secondary ion mass spectroscopy (SIMS) technique was used to obtain the concentration profile of Li atoms through the layers. Since we did not have a standard sample containing Li, we were not able to relate the number of counts from the SIMS to the actual Li concentration. Therefore, all SIMS data are given in arbitrary units, but a relative comparison is significant. The carrier concentration and the Hall mobility in the layers were evaluated by the Van der Pauw technique<sup>6</sup> between room temperature and 30 K. A AuCl<sub>3</sub> solution was used to form ohmic contacts, and the ohmicity of the contacts was checked systematically. A magnetic field strength of 2000 G was used for the Hall measurements.

Electrical measurements of the Li-doped MCT layers at 40 K are summarized in Table I. Figure 1 shows the variation of the carrier concentration (deduced from the Hall coefficient) versus  $1000/T(\text{K})$  for three samples. A typical freeze-out behavior cannot be seen for the larger doping levels. This happens even with mid  $10^{17}$  doping levels and above. Such an effect has been reported previously for phosphorus.<sup>7</sup> Furthermore, it can be seen from the figure that the mixed conduction *n* → *p* transition region diminishes when the doping level increases. For the higher doping levels, the carrier concentration is independent of temperature, indicating that electrically active acceptors are completely ionized. The total amount of electrically active Li concentration in the samples was determined from the low-temperature carrier concentration data.

The only layer (sample No. 1) which shows the freeze-out behavior has been analyzed numerically<sup>8</sup> using the charge neutrality equation:

$$n + N_a^- = p + N_d^+,$$

where *n*, *p*,  $N_d^+$ , and  $N_a^-$  are the concentration of electrons, holes, ionized donors, and ionized acceptors, respectively. For the donors, complete ionization is assumed and the concentration of ionized acceptors is given by

$$N_a^- = \frac{N_a}{1 + 4 \times \exp(x_a - \eta_f)},$$

where  $x_a$  is the reduced acceptor level with respect to valence band and  $\eta_f$  is the reduced Fermi level.

TABLE I. Electrical measurements of lithium-doped MCT at 40 K. Samples No. 1 and No. 2 represent *n*-type MBE grown MCT.

Sample No.	Thickness ( $\mu\text{m}$ )	Cd composition (%)	$N_a - N_d$ ( $\times 10^{18} \text{ cm}^{-3}$ )	Mobility at 40 K ( $\text{cm}^2/\text{V s}$ )	Li cell temp ( $^\circ\text{C}$ )
1	1.68	25	+ 0.84	370	205
2	1.38	17	+ 52.00	360	219
3	2.16	20	+ 200.00	330	245
4	2.18	23	+ 800.00	330	282
5	1.92	21	+ 440.00	340	270
6	1.00	20	- 1.00	$3.0 \times 10^3$	
7	6.20	19	- 1.00	$2.4 \times 10^3$	

From the Kane model<sup>9</sup> for nonparabolic bands,

$$n = \frac{K_B T}{2\pi^2} \left( \frac{3}{2P^2} \right)^{3/2} \int_0^\infty \frac{x^{1/2} (x + x_g)^{1/2} (2x + x_g)}{1 + \exp(x + x_g - \eta_f)} dx,$$

where  $P$  is the momentum matrix element of the Kane model and  $x_g$  is the reduced energy gap. For the band gap  $E_g$ , an empirical equation is used from Ref. 10. Since the equilibrium concentration of light hole is negligible,  $p$  is the heavy-hole concentration. Parabolic band with Fermi-Dirac statistics is assumed for the heavy holes. Since the mixed conduction dominates at high temperature, the concentration is deduced from the following equation:

$$c.c. = (p + nb)^2 / (p - nb^2),$$

where  $b$  is the ratio of electron-to-hole mobility and is given by

$$b = \mu_e / \mu_h = \tau m_h^* / m_e^*,$$

where  $m_e^* = 3 \hbar^2 E_g / 4P^2$ ,  $m_h^* = 0.63 m_e$ ,<sup>11</sup> and  $P = 8 \times 10^{-8} \text{ eV cm}$ .<sup>11</sup> When calculating,  $N_a$ ,  $N_d$ ,  $\tau$ , and  $E_g$  were adjusted to give the best fit for the experimental carrier concentration data. The solid line in Fig. 1 is the best fit. It was obtained with  $N_a = 1.89 \times 10^{16} \text{ cm}^{-3}$ ,  $N_d = 1.05 \times 10^{16} \text{ cm}^{-3}$ ,  $\tau = 0.24$ ,  $E_g = 8.3 \text{ meV}$ , and Cd composition = 25.8%.

Figure 2 shows mobility versus doping concentration at 40 K. It can be seen that the hole mobility in the Li-doped

samples at 40 K does not vary drastically with the hole concentration. Doping levels as high as  $8 \times 10^{18} \text{ cm}^{-3}$  were achieved. At low doping levels, experimental results indicate a large degree of compensation in the layers, since along the (100) growth orientation, only *n*-type MBE grown MCT(100) layers are currently achieved by stoichiometry adjustment (see Table I). This large degree of compensation accounts for the limitation of the hole mobility at low doping levels.

Figure 3 shows the concentration of Li atoms in the MCT layers calculated from the incident flux and from growth rate (assuming unity sticking coefficient) versus  $1000/T(\text{K})$ , where  $T$  is the Li cell temperature. The carrier concentration  $N_a - N_d$  (extracted from Hall measurements) and the SIMS Li counts are also plotted in Fig. 3. By comparing the concentration of electrically active Li atoms in the layers from Hall measurements and the concentration of Li atoms incorporated into layers calculated from the incident flux, it can be seen that there is good agreement within the experimental error. At this range of doping levels,  $N_a - N_d$  extracted from Hall measurements is approximately equal to the acceptor concentration  $N_a$ , since residual donor concentration is of the order of  $10^{16} \text{ cm}^{-3}$ . Therefore, this agreement is an indication that almost 100% of the Li is electrically efficient, and also that the incorporation of Li in MBE grown MCT layers is close to 1. As can be seen from Fig. 3, the SIMS data fall on a straight line, indicating that the number of Li atoms incorporated into the samples de-

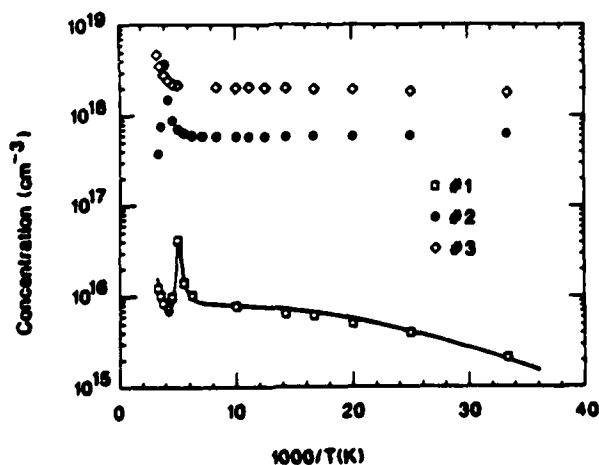


FIG. 1. Hole concentration as a function of  $1000/T(\text{K})$  for lithium-doped MCT layers grown by MBE. The solid line for sample No. 1 is the best fit obtained for the following parameters:  $N_a = 1.89 \times 10^{16} \text{ cm}^{-3}$ ,  $N_d = 1.05 \times 10^{16} \text{ cm}^{-3}$ ,  $\tau = 0.24$ , and  $E_g = 8.3 \text{ meV}$ .

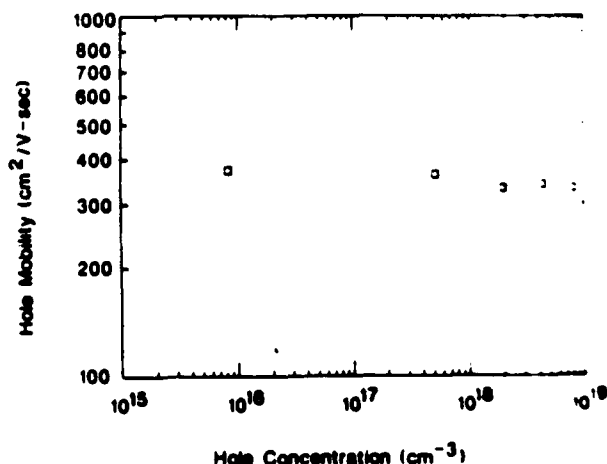


FIG. 2. Experimental hole mobility at 40 K as a function of the hole concentration for lithium-doped MCT layers.

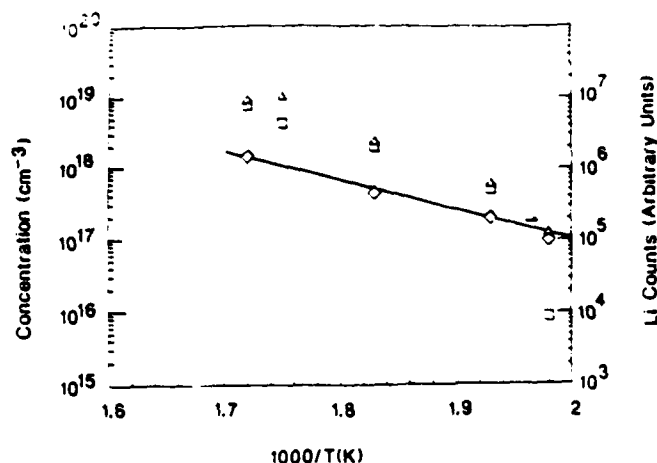


FIG. 3. Li counts ( $\diamond$ ) obtained by SIMS in the layers,  $N_a - N_d$  ( $\text{cm}^{-3}$ ) from Hall measurements ( $\square$ ) and Li concentration ( $\text{cm}^{-3}$ ) calculated from the incident flux ( $\triangle$ ) vs reciprocal of the Li cell temperature.

creases exponentially with the reciprocal of the Li cell temperature. Sample No. 1, which has the lowest Li cell temperature, exhibits a large discrepancy between Li concentration as calculated from the incident flux and as measured from Hall measurements. This discrepancy is due to the compensation in the layers because the level of electrically active impurities (Li) is not much larger than the intrinsic donors.

In order to investigate the diffusivity of Li, a sample consisting of a nondoped MCT layer ( $0.93\text{ }\mu\text{m}$  thick) on top of a Li-doped MCT layer ( $0.93\text{ }\mu\text{m}$  thick) has been grown. From the SIMS profile of this sample, Li can be seen in the undoped layer in amounts comparable to that in the intentionally doped one. This indicates that Li is highly mobile in MCT layers grown by MBE. At this point, we have no evidence from SIMS data that Li is diffusing in CdTe buffer layer and substrate.

In conclusion, we have demonstrated that Li behaves as

a  $p$ -type dopant in MBE grown  $\text{Hg}_{1-x}\text{Cd}_x\text{Te}$  (100). This represents the first successful attempt to incorporate electrically active acceptors during MBE growth. These Li-doped MCT layers have been estimated to have very shallow acceptor levels for sample No. 1, which showed the freeze-out. The calculated activation energy was 8.3 meV. Using Li as a  $p$ -type dopant, carrier concentrations up to  $8 \times 10^{18}\text{ cm}^{-3}$  have been achieved. At low doping levels, layers show compensation due to the residual donors from stoichiometry deviation. The doping level in the samples can be controlled by varying the Li cell temperature. An incorporation coefficient of 1 and almost 100% electrical efficiency for Li in MBE grown MCT layers were observed. However, the SIMS profile indicates that Li is highly mobile in MCT layers. This represents a limitation in the use of this element, especially for abrupt heterojunctions.

We wish to acknowledge G. Monfroy for performing the energy dispersive spectroscopy measurements for some of the samples, and Z. Ali and A. Farook for their technical assistance. This work was funded by the Defense Advanced Research Project Agency and monitored by the Air Force Office for Scientific Research under contract No. F49620-87-C-0021.

<sup>1</sup>J. P. Faurie and A. Million, *J. Cryst. Growth* **54**, 582 (1981).

<sup>2</sup>M. Boukerche, J. Reno, I. K. Sou, C. Hsu, and J. P. Faurie, *Appl. Phys. Lett.* **48**, 1733 (1986).

<sup>3</sup>P. Capper, *J. Cryst. Growth* **57**, 280 (1982).

<sup>4</sup>J. P. Faurie, DARPA II- VI Materials & Processing Conference, Washington, April 1987 (unpublished results).

<sup>5</sup>J. M. Arias, S. H. Shin, J. T. Chen, S. Sivananthan, J. Reno, and J. P. Faurie, *J. Vac. Sci. Technol. A* **5**, 3133 (1987).

<sup>6</sup>L. J. van der Pauw, *Philips Tech. Rev.* **20**, 220 (1958).

<sup>7</sup>H. R. Vydyanth, R. C. Abbot, and D. A. Nelson, *J. Appl. Phys.* **54**, 1323 (1983).

<sup>8</sup>M. Boukerche, P. S. Wijewarnasuriya, J. Reno, I. K. Sou, and J. P. Faurie, *J. Vac. Sci. Technol. A* **4**, 2072 (1986).

<sup>9</sup>E. O. Kane, *J. Phys. Chem. Solids* **1**, 249 (1957).

<sup>10</sup>E. Finkman and S. E. Schacham, *J. Appl. Phys.* **56**, 2896 (1984).

<sup>11</sup>E. Finkman, *J. Appl. Phys.* **54**, 1883 (1983).

## III-2-2-2 GROUP V ELEMENTS: ARSENIC-ANTIMONY

## 1. As doping: Photo assisted MBE growth

It has been previously been shown that under regular MBE growth conditions As and Sb are incorporated as donors in HgCdTe. Exposure to a U.V. Xenon Lamp of 1kW increased the  $N_D-N_A$  level when As was used.

However, report it was not concluded that As or Sb cannot be incorporated as p-type dopants in MBE grown layers. But it was clear that it was not a problem easy to solve. In order to find out the proper conditions to incorporate, if possible, the As in the p-type site a Nd-YAG pulsed laser operating at  $0.523\mu\text{m}$  was used during the growth process.

Numerous experiments were carried out. For the sake of clarity only some of them are reported in Table I.

TABLE I  
Photo assisted MBE growth  
Nd: YAG LASER - Green light  
Growth Temperature

Sample	x	t( $\mu\text{m}$ )	Growth rate layer HgTe CdTe			cc( $\text{cm}^{-3}$ )	Laser power mw/ $\text{cm}^2$	T <sub>As</sub>
CZT48HCT659	.245	2.57	7.14	5.39	1.75	$n-9.10 \times 10^{18}$	160	150
CZT49HCT660	.240	2.58	7.17	5.45	1.72	$n-2.80 \times 10^{18}$	0	150
CZT50HCT661	.300	2.18	6.06	4.25	1.81	$n-1.12 \times 10^{18}$	500	175
CZT52HCT663	.230	---	---	---	---	$n-3.50 \times 10^{18}$	0	175
CZT51HCT662	.280	2.25	6.25	4.50	1.75	$n-2.65 \times 10^{18}$	500	150
CT277HCT685	.260	2.94	6.53	4.84	1.69	$n-1.22 \times 10^{18}$	0	125
CZT69HCT686	.270	3.02	6.71	4.90	1.81	$n-1.45 \times 10^{18}$	25	125
CT278HCT687	.265	3.02	6.71	4.92	1.79	$n-7.24 \times 10^{18}$	50	125

From Table I it is clear that with or without the laser light during MBE growth As behave as a donor in HgCdTe layers. In fact, with the laser it has been observed a decrease of the Hg sticking coefficient. At low power the Hg vacancy

density increases, which enhances the p-type character. At high power, not only the stoichiometry but also the composition  $x$  changes. In the presence of arsenic during growth the n-type character observed without light in the (111)B orientation is in fact enhanced because more Hg vacancies are available for As atoms.

These experiments, however, cannot completely rule out the possibility of incorporating As in the right site. A lower growth temperature, a higher Hg flux, a different crystallographic orientation or a different laser (cw for example) have to be investigated before making any definite conclusion.

From the work achieved in the Microphysics Laboratory and in other institutions it appears that p-type doping is not yet under control in MBE grown MCT layers. Isothermal annealings at temperatures between 200 and 350°C also kept the samples n-type showing that the doping mechanism was stable.

## IV HOMOJUNCTIONS AND HETEROJUNCTIONS GROWN IN SITU

### IV-1 HETEROJUNCTIONS

Isotype n-N abrupt heterojunctions were grown in situ by MBE on CdTe(-111)//GaAs(100) combination substrates. The first devices tested had  $x = .18$  on the bottom and  $x = .26$  on the top. All the electrical and optical characterizations were consistent with the presence of narrow and strong composition burst right at the interface. The  $R_0A$  was limited by the wide-gap side (see attached publication #1

The later devices grown with care to avoid the problem had drastically different behavior. The compositions were slightly higher on both sides:  $x = .22$  for the bottom and  $.28$  for the top. Strong rectification was seen with quality factors varying from 2 at high temperatures to 2.5 at 80K. The forward bias occurred when the top material was biased negatively. One device had an  $R_0A$  as high as  $10^4 \Omega\text{cm}^2$  at 80K, but this value was only seen once. In the average it typically reaches  $10^3$  at 80K. The activation energy of  $I_0/T^2$  varies from .1eV at high temperature to .06eV at 80K. The spectral response shows a maximum at 8 $\mu\text{m}$  wavelength, without sharp peak at short wavelength as before. The capacitance measurements are unreliable since the top material thickness was as small as .5 $\mu\text{m}$ , and the top contact is suspected to have a smaller area than expected. A low current density  $10^{-2}\text{A}/\text{cm}^2$  can blow the devices open. These measurements are consistent with a Schottky type behavior at the heterojunction, most of the depletion occurring in the wide bandgap material, which is limiting the  $R_0A$ . Thermionic emission is not the only process involved in the transport since the quality factor is higher than 2. This renders the barrier height determination unreliable, even if it seems consistent with the expected bandgap difference between the two sides.

Unfortunately, the device performed like a metal semiconductor Schottky diode where the metal would be the degenerate narrow-bandgap material. A low quantum efficiency is expected from such a device.

#### ATTACHED PAPERS:

1. "Mercury cadmium telluride n-isotype heterojunctions grown in situ by molecular beam epitaxy."

2. "Mercury cadmium telluride junctions grown by molecular beam epitaxy"

# Mercury cadmium telluride *n*-isotype heterojunctions grown *in situ* by molecular-beam epitaxy

M. Boukerche, I. K. Sou, M. DeSouza, S. S. Yoo, and J. P. Faurie  
Department of Physics, University of Illinois at Chicago, Chicago, Illinois 60680

(Received 10 November 1986; accepted 7 May 1987)

Electrical characterizations of the first *n*-*N* HgCdTe heterojunctions grown *in situ* by molecular-beam epitaxy are reported. The cadmium concentrations of the two materials are 0.18 for the bottom layer and 0.26 for the top. The measurements by Hall, *IV*, *CV*, and spectral responsivity are consistent with the existence of a conduction-band barrier at the interface behaving as an insulator at low temperature. We suggest that transient effusion cell fluxes occurring during shutter sequencing created such barriers at the heterojunction interfaces during the growth. The high  $R_0A$  ( $600 \Omega \times \text{cm}^2$ ) measured suggests that this effect might be of interest for future heterojunction gate field-effect transistor investigations.

## I. INTRODUCTION

The  $\text{Hg}_{1-x}\text{Cd}_x\text{Te}$  (MCT) ternary alloy is currently the most important material for infrared applications in the 8–12  $\mu\text{m}$  wavelength range. It is also used for the 3–5  $\mu\text{m}$  window and considered for the optoelectronic range. This material can be grown for any cadmium composition  $x$  between 0 and 1, and can then be considered as a solid solution. The corresponding forbidden energy gap can be varied continuously between  $-0.22$  and  $1.6$  eV at 80 K. These unique properties plus the fact that the lattice mismatch between the extreme compositions is only 0.3% make this ternary semiconductor material very attractive for heterojunction investigations. The main motivation for such studies is to improve existing detector performances by tailoring wavelength response, decreasing parasitic currents, and increasing minority-carrier collection efficiencies.

LoVecchio *et al.*<sup>1</sup> studied the case of back-to-back MCT ( $x = 0.2$ )/CdTe heterojunctions. They concluded that a valence-band barrier was present in the devices. *n/p* MCT heterojunction photovoltaic devices were demonstrated by Bratt.<sup>2</sup> In certain cases, barrier formation was also reported.

Both groups used the liquid phase epitaxy (LPE) growth technique and reported substantial grading and/or diffusion at the interfaces. Vydyanath *et al.*<sup>3</sup> showed that such effects could actually be profitable since they presented exceptional LPE grown MCT heterojunction detector performances.

The possibility of including semimetallic, semiconducting, and semi-insulating materials within the same monocrystal could lead to important technological applications. The abrupt heterojunctions between these materials have to be further studied.

Kuech and McCaldin<sup>4</sup> reported characterizations of HgTe layers grown by the metalorganic chemical vapor deposition technique at 325–350 °C on *n*-type CdTe. A Schottky barrier behavior was seen, with a maximum barrier height of 0.92 eV.

The validity of the common anion rule for the HgTe/CdTe system has been questioned recently.<sup>5</sup> The reported values of the valence-band offset vary from 40 meV (Ref. 6) to 350 meV<sup>7,8</sup> depending on the technique used. The above workers<sup>4</sup> mention that inversion in the CdTe lay-

er could explain their low barrier height value. We suggest that interdiffusion effects might have played an important role. In any case, most of the band-gap difference should appear in the conduction-band discontinuity.

The molecular-beam epitaxy (MBE) technique is now recognized as a possible choice for the growth of MCT on CdTe and GaAs.<sup>9,10</sup> Its low growth temperature (190 °C) minimizes the interdiffusion effects and allows abrupt interfaces to be produced in thin epitaxial layers like superlattices. Several abrupt *n*-isotype heterojunctions between two narrow-band-gap compositions were grown for the first time in order to observe the transport properties of the electrons through the expected conduction-band discontinuity on the wide-band-gap side. We present here the characterization of mesa devices fabricated from these first samples.

## II. EXPERIMENTAL

The junctions were grown on CdTe(111)//GaAs(100) substrates with a Riber 2300 system modified to handle mercury. Both sides of the junction were doped *n* type with indium as previously described.<sup>11</sup> The narrow-gap side was first made with a thickness of 2 to 3  $\mu\text{m}$  before the growth conditions were abruptly changed to produce the wide-gap material up to a thickness of 1.0  $\mu\text{m}$ . The substrate temperature was kept at 190 °C all along the growth. The composition of the narrow gap was determined by infrared transmission measurements at room temperature. Its doping level  $4 \times 10^{16} \text{ cm}^{-3}$  was deduced from the Hall measurements neglecting the contribution of the wide-gap side. This was relevant since the doping level was intentionally lowered during the growth of the  $x = 0.26$  material. The composition and doping ( $\sim 5 \times 10^{15} \text{ cm}^{-3}$ ) of the top layer was estimated from the growth conditions on separate runs. To check the doping level, metal-insulator-semiconductor (MIS) structures were fabricated with gold and zinc sulfide on a different piece of the sample. The high-frequency capacitance versus voltage curves were measured at 80 K and 100 kHz with an LCR 4275 from Hewlett-Packard. The classical MIS calculation<sup>12</sup> was used to deduce the impurity level from the minimum to maximum capacitance ratio, where the minimum capacitance was calculated using the approximation of Ref.

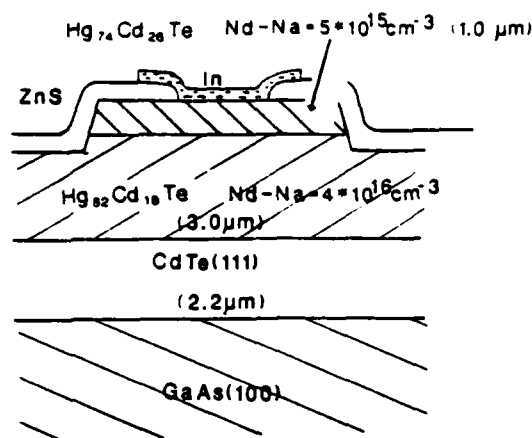


FIG. 1. Structure of the devices.

19. The doping level deduced was within a factor of 2 from the growth estimated value. The devices were made by standard photolithographic techniques and mesa etching. The metal was evaporated over the zinc sulfide passivation opened for contacts. Their structure can be seen in Fig. 1. The geometry is circular to minimize edge leakage but is obviously not optimized for detection applications. The junction area is  $7 \times 10^{-4} \text{ cm}^2$ . More than 150 dots were tested from 300 down to 80 K with a microprobe station from MMR Technologies, Inc. The probe connected to the top contact was positioned on the metal part overlapping the zinc sulfide to avoid piezoelectric effects. The current versus voltage measurements were made with an electrometer/voltage source model 617 from Keithley, modified to generate 5-mV steps. All the data acquisition was computerized.

### III. RESULTS

The current versus voltage curves measured can be seen in Fig. 2. They are representative of the average of the devices measured. Very weak forward rectification occurs when the top wide-band-gap material is biased negatively. They could

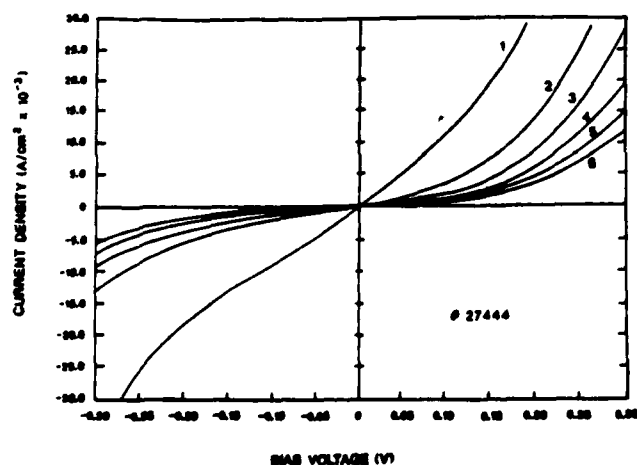


FIG. 2. Current/voltage curves vs temperature. Positive voltages correspond to negative bias on the top material. Temperatures: curve 1: 235 K, 2: 169 K, 3: 132 K, 4: 109 K, 5: 92 K, and 6: 80 K.

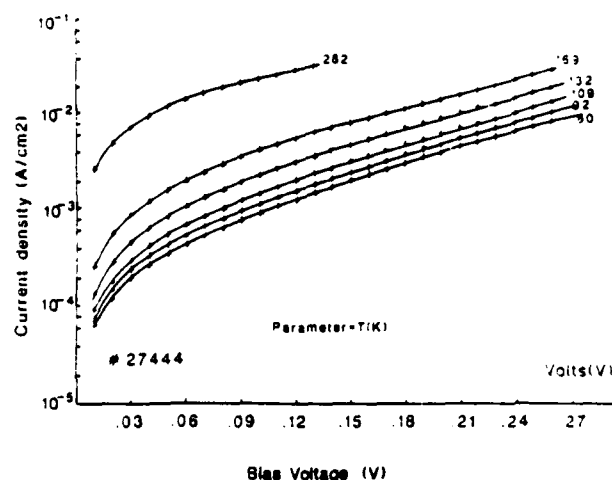


FIG. 3. Semilog plot of the  $I/V$  curves when the top material is biased negatively.

be simply described as showing double soft reverse breakdown at low temperature. The current is proportional to the voltage at low bias, and tends to a power of the voltage law (2–3) above 50–100 mV. A semilogarithmic plot of these curves is shown in Fig. 3 for the forward bias case. Notice that their slopes are nearly independent of temperature. The  $R_0A$  values could reach  $600 \Omega \text{ cm}^2$  at 80 K on several devices, showing that the active part of the device is on the wide-band-gap side. Its variation as a function of  $1/T$  can be seen in Fig. 4 in reverse bias. At high-temperature it follows an exponential law in a limited range only, and tends to saturate at low temperature. The corresponding high-temperature activation energies are systematically higher in reverse bias ( $\sim 105 \text{ meV}$ ) than in forward bias ( $\sim 80 \text{ meV}$ ). The  $I/V$  curves were fitted by the least-square method to the equation

$$I = I_s \{ \exp[(V - IR_s)/V_0] - 1 \}, \quad (1)$$

where  $I$  is the current density,  $I_s$  the saturated current den-

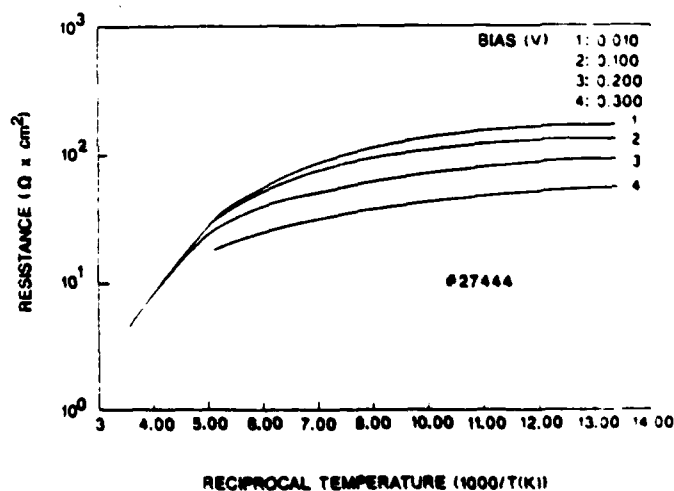


FIG. 4. Variation of the dc resistance of the device with reciprocal temperature.

sity,  $V$  the bias voltage,  $R_s$  the series resistance, and  $V_0$  the voltage defining the slopes of the curves. The precision of the parameters extracted was only questionable close to room temperature where the devices showed an ohmic behavior. Below 150 K,  $V_0$  was found constant and equal to 145 and 80 mV in reverse and forward bias, respectively, and  $R_s$  was negligible.  $V_0$  was increasing with temperature above 150 K.

A typical capacitance versus voltage curve is shown in Fig. 5. It clearly does not follow the classical Schottky diode depletion model but rather a metal-insulator-semiconductor device behavior. The frequency dependence is small. The admittance curves correlate the slope variation of the dc current/voltage measurements.

#### IV. DISCUSSION

The lack of strong rectification implies that thermionic emission is negligible. The current transport is limited by some form of tunneling since it varies as  $\exp(V/V_0)$  independently of temperature below 150 K. These properties are systematic for all the devices on several crystals, and are not resulting from a marginal contact process on the top contact which could create back-to-back Schottky diodes randomly. Furthermore, a sharp minimum in capacitance close to zero bias should be seen in this case.<sup>13</sup> Schottky barrier lowering with biasing voltage is not detected since the current should vary as  $\exp(\alpha V^{1/4}/T)$ ,<sup>12</sup> and  $V_0$  should be a function of temperature even at 80 K.

These results have similarities with the theory of thermionic field emission across Schottky barriers (TFS).<sup>14</sup> The ratio  $kT/E_0$  is an estimation of the relative importance of the thermionic and field emission processes,<sup>15</sup> where  $k$  is the Boltzmann constant,  $T$  the absolute temperature, and  $E_0$  an energy defined as

$$E_0 = (qh/4\pi)(N_D/m^*\epsilon)^{1/2}, \quad (2)$$

where  $q$  is the electronic charge,  $h$  the Planck's constant,  $N_D$  the donor concentration in the semiconductor (in our case the wide-band-gap side with  $x = 0.26$ ),  $m^*$  and  $\epsilon$  the electron effective mass and the static dielectric constant in the same material. When  $kT \gg E_0$  the current is mainly due to

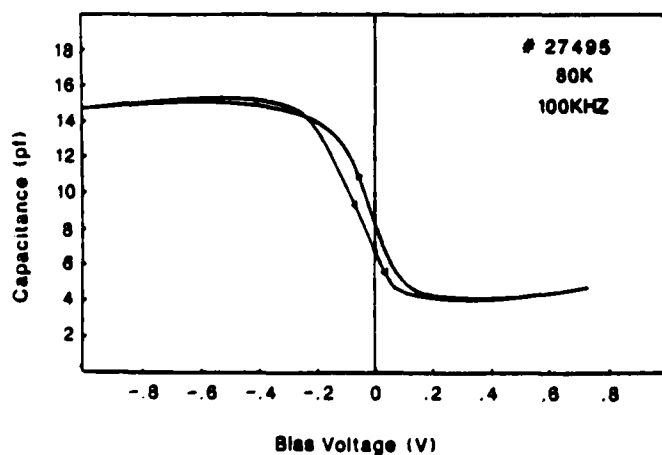


FIG. 5. High-frequency capacitance/voltage curve at low temperature. Positive voltages correspond to positive bias on the top material.

thermionic emission. When  $kT \ll E_0$  field emission (or tunneling from energies close to the conduction band) is the dominant transport mechanism. Both types of electron emission have to be considered when  $kT \approx E_0$ . In our case  $N_D \approx 5 \times 10^{15} \text{ cm}^{-3}$ , and for  $x = 0.26$  at  $T = 80 \text{ K}$ , the relative electron effective mass and dielectric constant are taken, respectively, as  $1.4 \times 10^{-2}$  and 16.9. The value of  $E_0$  is then 2.66 meV, much smaller than  $kT = 6.9 \text{ meV}$ . The fact that thermionic conduction is not seen in forward bias, together with the capacitance measurements results, make us conclude that a large conduction-band barrier is present at the heterojunction between the two materials. This is in agreement with the spectral response measured on one device in small reverse bias at 80 K, showing a wide response in the 3–6  $\mu\text{m}$  range and a peak more than three times higher in amplitude at 1.9- $\mu\text{m}$  wavelength. The root square of the photoresponse is shown versus wavelength in Fig. 6. The low-energy tail was close to the noise floor and was separated from the response of the  $x = 0.26$  material by more than 1  $\mu\text{m}$ . The measurement was made under vacuum with a glow bar infrared source, a monochromator, and a lock-in amplifier. The curve was corrected for blackbody radiation and grating dispersion. It can be interpreted as internal photoemission from a conduction-band barrier 0.56 eV above the Fermi level (being degenerate in the narrow-band-gap material). The TFS theory predicts that the current/voltage relation should be of the form<sup>14</sup>

$$I = I_s \exp(qV/E_0)$$

at high enough voltages, where  $E_0 = E_{00} \coth(E_{00}/kT)$  and  $I_s$  is a function of  $T$ , the barrier height, the doping level, and is a weak function of the bias.  $E_{00}$  has been previously introduced.

Since  $E_0 = 80 \text{ meV}$  below 150 K in our devices, we can see that the rise in  $E_0$  above this temperature cannot be accounted for by the TFS theory. Tunneling through a high and

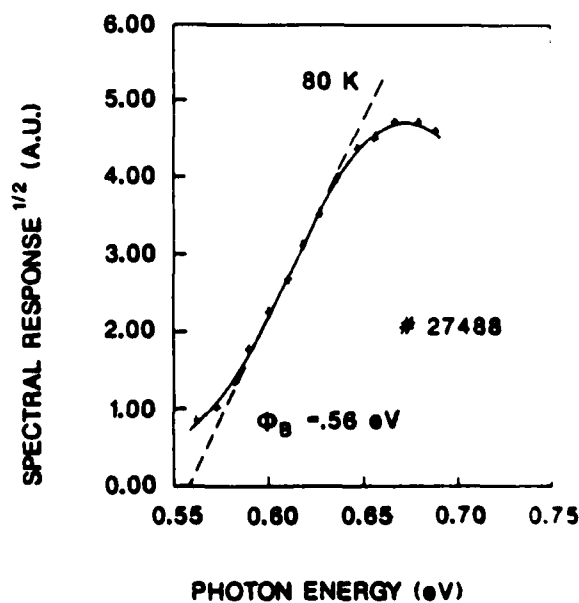


FIG. 6. Root square of the spectral response of the device vs photon energy. Only the high-energy tail is shown.

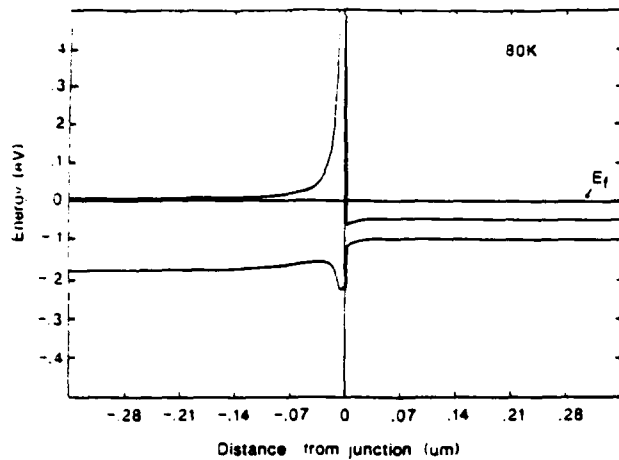


FIG. 7. Calculation of the assumed band profile of the structure at zero bias. Parameters used:  $m_{HH}^*/m_0 = 0.44$ , doping left-hand side =  $5 \times 10^{15} \text{ cm}^{-3}$ , doping right-hand side =  $4 \times 10^{16} \text{ cm}^{-3}$ , Cd composition left-hand side = 0.26, Cd composition right-hand side = 0.18, Cd composition at the barrier peak = 0.6,  $\Delta E_V = 0.15 \times \Delta E_g$ ,  $T = 80 \text{ K}$ .

sharp barrier is the suspected dominant transport at low  $T$ . Only a minor contribution to the current is due to band bending change with bias in the  $x = 0.26$  material. As will be discussed later, we think that the barrier resulted from abrupt composition change during growth. Its actual conduction-band profile is expected to be much steeper than the parabolic potential approximation made in the TFS theory.

A Poisson solution of the expected band profile of the device at 80 K is shown in Fig. 7. An abrupt Cd composition increase up to  $x = 0.6$  was assumed right at the interface, followed by a sharp exponential decrease down to  $x = 0.26$ . The minimum barrier thickness was set to be 100 Å. The valence-band offset between two different composition materials was assumed to be 15% of their band-gap difference. A heavy-hole effective mass independent of composition and equal to 0.44 has been used. The calculation is made with the relaxation method, using the two-band Kane<sup>16</sup> model and assuming fully ionized dopants without diffusion effects at the interface. Degeneracy is included. The details of this calculation will be presented elsewhere.<sup>17</sup> We can see that the Fermi level on the left-hand side is within 1 meV of the conduction band, whereas the narrow bandgap is heavily degenerate, the Fermi level lying 45 meV above the conduction band.

This structure basically looks like a metal-insulator-semiconductor device as suspected from the capacitance measurements. The semiconductor with  $x = 0.26$  is weakly degenerate. The use of a metal-insulator-metal tunneling model could be appropriate at low temperature where we established that tunneling transport is dominant. We used the model developed by Simmons<sup>18</sup> for its simplicity, modifying it slightly to make provision for different effective masses in the metal and the insulator. It assumes a rectangular barrier and is restricted to low temperatures where the tunneling is independent of temperature. We did not use it in the first place since it cannot demonstrate the existence of

the tunneling process by itself. The current density is given by

$$I = (1/R_0) \{ (\Phi_B - V/2) \exp(-A \sqrt{\Phi_B - V/2}) - (\Phi_B + V/2) \exp(-A \sqrt{\Phi_B + V/2}) \}$$

with  $A = 4\pi d \sqrt{2m_e q/h}$ ,

$$R_0 = (2\pi h d^2 / q^2) (m_i / m_m),$$

$V < \Phi_B$ ,  $d$  is the thickness of the barrier,  $\Phi_B$  the barrier height,  $V$  the bias,  $h$  the Planck's constant, and  $q$  the electronic charge.  $m_i^*$  and  $m_m$  are the electron effective masses in the insulator and the metal electrode acting as the cathode, respectively.  $R_0$  is not to be confused with the zero bias resistance of the device.

The effect of barrier height lowering is not considered since it could not be detected from the measurements and the barrier height is expected to be large. The fact that the curves in Fig. 3 are nearly symmetric is consistent with this model. The low-temperature curve of Fig. 3 was fitted in reverse bias since the tunneling is less affected than in forward bias by the actual barrier profile on the wide-band-gap side.  $\Phi_B$  and  $d$  were adjusted to produce the results shown in Fig. 8. The following effective masses have been used:  $m_i/m_0 = 0.058$  and  $m_m^*/m_0 = 0.0039$ . It can be seen that the best fit occurs for  $\Phi_B \approx 0.55 \text{ eV}$ , in excellent agreement with the optical result. The average matching barrier thickness is close to 110 Å.

The capacitance measurements can be interpreted as follows: the diode is essentially behaving as an MIS where the narrow-band-gap material is the metal electrode and the barrier is the insulator. The top semiconductor with  $x = 0.26$  is then seen *n*-type in depletion at zero bias. Calculation of the low-frequency differential capacitance of the structure shown in Fig. 7 was attempted using the same type of calcu-

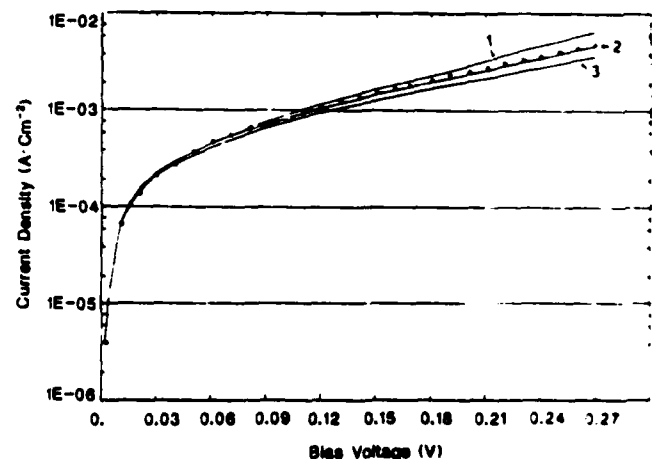


FIG. 8. Fitting of the Simmons model to the low-temperature curve of Fig. 2. The top material is biased positively. Parameters used:

	$\Phi_B$ (eV)	$d$ (Å)
Curve 1	0.45	119
Curve 2	0.55	109
Curve 3	0.65	101

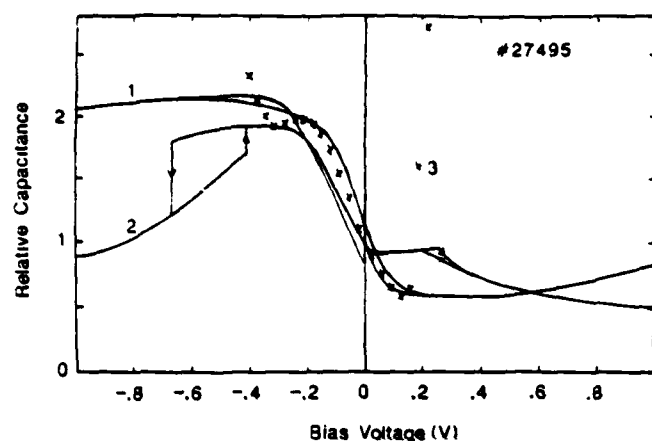


FIG. 9. Relative capacitance vs. voltage curves. Curve 1: second measurement of the *CV* data shown in Fig. 5.  $T = 80$  K, 100 kHz. Curve 2: measurement of the same device with the same frequency.  $T = 160$  K. Curve 3 =  $\times$  Low-frequency capacitance calculation at 80 K. Same parameters as in Fig. 7.

lation as before and the same parameters. The quasi-Fermi levels on each side of the heterojunction were assumed to be constant, their difference being abruptly accommodated at the interface. The result is shown in Fig. 9, together with measurements made at 80 and 160 K at 100 kHz on the same device. We can see that an accumulation plateau occurs below  $-0.2$  V. Its magnitude is much smaller than the capacitance of the pseudoinulator alone. This is due to the onset of depletion on the narrow-band-gap side which begins to be inverted below  $-0.3$  V. The high-frequency low-temperature *CV* curve then stays approximately constant thereon. The calculation also shows strong inversion of the wide-band-gap side to be occurring at  $+0.15$  V. Notice that these thresholds tend to precede the abrupt falls in capacitance measured at 160 K. We think that these transitions are linked to the collapse of their corresponding hole inversion layers through the valence side of the burst barrier, driving their respective material side in deep depletion. It demonstrates that hole confinement against this barrier occurred before. We conclude that a valence-band barrier is also present, and that the valence-band offset cannot be neglected. Even though no precise value can be deduced from this work, we should point out that the 15% of the band-gap difference value used in the calculations is consistent with all the measurements made as well as the recently published studies<sup>7,8</sup> when extrapolated to the HgTe/CdTe case. At the present time the reason why the capacitance only collapses at high temperatures is not clearly understood. It might be linked to two-dimensional quantized energy levels of the inversion layers interacting with deep levels within the bursting material. Even though the deep levels have been omitted from this study, they are known to be present since noticeable hysteresis has been seen in the *CV* measurements, and to a smaller degree in the *IV* measurements. They could also contribute to the enhanced tunneling process described.

The burst in composition which occurred at the interface is linked to the transient flux response of the effusion cell opened during the growth to increase the cadmium content of the top layer. When the shutter is closed, the cell has a higher quasiequilibrium pressure than with the shutter opened. This study shows that with the particular geometry used the time constant required by the cell to change from the closed to opened stable conditions was in the order 8 s. Once detected, this problem can be avoided. Recently grown devices trying to avoid this effect give credit to this hypothesis and will be published later.

## V. CONCLUSION

We showed that the electrical characterizations of the first abrupt *n*-isotype heterojunctions made by MBE were consistent with the presence of a sharp burst in composition at the heterojunction interface due to the growth conditions.

The measurements and the calculations presented are in agreement with the presence of a valence-band offset between the barrier material and the adjacent layers. When extrapolated linearly to the HgTe/CdTe case, the value assumed is in agreement with the recently published studies. The high  $R_0A$  values obtained even for a narrow-gap composition  $x = 0.17$  could be of interest for future gate field-effect transistor investigation.

## ACKNOWLEDGMENTS

This work was funded by DARPA Contract No. MDA903-85K-0030. One of us (M. E. D.) has also a scholarship from CNPq-Brazil.

- <sup>1</sup>P. LeVeechio, M. B. Reine, and M. N. Grimbergen, *J. Vac. Sci. Technol. A* 3, 246 (1985).
- <sup>2</sup>P. R. Bratt, *J. Vac. Sci. Technol. A* 1, 1687 (1983).
- <sup>3</sup>H. R. Vidyantath, S. R. Hampton, P. B. Ward, L. Fishman, J. Slawinski, and T. Krueger, 1986 IRS Detector Specialty Group Meeting, NASA AMES Research Center, Moffet Field, CA.
- <sup>4</sup>T. F. Kuech and J. O. McCaldin, *J. Appl. Phys.* 53, 3121 (1982).
- <sup>5</sup>J. Tersoff, *Phys. Rev. Lett.* 56, 2755 (1986).
- <sup>6</sup>Y. Guldner, G. Bastard, J. P. Vieren, M. Voos, J. P. Faurie, and A. Million, *Phys. Rev. Lett.* 51, 907 (1983).
- <sup>7</sup>S. P. Kowalczyk, J. T. Cheung, E. A. Kraut, and R. W. Grant, *Phys. Rev. Lett.* 56, 1605 (1986).
- <sup>8</sup>T. M. Duc, C. Hsu, and J. P. Faurie, *Phys. Rev. Lett.* 58, 1127 (1987).
- <sup>9</sup>J. P. Faurie, A. Million, R. Boch, and J. L. Tisot, *J. Vac. Sci. Technol. A* 1, 1593 (1983).
- <sup>10</sup>J. P. Faurie, S. Sivananthan, M. Boukerche, and J. Reno, *Appl. Phys. Lett.* 45, 1307 (1984).
- <sup>11</sup>M. Boukerche, J. Reno, I. K. Sou, C. Hsu, and J. P. Faurie, *Appl. Phys. Lett.* 48, 1733 (1986).
- <sup>12</sup>S. M. Sze, *Physics of Semiconductor Devices*, 2nd ed. (Wiley, New York, 1981).
- <sup>13</sup>C. N. Van Opdorp, thesis, Technical University of Eindhoven, 1989.
- <sup>14</sup>F. A. Padovani and R. Stratton, *Solid State Electron.* 9, 695 (1966).
- <sup>15</sup>G. R. Crowell and V. L. Rideout, *Solid State Electron.* 12, 89 (1969).
- <sup>16</sup>E. O. Kane, *J. Phys. Chem. Solids* 1, 249 (1957).
- <sup>17</sup>M. Boukerche and J. P. Faurie, *Solid State Electron.* (submitted).
- <sup>18</sup>J. G. Simmons, *J. Appl. Phys.* 34, 1793 (1963).
- <sup>19</sup>E. H. Nicollian and J. R. Brews, *MOS (Metal Oxide Semiconductor) Physics and Technology* (Wiley, New York, 1982), p. 164.

# Mercury cadmium telluride junctions grown *in situ* by molecular-beam epitaxy

M. Boukerche, S. Yoo, I. K. Sou, M. De Souza, and J. P. Faurie  
Department of Physics, University of Illinois at Chicago, Chicago, Illinois 60680

(Received 10 November 1988; accepted 17 February 1988)

The characterization of *n*-isotype mercury cadmium telluride heterojunctions made *in situ* by molecular-beam epitaxy is reported first. The cadmium composition of each side is 0.3 for the top material and 0.21 for the bottom. Both sides were doped with indium. Strong rectification with an ideality factor varying from 1.8 to 2.5 is shown. The forward bias occurs when the wide-band-gap material is biased negatively. The preliminary results of the first homojunctions made by the same technique are then presented. The cadmium composition was 0.27. The bottom *p*-type material was doped by stoichiometric deviation, whereas the top *n*-type material was doped with silicon. The device is sensitive to infrared radiation and it is found that the doping concentration is not uniform. We suggest that generation-recombination is limiting the device operation at high temperatures.

## I. INTRODUCTION

In recent years, the mercury cadmium telluride (MCT) alloy has been recognized as the most important material for midinfrared applications. Its tunable band gap is also considered for near-infrared detection. Modern technologies to manufacture high-density array detectors require large high-quality epitaxial materials. The growth technique most commonly used industrially today is liquid phase epitaxy. Molecular-beam epitaxy (MBE) is one possible alternative since it has been shown that MBE is able to produce high-quality material.<sup>1</sup> Furthermore, excellent uniformities in composition and thickness along with uniform properties have been obtained for MCT epitaxial layers on 2-in.-diam GaAs substrates.<sup>2</sup> The key issue now is to qualify the MBE material through device characterization. The demonstration of *in situ* doping and junction formation, without annealing treatments, is a very important contribution towards this goal. We reported last year unexpected barrier formation in the first *n*-isotype abrupt heterojunctions.<sup>3</sup> We will show here that such effects can be avoided. Strong rectification is then observed. We will also present the first results on homojunctions doped *in situ* with silicon.

## II. HETEROJUNCTIONS

*N*-isotype abrupt heterojunctions were grown on CdTe(111)/GaAs(100) combination substrates as previously reported. The CdTe buffer layer was 2.2  $\mu\text{m}$  thick. The narrow band-gap layer was then grown with a cadmium composition  $X = 0.21$  and a donor concentration of  $4 \times 10^{15} \text{ cm}^{-3}$ , as determined by Hall measurements. When the MCT material thickness reached 3  $\mu\text{m}$ , the Cd content was abruptly increased to 0.30. This final layer was then grown with a thickness of 0.5  $\mu\text{m}$ . Its donor concentration is not precisely known but is estimated to be in the low  $10^{15} \text{ cm}^{-3}$  range from the growth conditions. Both sides of the junction were doped with indium as previously reported.<sup>4</sup> The other effusion cells used contained Te, CdTe, and Hg, respectively. The substrate temperature was maintained at 190  $^{\circ}\text{C}$  and the growth rate was 5–7  $\text{\AA}/\text{s}$ . To avoid the composition burst

observed previously at the heterojunction interface,<sup>3</sup> the distance between the cells and their shutters was increased. Mesa devices were then made with In contacts and ZnS passivation. The top contact area was  $10^{-4} \text{ cm}^2$ . The processing temperature never exceeded 60  $^{\circ}\text{C}$ .

As seen in Fig. 1 strong rectification was observed. Forward conduction occurred for a positive bias applied to the narrow-band-gap material. The average  $R_0A$  of the 30 devices measured reached  $10^3 \Omega \times \text{cm}^2$  at liquid-nitrogen temperature. A value of  $10^4 \Omega \times \text{cm}^2$  was observed on one device. We conclude that the device operation is limited by the wide-band-gap material where most of the depletion occurs. The  $I/V$  curves were least-squares fitted at each temperature. Series resistance had to be included since it is unavoidable in such thin devices and low doping levels.

$$I = I_s \{ \exp [q(V - RI)/nkT] - 1 \}, \quad (1)$$

where  $I_s$  is the saturation current,  $R$ , the series resistance,  $n$  the ideality factor,  $I$  the current density,  $V$  the bias,  $k$  the Boltzman constant,  $q$  the electronic charge, and  $T$  the absolute temperature.

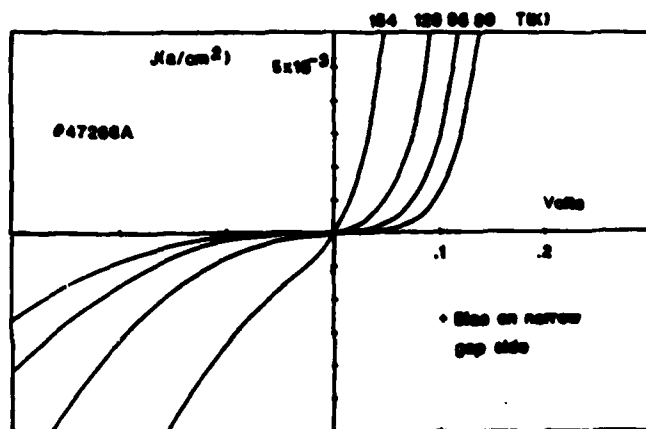


FIG. 1. Current vs voltage curves of the heterojunction device.

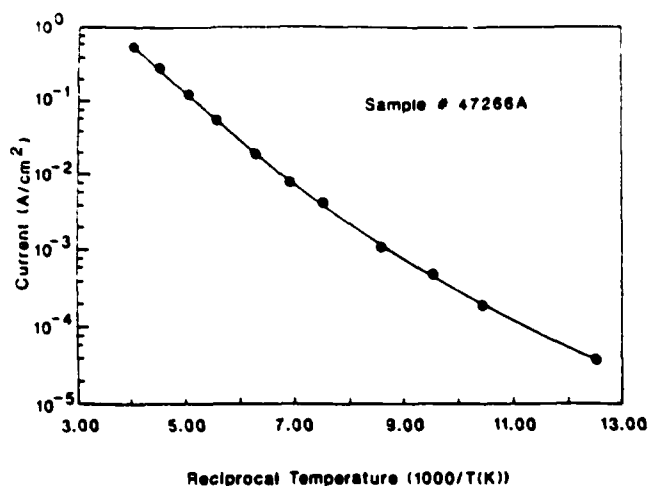


FIG. 2. Variation of the current prefactor  $I_0$  in Eq. (1) with the reciprocal temperature.

The quality of the fitting was excellent at all the temperatures with four decades of forward current variation. Its reliability above 200 K was questionable since the curves were basically Ohmic. The ideality factor  $n$  varied from 1.8 at 200 K to 2.5 at low temperatures. The activation energy of  $I_0$  was consistently close to 125 meV at high temperatures, whereas at low temperatures it decreased to around 80 meV depending on the device tested (Fig. 2). Capacitance measurements are believed to be unreliable since series resistance could not be neglected and the top material thickness was very thin. A calculation of the expected band profile of the heterojunction is shown in Fig. 3. The method used has been previously described.<sup>3</sup> We assumed a valence-band offset equal to 10% of the band-gap difference between the two sides at 80 K, and doping levels of  $4 \times 10^{15} \text{ cm}^{-3}$  and  $2 \times 10^{15} \text{ cm}^{-3}$  in the narrow- and wide-band-gap sides, respectively. (If the valence-band offset would be taken as 20% of the band gap, the phenomenologic discussion which follows would not be changed.) This calculation gives a depletion layer thickness

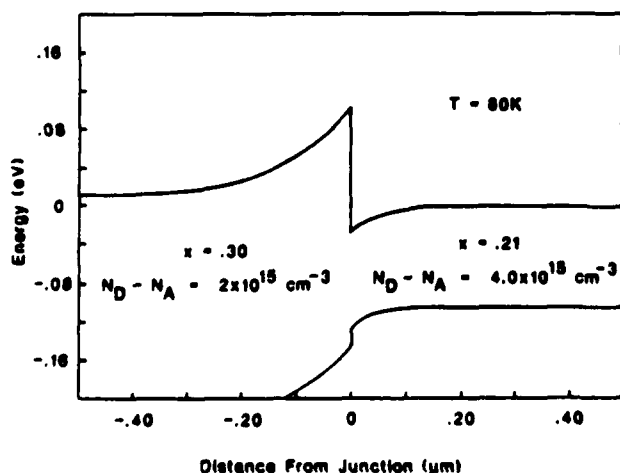


FIG. 3. Energy band profile calculated for the heterojunction. Two-dimensional quantization has been neglected. The energy reference is the Fermi level.

more than  $0.3 \mu\text{m}$  in the wide-band-gap material. This is very close to the top contact position. The barrier height between the top of the spike and the Fermi level is 104 meV. The spectral response of one device reverse biased at 50 mV is shown in Fig. 4. A maximum is seen at  $8\text{-}\mu\text{m}$  wavelength. It can be noticed that the photosignal does not seem to follow the usual internal photoemission theory on the cutoff side of the curve. The photoresponse signal displays a tendency towards a more linear relationship with the photon energy. This could be due in part to a photoconductive contribution of the series resistance around the mesa. The narrow-band-gap side near the heterojunction is believed to be heavily degenerate at 80 K, in strong accumulation (see Fig. 3). The energy distribution range of the photoemitted electrons is then limited to a few kT. This situation can lead to a linear relationship between the photon energy and the photosignal.<sup>5</sup> A linear extrapolation of the experimental curve in the cutoff region would then give a barrier height  $\phi_b$  equal to 130 meV. The device looks like a metal-semiconductor Schottky diode<sup>6</sup> where the metal would be the degenerate narrow-band-gap material. However, the equivalent barrier height, i.e., the energy difference between the top of the spike and the Fermi level, is a function of the bias. Anderson<sup>6</sup> showed that an ideality factor  $> 1$  is expected, and that the reverse current should not saturate. The built-in potential is 26 meV on the narrow band gap and 93 meV on the other side. At low forward bias the ideality factor should be close to 1.28. The fact that  $n$  equals or exceeds 2 makes us conclude that thermionic emission is not the only transport involved, even at high temperatures. This is also supported by the following argument. The variation versus temperature of  $I_0$  deduced from the fitting to Eq. (1) closely matches the variation of the current measured at low forward bias. According to the Anderson<sup>6</sup> model, at fixed low voltages, the current should vary as  $T^{1/2} \exp(-qV_D/kT)$ , where  $T$  is the absolute temperature and  $V_D$  is the electrostatic potential drop across the wide-band-gap material side. The calculation shows that  $V_D$ , at zero bias, should decrease when the temperature increases. For example, it should be approximately equal to 40 meV at 250 K. This is in contradiction with the measurements since the activation energy of  $I_0/T^{1/2}$

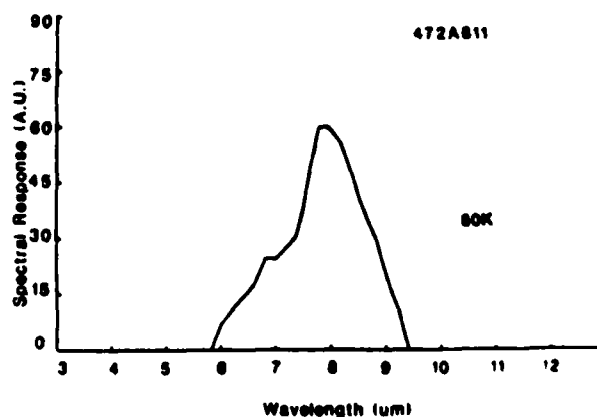


FIG. 4. Spectral response of the heterojunction at 80 K.

is equal to 120 meV at high temperatures.

We suggest that generation-recombination mechanisms in the  $x = 0.3$  material play an important role at high temperatures. Tunneling effects are expected at low temperatures in such narrow-band-gap materials, they are certainly responsible for the increase of  $n$  to 2.5 at 80 K. However, the slope of  $\log I/V$  still increases down to this temperature, and another transport process is still present. If thermionic emission is the main relevant mechanism in the intermediate temperature range, the activation energy of  $I$ , (82 meV) would be in reasonable agreement with the calculated value of  $V_{D2}$  (93 meV).

### III. HOMOJUNCTIONS

The epitaxial layer was grown on CdTe(111)/GaAs(100) substrate at the same temperature as before (190 °C). The stoichiometric conditions were adjusted to produce  $p$ -type material with a thickness of 4.2  $\mu\text{m}$ . The silicon  $n$ -type doping flux was then added on the crystal during the remaining 1  $\mu\text{m}$  material grown subsequently by opening the corresponding shutter. The other growth conditions were identical to the ones reported above. Hall measurement of the layer as grown gave an  $n$ -type doping level of  $5 \times 10^{16} \text{ cm}^{-3}$  in the top material neglecting the contribution of the  $p$ -type material. This was relevant since this measurement showed an  $n$ -type fully ionized behavior below 250 K (flat curve). After etching of the  $n$ -type material, the same technique showed that the remaining material was  $p$  type with a level of  $2 \times 10^{16} \text{ cm}^{-3}$ . Freeze out was present down to the lowest temperature measured (28 K). The cadmium composition was determined at room temperature by Fourier transform infrared (FTIR) transmission measurements. The value calculated for an absorption coefficient of  $1000 \text{ cm}^{-1}$  was  $X = 0.27$ . Mesa devices were subsequently processed at low temperature (below 65 °C). The  $n$ - and  $p$ -type materials were contacted with indium and gold, respectively. The area of the devices was  $1.5 \times 10^{-4} \text{ cm}^2$ . The  $I/V$  curves in Fig. 5 were measured with a cryogenic probe station. They show good rectification, forward bias occurring when the top  $n$ -type material is biased negatively as expected. We can see in Fig. 6 that illumination by a blackbody at

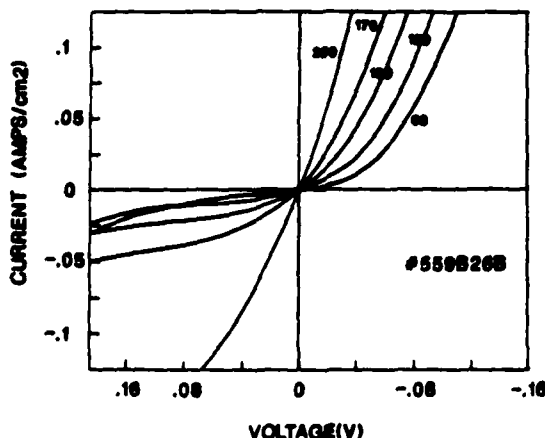


FIG. 5. Current vs voltage curves for the homojunction device.

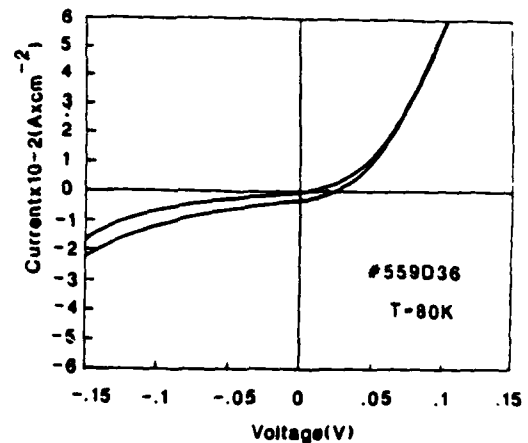


FIG. 6.  $I/V$  curve of the homojunction at 80 K, with and without illumination from a blackbody at 600 K. The room-temperature background field of view is 180°.

600 K generates a reverse photocurrent. The variation of  $R_0A$  versus temperature in Fig. 7 follows a constant slope at high temperatures, and progressively saturates down to 90 K, decreasing slightly thereafter. At liquid-nitrogen temperature, the device is expected to be limited by tunneling and edge leakage since no passivation was used and the structure is not gated. Also, the field of view of the room-temperature background was 180°, so the value of  $R_0A$  is not entirely limited by the junction material. Since the  $n$ -type material is degenerate at 80 K, most of the depletion layer should be on the  $p$  side. At zero bias the capacitance is 30% smaller than expected from the doping levels. It decreases with reverse bias but  $1/C^2$  does not follow a straight line. We conclude that the doping is not uniform, and that the silicon probably diffused in the  $p$  side. The  $I/V$  data were fitted to Eq. (1). The ideality factor varied from 2.1 at high temperature to 3.0 at 80 K. Since the same time  $R_0A$  varies nearly as  $1/n_i$ , where  $n_i$  is the intrinsic carrier concentration, we suggest that generation-recombination currents in the depletion region could be dominant above 160 K.<sup>7</sup> Further analysis of these devices will be published elsewhere.<sup>8</sup>

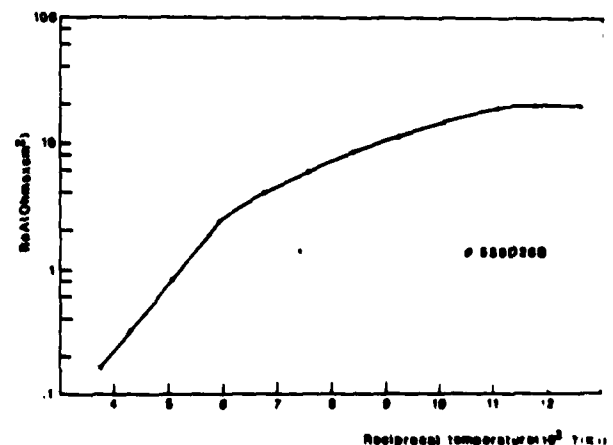


FIG. 7. Variation of the zero bias resistance of the homojunction vs reciprocal temperature. Background field of view is 180°.

#### IV. CONCLUSION

The first rectifying MCT devices made *in situ* by MBE have been described. The previous composition burst during heterojunction formation could be eliminated by proper growth conditions. The strong rectification measured shows that the conduction-band discontinuity is abrupt, and that the interface state density between the two materials is negligible.

The homojunction presented also showed strong rectification and generated a photovoltaic current upon infrared illumination.

These preliminary results are intended to represent a first step in the understanding of *in situ* junction formation using the MBE technique. All the native defects are still present in the material since it is not annealed under mercury pressure, as is commonly the case for *ex situ* made junctions. The control of doping is also a very difficult task to achieve in this II-VI ternary alloy. In addition all the measurements were made with 180° field of view and a probe station where some residual strain is unavoidable during probing.

Further material characterizations and device modeling are then needed to confirm the generation-recombination

process suggested and also why the diffusion limited regime is not observed in the homojunction at high temperature.

#### ACKNOWLEDGMENTS

The technical help of Z. Ali and S. Farook was greatly appreciated. This work was funded by DARPA under Contract No. F49620-87-C-0021. One of us (MDS) is also supported by a scholarship from C. N. Pq, Brazil.

<sup>1</sup>S. Sivananthan, M. D. Lange, G. Monfroy, and J. P. Faurie, *J. Vac. Sci. Technol. B* **6**, 788 (1988).

<sup>2</sup>M. D. Lange, S. Sivananthan, X. Chu, and J. P. Faurie, *Appl. Phys. Lett.* **52**, 978 (1988).

<sup>3</sup>M. Boukerche, I. K. Sou, M. De Souza, S. Yoo, and J. P. Faurie, *J. Vac. Sci. Technol. A* **5**, 3119 (1987).

<sup>4</sup>M. Boukerche, J. Reno, I. K. Sou, C. Hsu, and J. P. Faurie, *Appl. Phys. Lett.* **48**, 1733 (1986).

<sup>5</sup>R. Williams, *Semiconductors and Semimetals* (Academic, New York, 1970), Vol. 6.

<sup>6</sup>R. L. Anderson, *Solid State Electron.* **5**, 341 (1962).

<sup>7</sup>M. B. Reine, A. K. Sood, and T. J. Tredwell, *Semiconductors and Semimetals* (Academic, New York, 1981), Vol. 18.

<sup>8</sup>M. Boukerche, S. Yoo, I. K. Sou, M. D. Souza, and J. P. Faurie (unpublished results).

#### IV-2 HOMOJUNCTIONS

N-p homojunctions have also been fabricated in situ. The epitaxial layer was grown on CdTe(111)B/GaAs(100) substrate at 190°C. The stoichiometric conditions were adjusted to produce p-type material with a thickness of 4.2 $\mu$ m. Silicon was used as the n-type dopant to a level of  $5 \times 10^{16}\text{cm}^{-3}$

The homojunctions showed strong rectification and generated a photovoltaic current upon infrared illumination. Diffusion limited regime was not observed in the homojunctions at high temperature which suggests what native defects were controlling the diode performance. These results are describe in the paper entitled, "MCT n-isotype heterojunctions grown in situ by molecular beam epitaxy" attached to section IV-1.

#### IV-3 COMMENTS

It is important to point out that the Microphysics Laboratory has described the first rectifying MCT devices made in situ by MBE. This work has been carried out in 1987 (see Semi Annual Technical Report dated June 30, 1987). Since then the effort has been put in the control of microstructural defect. Therefore it is not fair to think that these results represent the state-of-the-art of the Microphysics Laboratory as pointed out in the introduction of this report. Hence taking into consideration (i) the progress achieved in the control of twin formation during the year 1989 (ii) the growth of n-type doping using indium (iii) the growth of high quality p-type HgCdTe in (211)B orientation the Microphysics Laboratory has currently the potential of growing much better in situ homo- and heterojunctions.

## V PHOTODIODES MADE EX SITU

### V-1 ION IMPLANTED PHOTODIODES

Ion implanted photodiodes have been fabricated by Rockwell International Science Center on HgCdTe(111)B MBE layers grown in the Microphysics Laboratory. These junctions have been made on as-grown p-type layers, 12 $\mu$ m thick. The diode dark currents in the diffusion regime and the spectral response attest to the excellent uniformity in composition of the layer. We have also established that in the diffusion regime, the data can be explained by the ideal diode equation with electrical parameters measured on the as-grown MBE layers.

The problems at low temperature are complex because factors in material and fabrication are independent and the dark currents are likely dominated by grown induced and process induced defects difficult to separate. The results are detailed in the attached paper.

Several layers have been implanted but it turned out that for most of them only a few diodes were working. We concluded that high EPD (high  $10^6\text{cm}^{-2}$ ) due to twinning was responsible for low yield. These results obtained in 1987 and early 1988 have triggered our effort related to the twinning problem as explained in the introduction and in part II.

#### ATTACHED PAPERS:

1. "Characteristics of p-n junctions fabricated on MCT grown by MBE"

# Characteristics of $p$ - $n$ junctions fabricated on $\text{Hg}_{1-x}\text{Cd}_x\text{Te}$ epilayers grown by molecular beam epitaxy

J. P. Faurie, S. Sivananthan, and M. Lange

University of Illinois at Chicago, Physics Department, Chicago, Illinois 60680

R. E. Dewames, A. M. B. Vandewyck, G. M. Williams, Dan Yamini, and E. Yao

Rockwell International Science Center, Thousand Oaks, California 91360

(Received 7 December 1987; accepted for publication 22 April 1988)

$p$ - $n$  junctions have been fabricated, using the ion implantation technique, on a  $\text{Hg}_{1-x}\text{Cd}_x\text{Te}$  epilayer grown by molecular beam epitaxy (MBE) on a  $\text{CdTe}(111)B$  substrate. These junctions have been made on as-grown  $p$ -type layers, 12  $\mu\text{m}$  thick. The layer ( $x = 0.34$ ) exhibits at 77 K a hole mobility of  $800 \text{ cm}^2 \text{ V}^{-1} \text{ s}^{-1}$  and a carrier concentration of  $3.6 \times 10^{15} \text{ cm}^{-3}$ . The diode dark currents in the diffusion regime and the spectral response attest to the excellent uniformity in composition of the layer. We have also established that in the diffusion regime the data can be explained by the ideal diode equation with electrical parameters measured on the as-grown MBE layers. We consider this an important step in the understanding of the relationship between material parameters and device performance.

Since the first successful attempt to grow  $\text{Hg}_{1-x}\text{Cd}_x\text{Te}$  by molecular beam epitaxy (MBE) reported in 1981,<sup>1</sup> the quality of MBE  $\text{Hg}_{1-x}\text{Cd}_x\text{Te}$  epilayers has been improved drastically.<sup>2-5</sup> Surprisingly, whereas extensive effort has been devoted towards the making of photovoltaic devices on bulk and liquid phase epitaxy (LPE) material, the only published device data on MBE  $\text{HgCdTe}$  epitaxial layers were reported in 1983<sup>2</sup> and very recently in 1988.<sup>6</sup>

The reason is probably due to the fact that MBE was used more as a tool to understand the growth and to grow microstructures such as superlattices,<sup>7</sup> than to grow thick epilayers. With the development of Hg cells with large capacity, the MBE technique has been able to overcome one of its drawbacks, i.e., the low Hg condensation coefficient. It is now possible to grow epilayers of 10–15  $\mu\text{m}$  thickness or even more, thickness that is required for infrared (IR) photovoltaic devices.<sup>3-5</sup> In addition to that, the reproducibility in the growth conditions and the excellent uniformity achieved in composition and carrier concentration on 2-in.-diam GaAs substrates<sup>8</sup> prove that MBE  $\text{HgCdTe}$  material should be taken into consideration as a valuable candidate for conventional infrared detectors.

The purpose of this study is to establish the relationships between electrical parameters measured on the active layer, the junction characteristics, and the device figures of merit. Material properties and processing of devices are interdependent and in general difficult to separate, but it is reasonable to expect that in the diffusion regime of the diode operation the correlation between average electrical parameters, junction parameters, and device figures of merit can be validated.

One epitaxial layer of  $\text{Hg}_{1-x}\text{Cd}_x\text{Te}$ , whose characteristics are presented in Table I, has been investigated here. It has been grown on a  $\text{CdTe}(111)B$  substrate at 195 °C in a Riber 2300 MBE system, under a growth procedure previously described.<sup>9</sup> The layer is  $p$ -type as currently observed in our laboratory for (111) $B$  layers of  $x > 0.22$  grown at this temperature. MBE growth occurs under Te-rich conditions; therefore, it is likely that the acceptor character is mainly related to the presence of Hg vacancies. The carrier concen-

tration and hole mobility of the layer are in the range of the best values obtained for such a composition.<sup>5</sup> Minority-carrier lifetime measurements have been performed using the photodecay technique.

The composition of the  $\text{Hg}_{1-x}\text{Cd}_x\text{Te}$  alloy is determined from IR transmission spectra obtained at 300 K. The energy gap has been defined to correspond to an absorption coefficient of  $500 \text{ cm}^{-1}$ .

In this experiment a  $1 \times 32$  planar array of  $n^+/p$  photovoltaic devices was used for characterization. Ion implantation was used to form the junction and the structure is passivated with  $\text{ZnS}/\text{SiO}_2$ . Ion implantation is done at 300 K on the as-grown MBE  $\text{HgCdTe}$  material coated with a thin layer of ZnS. Typical elements used are boron and beryllium and the energy range is between 200 and 250 keV with a dose range of  $10^{13}$ – $10^{14} \text{ cm}^{-2}$ . The detector array was of planar structure with an implant area of  $110 \mu\text{m}^2$  on 125  $\mu\text{m}$  center to center spacing. The thickness of the layer  $\sim 12 \mu\text{m}$  was measured by optical micrograph on a cleaved portion of the layer and the junction depth was measured to be 2–2.5  $\mu\text{m}$  deep in the material.

Figure 1 demonstrates the uniformity of the spectral response for six diodes across the wafer. The relative spectral response per watt was measured at 77 K on an 8 mm<sup>2</sup> processed array. The spectral response, which exhibits excellent uniformity over this area (see Fig. 1), was illuminated on the implant side through the passivated layer on randomly bonded detector elements. During this measurement adjacent diodes are floating. The quantum efficiency measured from the top side of the device (through the  $n^+$  implanted region) was 25%. The spectral response curves are some-

TABLE I.  $\text{HgCdTe}$  material characteristics.

$T = 77 \text{ K}$						
Sample	$x$	$d$ ( $\mu\text{m}$ )	$N_A - N_D$ ( $\text{cm}^{-3}$ )	Hole mobility ( $\text{cm}^2/\text{V s}$ )	Carrier lifetime ( $10^{-9} \text{ s}$ )	$\lambda_m$ ( $\mu\text{m}$ )
216 528	0.34	12.1	$3.6 \times 10^{15}$	800	100	3.57

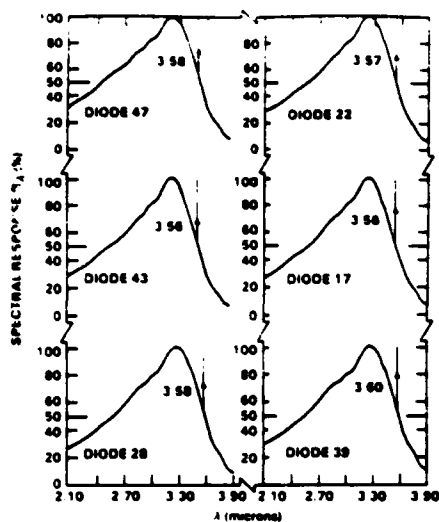


FIG. 1. Spectral response uniformity at 77 K of MBE photodiodes fabricated on layer No. 216 528.

what narrow band. This may be due to the fact that infrared radiation was incident through the implanted region of the detector instead of through the CdTe substrate. Short wavelength photons will be preferentially absorbed near the damaged implanted material and recombine before collection by the  $p$ - $n$  junction. This effect may also relate to the low quantum efficiency. The measured cutoff wavelengths are observed to be uniform and in accord with the IR transmission data (taken at 300 K and extrapolated at 77 K), i.e., 3.57  $\mu\text{m}$  compared to 3.60  $\mu\text{m}$ .

Figure 2 is a statistical display of  $R_0A$  products measured at 195 K. In Fig. 2(b) we have used the Weibull probability paper to illustrate the cumulative distribution function.<sup>10</sup> Figure 2(a) is a histogram and the curve is a fit of the data to a Weibull distribution with parameters derived from the Weibull cumulative distribution function. The steepness of the Weibull distribution curve illustrates the excellent uniformity of the diodes. The devices with  $R_0A$  products which clearly do not fit the Weibull curve are limited by

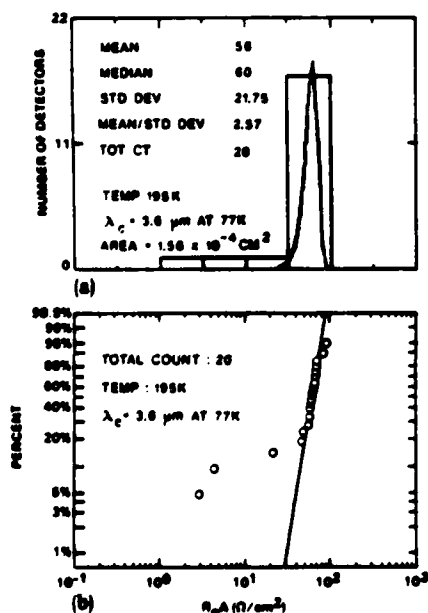


FIG. 2. Statistical display of  $R_0A$  products at 195 K: (a) histogram, (b) Weibull probability.

gross imperfections of yet unknown origin.

In Fig. 3 we illustrate the current-voltage characteristics for a diode operating in the diffusion regime at 183 K. The data can be explained by Shockley's ideal diode equation  $J = J_0[\exp(qV/kT) - 1]$ , where  $q$  is the electronic charge,  $V$  the applied voltage,  $k$  the Boltzmann constant,  $T$  the absolute temperature, and  $J_0$  the saturation current density. Both forward and reverse bias characteristics are shown in Fig. 3. The linear line labeled "calculated from reverse bias" is based on the ideal diode equation taking  $J_{SAT}$  measured from reverse bias. The currents in reverse bias are usually observed to be slightly larger than currents in forward bias suggesting the presence of a small ohmic current component. The second line is the best fit to the forward bias current corrected for series resistance effects observed at large forward bias. For the layer processed, the measured electrical parameters at 195 K are  $N_A = 6.5 \times 10^{15} \text{ cm}^{-3}$ ,  $\mu_n = 320 \text{ cm}^2/\text{V s}$ ,  $\tau_n = 1.60 \times 10^{-7} \text{ s}$ . Taking  $\mu_p = 4 \times 10^4 \text{ cm}^2/\text{V s}$  we obtain for the diffusion coefficient  $D = (kT/q)\mu = 6.7 \times 10^2 \text{ cm}^2 \text{ s}^{-1}$ , and for the diffusion length  $L_n = 104 \mu\text{m}$ . Since our thickness  $t$  is  $\sim 12 \mu\text{m}$  in the perpendicular direction, we have a short diode and in the direction parallel to the surface a long diode. We have a two-dimensional problem which we approximate by a linear superposition of two currents. The current density in the direction normal to the surface is taken as  $J_0 = q(n_i^2/N_A)(t/\tau_n)$  and parallel to the surface as  $J_0 = q(n_i^2/N_A)(L_n/\tau_n)$ . The effective area of the device in the perpendicular direction is taken to be  $a^2 = 1.6 \times 10^{-4} \text{ cm}^2$ ,  $a = 125 \mu\text{m}$  and  $4ah$  in the parallel direction where  $h \approx 3 \times 10^{-4} \text{ cm}$ . From the electrical data we obtained  $\lambda_c^{(e)}(0 \text{ K}) = 4.16 \mu\text{m}$ . This value is larger than what was expected from the measurement of the photoreponse  $\lambda_c^{(p)}(0 \text{ K}) = 3.72 \mu\text{m}$ . Such discrepancies are usually observed between cutoff wavelengths deduced from electrical and optical data. Taking the gap obtained from electrical data (see Fig. 4) the intrinsic carrier concentration  $n_i^{(e)}(195 \text{ K})$  is calculated to be  $2.87 \times 10^{13} \text{ cm}^{-3}$ . Inserting this value plus the electrical data cited before we calculate  $J_{SAT}^{theor} = 4.4 \times 10^{-8} \text{ A}$ . The measured value is  $4.5 \times 10^{-8} \text{ A}$ .

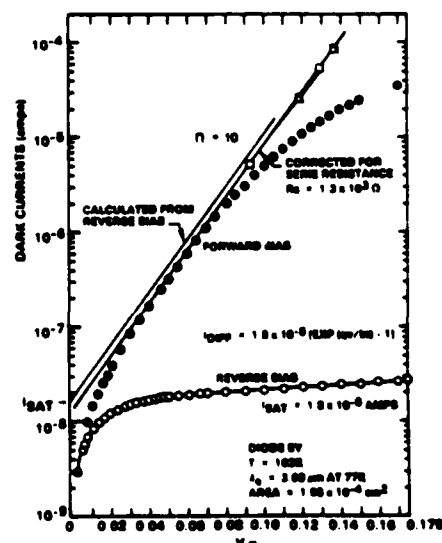


FIG. 3. Current-voltage characteristics at 183 K of MBE photodiodes fabricated on layer No. 216 528.  $\lambda_c = 3.60 \mu\text{m}$  at 77 K.

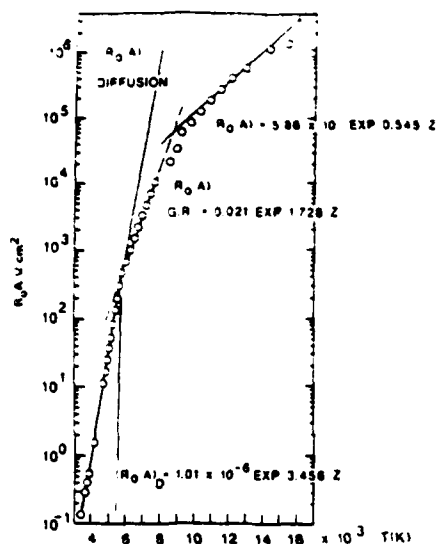


FIG. 4. Zero bias resistance-area ( $R_0A$ ) product vs temperature of MBE epilayer No. 216 528.  $x = 0.341$ ,  $\lambda_c$  (optical) =  $3.60 \mu\text{m}$  at  $77 \text{ K}$ ,  $3.74 \mu\text{m}$  at  $0 \text{ K}$ ,  $E_g$  (optical) =  $0.332 \text{ eV}$  at  $0 \text{ K}$ ,  $\lambda_c$  (electrical) =  $4.16 \mu\text{m}$  at  $0 \text{ K}$ ,  $E_g$  (electrical) =  $0.298 \text{ eV}$  at  $0 \text{ K}$ . Area of the diode:  $1.56 \times 10^{-4} \text{ cm}^2$ , the parameter  $z$  is equal to  $10^3/T$ .

Hence taking the gap deduced from electrical data (see Fig. 4) plus the electrical parameters measured for the layer, an excellent agreement is obtained between theory and experiment. For analysis we have used a simple model for the  $n^+p$  device structure. We have assumed that recombination velocities associated with surfaces and interfaces can be neglected and that the current contribution from the  $n^+$  side is negligible. This appears to be valid since by neglecting those contributions the data can be explained. The calculations are sensitive to the value of  $\lambda_c$  used for calculating  $n_i$  as well as the values assumed for the junction parameters.

As shown in Fig. 4 the  $R_0A$ 's monotonically increase with lowering of the temperature. We have fitted the transition region to a  $G-R$  expression of the form  $\exp E_g/2kT$ . The temperature dependence appears to support the thesis that currents in the transition region originate from carrier generation in the depletion region. The forward bias characteristics, however, do not show the expected voltage dependence of  $\exp qV/2kT$ . This observation is not necessarily inconsistent with the temperature dependence.<sup>11,12</sup>

The fit to the data in the transition region and at lower temperature represents an empirical fit of the data and should not be considered as a validation of physical mechanisms. At temperatures below  $65 \text{ K}$  we observe a decrease in  $R_0A$  products or increase in dark currents. Dark current components with negative temperature coefficient are expected from tunneling mechanism since the band gap decreases with decreasing temperature.<sup>13</sup>

In summary,  $n^+p$  junctions have been made on  $\text{HgCdTe}$   $p$ -type layers grown by MBE on  $\text{CdTe}(111)$   $B$  substrates using the ion implantation technique. The spectral response of the diodes confirms the excellent uniformity in composition achieved in these layers along the growth axis and over the surface area investigated.

We have also established that in the diffusion regime the data can be explained, at small bias and forward bias, by the

ideal diode equation with electrical parameters measured on as-grown MBE layers. We consider this as the first important step in the understanding of the relationship between material parameters and device performance.

The problems at low temperatures are complex because factors in material and fabrication are interdependent and the dark currents are likely dominated by grown-in and process-induced defects difficult to separate. At low temperatures the currents are small but generated at the metallurgical junction. Hence, the features of the junction are of critical importance. Understanding the technological limits is still a critical issue in devices fabricated by conventional techniques.<sup>13,14</sup> The hope is that MBE technology with its *in situ* diagnostic capabilities and the capability to produce devices *in situ* will provide the needed insight to identify and reduce factors limiting performance in current state of the art device fabricated by conventional techniques. The capability of growing highly uniform layers on substrate as large as  $2 \text{ in.}$  in diameter along with the demonstration that good diodes can be obtained even on the first attempts on as-grown material should attract attention to MBE  $\text{HgCdTe}$  for IR focal plane arrays. In parallel with the fabrication of MBE diodes we have processed a post-growth annealed layer grown by liquid phase epitaxy. The performance was observed to be similar. However, these devices were not annealed after the implantation step usually included in the baseline LPE processing.

This work has been supported at the University of Illinois by Defense Advanced Research Projects Agency (DARPA) under contract No. F49620-87-C-0021 and by DARPA/Night Vision Laboratory (NVL) under contract No. DAAL03-87-K-0092. The work on device fabrication and analysis was supported in part by Rockwell International discretionary funds and by DARPA/NVL under contract DAAL03-87-C-0014.

<sup>1</sup>J. P. Faurie and A. Million, *J. Cryst. Growth* **54**, 582 (1981).

<sup>2</sup>J. P. Faurie, A. Million, R. Boch, and J. L. Tissot, *J. Vac. Sci. Technol. A* **1**, 1593 (1983).

<sup>3</sup>J. M. Arias, S. H. Shin, J. T. Cheung, J. S. Chen, S. Sivananthan, J. Reno, and J. P. Faurie, *J. Vac. Sci. Technol. A* **5**, 3133 (1987).

<sup>4</sup>T. H. Myers, R. W. Yanka, J. P. Karina, K. A. Harris, J. W. Cook, and J. F. Schetzina, in *Proceedings of MRS Meeting*, Boston, Dec. 1986.

<sup>5</sup>S. Sivananthan, M. D. Lange, X. Chu, and J. P. Faurie, *J. Vac. Sci. Technol.* (to be published).

<sup>6</sup>J. M. Arias, S. H. Shin, J. G. Pasko, and E. R. Gertner, *Appl. Phys. Lett.* **52**, 39 (1988).

<sup>7</sup>J. P. Faurie, *IEEE J. Quantum Electron.* **22**, 1656 (1986) and references therein.

<sup>8</sup>M. D. Lange, S. Sivananthan, X. Chu, and J. P. Faurie, *Appl. Phys. Lett.* **52**, 978 (1988).

<sup>9</sup>J. P. Faurie, J. Reno, S. Sivananthan, I. K. Sou, X. Chu, M. Bouharcha, and P. S. Wijewarnasuriya, *J. Vac. Sci. Technol. B* **4**, 586 (1986).

<sup>10</sup>A. J. Cross and V. A. Clark, *Survival Distributions—Reliability Applications in Biomedical Sciences* (Wiley, New York, 1975).

<sup>11</sup>C. T. Sah, R. N. Noyce, and W. Shockley, *Proc. IRE* **45**, 1228 (1957).

<sup>12</sup>S. C. Choo, *Solid-State Electron.* **11**, 1069 (1968).

<sup>13</sup>R. E. Dewames, G. M. Williams, J. G. Pasko, and A. M. B. Vandewyck, *J. Cryst. Growth* **86**, 849 (1988).

<sup>14</sup>R. E. Dewames, J. G. Pasko, E. S. Yao, and A. M. B. Vandewyck, *J. Vac. Sci. Technol.* (to be published).

## V-2 LOW ENERGY ION SPUTTERING PHOTODIODES

The effect of low energy ions (LEI) on HgCdTe has been investigated in the Microphysics Laboratory where it has been found that n-p junction is formed when a p-type material is bombarded.

This approach which has been entirely developed in the MPLab has been used to fabricate photodiodes on HgCdTe layers grown by MBE in the laboratory. The technique along with diode performances have been described in the attached paper.

The first epilayers tested showed that HgCdTe grown by MBE can be of excellent quality. Fig. 1 illustrates  $R_0A$  vs  $T$  for diodes fabricated on MBE grown HgCdTe epilayers of different  $x$ . It can be seen that high  $R_0A$ s are obtained even though all the layers tested were twinned epilayers.

We have found that this method is not only inexpensive but also fast and reliable. Fig. 2 and 3 compare  $R_0A$ s for diodes fabricated on the same MBE layers either by ion implantation at Rockwell or by low energy ion in the MPLab. For both of them  $R_0A$ s in the diffusion regime show nearly identical slopes. In addition, the diodes fabricated using this new method are very stable.

Therefore, this technique appears to have potential in terms of diode manufacturing. These very encouraging results call for additional work. Compared to conventional ion implantation technique, LEI technique is much less damaging for HgCdTe. In addition this technique might be developed in situ.

### FIGURE CAPTIONS:

Fig. 1  $R_0A$  of MBE  $Hg_{1-x}Cd_xTe(111)B$  photodiodes

Fig. 2 Arrhenius plot of  $R_0A$  for diodes made on the same

Fig. 3 Epilayer using either ion implantation or low energy ion

### ATTACHED PAPER:

1. "Planar heterojunctions made on molecular beam epitaxially grown mercury cadmium telluride using low energy ion sputtering"

$R_{0A}$  of MBE  $Hg_{1-x}Cd_xTe$  PHOTO DIODE (Aug. 5 1989)

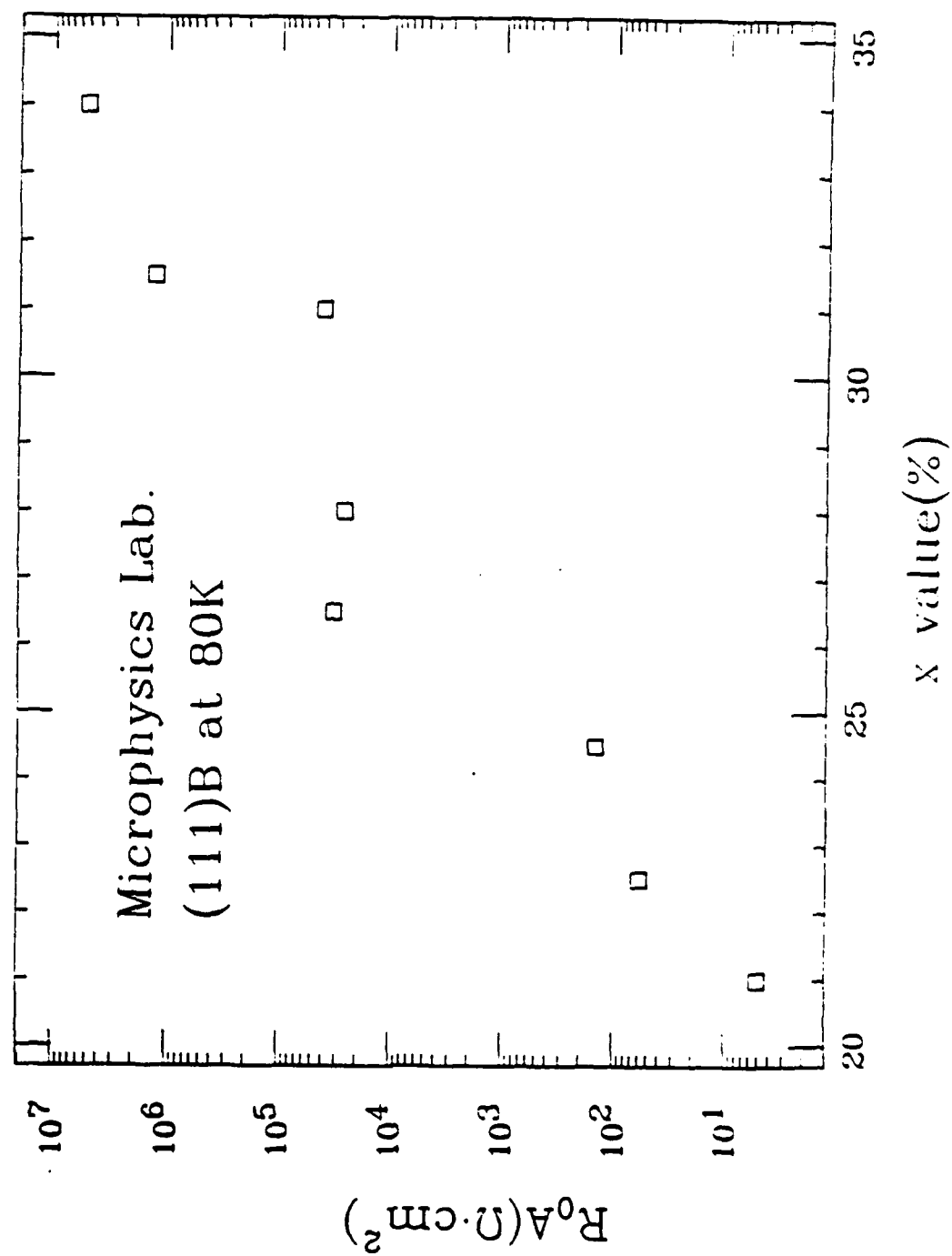


Fig. 1

# ARRHENIUS PLOT OF THE ZERO BIAS RESISTANCE-AREA ( $R_0A$ ) PRODUCT

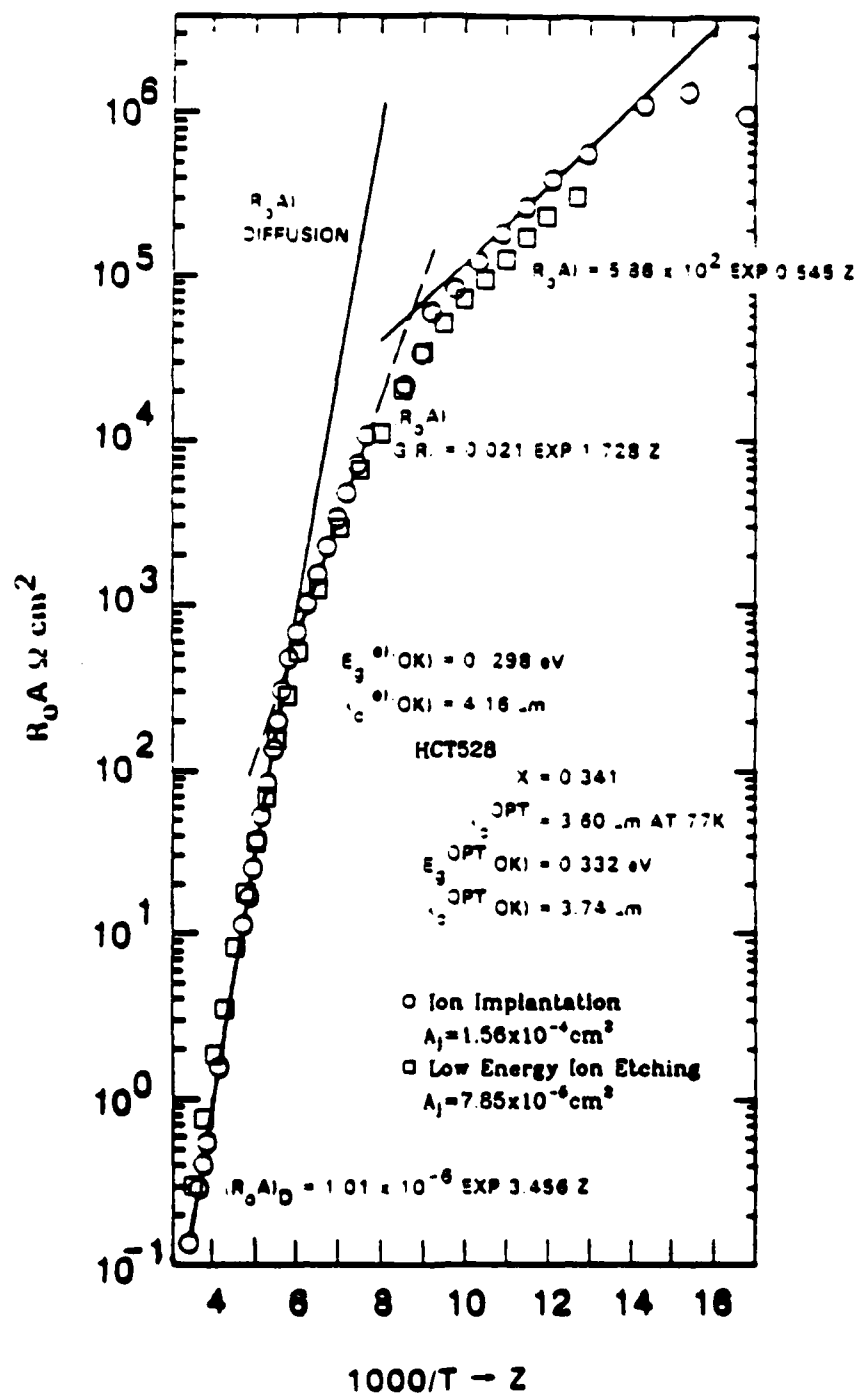


Fig. 2

# ARRHENIUS PLOT OF THE ZERO BIAS RESISTANCE-AREA ( $R_0A$ ) PRODUCT

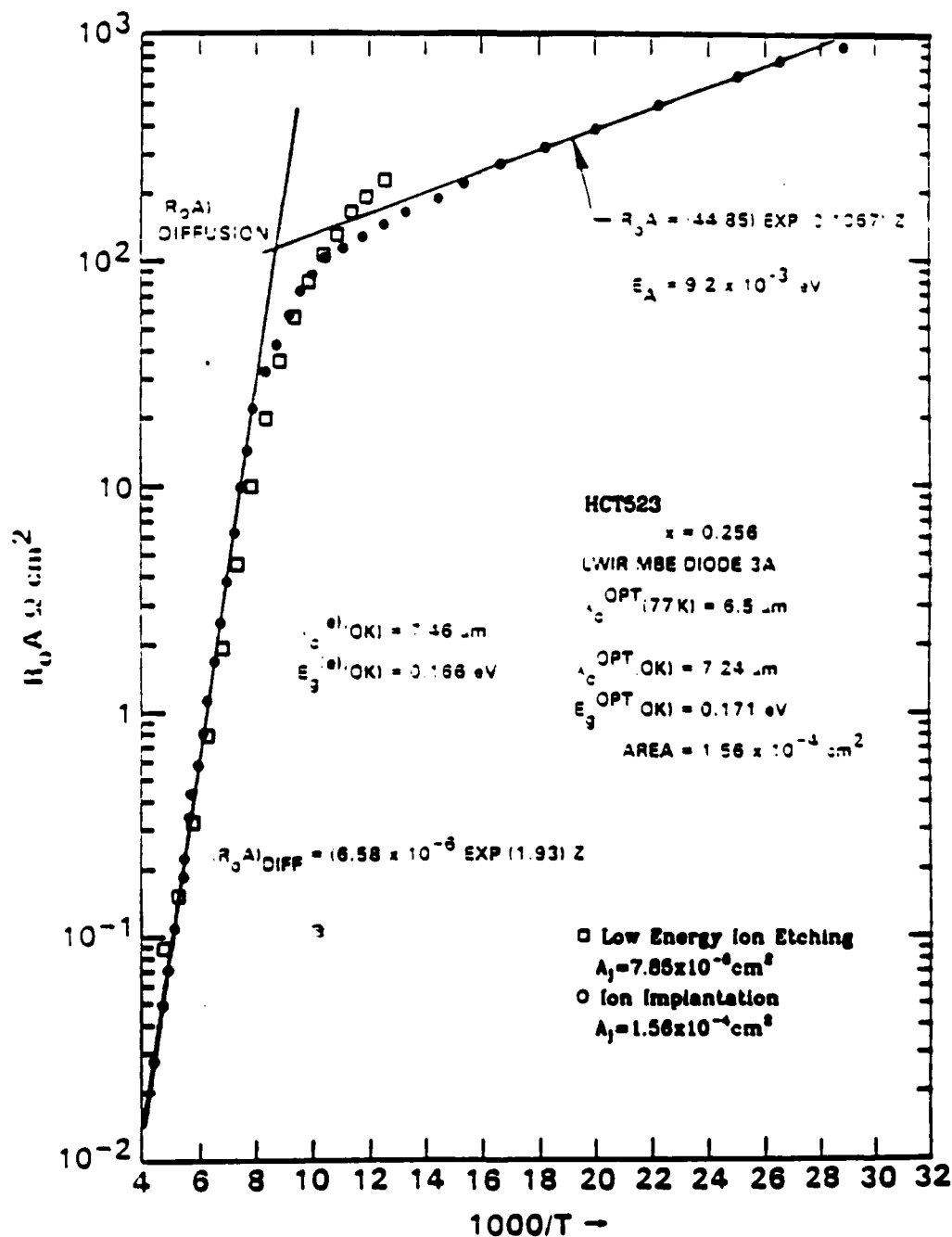


Fig. 3

**Planar heterojunctions made on MBE grown mercury cadmium telluride using low energy ion sputtering**

**S. S. Yoo\*, M. Boukerche, M. DeSouza and J. P. Faurie**

**Department of Physics  
\*Electrical Engineering and Computer Science  
University of Illinois at Chicago  
Chicago, Illinois 60680**

**ABSTRACT**

Planar heterojunctions were fabricated on mercury cadmium telluride layers grown by Molecular Beam Epitaxy. P-type (111)B  $\text{Hg}_{1-x}\text{Cd}_x\text{Te}$  having an x value gradually increasing to the surface have been grown. The sputtering technique has been used to form the junctions. For the first time, electrical and optical characterizations of a representative junction are presented in this report. The resistance-area product at zero bias and at 80 K is  $2.4 \times 10^3 \text{ ohm-cm}^2$  for  $x=0.27$ . The spectral response of this device shows that two junctions, one with  $x=0.27$  and the other with  $x=0.33$ , exist. However, Responsivities as high as 7.2 A/W at 80 K were recorded due to the electrically reflecting boundary on the p-type surface.

## 1. INTRODUCTION

The ternary alloy  $\text{Hg}_{1-x}\text{Cd}_x\text{Te}$ , with  $x$  values ranging from 0.2 to 0.3, is currently the most important narrow band gap semiconductor for infrared (IR) detection. Its interesting features for infrared detection applications have been studied for more than two decades. The photovoltaic rather than the photoconductive detection has been favored because of the low  $1/f$  noise, high detectivity and the high density of devices mainly for application to focal plane arrays.

Great effort has been made, for several years, to grow epitaxial layers using different methods, such as: LPE, MOCVD, LADA, and MBE. However up to now, only the LPE technique seems to have reached a sufficient maturity to give layers suitable for device processing. This is probably due to the fact that MBE was more often utilized as a tool to grow heterostructures, such as superlattices. However, reports have recently been published on IR photodiodes made on (111)B  $\text{Hg}_{1-x}\text{Cd}_x\text{Te}$  grown by MBE.<sup>1,2,3</sup> According to these publications, the as grown MBE  $\text{Hg}_{1-x}\text{Cd}_x\text{Te}$  layers exhibited IR photodiode performances not as good as those fabricated on annealed LPE layers for device applications. More recently, IR photodiodes fabricated on  $\text{Hg}_{1-x}\text{Cd}_x\text{Te}$  layers grown by MBE in a different orientation, namely (211)B, displayed performances equivalent to those made with LPE layers.

The ion implantation technique is one of the techniques most commonly used to make p-n junctions. This technique allows a precise control of the junction depth, avoids heating of this metallurgically sensitive material and is more suitable for microdevices than mercury diffused junctions made by annealing.<sup>5</sup> In general, ion implantation employs a high ion energy ranging from 100 KeV to 400 KeV. Since the lower binding energies of ionic bonds are dominant in II-VI compound semiconductors, the damages induced by the implanted ions can propagate well beyond the depth where ions stop. This effect is not so dramatic for III-V compound semiconductors. Therefore, the junction is believed to be formed several times deeper than the mean range of the ions. A variety of dopants, such as B, Al, P, and even inert Ar, have been implanted with different ion energies to form p-n junctions whose results were compared in the experiment of Kolodny et al.<sup>6</sup> They concluded that the conversion to n-type conductivity was due to defects or damages created by the implanted ions, rather than by the implanted dopants and the number of implanted ions because the sheet carrier density was not sensitively changed by the ion doses and the ion energies. More recently, Bubulac et al.<sup>7</sup> found that mercury atoms activated by implanted ions diffuse more effectively into the stoichiometrically doped p-type layers than ones doped by impurities, such as As. Furthermore, the junction could be improved, and be defect free, by driving the mercury atoms further into the p-type region by successive annealings.

By analogy, if a low energy ion bombardment such as sputtering is sufficient to create defects or damages at the surface of p-type  $\text{Hg}_{1-x}\text{Cd}_x\text{Te}$  layers, the damaged surface should be converted to n-type, thus forming p-n junctions similar to ion implanted junctions. This technique was first investigated by Wotherspoon in 1981.<sup>8</sup> He claimed that the etched-away part of the p-type layer leaves the excess carriers

of mercury, which act as dopant sources converting the p-type surface to n-type. Surprisingly, despite the wide use of dry etching techniques, to our knowledge, only few reports have been published on the study of sputter etching effects.<sup>9,10</sup>

For the first time, we present, in this report, the performance of p-n junctions, fabricated on compositionally graded p-type  $\text{Hg}_{1-x}\text{Cd}_x\text{Te}$  grown by MBE, using a simple diode sputtering system.

## 2. FABRICATION

The starting materials were p-type (111)B  $\text{Hg}_{1-x}\text{Cd}_x\text{Te}$  layers grown in a RIBER-2300 Molecular Beam Epitaxy system.<sup>11</sup> P-type  $\text{Hg}_{1-x}\text{Cd}_x\text{Te}$ , 5  $\mu\text{m}$  thick with a cadmium composition  $x$  equal to 0.27, was grown initially, then the  $x$  value was gradually increased in a controlled manner during the growth of the remaining 0.7  $\mu\text{m}$   $\text{Hg}_{1-x}\text{Cd}_x\text{Te}$ . A thin cadmium telluride cap layer was evaporated in situ to protect the  $\text{Hg}_{1-x}\text{Cd}_x\text{Te}$  surface. The overall  $x$  value of the layer was deduced to be 0.27 from IR Transmission measurement at 300 K. The carrier concentration and the mobility were determined to be  $2.3 \times 10^{16} \text{ cm}^{-3}$  and  $100 \text{ cm}^2/\text{V-sec}$  respectively at 80 K from the Hall measurement. The minority carrier lifetime was measured to be 140 nsec at 77 K by the photodecay technique. Secondary Ion Mass Spectroscopy measurements were carried out to confirm the gradual change of the  $x$  value. At the surface of the layer,  $x$  was deduced to be 0.33 by taking the relative change in the Cd/Te ratio. This was in good agreement with the growth condition. The device areas were defined by conventional photolithography, which are 100  $\mu\text{m}$  diameter dots. The contact opening was made by a slight etching of the cadmium telluride cap layer in a 0.01% solution of  $\text{Br}_2$  in  $\text{HBr}$ . The sputter etching was carried out at an ion energy of 400 eV using a diode sputtering system. Immediately after sputtering, Ni was deposited on the n-type area. The contact metal was defined using the lift off technique. Long stripes of Au contacts were electrochemically deposited on the p-type layer. During the processing, the temperature never exceeded 60 C and the layer was not subsequently annealed. The schematic diagram of the resulting device structure is shown in Fig. 1. The current-voltage characteristic and the photovoltaic effect at 80 K are shown in Fig. 2.

## 3. ELECTRICAL AND OPTICAL MEASUREMENTS

The electrical measurements were taken in a Joule Thomson refrigerator. Fig. 3 shows the current-voltage characteristics of a representative device at three different temperatures: 143 K in the diffusion region, 111 K in the generation-recombination region and 83 K in the tunneling region of the zero bias resistance-area product dependence on temperature. The analysis, in forward bias, was carried out by fitting the current-voltage data points to the modified Shockley's diode equation, considering the series resistance effect in the high current region:

$$V = IR_s - I_s (\exp(qV/nKT) - 1)$$

$q$  is the electronic charge,  $V$  the applied voltage,  $k$  the Boltzman constant,  $T$  the absolute temperature,  $I_s$  the saturation current,  $n$  the

ideality factor and  $R_s$  the series resistance. After the fitting of the current-voltage curves at various temperatures, the series resistance extracted from the fitting was compared with the resistivity measured by Hall effect measurements. They were in good agreement. The fitting at 142 K was excellent for explaining the ideal diode behavior of the current-voltage characteristics in the diffusion region, where the ideality factor is unity. The saturation current in forward bias is slightly less than in reverse bias. This is consistent with the results of Faurie et al.<sup>3</sup> The temperature dependence of the zero bias resistance-area product is shown in Fig. 4. For the diffusion region at temperatures above 125 K, the temperature dependence of the zero bias resistance-area product gives an activation energy of 200 meV, which is less than the optical band gap (243 meV at 83 K). However, this discrepancy is usually observed between electrical and optical data. As the temperature decreases, the current-voltage curve in forward bias shows two separate slopes in small bias region and large bias region. In this case, the fitting was carried out in two separate current regions. From the current-voltage curve at 111 K, the ideality factors were determined to be 2 in the small bias region and 1.17 in the large bias region. The generation-recombination current becomes dominant in the small bias whereas the diffusion current still prevails in large forward bias regions. This illustrates the fact that the zero bias resistance-area product in the temperature range, 100 K to 120 K, is due to generation-recombination in the depletion region, thus showing the temperature dependence of  $E_g/2$ . For temperatures lower than 100 K, the ideality factor in the high current region increases slowly up to 1.7 at 83 K and the change in the slope becomes insensitive to temperature variations at small biases. This indicates that the current in small bias is related to the thermally assisted tunneling mechanism.<sup>12</sup> The performance of a linear array of detectors can be represented by the histogram of the dynamic resistance of the junctions as shown in Fig. 5. These were 32 devices within a certain area and were measured at 150 K in the diffusion region of the zero bias dynamic resistance. It shows the very good uniformity of the devices at the operating temperature.

The junction depth was characterized by the differential Hall and the spreading resistance measurements. They give depths of 1 and 0.8  $\mu\text{m}$ , respectively for this layer. Considering the junction depth of ion implanted diodes, which is typically 2 to 5  $\mu\text{m}$ , the investigated junction was shallower. However the measured junction depth for other processed MBE grown layers varied from layer to layer. This is probably due to the preferential mercury diffusion along the defects, such as dislocations and twin boundaries often present in MBE grown (111)B layers. Further study is currently being carried out to determine the junction depth, the carrier concentration and the minority carrier lifetime of the converted n-type layer.

One interesting feature of these devices is the spectral response, as shown in Fig. 6. It shows double peaks, one at 3.8  $\mu\text{m}$  and the other at 2.8  $\mu\text{m}$  and the signals are comparable. This can be explained by considering the planar junction with two diodes connected in parallel, one with a low  $x$  value (0.27) in the vertical direction and the other with high  $x$  value (0.33) in a direction parallel to the surface. Since the vertical junction area is assumed to be much larger, it is dominant

in the electrical measurement. But for the optical measurement, the junction of the high  $x$  value becomes dominant in the short wavelength region, where the junction of the low  $x$  value has less spectral response. The minority carriers generated by the radiation in the high  $x$  value p-type layer can either diffuse into the depletion region of the high  $x$  value junction, or be swept to the low  $x$  value layer and then diffuse into the depletion region of the low  $x$  value junction. The responsivity was measured with a 500 K blackbody radiation source at 80 K. It was determined to be 7.2 A/W. Since the compositionally graded layer at the p-type surface acts as an electrically reflecting boundary for the minority carriers,<sup>13</sup> the minority carriers generated by the radiation are repelled by the high  $x$  value layer.

#### 4. SUMMARY

We have presented the fabrication of junctions on  $\text{Hg}_{1-x}\text{Cd}_x\text{Te}$  grown by MBE, using low energy ion sputter etching. Several groups<sup>7,10,11</sup> have shown that the origin of the n-type conversion is due to the mercury diffusion into the bulk of the layer from the very thin surface layer within the projected energy range of the ions. In contrast to ion implantation creating n-type conversion mainly by extended induced damages, this technique can actually improve n-type material properties by decreasing its degree of compensation.<sup>11</sup> This technique is comparable to the ion implantation for the fabrication of microdevices, except for the fact that it uses lower ion energies. Low energy ion sputtering might be expected to be better than ion implantation in view of less process-induced damages during the junction formation, the control of the shallow junction depth and the n-type layer carrier concentration. This technique can be applied for in situ junction technology in a MBE chamber. Furthermore, the fabrication costs using this technique are very inexpensive compared to the ion implantation.

The current-voltage characteristics in three different temperature regions along with the zero bias resistance-area product corresponding to the diffusion, generation-recombination and tunneling regimes were presented. The current-voltage characteristics show the diffusion behavior at small bias, for temperatures higher than 125 K. The generation-recombination current is dominant for the temperature range 100 K to 125 K and the tunneling current is dominant at temperatures below 100 K, at small bias. The product of zero bias resistance-area is  $2.4 \times 10^3 \text{ ohm-Cm}^2$  at 80 K. Finally double peaks are seen in the spectral response, which is due to the compositional heterojunction at the surface. This is advantageous for the optical detection because the large band gap layer acts as the electrical reflecting boundary in the long wavelength where the low  $x$  value layer is active. It also prevents the exposure of the sensitive narrow band gap semiconductor surface. A responsivity as high as 7.2 A/W was achieved owing to the larger  $x$  value layer on the surface. This value was higher than that of other homojunctions grown by MBE with the same process. The structure could also be utilized for the double wavelength detection by controlling the band gap of the compositional heterojunction.

## 5. ACKNOWLEDGEMENTS

This work has been supported by DARPA and monitored by ARO under the contract # F49620-87-0021. One of us (M.DeSouza) has also a scholarship from CNPQ(Brazil).

## 6. REFERENCES

1. J. P. Faurie, A. Million, R. Boch and J. L. Tissot, J. Vac. Sci. Technol. A 1, 1953 (1983)
2. J. M. Arias, S. H. Shin, J. G. Pasko and E. R. Gertner, Appl. Phys. Lett. 52, 39 (1988)
3. J. P. Faurie, S. Sivananthan, M Lange, R. E. Dewames, A. M. B. Vandewyck, G. M. Williams, D. Yamini and E. Yao, Appl. Phys. Lett. 52, 2151 (1988)
4. J. M. Arias, S. H. Shin, J. G. Pasko, R. E. DeWames and E. R. Gerter, J. Appl. Phys., 65, 1747 (1989)
5. G. L. Destefanis, Journal of Crystal Growth, 86, 700, (1988)
6. A. K. Kolodny and I. Kidron, IEEE ED-27, no.1, 37, (1980)
7. L. O. Bubulac, J of Crystal Growth, 86, 723, (1988)
8. J. T. M. Wotherspoon, UK Patent GB 2095898, 1981
9. H. M. Nitz, O. Ganschow, U. Kaiser, L. Wiedmann and A. Bennighoven, Surface Science 104, 365 (1981)
10. G. Bahir and E. Finkman, J. Vac. Sci. Technol. A7, 348 (1989)
11. J. P. Faurie, J. Reno, S. Sivananthan, I. K. Sou, X. Chu, M. Boukerche and P. S. Wijewarnansuriya, J. Vac. Sci. Techol. A4, 586 (1986)
12. R. E. DeWames, G. M. Williams, J. G. Pasko and A. H. B. Vanderwyck, J. Cryst. Growth 86, 849 (1988)
13. M. B. Reine, A. K. Sood and T.J.Tredwell, in Semiconductor and Semimetals, vol. 18, p299, Academic Press, New York (1981)

## VI SURFACE AND INTERFACE STUDIES

### VI-1 HgTe-CdTe SUPERLATTICES: Hg INCORPORATION IN CdTe LAYERS DURING MBE GROWTH

It has been shown in 1982 that HgTe-CdTe superlattices (SLs) could be grown by MBE. But due to the noncongruent evaporation of Hg from HgTe, the Hg flux must be maintained even during the growth of the CdTe layers. This means that some Hg is incorporated in the CdTe during its growth. There are two important questions that arise. First, how will this Hg incorporation affect the bandgap of the SL. Second, how much Hg is in the CdTe.

We determine the period of the SL by the position of the X-ray satellite peaks. The average Hg composition in the SL is then measured by EDS. The period and the average Hg composition are then used to compute the individual layer thicknesses if the percentage of Hg in the CdTe is known. Using this method, for the same period and average Hg composition, as the amount of Hg in the CdTe increases several things will occur. First, the thickness of the HgTe layers will decrease. This will tend to increase the bandgap. Second, the CdTe will become  $\text{Hg}_x\text{Cd}_{1-x}\text{Te}$  with a smaller bandgap. This decrease in the barrier height will tend to decrease the SL bandgap. Finally, the width of the  $\text{Hg}_x\text{Cd}_{1-x}\text{Te}$  will increase. This will have a small tendency to increase the bandgap. The total effect on the SL bandgap of all these changes would be small.

We have grown, with a Hg flux, thick layers of CdTe under the same conditions as in our SLs [190 to 200°C on (111)B]. The amount of Hg measured in the layer by EDS was less than 5%. On a series of thin CdTe (111)B layers grown under a Hg flux the amount of Hg was carefully measured by XPS. This is done using both the ratio of the peak areas and the difference in energy between the core level and valence band maximum. For the growth conditions that we actually use in our SLs, these results agree with those obtained for the thick layers. The Hg incorporation varies, up to 9%, depending on the growth conditions. This should only slightly affect the characteristics of the HgTe-CdTe SLs and other microstructures, such as single and double barrier tunneling structures.

These results indicate that some Hg is incorporated in the CdTe but that under our normal conditions this amount is small. The Hg incorporation is crystal orientation dependent. For the (100) surfaces, about 15% Hg are observed for

growth conditions identical to those used for the (111). For more information see the attached paper.

**ATTACHED PAPER:**

1. "Hg incorporation in CdTe during the growth of HgTe-CdTe superlattices by molecular beam epitaxy."

# Hg incorporation in CdTe during the growth of HgTe-CdTe superlattices by molecular beam epitaxy

J. Reno,<sup>a)</sup> R. Sporken,<sup>b)</sup> Y. J. Kim, C. Hsu, and J. P. Faurie  
Department of Physics, University of Illinois at Chicago, Chicago, Illinois 60680

(Received 3 August 1987; accepted for publication 9 September 1987)

HgTe-CdTe superlattices and other microstructures such as single and double barrier tunneling structures are commonly grown by molecular beam epitaxy with the mercury flux continuously on the sample during the growth. This means that some mercury will be incorporated in the CdTe layers. We present here, for the first time, a measurement of the amount of mercury incorporated in thin layers of CdTe. X-ray photoelectron spectroscopy was used to measure the amount of mercury. The amount of mercury was found to be between 3 and 9% for CdTe (111) $\bar{B}$ , depending on the growth conditions. The amount of mercury was found to increase with mercury flux and to decrease as the substrate temperature was increased. Under the same conditions, it was found that much more mercury was incorporated in the (100) orientation. The type of substrate (CdTe or GaAs) was not found to influence the results. These results indicate that the amount of mercury in the CdTe layers of HgTe-CdTe superlattices is not quite as low as expected from measurements of thick CdTe layers, but it can be low enough that it does not influence significantly the results on the superlattice system in the (111) orientation.

HgTe-CdTe superlattices have been proposed as a new, interesting infrared material.<sup>1,2</sup> It has been shown that they can be grown by molecular beam epitaxy (MBE).<sup>3</sup> It has also been shown that the best growth temperature is 180–200 °C.<sup>3</sup> At this temperature the mercury condensation coefficient is about  $10^{-3}$ .<sup>4</sup> This means that a large mercury overpressure is needed to grow HgTe. It also implies that mercury will easily and noncongruently evaporate from HgTe. Due to this problem, the common growth technique for HgTe-CdTe superlattices and other microstructures such as single and double barrier tunneling structures involves leaving the Hg source open at all times.<sup>5,6</sup> Thus, there is a mercury flux on the sample during the growth of the CdTe layers. A competition then occurs between the Hg and Cd atoms for lattice sites. As a result, the CdTe layers may not be pure CdTe but instead be Hg<sub>1-x</sub>Cd<sub>x</sub>Te with some percentage of mercury.

This problem was recognized by the first people to grow HgTe-CdTe superlattices on CdTe (111) $\bar{B}$  substrates. They grew thick layers of CdTe under the same conditions as in the superlattice, including the presence of the Hg flux. The Hg content was then measured by energy dispersive spectroscopy (EDS). It was found that the CdTe contained less than 5% mercury.<sup>7</sup> When we began to grow HgTe-CdTe superlattices at the University of Illinois, we repeated these experiments with the same results.<sup>5</sup> This small amount of mercury should only slightly influence the characteristics of the superlattices such as the band gap and the valence-band discontinuity. Therefore, it was neglected. The only question was whether the results for a thick layer were the same for the thin layer in the superlattice.

Recently, it has been suggested that the amount of mercury in the CdTe layers of the superlattice might not be as

small as previously thought.<sup>8</sup> For this reason we have performed the first measurements of the amount of mercury incorporated in *thin* CdTe layers grown with a mercury flux. We have also looked at how the amount of mercury incorporated depends upon the substrate temperature, the mercury flux, the CdTe growth rate, and on the type and orientation of the substrate.

The samples were all grown at the University of Illinois in a Riber 2300 MBE machine. CdTe substrates oriented in the (100) and the (111) $\bar{B}$  were used. Additionally, GaAs(100) with both (100) and (111) $\bar{B}$  CdTe buffer layers were used. The substrate preparation and the growth of the appropriate buffer layer have been discussed elsewhere.<sup>5</sup> The Te flux was kept constant throughout the experiment. The flux was chosen so that the HgTe growth rate was about 5 Å/s on a CdTe(111) $\bar{B}$  substrate. A CdTe growth rate of 1 Å/s was used throughout the experiment, except when that growth rate was the parameter being varied. These growth rates are typical of those used in the growth of HgTe-CdTe superlattices. The substrate temperature was measured using a chromel-alumel thermocouple in contact with the sample holder and by an infrared pyrometer. These measurements have been calibrated using the melting temperatures of indium and tin.

The structure of the samples was chosen to be similar to that of the superlattices. On the buffer layer a HgTe layer with a thickness of 80–100 Å was grown first. This was immediately followed by a CdTe layer 150–170 Å thick. The CdTe layer was grown with the Hg flux still on the sample. The Hg concentration in the CdTe layers was measured by x-ray photoelectron spectroscopy (XPS) using both the ratio of peak areas and the energy difference between the Hg 5d or Cd 4d core level and the valence-band maximum (VBM). For Hg<sub>1-x</sub>Cd<sub>x</sub>Te, this energy difference can be shown to reflect the position of the VBM on an absolute energy scale, because the cation core levels are virtually independent on the alloy composition  $x$ .<sup>9,10</sup> The position of the VBM is

<sup>a)</sup> Present address: Sandia National Laboratory, Organization 1144, Albuquerque, NM 87185.

<sup>b)</sup> Permanent address: Facultes Universitaires Notre-Dame de la Paix, B-5000 Namur, Belgium.

known in turn to be very sensitive to the composition  $x$ .<sup>9,10</sup> Therefore, the binding energy of the Hg 5d and Cd 4d core levels with respect to the VBM can be used to determine the alloy composition  $x$ . Several samples were grown without the HgTe layer on the bottom to see if its presence changed the measurement. No difference was found in the Hg concentration in the CdTe whether the HgTe was present or not. First with the Te and CdTe fluxes constant, the substrate temperature and the Hg flux were varied to determine their influence on the Hg incorporation.

The samples were kept under ultrahigh vacuum conditions as they were transferred to the XPS chamber. The XPS measurements were performed with an SSX-100 spectrometer from Surface Science Laboratories. A monochromatized and focused Al K $\alpha$  excitation line was used. The overall energy resolution measured on the Au 4f<sub>7/2</sub> core level is 0.7 eV. The core levels used in this work were the Hg 4f and 5d, the Cd 4d and 3d, and the Te 4d and 3d. The values of the peak areas and positions of all the core levels were determined by a detailed analysis of the spectra by a least-squares fit of individual spin-orbit doublets to the data. The line shape used for the fits was a Lorentzian convoluted with a Gaussian. A nonlinear background was subtracted from the spectra prior to the fitting procedure.

Figure 1 shows a typical result for the spectrum of the Cd 4d and the Hg 5d core levels. This is the most difficult case due to the large number of overlapping peaks. The fit reveals the existence of two Hg components. These two components will be called Hg<sup>(1)</sup> and Hg<sup>(2)</sup> in the following discussion. From its binding energy with respect to the VBM,<sup>10</sup> Hg<sup>(1)</sup> can be clearly identified as Hg in Hg<sub>1-x</sub>Cd<sub>x</sub>Te. The origin of Hg<sup>(2)</sup>, at about 600 meV higher binding energy, is not yet fully understood. We believe that Hg<sup>(2)</sup> is some sort of surface mercury. Further experiments are still in progress to clarify this point. Only the component Hg<sup>(1)</sup>, associated with Hg in Hg<sub>1-x</sub>Cd<sub>x</sub>Te, was used in our measurements. It

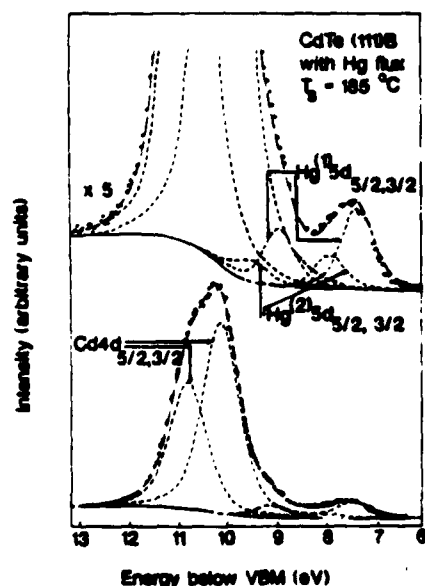


FIG. 1. Typical XPS spectrum from a CdTe layer grown with a mercury flux. The dash-dotted line is the result of a least-squares fit to the data. The dashed lines represent the individual components used for this fit. The background is represented by the solid line. The dots are the experimental data.

is the only one that should influence the band gap, if Hg<sup>(2)</sup> is indeed a surface phenomenon.

To obtain the binding energies ( $E_{C1} - E_V$ ) used for the determination of the Hg concentration, the position of the VBM was determined simply by a linear extrapolation of the valence-band leading edge. This procedure has proven to be reproducible and very accurate for Te-based II-VI semiconductors.<sup>11</sup> Since the binding energy defined above is very sensitive to the Hg concentration in Hg<sub>1-x</sub>Cd<sub>x</sub>Te,<sup>10</sup> it can be used to determine the amount of Hg in the CdTe. As can be seen in Table I, there is good agreement between the two methods. This gives us confidence in our results and in neglecting the Hg<sup>(2)</sup> component. This procedure implies the measurement of the valence-band energy distribution curve and is thus highly time consuming. Therefore, it was not applied systematically to all the samples.

In order to compare our previous results for a thick layer with these for a thin layer, we grew a thick CdTe layer and checked the Hg concentration with both XPS and EDS. The growth conditions were similar to those used for the thin layers ( $T_s = 195^\circ\text{C}$ , Hg flux =  $1.6 \times 10^{17} \text{ cm}^{-2} \text{ s}^{-1}$ , and CdTe growth rate  $1 \text{ Å s}^{-1}$ ). The results from EDS agreed with all of our earlier work and gave a value of about 3% Hg in the CdTe. The XPS results on this layer gave a Hg concentration of 5%. This difference is within the range of experimental error, but it may also indicate that there is a slight difference in the Hg concentration with depth.

The homogeneity of the Hg distribution with depth can be checked by comparing results from core levels at different binding energies. In our case the determinations using the Hg 4f, Cd 3d, and Te 3d core levels are more surface sensitive than those using the Hg 5d, Cd 4d, and Te 4d lines. This is due to the smaller escape depth for the Cd 3d and Te 3d photoelectrons ( $\lambda \approx 15 \text{ Å}$ ) compared to the Cd 4d and Te 4d ( $\lambda \approx 20 \text{ Å}$ ). We found that the more surface-sensitive determinations systematically yielded slightly higher concentrations. Compared with EDS, XPS is primarily a surface technique. The observed surface enrichment is thus consistent with the difference between the bulk results from EDS and the XPS results. Further investigations with good depth resolution would certainly be very desirable to confirm (or infirm) this point.

Table I summarizes the Hg concentrations determined by XPS for the different substrate and Hg cell temperatures. The Hg concentrations determined by both XPS methods are given. The values given in the table based on peak area

TABLE I. Hg to Te ratio in CdTe grown with a Hg flux on CdTe substrates, along with the growth conditions.  $T_s$  is the substrate temperature. The CdTe growth rate was held constant at about  $1 \text{ Å/s}$ .

Substrate orientation	$T_s$ (°C)	Hg flux ( $10^{17} \text{ cm}^{-2} \text{ s}^{-1}$ )	$1-x$ (area ratios)	$1-x$ (binding energies)
(111)B	175	1.6	$0.085 \pm 0.009$	$0.087 \pm 0.020$
(111)B	185	1.6	$0.065 \pm 0.015$	$0.051 \pm 0.020$
(111)B	195	1.6	$0.057 \pm 0.016$	
(111)B	195	0.89	$0.045 \pm 0.010$	$0.070 \pm 0.020$
(111)B	195	1.6	$0.057 \pm 0.016$	
(111)B	195	2.2	$0.085 \pm 0.016$	$0.100 \pm 0.020$
(100)	185	1.6	$0.147 \pm 0.016$	

ratios are average values from four different sets of core level spectra. Relative sensitivity factors were determined for our instrument from MBE grown HgTe (111) and CdTe (111) samples.

The Hg flux was determined using Knudsen's effusion law, which is a good approximation in this case for the direction normal to the evaporating surface. A change of the substrate temperature by 10 °C will change the Hg condensation coefficient by about a factor of 1.5.<sup>4</sup> Several striking features are observed from this table. First, for these growth conditions on CdTe (111)B the amount of Hg incorporated is much less than 20%.<sup>12</sup> Second, the overall agreement between the area ratio and the binding energy results is good. Third, the amount of Hg incorporated follows the general trends expected from the growth conditions, and the relative magnitudes are in reasonable agreement with the Hg flux and condensation coefficient variations. Fourth, a Hg concentration of 5% was obtained by the correct selection of the growth conditions and we have obtained a value as low as 3% in a second set of experiments.

It has been reported that for a CdTe (211) substrate the amount of Hg incorporated is about 20%.<sup>13</sup> We have also shown that the Hg condensation coefficient varies depending on the orientation of the substrate.<sup>14</sup> For this reason, we have also investigated CdTe (100). The fluxes were the same as used for the (111)B. The results are also given in Table I. The difference in the Hg incorporation is very large and opposite to our initial expectations, since Hg on CdTe (100) has the smaller condensation coefficient of these two orientations. We do not understand these results, but they show once again that MBE growth cannot be treated by a classical thermodynamic approach using the law of mass action and neglecting surface kinetics.

We performed a second set of experiments to check the dependence of the Hg incorporation on the CdTe growth rate and on the type of substrate. The Te and Hg fluxes were kept constant. The results are given in Table II.

The first point that can be seen from these results is that it does not matter whether a CdTe (111)B substrate or a GaAs (100) substrate with a CdTe (111)B buffer is used to grow the layers. The Hg incorporation is about the same for the two different substrates. The second point is that the Hg incorporation appears to increase with the CdTe growth rate. We do not have much data, but the trend appears to be in this direction.

It was also found that the quality of the surface prior to the growth of our structures could dramatically influence the amount of Hg incorporated. If the same substrate was reused frequently and thus re-etched several times or an inadequate buffer layer was grown, a significantly larger Hg incorporation was found. This means that extreme care must be taken not only when doing this type of experiment but also when preparing a substrate on which to grow a superlattice.

In conclusion, we have presented for the first time a measurement of the amount of mercury incorporated in thin layers of CdTe grown under mercury flux. The growth conditions and the structures were chosen to be similar to those in HgTe-CdTe superlattices. When carefully prepared, lay-

TABLE II. Hg to Te ratio in CdTe grown with a Hg flux along with the growth conditions. All were grown on a CdTe (111)B buffer layer but the initial substrate was varied.  $T_s$  is the substrate temperature. Estimated Hg flux:  $1.6 \times 10^{17} \text{ cm}^{-2} \text{ s}^{-1}$ .

Substrate	$T_s$ (°C)	CdTe growth rate ( $\text{\AA}/\text{s}$ )	$1-x$ (area ratios)	$1-x$ (binding energies)
CdTe	195	0.5	$0.030 \pm 0.004$	$0.043 \pm 0.020$
CdTe	195	1.0	$0.057 \pm 0.016$	...
CdTe	195	2.0	$0.078 \pm 0.008$	...
GaAs	185	1.0	$0.065 \pm 0.007$	$0.043 \pm 0.020$
GaAs	195	1.0	$0.036 \pm 0.008$	...

ers grown on CdTe (111)B were found to contain between 3 and 9% mercury. The amount of mercury was found to increase with the mercury flux and the CdTe growth rate, and to decrease as the substrate temperature was increased. We did not observe any significant dependence of the amount of mercury incorporated on the type of substrate but there was a large dependence on the orientation of the substrate. We found that much more mercury was incorporated for (100) than for (111)B prepared under the same conditions. We thus expect the Hg incorporation in CdTe (100) to be even more important under normal growth conditions.<sup>14</sup> This dependence of the amount of mercury incorporated on the growth conditions and the substrate orientation means that care must be taken when comparing results between different groups. Also, dramatic increases in the amount of Hg incorporated can occur if the initial surface is not properly prepared. These results indicate that the amount of mercury incorporated into carefully prepared (111)B superlattices is small enough that it should not significantly influence the characteristics of the superlattices previously reported, and in particular the value of the valence-band discontinuity and the band gaps.

This work carried out at the University of Illinois at Chicago was supported by the Defense Advanced Research Projects Agency and monitored by the Air Force Office of Scientific Research under contract No. F4920-87-C-0021. One of us (R. S.) is supported in part by the National Belgian Foundation for Scientific Research (FNRS).

<sup>1</sup>J. N. Schulman and T. C. McGill, *Appl. Phys. Lett.* **34**, 663 (1979).

<sup>2</sup>D. L. Smith, T. C. McGill, and J. N. Schulman, *Appl. Phys. Lett.* **43**, 180 (1983).

<sup>3</sup>J. P. Faurie, A. Million, and J. Piagnet, *Appl. Phys. Lett.* **41**, 713 (1982).

<sup>4</sup>J. P. Faurie, A. Million, R. Boch, and J. L. Timot, *J. Vac. Sci. Technol. A* **1**, 1593 (1983).

<sup>5</sup>J. P. Faurie, *IEEE J. Quantum Electron.* **QE-22**, 1656 (1986).

<sup>6</sup>K. A. Harris, S. Hwang, D. K. Blanka, J. W. Cook, J. F. Schetzma, N. Otsuka, J. P. Bankus, and A. T. Hunter, *Appl. Phys. Lett.* **48**, 396 (1986).

<sup>7</sup>J. P. Faurie, A. Million, and J. Piagnet (unpublished results, 1982).

<sup>8</sup>S. Perkowitz, D. Rajaval, I. K. Sou, J. Reno, J. P. Faurie, C. E. Jones, T. Caselman, K. A. Harris, J. W. Cook, and J. F. Schetzma, *Appl. Phys. Lett.* **49**, 806 (1986).

<sup>9</sup>C. K. Shih and W. E. Spicer, *Phys. Rev. Lett.* **58**, 2594 (1987).

<sup>10</sup>C. Hsu, T. M. Duc, and J. P. Faurie (unpublished).

<sup>11</sup>T. M. Duc, C. Hsu, and J. P. Faurie, *Phys. Rev. Lett.* **58**, 1127 (1987).

<sup>12</sup>S. Perkowitz, R. Sudharsanan, and S. S. Yom, *J. Vac. Sci. Technol. A* **5**, 3157 (1987).

<sup>13</sup>M. W. Goodwin, M. A. Kinch, R. J. Koestner, M. C. Chen, D. G. Seler, and R. J. Justice, *J. Vac. Sci. Technol. A* **5**, 3110 (1987).

<sup>14</sup>S. Sivananthan, X. Chu, J. Reno, and J. P. Faurie, *J. Appl. Phys.* **60**, 1359 (1986).

## VI-2 X-RAY PHOTOEMISSION STUDY OF Hg CLUSTERS ON $\text{Hg}_{1-x}\text{Cd}_x\text{Te}$ SURFACES

The (111)B surface of MBE-grown  $\text{Hg}_{1-x}\text{Cd}_x\text{Te}$  samples has been studied in detail using x-ray photoemission spectroscopy (XPS). The composition of the samples was in the range  $x = 0.15$  to  $0.97$ . The smaller  $x$  values were obtained with three MBE sources (CdTe, Te and Hg) as usual, whereas only two sources (CdTe and Hg) were used to obtain the larger values. A monochromatized and focussed Al  $K_{\alpha}$  excitation line was used for the XPS measurements.

Two types of Hg have consistently been found for all the samples. These two types of Hg will be labeled Hg[1] and Hg[2] hereafter. From the binding energy with respect to the valence-band maximum, Hg[1] is clearly identified as Hg in  $\text{HgCdTe}$ . The second component is found at higher binding energy and is attributed to the presence of small Hg clusters on the  $\text{HgCdTe}$  surface. The radius of these clusters is deduced from the  $\text{Hg}[2]4f_{7/2}$  intensity measured with XPS. Values between  $5\text{--}20\text{\AA}$  are obtained. The  $\text{Hg}[2]4f_{7/2}$  binding energy increases with decreasing cluster size. This is explained by the Coulomb energy  $\sim e^2/r$  due to the unit charge appearing on the cluster during the photoemission process<sup>(1)</sup>. This charge is not neutralized within the time scale relevant for photoemission, due to the semiconducting nature of the substrate. A good agreement between the experimentally observed binding energy shift and the calculated  $e^2/r$  behavior is observed. For large cluster sizes, a binding energy of  $100.2 \pm 0.2$  eV is deduced. This is close to the value for bulk Hg (99.9 eV)<sup>(2)</sup>.

The apparent spin-orbit splitting of the  $\text{Hg}[2]5d$  levels decreases with decreasing cluster size. A total variation of 0.5 eV is measured. Our results are smaller than the value for free Hg atoms, except for the largest cluster sizes. This is attributed to the repulsion between the Cd4d and Hg5d levels, as initially discussed by Moruzzi et al.<sup>(3)</sup>.

From the influence of the sample preparation conditions on the amount of Hg in the clusters, we conclude that Hg outdiffusion is probably the major reason for the formation of these clusters.

### REFERENCES:

1. G.K. Wertheim et al., Phys. Rev. Lett. 51, 2310 (1983)
2. S. Svensson et al., J. Elec. Spectrosc. 9, 51 (1976)
3. V.L. Moruzzi et al., Phys. Rev. B 10, 4856 (1974)

**ATTACHED PAPERS:**

1. "X-ray photoemission from small mercury clusters on II-VI semiconductor surfaces"
2. "X-ray photoemission study of Hg clusters on  $\text{Hg}_{1-x}\text{Cd}_x\text{Te}$  surfaces"

# X-ray photoemission from small mercury clusters on II-VI semiconductor surfaces

R. Sporken,\* S. Sivananthan, J. Reno,<sup>†</sup> and J. P. Faurie

*Department of Physics, University of Illinois at Chicago, P.O. Box 4348, Chicago, Illinois 60680*

(Received 16 October 1987)

The presence of small Hg clusters ( $R = 5\text{--}20\text{ \AA}$ ) on  $\text{Hg}_{1-x}\text{Cd}_x\text{Te}$  samples grown by molecular-beam epitaxy has been deduced from a careful analysis of the x-ray-induced photoemission spectra. The positive binding-energy shift measured for these clusters is explained by the appearance of a positive charge on the clusters during the photoemission process. (The experimental results are compared with the calculated  $e^2/2R$  behavior.) The apparent spin-orbit splitting for the Hg  $5d$  levels is reduced, compared to bulk Hg and to isolated Hg atoms. This is attributed to the repulsion between the Cd  $4d$  and Hg  $5d$  orbitals. It is shown that Hg out-diffusion is the main reason for the formation of these clusters.

## I. INTRODUCTION

Studies of surfaces and interfaces of semiconducting materials are very important for the development and understanding of modern microelectronic devices. Detailed investigation of the phenomena occurring during the growth of such surfaces and interfaces is very important due to the still increasing miniaturization of the devices presenting a challenge to both theoreticians and experimentalists. This paper deals with one particular aspect of surface studies on II-VI compound semiconductors, which is the formation of small mercury clusters on the surfaces of these semiconductors.

Photoemission has been demonstrated to be very powerful for examining the electronic properties of supported small metal clusters.<sup>1-3</sup> The study of such small particles was initially motivated by their technological importance in heterogeneous catalysis.<sup>4</sup> Small metal clusters have also been detected in many cases during the early stages of metal-semiconductor interface formation.<sup>5-7</sup> Amorphous carbon has been the most widely used substrate for detailed studies of the electronic properties of small metal clusters, but other substrates, mostly insulators, have been used as well. In this paper we present a photoemission study of Hg clusters on CdTe(111) and  $\text{Hg}_{1-x}\text{Cd}_x\text{Te}(111)$  substrates. To the best of our knowledge, this is the first detailed photoemission study of metal clusters on a semiconducting substrate.

This work was first motivated by an unexpected result obtained during the study of the Hg incorporation in CdTe during the growth of HgTe-CdTe superlattices by molecular-beam epitaxy (MBE).<sup>8</sup> The common growth technique for HgTe-CdTe superlattices and other superstructures, such as single and double barrier tunneling structures, involves leaving the Hg cell open at all times.<sup>9,10</sup> As a result, the CdTe layers are not pure CdTe layers, but instead  $\text{Hg}_{1-x}\text{Cd}_x\text{Te}$  with typically 3-9% of mercury for the (111)  $B$  orientation.<sup>8</sup> In addition to Hg bound to Te atoms, the x-ray photoemission (XPS) analysis of such spectra revealed the existence of a second type of mercury with about 600 meV higher binding ener-

gy.<sup>8</sup> In the present work, we show that this second mercury component in the Hg  $5d$  and  $4f$  spectra is due to the presence of small Hg clusters on CdTe and  $\text{Hg}_{1-x}\text{Cd}_x\text{Te}$  surfaces. The electronic properties as well as the origin of these clusters will be discussed.

## II. EXPERIMENT

The samples were all prepared at the University of Illinois at Chicago in a Riber MBE 2300 machine. CdTe substrates oriented in the (111)  $B$  direction as well as GaAs substrates with a CdTe(111)  $B$  buffer layer were used. The substrate preparation and the growth of the appropriate buffer layer have been discussed elsewhere.<sup>3</sup> The layers analyzed here are  $\text{Hg}_{1-x}\text{Cd}_x\text{Te}$  with  $x$  in the range of 0.15-0.97. The smaller  $x$  values were obtained with three MBE sources (CdTe, Te, and Hg) following the usual procedure.<sup>9</sup> The larger values are obtained with only two sources (CdTe and Hg) as described in Ref. 8. The sample temperatures quoted here were measured using a Chromel-Alumel thermocouple and—whenever possible—by an infrared pyrometer. These measurements have been calibrated using the melting points of indium and tin.

The samples were kept under ultrahigh-vacuum conditions as they were transferred to the XPS chamber. The XPS measurements were performed with a SSX-100 spectrometer from Surface Science Laboratories. A monochromatized and focussed Al  $K\alpha$  excitation line was used. The overall energy resolution measured on the Au  $4f$  core level is 0.7 eV. The reference levels used for this study will be specified as necessary. The position of the Fermi level was determined from the position of the Au  $4f_{7/2}$  line measured from a bulk gold sample. The corresponding binding energy was fixed at 83.93 eV. The core levels used in this work are the Hg  $4f$  and  $5d$ , the Cd  $3d$  and  $4d$ , and the Te  $4d$  and  $3d$ . For all the peaks, the values of the area, position, and full width at half maximum (FWHM) were determined by a least-squares fit of individual spin-orbit doublets to the data.

### III. RESULTS AND DISCUSSION

The discussion of the results will be organized in three parts. First, we will focus on a detailed analysis of the XPS spectra from  $\text{Hg}_{1-x}\text{Cd}_x\text{Te}$  samples. It will be shown that two types of Hg exist in these samples, one being Hg bound to Te and the other due to the presence of small mercury clusters on the sample surface. Thereafter, it will be shown that such Hg clusters can be obtained by depositing Hg on CdTe(111) *B* surfaces at room temperature. Finally, we will try to identify the origin of these clusters obtained unintentionally on MBE-grown  $\text{Hg}_{1-x}\text{Cd}_x\text{Te}$  surfaces.

Typical photoemission spectra from  $\text{Hg}_{1-x}\text{Cd}_x\text{Te}$  are shown in Fig. 1. The peaks are the Cd 4*d* and Hg 5*d* spin-orbit doublets and the Hg 4*f*<sub>7/2</sub>. These spectra have been analyzed for all the samples by means of a least-squares curve-fitting procedure as mentioned above. A nonlinear background was subtracted from the spectra prior to the fitting procedure. The line shape used for the fits was a Lorentzian convoluted with a Gaussian. This procedure is justified for the photoemission from semiconductors. It might be argued, however, that the Doniach-Šunjić line shape<sup>11</sup> has to be used in the case of small metal clusters. The quality of the fits obtained with the symmetric line shape is very good. This might indicate that the final-state screening in very small clusters is different from bulk metals, resulting in a different (and smaller) singularly index for the Doniach-Šunjić line shape for these clusters as compared to the bulk metal.

Two types of Hg have consistently been found for all the samples. These two types of mercury will be labeled

$\text{Hg}^{(1)}$  and  $\text{Hg}^{(2)}$  in the following discussion. From its binding energy with respect to the valence-band maximum (VBM),<sup>12</sup>  $\text{Hg}^{(1)}$  is clearly identified as Hg in  $\text{Hg}_{1-x}\text{Cd}_x\text{Te}$ . The second component  $\text{Hg}^{(2)}$  is observed at higher binding energy. We have suggested earlier that  $\text{Hg}^{(2)}$  is due to some kind of surface mercury.<sup>3</sup> This was inferred from two observations. First, on a 1.5- $\mu\text{m}$ -thick CdTe layer grown with a Hg flux, the amount of incorporated Hg as measured with energy-dispersive x-ray spectroscopy (EDS) agrees with the results from XPS obtained by neglecting  $\text{Hg}^{(2)}$ . Including  $\text{Hg}^{(2)}$  yields significantly higher concentrations. As the depth probed by XPS is small compared to EDS,  $\text{Hg}^{(2)}$  should be located in the surface region. Second, the Hg concentration in the CdTe layers can be determined from the binding energy of the Cd 4*d* and Hg 5*d* levels with respect to the VBM. This procedure is described in Ref. 8. Once again these results agree with concentrations deduced from XPS peak areas, neglecting  $\text{Hg}^{(2)}$ . This also suggests that  $\text{Hg}^{(2)}$  is located at the surface. Otherwise it would affect the position of the VBM.

Now that we have established that  $\text{Hg}^{(2)}$  is some sort of surface mercury, we need to find its exact nature. From the chemical shift measured on the Hg 5*d* and Hg 4*f* lines,  $\text{Hg}^{(2)}$  could be tentatively identified as  $\text{HgTe}_2$ . This is not a stable compound, but could exist at the surface of  $\text{Hg}_{1-x}\text{Cd}_x\text{Te}$  samples. However, if  $\text{Hg}^{(2)}$  is located in a two-dimensional surface layer, coverages up to 0.8 monolayers (ML) are deduced from the  $\text{Hg}^{(2)}$  peak areas. Such a coverage should then affect the characteristics of a surface component detected in the Te 4*d* spectra. The surfaces studied here are (111) *B* surfaces which are ter-

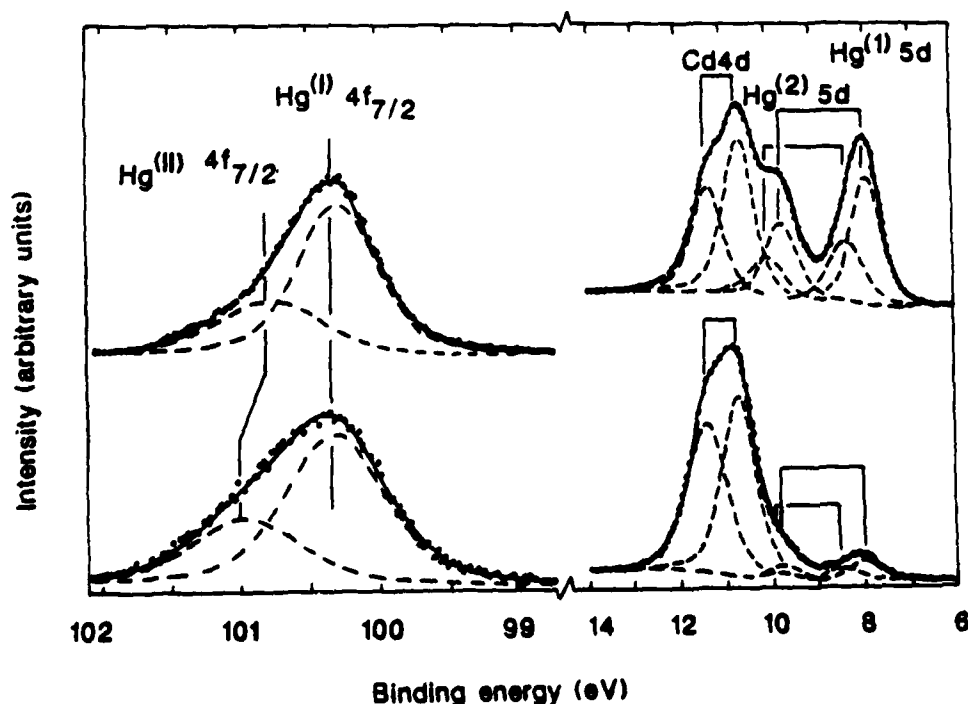


FIG. 1. Typical XPS core-level spectra from  $\text{Hg}_{1-x}\text{Cd}_x\text{Te}$ . The composition is  $x = 0.94$  (lower spectrum) and  $x = 0.60$  (upper spectrum). The number of atoms in the  $\text{Hg}^{(2)}$  estimated using relation (1) is  $7 \times 10^{13}$  and  $6 \times 10^{14} \text{ cm}^{-2}$ , respectively. The binding energy is referred to the Fermi level. The solid line is obtained by least-squares fitting of individual components (dashed lines) to the data.

minated by threefold-bonded Te atoms. From the Te 4d core-level spectra, a surface shift<sup>13</sup> of  $475 \pm 75$  meV towards higher binding energy was unambiguously determined by very careful curve fitting (Fig. 2). Close examination of the residuals, i.e., the difference between the calculated and the measured spectra, was particularly useful for the determination of this surface component. The characteristics (relative intensity, FWHM, and shift) of this surface component are independent of the amount of  $\text{Hg}^{(2)}$ . This rules out the existence of a two-dimensional layer of  $\text{HgTe}_2$ .

Based on this observation and on the fact that the Te 4d core-level intensity is reduced by only 5% for a  $\text{Hg}^{(2)}$  coverage corresponding to 1 ML in the case of a two-dimensional layer, we suggest that  $\text{Hg}^{(2)}$  must be related to the existence of small Hg clusters on the sample surface. The spectral characteristics of such small metal clusters are now well established<sup>1-3,14,15</sup> although the detailed explanation of these same characteristics is still a matter of debate. For almost all cases of small metal clusters, the core-level binding energies are higher than for the corresponding bulk material. This binding energy generally decreases with increasing cluster size, and sometimes a saturation or even a slight decrease is observed for very small cluster sizes.<sup>3,14</sup>

Figure 3 shows the binding energy  $E_B$  with respect to the Fermi level for the  $\text{Hg}^{(2)} 4f_{7/2}$  core level versus the  $A(\text{Hg}^{(2)} 4f_{7/2})/A(\text{Te } 3d_{5/2})$  area ratio. These data have been measured from many different samples and the different area ratios are the results of different preparation conditions. The relation between this area ratio and the preparation conditions will be discussed in the last section of this paper. The  $A(\text{Hg})/A(\text{Te})$  area ratio is related to the average cluster radius. The intensity model described in Ref. 14 can be adapted to the present problem and the following relation is obtained:

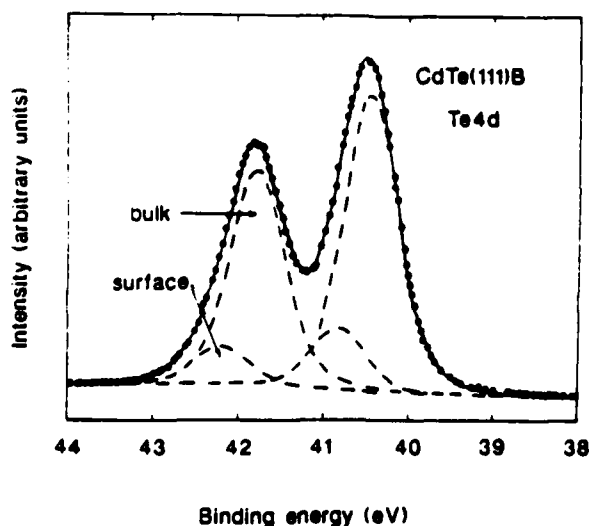


FIG. 2. Te 4d core-level spectrum from CdTe(111) B. The solid line is obtained by least-squares fitting of individual components (dashed lines) to the data. The binding-energy scale is referred to the Fermi level.

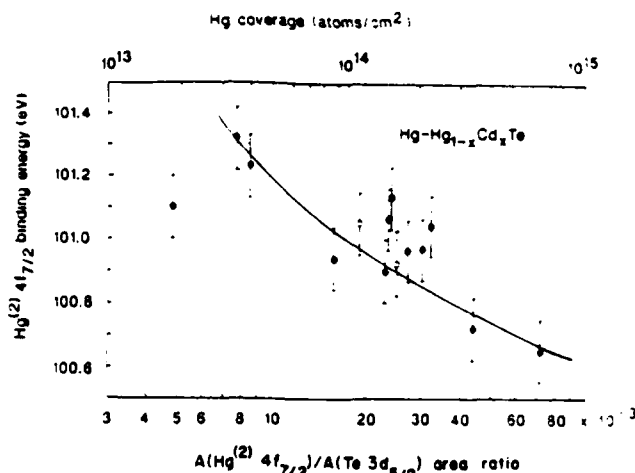


FIG. 3.  $\text{Hg}^{(2)} 4f_{7/2}$  binding energy with respect to the Fermi level vs  $A(\text{Hg}^{(2)} 4f_{7/2})/A(\text{Te } 3d_{5/2})$  area ratio. The solid circles are results from  $\text{Hg}_{1-x}\text{Cd}_x\text{Te}$  samples, whereas the open circles are obtained after the Hg absorption on CdTe at room temperature. The Hg coverage has been estimated using relation (1) with  $N_c = 6 \times 10^{11} \text{ cm}^{-2}$ . The solid line represents the calculated  $e^2/2R$  behavior. For details see the text.

$$\Gamma = A(\text{Hg}^{(2)} 4f_{7/2})/A(\text{Te } 3d_{5/2})$$

$$= N_c k \lambda_e \{ R^2 - 2[\lambda_e^2 - (R\lambda_e + \lambda_e^2) \exp(-R/\lambda_e)] \} \quad (1)$$

This relation is valid as long as the area covered by the clusters is small compared to the total sample area.  $R$  is the average cluster radius,  $N_c$  the cluster concentration,  $\lambda_e$  the effective photoelectron escape depth, and  $k$  is a constant depending on XPS sensitivity factors and on the density of the Hg clusters.  $\lambda_e$  is related to the photoelectron escape depth  $\lambda$  and to the mean electron escape angle  $\beta$  ( $\lambda_e = \lambda \cos \beta$ ). If  $N_c$  has approximately the same value for all the samples studied here, a plot of  $E_B$  versus  $\Gamma$  is equivalent to a plot of  $E_B$  versus  $R$  on a nonlinear scale. Some scatter observed from our data is most likely due to slight differences in  $N_c$  between different samples. The binding-energy decrease observed in Fig. 3 with increasing cluster size is a common feature for small metal clusters. In the case of metal clusters supported on insulating substrates, Wertheim *et al.*<sup>3,15</sup> have shown that positive binding-energy shifts with decreasing cluster size can be attributed to the Coulomb energy  $\sim e^2/2R$  which is due to the positive charge appearing on the cluster surface during the photoemission process. The unit charge in the photoemission final state is not neutralized during the time scale relevant to photoemission. The resulting Coulomb attraction will therefore increase the measured binding energy of the photoelectrons from the cluster. The same explanation was used in Ref. 14 for the case of Al clusters on Sb(111) substrates. We now suggest that this explanation may also be extended to the case of small metal clusters on certain semiconducting surfaces. For a typical cluster concentration of  $N_c = 6 \times 10^{11} \text{ cm}^{-2}$ , the cluster radii corresponding to Fig. 3 are found in the range of 5–20 Å using Eq. (1). A rough estimation of the

corresponding  $\text{Hg}^{(2)}$  coverages  $\Theta$  yields  $10^{13}$ – $10^{15}$  atoms/cm<sup>2</sup>. These coverage values are rather insensitive to the values of  $N_c$ , whereas the quoted radii are more strongly dependent on  $N_c$ . The reasonably smooth behavior of the data in Fig. 3 over a narrow range for the cluster radii (5–20 Å) is an indirect evidence for  $N_c$  being relatively independent on the details of the sample preparation. Figure 3 compares very well with results published in the recent literature concerning Au on amorphous carbon<sup>2,3</sup> and Ag on amorphous carbon.<sup>15</sup> In all the cases, the binding energy for the bulk metal was obtained for coverages between  $10^{15}$  and  $10^{16}$  atoms/cm<sup>2</sup>. Extrapolation of our results, according to a  $e^2/2R$  dependence, yields  $E_B(\text{Hg}^{(2)} 4f_{7/2}) = 100.2 \pm 0.2$  eV for large cluster sizes. This is close to the value for bulk Hg (99.9 eV).<sup>16</sup> The solid line in Fig. 3 shows this  $e^2/2R$  behavior adjusted to our data, using the values for  $R$  deduced from Eq. (1) with  $N_c = 6 \times 10^{11}$  cm<sup>-2</sup>. There might be a saturation or even a slight decrease for very small cluster sizes, as already reported for Al on Sb(111).<sup>14</sup> However, we do not want to draw this conclusion, due to the insufficient number of data in this particular region.

Another striking feature of  $\text{Hg}^{(2)}$  is the variation of the apparent spin-orbit splitting of the  $\text{Hg}^{(2)}$  5d levels with  $\text{Hg}^{(2)}$  coverage  $\Theta$ . Figure 4 shows this energy separation versus the intensity ratio  $\Gamma$  defined above. A total increase of 0.5 eV is observed with increasing cluster size. A saturation occurs at 1.7 eV, which is close to the value for bulk Hg (1.86 eV).<sup>17</sup> The spin-orbit splitting for isolated Hg atoms is known to be equal to the value for liquid Hg.<sup>17</sup> Our measured values of the apparent spin-orbit splitting are thus even smaller than the value for isolated atoms. This can be explained by the repulsion between the Cd 4d and Hg 5d levels, as initially discussed by Moruzzi *et al.*<sup>18</sup> In systems with two  $d$  metals, even

with no direct energy overlap, the two sets of  $d$  levels interact. The result is a repulsion between these  $d$  states proportional to their original energy separation, which then reduces the apparent spin-orbit splitting of either subsystem. For the smallest clusters, almost all the  $\text{Hg}^{(2)}$  atoms are in contact with the  $\text{Hg}_{1-x}\text{Cd}_x\text{Te}$  surface, whereas the repulsion is reduced for the larger clusters due to the increased Cd– $\text{Hg}^{(2)}$  distance. A similar explanation has been invoked by Eberhardt *et al.* in the case of  $\text{Cu}_3\text{Au}$  alloys.<sup>19</sup>

We have adsorbed Hg on MBE-grown  $\text{CdTe}(111)$  samples. The samples were kept at room temperature and the estimated Hg flux was approximately  $2.5 \times 10^{17}$  atoms cm<sup>-2</sup> s<sup>-1</sup>. This value was determined using Knudsen's effusion law. Hg 4f, Cd 3d, and Te 3d spectra have been measured after exposures of 35 and 45 min, respectively. Only one component was then detected in the Hg 4f<sub>7/2</sub> spectra. The corresponding results are represented by the open circles in Fig. 3. These results agree with values measured for  $\text{Hg}^{(2)}$  on  $\text{Hg}_{1-x}\text{Cd}_x\text{Te}$ . This is a further evidence that our interpretation of  $\text{Hg}^{(2)}$  is correct. We also note that for these two exposures, the ratio of the Hg coverages quoted in Fig. 3 is in excellent agreement with the ratio of the Hg exposures.

The last section of this paper is devoted to a tentative identification of the origin of the Hg clusters on  $\text{Hg}_{1-x}\text{Cd}_x\text{Te}$  surfaces. Two possible sources of these Hg clusters are readily identified: either the Hg in the  $\text{Hg}_{1-x}\text{Cd}_x\text{Te}$  crystals or the residual Hg in the growth chamber during the cooling of the grown layers.

The cooling of the layers from the growth temperature (175–195°C) to a temperature low enough to take the samples out of the growth chamber (typically 50°C) takes on the order of 1 h. During this time, the Hg flux is progressively reduced from a value of typically  $1.5 \times 10^{17}$  atoms cm<sup>-2</sup> s<sup>-1</sup> to zero. The amount of Hg in the clusters obtained by this procedure is comparable with the amount obtained by exposing a  $\text{CdTe}(111)$   $B$  surface at room temperature to an estimated Hg flux of  $2.5 \times 10^{17}$  atoms cm<sup>-2</sup> s<sup>-1</sup> during at least 30 min. As the Hg sticking coefficient on CdTe is expected to decrease with increasing temperature and based on the fact that the Hg flux used for the adsorption experiment was always higher than during the cooling of the  $\text{Hg}_{1-x}\text{Cd}_x\text{Te}$  samples, we conclude that Hg adsorption on the  $\text{Hg}_{1-x}\text{Cd}_x\text{Te}$  surfaces during the cooling cannot be the only reason for the formation of Hg clusters on these surfaces. We therefore suggest that out-diffusion of Hg from the samples contributes significantly to the formation of the Hg clusters.

A mercury atom reaching the surface of a  $\text{Hg}_{1-x}\text{Cd}_x\text{Te}$  sample can (1) combine with any available free Te atom, (2) migrate on the surface until it reaches a nucleation site and contribute to the formation of Hg clusters, or (3) desorb from the surface. Parameters like the substrate temperature or the number and type of surface defects certainly play a major role in determining which of these steps will be the dominant one. The three possibilities exist regardless of whether the Hg atom reaches the surface by out-diffusion from the bulk or by condensation from the Hg vapor. However, it is clear

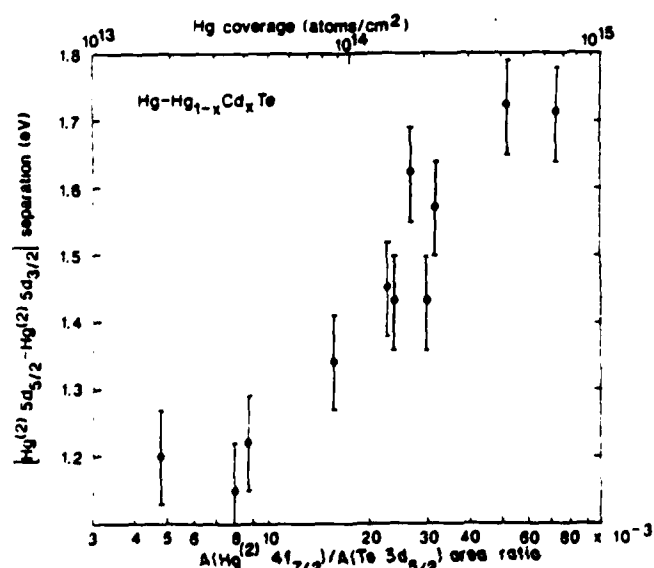


FIG. 4.  $\text{Hg}^{(2)}$  5d apparent spin-orbit splitting vs  $A(\text{Hg}^{(2)} 5f_{7/2})/A(\text{Te } 3d_{5/2})$  area ratio. The Hg coverage has been estimated using relation (1) with  $N_c = 10^{11}$  cm<sup>-2</sup>. For details see the text.

that the amount of Hg in the sample should affect the amount of Hg in the clusters if out-diffusion is the major source of Hg atoms going into the clusters. Such a relation has been observed (Table I). For different samples prepared at the same temperature, the amount of Hg in the clusters is found to increase with the Hg concentration in the  $\text{Hg}_{1-x}\text{Cd}_x\text{Te}$  samples. The exact relationship between the two intensities certainly depends on the distribution of the Hg in the clusters and in the  $\text{Hg}_{1-x}\text{Cd}_x\text{Te}$ , as well as on the details of the diffusion mechanism. Furthermore, the data in Table I are consistent with the assumption that the amount of Hg in the clusters increases with increasing temperature for a given sample composition. This would not be easy to explain if condensation from Hg vapor was the main reason for the cluster formation, whereas enhanced out-diffusion combined with higher surface mobility is likely to increase the amount of Hg in the clusters. However, increasing the substrate temperature also favors the Hg desorption. Many more experimental results as well as a detailed study of the corresponding surface kinetics are thus called for. A future study should also reveal whether the out-diffusing Hg was initially bound to Te or instead located in interstitial lattice sites. This is very important for an understanding of the thermal stability of these materials. The existence of interstitial Hg is indeed expected due to the high Hg overpressure needed during the growth of  $\text{Hg}_{1-x}\text{Cd}_x\text{Te}$ .<sup>20</sup>

#### IV. CONCLUSION

We have shown that Hg clusters are found on MBE-grown  $\text{Hg}_{1-x}\text{Cd}_x\text{Te}$  samples. The typical radius of these clusters is in the range of 5–20 Å. The Hg core levels measured with XPS show the typical positive binding-energy shift which increases with decreasing cluster size. This shift is explained by the Coulomb energy  $e^2/2R$  due to the positive charge appearing on the cluster during the photoemission process. For small clusters, the apparent

TABLE I. Intensity ratio  $A(\text{Hg}^{2+} 4f_{7/2})/A(\text{Te } 3d_{5/2})$  for the Hg clusters along with the growth temperature and the composition of the  $\text{Hg}_{1-x}\text{Cd}_x\text{Te}$  samples.

$T_s$ (°C)	$1-x$	$A(\text{Hg}^{2+} 4f_{7/2})/A(\text{Te } 3d_{5/2})$
185	0.065	$9.7 \times 10^{-3}$
185	0.740	$4.4 \times 10^{-2}$
195	0.045	$4.8 \times 10^{-3}$
195	0.057	$9.3 \times 10^{-3}$
195	0.085	$1.6 \times 10^{-2}$
175	0.095	$7.7 \times 10^{-3}$
185	0.065	$9.7 \times 10^{-3}$
195	0.057	$9.3 \times 10^{-3}$

spin-orbit splitting of the Hg 5d levels is smaller than for bulk Hg and even smaller than for isolated Hg atoms. This is attributed to repulsion between the Cd 4d and Hg 5d orbitals for the smallest clusters, where almost all the Hg atoms are in contact with the  $\text{Hg}_{1-x}\text{Cd}_x\text{Te}$  substrate. Finally, we have shown that Hg out-diffusion from the bulk is probably the major reason for the formation of these clusters.

#### ACKNOWLEDGMENTS

We are grateful to Y. J. Kim for the preparation of some of the samples used for this work. This work carried out at the University of Illinois at Chicago, was supported by the U. S. Defense Advanced Research projects Agency and monitored by the U. S. Air Force Office of Scientific Research under Contract No. F4920-87-C-0021. One of us (R.S.) is supported in part by the Belgian National Foundation for Scientific Research [Fonds National Belge pour la Recherche Scientifique (FNRS)].

\*Permanent address: Facultés Universitaires Notre-Dame de la Paix, B-5000 Namur, Belgium.

†Present address: Sandia National Laboratories, Organization 1144, Albuquerque, NM 87185-5800.

<sup>1</sup>K. S. Liang, W. R. Salaneck, and I. A. Aksay, *Solid State Commun.* **19**, 329 (1976).

<sup>2</sup>M. G. Mason, *Phys. Rev. B* **27**, 748 (1983).

<sup>3</sup>G. K. Wertheim, S. B. DiCenzo, and S. E. Younquist, *Phys. Rev. Lett.* **51**, 2310 (1983).

<sup>4</sup>J. C. Slater and K. H. Johnson, *Phys. Today* **27**, 34 (1974).

<sup>5</sup>T. Kendelewicz, W. G. Petro, I. Lindau, and W. E. Spicer, *Phys. Rev. B* **30**, 5800 (1984).

<sup>6</sup>F. Houzay, M. Bensoussan, C. Guille, and F. Barthe, *Surf. Sci.* **162**, 617 (1985).

<sup>7</sup>R. Sporken, P. Xhonneux, R. Caudano, and J. P. Delrue, *Surf. Sci.* (to be published).

<sup>8</sup>J. Reno, R. Sporken, Y. J. Kim, C. Hsu, and J. P. Faurie, *Appl.*

*Phys. Lett.* **51**, 1545 (1987).

<sup>9</sup>J. P. Faurie, *IEEE J. Quantum Electron.* **QE-22**, 1656 (1986).

<sup>10</sup>K. A. Harris, S. Hwang, D. K. Blanks, J. W. Cook, J. F. Schetzina, N. Otsuka, J. B. Baukus, and A. T. Hunter, *Appl. Phys. Lett.* **48**, 396 (1986).

<sup>11</sup>S. Doniach and M. Šunjić, *J. Phys. C* **3**, 285 (1970).

<sup>12</sup>C. Hsu, T. M. Duc, and J. P. Faurie (unpublished).

<sup>13</sup>T. Miller, A. P. Shapiro, and T. C. Chiang, *Phys. Rev. B* **31**, 7915 (1985).

<sup>14</sup>R. Sporken, P. A. Thiry, E. Petit, J. J. Pireaux, R. Caudano, J. Ghijsen, R. L. Johnson, and L. Ley, *Phys. Rev. B* **35**, 7927 (1987).

<sup>15</sup>G. K. Wertheim, S. B. DiCenzo, and D. N. E. Buchanan, *Phys. Rev. B* **33**, 5384 (1986).

<sup>16</sup>S. Svensson, N. Martensson, E. Basilier, P. A. Mamquist, U. Gelius, and K. Siegbahn, *J. Electron Spectrosc. Relat. Phenom.* **9**, 51 (1976).

- <sup>17</sup>L. Ley, S. P. Kowalczyk, F. R. McFeely, and D. A. Shirley, Phys. Rev. B **10**, 4881 (1974).
- <sup>18</sup>V. L. Moruzzi, A. R. Williams, and J. F. Janak, Phys. Rev. B **10**, 4856 (1974).
- <sup>19</sup>W. Eberhardt, S. C. Wu, R. Garrett, D. Sondericker, and F. Jona, Phys. Rev. B **31**, 8285 (1985).
- <sup>20</sup>J. P. Faurie, A. Million, R. Roch, and J. L. Tissot, J. Vac. Sci. Technol. A **1**, 1593 (1983); S. Sivananthan, X. Chu, J. Reno, and J. P. Faurie, J. Appl. Phys. **60**, 1359 (1986).

# X-ray photoemission study of Hg clusters on $\text{Hg}_{1-x}\text{Cd}_x\text{Te}$ surfaces

R. Sporken,<sup>a)</sup> S. Sivananthan, J. Reno,<sup>b)</sup> and J. P. Faurie

Department of Physics, University of Illinois at Chicago, Chicago, Illinois 60680

(Received 2 February 1988; accepted 25 April 1988)

$\text{Hg}_{1-x}\text{Cd}_x\text{Te}$  (111)B surfaces have been studied with x-ray photoelectron spectroscopy (XPS). A surface shift is deduced from a careful analysis of Te 4d core-level spectra. The presence of small Hg clusters on these surfaces is observed, and the size is estimated from the XPS data ( $R = 5\text{--}20 \text{ \AA}$ ). The positive binding energy shift for these clusters agrees very well with the calculated Coulomb energy due to the positive charge which appears on the clusters during the photoemission process. The origin of these clusters is briefly discussed.

## I. INTRODUCTION

The study of the microscopic properties of surfaces and interfaces of semiconducting materials is very important for the understanding and development of modern microelectronic devices. A detailed investigation of the growth of such surfaces and interfaces is necessary due to the dramatic miniaturization of the devices. In this paper, we report on the study of small mercury clusters on  $\text{Hg}_{1-x}\text{Cd}_x\text{Te}$  surfaces.

The presence of small Hg clusters on the surfaces of some II-VI semiconductors has first been suggested by Reno *et al.*<sup>1</sup> to explain some x-ray photoelectron spectroscopy (XPS) results concerning the Hg incorporation in CdTe during the growth of HgTe-CdTe superlattices by molecular-beam epitaxy (MBE). The common growth technique for HgTe-CdTe superlattices and other superstructures, such as single and double barrier tunneling structures, involves leaving the Hg cell open at all times.<sup>2,3</sup> As a result, the CdTe layers are not pure CdTe layers but instead  $\text{Hg}_{1-x}\text{Cd}_x\text{Te}$  with typically 3%–9% of mercury for the (111)B orientation.<sup>1</sup> In addition to Hg bound to Te atoms, the XPS analysis of these samples revealed the existence of a second type of mercury with about 600 meV higher binding energy.<sup>1,4</sup> In the present work, we show that this second type of mercury is due to the presence of small Hg clusters on CdTe and  $\text{Hg}_{1-x}\text{Cd}_x\text{Te}$  surfaces. We also show how the size of these clusters can be estimated and used to explain the characteristics of such clusters. The origin of these clusters will be discussed in the last section of this paper.

## II. EXPERIMENTAL PROCEDURE

The samples were all prepared at the University of Illinois at Chicago in a Riber MBE 2300 machine. CdTe substrates oriented in the (111)B direction as well as GaAs substrates with a CdTe(111)B buffer layer were used. The substrate preparation and the growth of the appropriate buffer layer have been discussed elsewhere.<sup>2</sup> The layers analyzed here are  $\text{Hg}_{1-x}\text{Cd}_x\text{Te}$  with  $x$  in the range of 0.15–0.97. The smaller  $x$  values were obtained with three MBE sources (CdTe, Te, and Hg) as usual.<sup>2</sup> The larger values are obtained with only two sources (CdTe and Hg) as described in Ref. 1. CdTe samples on which we have adsorbed some Hg at a typical exposure of  $5 \times 10^{20} \text{ atoms cm}^{-2}$  have also been analyzed.

The samples were grown at temperatures between 175 and 195 °C. These sample temperatures were measured using a

Chromel-Alumel thermocouple and, whenever possible, by an infrared pyrometer. The measurements have been calibrated using the melting points of indium and tin.

The samples were kept under ultrahigh vacuum conditions as they were transferred to the XPS chamber. The measurements were performed with a SSX-100 spectrometer from Surface Science Instruments. A monochromatized and focused Al  $K_\alpha$  excitation line was used with the spot diameter set at 300  $\mu\text{m}$ . The overall energy resolution measured on the Au 4f core level is 0.7 eV. The position of the Fermi level was determined from the position of the Au 4f<sub>7/2</sub> line measured from a bulk gold sample. The corresponding binding energy was fixed at 83.93 eV.

## III. RESULTS AND DISCUSSION

The discussion of the results will be organized as follows: First, we will focus on a detailed analysis of the XPS spectra from  $\text{Hg}_{1-x}\text{Cd}_x\text{Te}$  samples. It will be shown that two types of mercury exist on these surfaces. The existence of a surface shift on the Te 4d core level will be discussed. Thereafter, it will be shown that one Hg component is related to Hg bound to Te atoms and that the other is due to the presence of small Hg clusters on the sample surface. Finally, the size of these clusters will be estimated, and their origin will be briefly discussed.

Typical photoemission spectra from  $\text{Hg}_{1-x}\text{Cd}_x\text{Te}$  are shown in Fig. 1. The peaks are the Cd 4d and Hg 5d spin-orbit doublets and the Hg 4f<sub>7/2</sub>. These spectra have been analyzed for all the samples by a least-squares curve fitting procedure. The line shape used for the fits was a Lorentzian convoluted with a Gaussian.

Two types of Hg have been found for all the samples. These two types of mercury will be labeled Hg<sup>(1)</sup> and Hg<sup>(2)</sup> in the following discussion. The existence of two components, quite obvious from the Hg 4f<sub>7/2</sub> spectra, is also deduced from the Hg 5d spectra by the curve fitting procedure as mentioned above. The energy separation between the two components, as well as their intensity ratio are deduced from both the Hg 4f and Hg 5d core level spectra. These two results are always in very close agreement.

The identification Hg<sup>(1)</sup> is based on the following method. For  $\text{Hg}_{1-x}\text{Cd}_x\text{Te}$ , the position of the valence band maximum is known to be very sensitive to the alloy composition  $x$ .<sup>5,6</sup> As the cation core levels are known to be virtually inde-

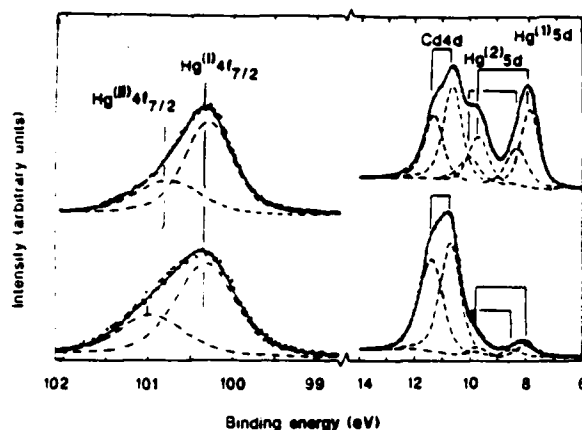


FIG. 1. Typical XPS core-level spectra from  $\text{Hg}_{1-x}\text{Cd}_x\text{Te}$ . The composition is  $x = 0.94$  (lower spectrum) and  $x = 0.60$  (upper spectrum). The number of atoms in the  $\text{Hg}^{(2)}$  estimated using relation (5) is  $7 \times 10^{13}$  and  $6 \times 10^{14} \text{ cm}^{-2}$ , respectively. The binding energy is referred to the Fermi level. The solid line is obtained by least-squares fitting of individual components (---) to the data.

pendent of the alloy composition,<sup>5,6</sup> the energy difference between the Hg 5d or Cd 4d core levels and the valence band maximum (VBM) reflects the position of the VBM on an absolute energy scale.

Therefore, the binding energy of the Hg 5d and Cd 4d core levels with respect to the VBM can be used to determine the alloy composition  $x$ . The same alloy composition is easily determined from the ratio of the peak areas in the XPS spectra. A comparison of these results shows that  $\text{Hg}^{(1)}$  is related to Hg in  $\text{Hg}_{1-x}\text{Cd}_x\text{Te}$ .

We have shown earlier that  $\text{Hg}^{(2)}$  is due to some mercury located in the surface region.<sup>1,4</sup> It is therefore important to investigate the spatial distribution of this second type of mercury.

Figure 2 shows a typical Te 4d core level spectrum measured on a  $\text{CdTe}(111)\text{B}$  surface. From these spectra, a surface shift<sup>7,8</sup> of  $475 \pm 75 \text{ meV}$  towards higher binding energy was determined by very careful curve fitting. Close examination of the residuals, i.e., the difference between the calculated and the measured spectra was necessary for the determination of this surface component. Figure 2 shows this difference spectrum for the same experimental data, fitted with one or two doublets, respectively. In the first case, the existence of nonrandom oscillations clearly indicates that the fit result is not an adequate representation of the experimental data. In the second case, where the sum of two doublets is used to fit the data, the difference spectrum contains only the random noise which affects the original data.

Spectra with the same characteristics have been observed on  $\text{Hg}_{1-x}\text{Cd}_x\text{Te}(111)\text{B}$  surfaces. All these surfaces are terminated by threefold bound Te atoms. In bulk  $\text{Hg}_{1-x}\text{Cd}_x\text{Te}$ , the Te atoms form four tetrahedral bonds with their nearest neighbors. This is consistent with the sign of the observed surface shift.

A simple layerwise attenuation model predicts

$$I_s/I_b = \exp(d/\lambda_e) - 1, \quad (1)$$

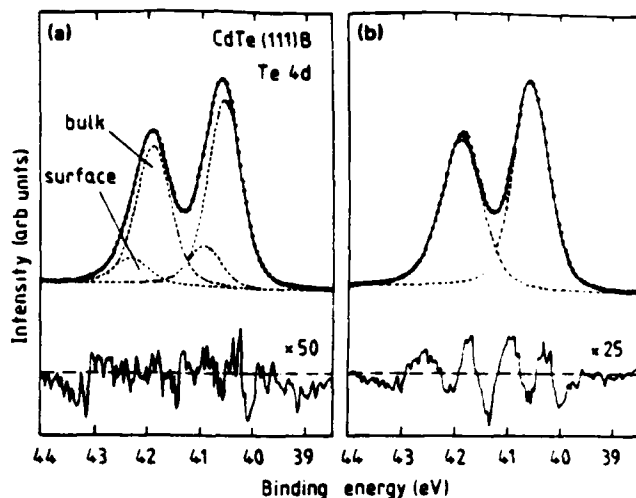


FIG. 2. Upper part: Te 4d core-level spectrum from  $\text{CdTe}(111)\text{B}$ . The solid line is obtained by least-squares fitting of individual components (---) to the data. The binding energy scale is referred to the Fermi level. Lower part: difference between the experimental data and the calculated spectrum. The same spectrum has been fitted with (a) two doublets or (b) one doublet.

where  $I_s$  and  $I_b$  are the intensities of the surface and bulk components,  $d$  is the distance between (111)B planes, and  $\lambda_e$  is the effective electron escape depth.  $\lambda_e$  is related to the electron escape depth  $\lambda$  and to the mean electron escape angle  $\beta$  ( $\lambda_e = \lambda \cos \beta$ ,  $\beta = 53^\circ$ ). For our experiment, we obtain  $I_s/I_b = 0.20 \pm 0.03$ . The corresponding escape depth as deduced from relation (1) is  $3.4 \pm 0.4 \text{ nm}$ . The characteristics of the surface component (relative intensity, FWHM, and energy shift) are independent of the amount of  $\text{Hg}^{(2)}$ . The intensity ratio between  $\text{Hg}^{(2)}$  and the surface tellurium component, corrected for the different sensitivity factors, is in the range of 0.1–1. We therefore suggest that  $\text{Hg}^{(2)}$  is related to the presence of small Hg clusters at the surface.

The spectral characteristics of such small metal clusters are now well established.<sup>4,9–11</sup> The most striking feature is a size dependent binding energy shift in the case of small metal clusters on poorly conducting substrates. During the photoemission process, the cluster is left with a unit positive charge which is not neutralized during the core-hole lifetime.<sup>11</sup> The final-state energy is thus increased by the Coulomb energy, which is  $e^2/2R$  for a charged conducting sphere or  $e^2/1.7R$  for unsupported hemispherical clusters. In the case of small mercury clusters, on  $\text{Hg}_{1-x}\text{Cd}_x\text{Te}$ , the contribution from the clusters is thus expected to shift towards higher binding energies for small cluster sizes.

The cluster radius is the relevant parameter for the determination of the binding energy shift. The following section of this paper shows how this radius is determined in a straightforward manner from the photoemission data.

First a series of  $\text{Hg}_{1-x}\text{Cd}_x\text{Te}$  samples is grown. These samples are analyzed with XPS, and it is found that the preparation conditions (Cd concentration  $x$ , substrate temperature  $T_s$  during the growth, Hg flux during the growth,...) influence the intensity of  $\text{Hg}^{(2)}$ . The relation between these preparation conditions and the intensity of  $\text{Hg}^{(2)}$  has been

described elsewhere.<sup>4</sup> If one assumes a simple exponential attenuation of the XPS signals, and if  $\text{Hg}^{(2)}$  is due to mercury in hemispherical clusters on the surface, the intensity of  $\text{Hg}^{(2)}$  is given by<sup>12</sup>

$$A(\text{Hg})^{(2)} = k\pi Nc\lambda_e \{R^2 - 2[\lambda_e^2 - (R\lambda_e + \lambda_e^2) \times \exp(-R/\lambda_e)]\}, \quad (2)$$

where  $R$  is the average cluster radius,  $Nc$  the cluster concentration,  $\lambda_e$  the effective photoelectron escape depth, and  $k$  is a constant depending on the XPS sensitivity factors and on the density of the Hg clusters.

Relation (1) is valid as long as the area covered by the cluster is small compared to the total sample area. The Te signal is then virtually not attenuated by the Hg clusters. Furthermore, the Te signal is independent of the Cd content in  $\text{Hg}_{1-x}\text{Cd}_x\text{Te}$ . Therefore,

$$\Gamma = A(\text{Hg}^{(2)} 4f_{7/2}) / A(\text{Te } 3d_{5/2}) \\ = k'Nc\lambda_e \{R^2 - 2[\lambda_e^2 - (R\lambda_e + \lambda_e^2)\exp(-R/\lambda_e)]\} \quad (3)$$

as long as  $Nc\pi R^2 \ll 1$ .  $k'$  is a constant depending again on the XPS signal strength from one Hg atom relative to one Te atom, on the Te concentration in  $\text{HgCdTe}$ , on the density of the Hg clusters and on the shape of the clusters. A straightforward calculation yields  $k' \approx 0.4$ . From our data,  $\Gamma$  is in the range of  $4 \times 10^{-3}$  to  $10^{-1}$ . For a typical cluster concentration of  $6 \times 10^{11} \text{ cm}^{-2}$ , the cluster radii are then found in the range of 5–20 Å using Eq. (3). A value of 3.0 nm was used for  $\lambda_e$ , which is quite reasonable for electrons with a kinetic energy of about 1400 eV.

Figure 3 shows the  $\text{Hg}^{(2)} 4f_{7/2}$  binding energy versus the cluster radius  $R$ , deduced from relation (2). The solid curve is obtained by the following relation:

$$E_B^{\text{cluster}} = E_B^{\text{bulk}} + E^2 / (1.7 R). \quad (4)$$

$E_B^{\text{bulk}}$  is the Hg  $4f_{7/2}$  binding energy for bulk Hg. A good agreement between the experimental binding energies and the value from Eq. (4) is obtained for  $E_B^{\text{bulk}} = 100.2 \text{ eV}$ , which is indeed close to the value for bulk Hg (99.9 eV).<sup>13</sup> In practice, an initial guess is made for the parameters  $Nc$  and  $\lambda_e$ . The cluster radii are then determined, and the value of  $E_B^{\text{bulk}}$  is adjusted so that a good fit of the experimental data is obtained from Eq. (3). The result can be used to optimize the values of  $\lambda_e$  and  $Nc$ , and all the parameters are adjusted by an iterative procedure. The final result is shown in Fig. 3 for the following values of the parameters:  $\lambda_e = 3.0 \text{ nm}$ ,  $Nc = 6 \times 10^{11} \text{ cm}^{-2}$ ,  $E_B^{\text{bulk}} = 100.2 \text{ eV}$ .

The coverage corresponding to  $\text{Hg}^{(2)}$  is given by

$$\theta = \frac{2}{3} \frac{\pi R^3 \rho}{M} Nc, \quad (5)$$

where  $\rho$  is the density of the Hg clusters and  $M$  is the Hg atomic mass. If  $\rho$  is taken equal to the density of bulk Hg,  $\theta$  is found in the range from  $10^{13}$  to  $10^{15} \text{ atoms/cm}^2$ . Figure 3 compares very well with results published in the recent literature concerning Au on amorphous carbon<sup>13,14</sup> and Ag on amorphous carbon.<sup>11</sup> In all the cases, the binding energy for the bulk metal was obtained for coverages between  $10^{15}$  and  $10^{16} \text{ atoms/cm}^2$ .

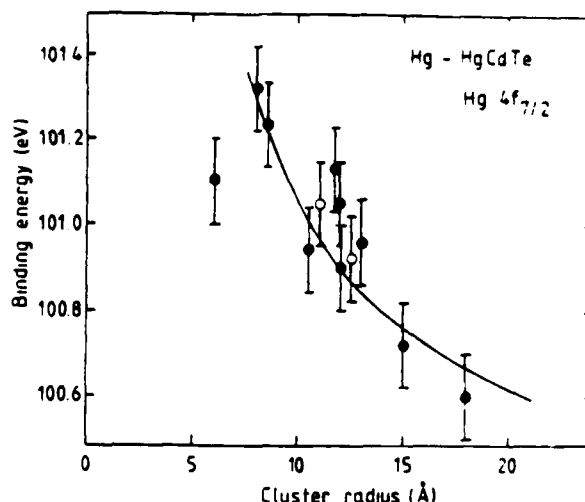


FIG. 3.  $\text{Hg}^{(2)} 4f_{7/2}$  binding energy with respect to the Fermi level, vs cluster radius  $R$ . ● are results from  $\text{HgCdTe}$  samples, whereas the ○ are obtained after the Hg adsorption on CdTe at room temperature. The solid line is a result of Eq. (4). The cluster radius has been obtained using Eq. (3).

Obviously, the final state charge model cannot be applied to nonmetallic clusters. The transition from nonmetallic to metallic clusters when the spacing between valence levels is comparable to  $kT$ . The corresponding cluster radius has been calculated for Pt by Diczieno and Wertheim.<sup>15</sup> They expect metallic behavior in hemispherical Pt clusters with  $R = 6 \text{ Å}$ . As the electronic structure of Hg is similar to the Pt one, the onset of metallic behavior is expected for clusters of the same size. In our case, the cluster sizes deduced from relation (3) are thus all in the range where metallic behavior is expected. Together with the reasonable values obtained for  $E_B^{\text{bulk}}$ ,  $\lambda_e$ , and  $Nc$ , this is an indication that our interpretation is correct.

The formation of small Hg clusters on  $\text{Hg}_{1-x}\text{Cd}_x\text{Te}$  or CdTe surfaces is also confirmed by another experiment. We have adsorbed Hg on MBE grown CdTe(111) samples. The samples were kept at room temperature and the Hg flux was  $\sim 2.5 \times 10^{17} \text{ atoms cm}^{-2} \text{ s}^{-1}$ . This value was estimated using Knudsen's effusion law. The samples have been analyzed with XPS after exposures of 35 and 45 min, respectively. Only one component was then detected in the Hg  $4f_{7/2}$  spectra. The corresponding binding energies are represented by the open circles in Fig. 4. These results agree very well with those measured for  $\text{Hg}^{(2)}$  on  $\text{Hg}_{1-x}\text{Cd}_x\text{Te}$ . The corresponding coverages as deduced from Eq. (5) are  $1.6 \times 10^{14}$  and  $2.3 \times 10^{14} \text{ atoms cm}^{-2}$ , respectively. The ratio of these coverages agrees with the ratio of the Hg exposures. The sticking coefficient for Hg on CdTe(111)B surfaces is then found on the order of  $3 \times 10^{-7}$ , which is still about three orders of magnitude lower than the sticking coefficient of Hg during the MBE growth of  $\text{HgCdTe}(111)$ .<sup>16</sup> This value should however be taken with caution, because it is based on the application of Knudsen's effusion law, which is only an approximation in this case, due to the relatively high Hg vapor pressure in the cell. Furthermore, the density of the Hg clusters might deviate from its bulk value, and this affects the results of Eq. (5).

In the last section of this paper, we will summarize the influence of the preparation conditions on the intensity ratio  $\Gamma$  and thus on the cluster  $R$ . The amount of  $\text{Hg}^{(2)}$  on  $\text{HgCdTe}$  is significantly influenced by the Hg concentration  $1 - x$  in the  $\text{Hg}_{1-x}\text{Cd}_x\text{Te}$  samples and by the substrate temperature  $T_s$ . For different samples prepared at the same temperature, the amount of Hg in the clusters is found to increase with the Hg concentration in the  $\text{HgCdTe}$  samples. Furthermore, the amount of  $\text{Hg}^{(2)}$  seems to increase with  $T_s$  for a given sample composition. These two parameters  $1 - x$  and  $T_s$  have been adjusted to prepare the samples studied in this work.

In an earlier paper,<sup>4</sup> we have shown that the two possible sources of Hg clusters are the outdiffusion of some Hg from the  $\text{Hg}_{1-x}\text{Cd}_x\text{Te}$  samples, as well as the condensation of the residual Hg in the growth chamber during the cooling of the grown layers. We have also shown that outdiffusion is probably the major reason for the formation of these clusters. A detailed study of the exact mechanism leading to the formation of these clusters is still to be done. This is very important for an understanding not only of the electrical properties but also of the thermal stability of these materials.

#### IV. CONCLUSION

We have shown that small Hg clusters are present on MBE-grown  $\text{Hg}_{1-x}\text{Cd}_x\text{Te}$  samples. The radius and the concentration of these clusters have been determined from the XPS data. The typical radius of these clusters is in the range of 5–20 Å. The identification of these clusters is based on the following arguments: (1) in addition to Hg bound to Te, a second mercury component ( $\text{Hg}^{(2)}$ ) is observed in the Hg core level spectra; (2) the presence of  $\text{Hg}^{(2)}$  does not affect the characteristics of a surface peak in the Te 4d spectra; (3) a positive binding energy shift is observed for  $\text{Hg}^{(2)}$ . This shift increases with decreasing cluster size; (4) this binding energy shift agrees well with calculated values of the Coulomb energy  $e^2/1.7 R$  which is due to the unit charge appearing on the clusters during the photoemission process. The composition of  $\text{Hg}_{1-x}\text{Cd}_x\text{Te}$  samples and the substrate temperature during the growth of these samples are the most important parameters influencing the amount of  $\text{Hg}^{(2)}$ . We suggest that Hg outdiffusion from the bulk is the major rea-

son for the formation of these clusters. Finally, we have shown that such clusters can be obtained by adsorbing some Hg on  $\text{CdTe}(111)$ .

#### ACKNOWLEDGMENTS

We are grateful to Professor R. Caudano for support and encouragement, to Professor A. A. Lucas for helpful discussion, and to Y. J. Kim for the preparation of some of the samples. This work carried out at the University of Illinois at Chicago was supported by the Defense Advanced Research Project Agency and monitored by the Air Force Office of Scientific Research under Contract No. F4920-87-C-0021. One of us (R. S.) was supported in part by the National Belgian Foundation for Scientific Research (FNRS).

<sup>1</sup> Permanent address: Facultés Universitaires Notre-Dame de la Paix, B-5000 Namur, Belgium.

<sup>2</sup> Present address: Sandia National Laboratory, Organization 1144, Albuquerque, New Mexico 87185.

<sup>3</sup> J. Reno, R. Sporken, Y. J. Kim, C. Hsu, and J. P. Faurie, *Appl. Phys. Lett.* **51**, 1545 (1987).

<sup>4</sup> J. P. Faurie, *IEEE J. Quantum Electron.* **22**, 1656 (1986).

<sup>5</sup> K. A. Harris, S. Hwang, D. K. Blanks, J. W. Cook, J. F. Schetzina, N. Otsuka, J. B. Bankus, and A. T. Hunter, *Appl. Phys. Lett.* **48**, 396 (1986).

<sup>6</sup> R. Sporken, S. Sivananthan, J. Reno, and J. P. Faurie, *Phys. Rev. B* (to be published).

<sup>7</sup> C. K. Shih and W. E. Spicer, *Phys. Rev. Lett.* **58**, 2594 (1987).

<sup>8</sup> C. Hsu, T. M. Due, and J. P. Faurie (unpublished).

<sup>9</sup> T. Miller, A. P. Shapiro, and T. C. Chiang, *Phys. Rev. B* **31**, 7915 (1985).

<sup>10</sup> G. K. Wertheim, P. H. Citrin, and J. F. van der Veen, *Phys. Rev. B* **30**, 4343 (1984).

<sup>11</sup> M. G. Mason, *Phys. Rev. B* **27**, 748 (1983).

<sup>12</sup> G. K. Wertheim, S. B. DiCenzo, and S. E. Younquist, *Phys. Rev. Lett.* **51**, 2310 (1983).

<sup>13</sup> G. K. Wertheim, S. B. DiCenzo, and D. N. E. Buchanan, *Phys. Rev. B* **33**, 5384 (1986).

<sup>14</sup> R. Sporken, P. A. Thiry, E. Petit, J. J. Pireaux, R. Caudano, J. Ghijsen, R. L. Johnson, and L. Ley, *Phys. Rev. B* **35**, 7927 (1987).

<sup>15</sup> S. Svensson, N. Martensson, E. Basilier, P. A. Mamquist, C. Gelius, and K. Siegbahn, *J. Electron. Spectrosc.* **9**, 51 (1976).

<sup>16</sup> M. G. Mason, *Phys. Rev. B* **27**, 748 (1983).

<sup>17</sup> S. B. DiCenzo and G. K. Wertheim, *J. Electron. Spectrosc.* **43**, c7 (1987).

<sup>18</sup> J. P. Faurie, A. Million, R. Roch, and J. L. Tissot, *J. Vac. Sci. Technol. A* **1**, 1593 (1983); S. Sivananthan, X. Chu, J. Reno, and J. P. Faurie, *J. Appl. Phys.* **60**, 1359 (1986).

### VI-3 HgTe-CdTe: VALENCE BAND DISCONTINUITY

#### VI-3-1 DIRECT MEASUREMENT OF THE VALENCE BAND DISCONTINUITY AT 300K BY XPS

The valence band discontinuity ( $\Delta E_v$ ) of the HgTe-CdTe heterojunction has attracted much attention since its first determination in 1982 along with much controversy, both theoretical and experimental, concerning its value. The magneto-optical and resonant Raman scattering<sup>1</sup> measurements performed at low temperature yield a value of less than 120 meV for  $\Delta E_v$  of the HgTe-CdTe(111)B heterojunction. This result agrees with the prediction of the common anion rule<sup>2</sup>. The core level X-ray photoelectron spectroscopy (XPS) measured 0.36 eV<sup>3,4</sup> at room temperature in agreement with other theoretical predictions<sup>5,6</sup>. The method of determination using only the cation core level difference is questionable because there is no proof that the difference between the core level and the valence band maximum in the two semiconductors does not change when the heterojunction is formed. This change, which could be due to band bending and/or interface chemical effect, would make such an indirect determination inappropriate. Therefore, we have investigated the valence band structure (VBS) of the heterojunction and present here the first direct measurement of the valence band discontinuity of the HgTe-CdTe heterojunction.

The HgTe-CdTe(111)B interface was grown in the MBE chamber and transferred under UHV conditions into the analysis chamber. The thickness of the thin overlayer, as determined from the core level XPS peak area, was chosen between 15 Å and 30 Å. The X-ray source used here is the Al  $K_{\alpha,2}$  line which has the energy of 1486.6 eV.

Since the escape depth of the valence electrons of the interface, here, is comparable with the thickness of the overlayer, the interface XPS spectrum covers the VBSs of the overlayer, substrate, and interface region. We have reported that the intensities of the substrate and overlayer core level peaks vary with thickness in a manner consistent with an exponential attenuation, indicating that the interface is abrupt in the monolayer range<sup>1</sup>. In other words, the interface region is so narrow that the contribution of it in the interface XPS spectrum of the VBS can be neglected.

The principle of the direct measurement of the  $\Delta E_v$  of HgTe-CdTe interface is to deconvolute the VBS of the interface spectrum using the normalized HgTe and

CdTe valence band distribution. This normalization considers two parameters. One is the attenuated intensities of the clean substrate due to the overlayer. The other one is energy shifts due to the interface band-bending effect. After least-square fitting process, the value of  $\Delta E_v$  can be obtained. We report here that the best fit gives an average value of 0.40eV for the valence band discontinuity of HgTe-CdTe(111)B interface with different thicknesses and growth sequences. This result agrees with the result measured from the core level XPS method<sup>3,4</sup>. We have also extended this method to the measurement on the  $\Delta E_v$  of the HgTe-CdTe heterojunction in the (100) orientation and found that  $\Delta E_v$  is equal to 0.290 eV.

#### REFERENCES:

1. J.P. Faurie, C. Hsu, and Tran Minh Duc, J. Vac. Sci. Technol. A5, 3074 (1987) and references therein.
2. J. O. McCaldin, T. C. McGill and C. A. Mead, Phys. Rev. Lett. 36, 56 (1976).
3. S. P. Kowalczyk, J. T. Cheung, E. A. Kraut, and R. W. Grant, Phys. Rev. Lett. 56, 1605 (1986).
4. Tran Minh Duc, C. Hsu, and J.P. Faurie, Phys. Rev. Lett. 58, 1127 (1987).
5. J. Tersoff, Phys. Rev. Lett. 56, 2755 (1986).
6. S. H. Wei and A. Zunger, Phys. Rev. Lett. 59, 144 (1987).

## VI-3-2 ELECTRICAL DETERMINATION

Several  $\text{Hg}_{1-x}\text{Cd}_x\text{Te}-\text{CdTe}-\text{Hg}_{1-x}\text{Cd}_x\text{Te}$  heterostructures with different  $x$ , doping level and barrier thickness have been grown by MBE at the University of Illinois.

The study of the current voltage behavior resulted in a determination of a valence-band discontinuity  $\Delta E_v = 390 \pm 75\text{meV}$  at  $T = 300\text{K}$ . This result is in reasonable agreement with XPS results.

This work has been done in collaboration with Prof. McGill group at Caltech. For more details see the attached paper. However, similar analyses of current-voltage data taken at 190-300K suggest that the valence-band offset decreases at low temperatures in this heterojunction.

### ATTACHED PAPERS:

1. "Electrical determination of the valence-band discontinuity in  $\text{HgTe}-\text{CdTe}$ "

# Electrical determination of the valence-band discontinuity in HgTe-CdTe heterojunctions

D. H. Chow, J. O. McCaldin, A. R. Bonnefoi, and T. C. McGill  
T. J. Watson, Sr., Laboratory of Applied Physics, California Institute of Technology, Pasadena, California 91125

I. K. Sou and J. P. Faurie  
Department of Physics, University of Illinois at Chicago, Chicago, Illinois 60680

(Received 17 August 1987; accepted for publication 22 October 1987)

Current-voltage behavior is studied experimentally in a  $\text{Hg}_{0.78}\text{Cd}_{0.22}\text{Te}$ -CdTe- $\text{Hg}_{0.78}\text{Cd}_{0.22}\text{Te}$  heterostructure grown by molecular beam epitaxy. At temperatures above 160 K, energy-band diagrams suggest that the dominant low-bias current is thermionic hole emission across the CdTe barrier layer. This interpretation yields a direct determination of  $390 \pm 75$  meV for the HgTe-CdTe valence-band discontinuity at 300 K. Similar analyses of current-voltage data taken at 190–300 K suggest that the valence-band offset decreases at low temperatures in this heterojunction.

The HgTe-CdTe heterojunction is the building block for a number of interesting device structures which have been experimentally realized. These include the HgTe-CdTe superlattice,<sup>1–7</sup> the resonant tunneling HgTe- $\text{Hg}_{1-x}\text{Cd}_x\text{Te}$  double barrier heterostructure,<sup>8,9</sup> and the single barrier  $\text{Hg}_{1-x}\text{Cd}_x\text{Te}$  negative differential resistance heterostructure.<sup>10,11</sup> In all of these structures, the valence-band offset,  $\Delta E_v$ , at the HgTe-CdTe interface is an important quantity in determining device behavior. Several theoretical and experimental values of  $\Delta E_v$  have been reported.<sup>12–20</sup> Most recently, x-ray photoemission spectroscopy (XPS) experiments on HgTe-CdTe heterojunctions have yielded values of approximately 350 meV for  $\Delta E_v$  at room temperature.<sup>16–18</sup> These results are in serious disagreement with most interpretations of published superlattice photoluminescence data, which indicate that  $\Delta E_v$  must be nearly 0 meV to explain the observed high-energy luminescence.<sup>3–7</sup> The XPS results are also in apparent disagreement with earlier low-temperature magnetoabsorption experiments which yielded a value of 40 meV for  $\Delta E_v$ ,<sup>20</sup> although it has been suggested that these two measurements could be consistent with each other if  $\Delta E_v$  is temperature dependent.<sup>21</sup>

In this letter, we report a direct electrical measurement of the valence-band discontinuity at the HgTe-CdTe interface. The sample studied was grown on a semi-insulating GaAs substrate by molecular beam epitaxy (MBE) in a Riber 2300 system. The active region consisted of a CdTe barrier layer sandwiched between two  $\text{Hg}_{0.78}\text{Cd}_{0.22}\text{Te}$  electrodes. Transmission electron microscopy (TEM) showed that the CdTe layer was 180 Å thick. The  $\text{Hg}_{0.78}\text{Cd}_{0.22}\text{Te}$  electrodes were doped *n* type with indium, to a carrier concentration of  $3.6 \times 10^{16} \text{ cm}^{-3}$  at 30 K. The top (bottom) electrode was 0.5 μm (3 μm) thick. A 2.5-μm CdTe buffer layer preceded the growth of the active device region of the heterostructure. Mesas were fabricated in the sample by wet etching with  $\text{Br}_2\text{:HBr:H}_2\text{O}$  in a 0.005:1:3 ratio. Au was used to make ohmic contacts to both the tops of the mesas and the etched  $\text{Hg}_{0.78}\text{Cd}_{0.22}\text{Te}$  surface, forming a set of isolated two-terminal devices. The mesas were circular, with diameters ranging from 35 to 70 μm. Several distinct preparations of

the sample were performed, with over 100 devices tested in total at room temperature. Roughly 25% of the devices were "short-circuits," with markedly higher currents and nearly linear current-voltage (*I-V*) curves. The remainder of the devices displayed uniform behavior, with overall current densities deviating by no more than 20%. Measured currents from the fabricated devices were found to be proportional to device area, indicating that edge transport mechanisms were not significant.

Figure 1 is an energy-band diagram for the heterostructure under an applied bias of 50 mV, calculated by solving Poisson's equation self-consistently via the method of Bonnefoi *et al.*<sup>22</sup> It should be noted that the calculated band diagram is independent of the values of the band offsets, except for an overall shift of the conduction- and valence-band edges in the CdTe layer. Figure 1 suggests that the dominant source of current at high temperatures is the thermionic emission of holes from the  $\text{Hg}_{0.78}\text{Cd}_{0.22}\text{Te}$  cladding layers across the CdTe valence-band barrier. It is important to note that the *n*-type doping of the electrodes does not

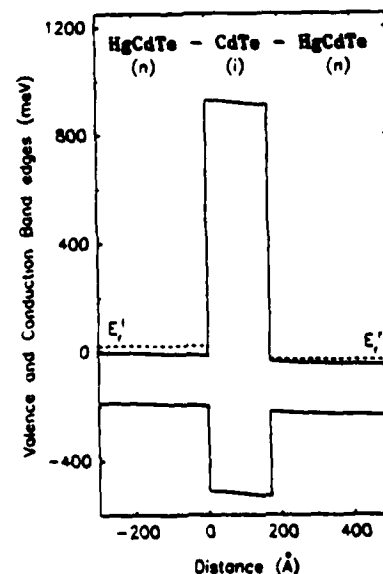


FIG. 1. Calculated band diagram for the  $\text{Hg}_{0.78}\text{Cd}_{0.22}\text{Te}$ -CdTe- $\text{Hg}_{0.78}\text{Cd}_{0.22}\text{Te}$  single barrier heterostructure, under an applied voltage of 50 mV. The upper (lower) solid line represents the conduction (valence) band edge as a function of distance in the direction of growth. The dashed line represents the Fermi energy in each of the electrodes, which are doped *n* type at  $3.6 \times 10^{16} \text{ cm}^{-3}$ . The CdTe barrier is 180 Å thick.

prohibit this transport mechanism because the band gap in  $\text{Hg}_{0.78}\text{Cd}_{0.22}\text{Te}$  is small ( $\approx 200$  meV).<sup>23</sup> At zero applied bias, the size of the potential energy barrier which the holes cross is given by

$$\phi_{\text{hole}} = E_f + E_g^{(x=0.22)} + \Delta E_v^{(x=0.22)},$$

where  $E_f$  is the Fermi energy relative to the conduction-band edge in the  $\text{Hg}_{0.78}\text{Cd}_{0.22}\text{Te}$  electrodes,  $E_g^{(x=0.22)}$  is the electrode band gap, and  $\Delta E_v^{(x=0.22)}$  is the valence-band offset between  $\text{Hg}_{0.78}\text{Cd}_{0.22}\text{Te}$  and  $\text{CdTe}$ . For all reported theoretical and experimental values of  $\Delta E_v$ , the potential energy barrier for thermionic emission of electrons is much larger than  $\phi_{\text{hole}}$ . It follows that thermionic electron currents can be ignored for this heterostructure.

A simple theoretical treatment, similar to the Bethe model for Schottky barriers,<sup>24</sup> can be employed to calculate thermionic hole current densities across the  $\text{CdTe}$  barrier as a function of applied voltage. The resulting expression is

$$J_{\text{therm}} = A^* T^2 \exp\left(\frac{-\phi_{\text{hole}} + cqV}{kT}\right) \left[1 - \exp\left(\frac{-qV}{kT}\right)\right],$$

where  $A^*$  is the modified Richardson constant,  $T$  is the temperature,  $V$  is the applied voltage,  $q$  is the hole charge,  $k$  is the Boltzmann constant, and  $c$  is the fraction of the total applied voltage which drops across the positively biased  $\text{Hg}_{0.78}\text{Cd}_{0.22}\text{Te}$  electrode. For this single barrier heterostructure,  $A^*$  is  $120/(m_h^*)$  in  $\text{A}/\text{cm}^2 \text{K}^2$ , where  $m_h^*$  is the unitless hole mass. The contributions from the light- and heavy-hole bands are summed to give the total current from this mechanism. It is important to note that the factor  $c$  is a function of the voltage applied across the heterostructure, and must therefore be calculated from the energy-band diagram for each individual bias condition. The value of  $c$  generally is in the range 0.25–0.40 for the heterostructure studied here, as compared to the case of a Schottky barrier, where  $c = 1$ .

For applied voltages of approximately 50 mV and higher, tunneling of holes across the "triangular-shaped"  $\text{CdTe}$  barrier makes a contribution to the total current through the heterostructure. This transport mechanism can be treated theoretically in a manner which is analogous to the model for the thermionic hole current. The resulting expression for the hole tunneling current density,  $J_{\text{tun}}$ , differs from that for  $J_{\text{therm}}$  by an integral term which replaces the factor  $\exp(-\Delta E_v^{(x=0.22)}/kT)$ :

$$J_{\text{tun}} = A^* T^2 \exp\left(\frac{-E_f - E_g^{(x=0.22)} + cqV}{kT}\right) \times \left[1 - \exp\left(\frac{-qV}{kT}\right)\right] \int_0^\infty (t^* t) u \exp\left(\frac{-u^2}{2}\right) du.$$

In this expression,

$$u^2/2 = m_h^* v_i^2/kT,$$

where  $v_i$  is the group velocity of the holes in the growth direction,  $u_0 = (2\Delta E_v^{(x=0.22)}/kT)^{1/2}$ , and  $t^* t$  is the transmission coefficient for holes tunneling through the  $\text{CdTe}$  barrier. In this study, we have calculated  $t^* t$  via the Wentzel-Kramers-Brillouin (WKB) method. A two-band  $k \cdot p$  theory formula<sup>25</sup> was used to find imaginary light-hole wave vectors in the  $\text{CdTe}$  barrier, while imaginary heavy-hole

wave vectors were determined from the simple "one-band" formula.

The total current density  $J$  is the sum of  $J_{\text{therm}}$  and  $J_{\text{tun}}$ . In general, the thermionic current density is calculated more accurately than the tunneling current density because  $t^* t$  is strongly dependent on many parameters, such as the barrier thickness,  $\text{CdTe}$  effective masses, and the applied voltage. It is therefore prudent to restrict analysis of experimental data to those voltages at which  $J_{\text{therm}}$  is expected to dominate. For this heterostructure, it has been estimated that  $J_{\text{tun}}$  becomes large (greater than 30% of the current) when  $V > 100$  mV. At room temperature,  $J_{\text{therm}}$  and  $J_{\text{tun}}$  are much greater than the electron tunneling current  $J_{\text{etun}}$ . However, negative differential resistance regions have been observed in  $I$ - $V$  characteristics taken at  $T = 4.2$  K, indicating that electron tunneling becomes an important transport mechanism at low temperatures. These results will be reported elsewhere.<sup>11</sup>

Figure 2 contains a typical experimental current density-voltage ( $J$ - $V$ ) characteristic, taken at room temperature. Also shown is a theoretical curve, which is obtained by setting  $\Delta E_v^{(x=0.22)} = 285$  meV in our simple model of the  $J$ - $V$  behavior.  $\Delta E_v^{(x=0.22)}$  was chosen by requiring the calculated and experimental currents to be the same at 50 mV, and was the only adjustable parameter used. Selecting different values of the applied bias results in variations of  $\Delta E_v^{(x=0.22)}$  by roughly  $\pm 10$  meV over the voltage range 0–200 mV, well beyond the 100-mV limit discussed above. This supports the assertion that virtually all of the current in the heterostructure is due to  $J_{\text{therm}}$  and  $J_{\text{tun}}$ . In fact, the shape of the theoretical  $J$ - $V$  curve is nearly independent of the choice of  $\Delta E_v^{(x=0.22)}$ , which enters the expression for  $J_{\text{therm}}$  only in a voltage-independent multiplicative factor. Over 75 devices (those which were not shorted, as described previously) were tested at room temperature. In all cases,  $\Delta E_v^{(x=0.22)}$  was found to be within 10 meV of the value obtained in Fig. 2. Due to the presence of Hg flux during the growth of  $\text{CdTe}$  layers, it is expected that the barrier material is actually  $\text{Hg}_{0.05}\text{Cd}_{0.95}\text{Te}$ .<sup>26</sup> Therefore, the experimentally obtained value of  $\Delta E_v^{(x=0.22)}$  actually represents the valence-band discontinuity at a  $\text{Hg}_{0.78}\text{Cd}_{0.22}\text{Te}$ - $\text{Hg}_{0.05}\text{Cd}_{0.95}\text{Te}$  interface.

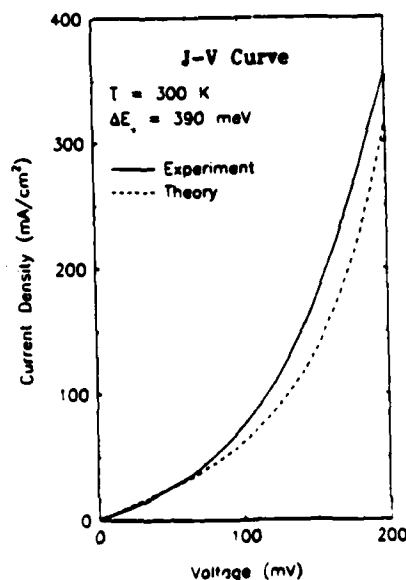


FIG. 2. Experimental  $J$ - $V$  curve (solid line) taken at room temperature. Also plotted is a best fit curve calculated for a  $\text{HgTe-CdTe}$  valence-band offset of 390 meV (dashed line).  $\Delta E_v$  is the only adjustable parameter used to generate the best fit curve.

Assuming a linear variation of the valence-band edge in  $\text{Hg}_{1-x}\text{Cd}_x\text{Te}$  with  $x$ ,  $\Delta E_v$  is then determined to be  $390 \pm 75$  meV. The estimated error has been assigned by combining the previously discussed variation in  $\Delta E_v$  ( $x = 0.22$ ) with the following sources of uncertainty: (i) nonuniformity across the sample, (ii) uncertainty in cladding layer compositions and band gaps, (iii) the percentage of alloying of the CdTe barrier due to incorporation of Hg during growth, and (iv) errors made in determining the transmission coefficients for hole tunneling.

Further  $I$ - $V$  measurements were made on over 20 devices in a low-temperature microprobe station. Electron tunneling currents were found to be insignificant for temperatures above 160 K. Consequently, we report data here for 190 K and higher. Analysis of the low-temperature data was performed in the same manner as described previously for room-temperature measurements, producing theoretical  $J$ - $V$  curves which agreed within 5% of the experimental characteristics over the voltage range 0–100 meV.

Figure 3 is a plot of the values of  $\Delta E_v$  which were determined as a function of temperature, along with a corresponding scale for  $\Delta E_v$  ( $x = 0.22$ ). Examination of Fig. 3 reveals that the band offset is found to vary strongly with temperature—an effect that has not been reported previously, to the best of the authors' knowledge. For example, it is found that  $\Delta E_v = 245 \pm 70$  meV at  $T = 190$  K. Band offset theories are at an early stage of development, with no temperature dependence yet estimated. It is possible that a transport mechanism which has not been considered may be contributing to the observed currents. This could lead to false determinations of the low-temperature band offsets. However, the observed agreement between the theoretical and experimental  $J$ - $V$  curves, without the use of any free parameters other than  $\Delta E_v$  ( $x = 0.22$ ), suggests that the correct current transport mechanisms have been included. It should be noted that the observed current decreases exponentially as the temperature decreases (as is expected for thermionic mechanisms), despite the decrease in  $\Delta E_v$ . This is reasonable because  $\phi_{\text{hole}}$  includes terms which do not vanish at  $T = 0$  K. Furthermore, the recent observation of negative differential resistance at  $T = 4.2$  K is consistent with a valence-band offset

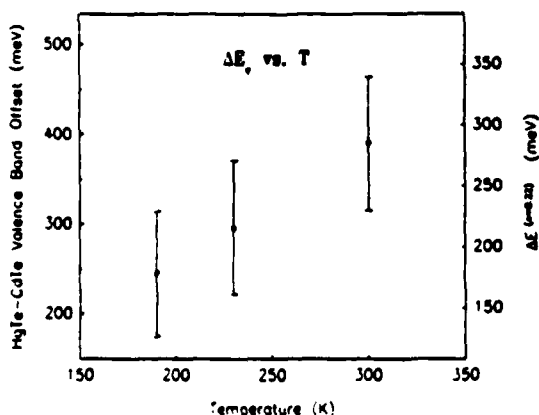


FIG. 3. Temperature dependence of HgTe-CdTe valence-band offset, as determined from experimental  $J$ - $V$  curves. Also plotted is the corresponding scale for the offset at the  $\text{Hg}_{0.78}\text{Cd}_{0.22}\text{Te}$ - $\text{Hg}_{0.05}\text{Cd}_{0.95}\text{Te}$  interface,  $\Delta E_v$  ( $x = 0.22$ ), assuming a linear dependence on composition, i.e.,  $\Delta E_v$  ( $x = 0.22$ ) =  $0.73\Delta E_v$ .

which is much smaller than the room-temperature value.

In this letter, we have experimentally and theoretically studied the current-voltage behavior of a  $\text{Hg}_{0.78}\text{Cd}_{0.22}\text{Te}$ - $\text{CdTe}$ - $\text{Hg}_{0.78}\text{Cd}_{0.22}\text{Te}$  heterostructure. Interpretation of the measured current as being dominated by thermionic and tunneling hole currents resulted in a determination of  $\Delta E_v = 390 \pm 75$  meV at  $T = 300$  K. This result is in reasonable agreement with recent XPS measurements. A similar analysis of low-temperature data indicates that the valence-band offset has a strong and previously unreported temperature dependence, with  $\Delta E_v$  becoming smaller for low  $T$ . However, other transport mechanisms may have contributed to the low-temperature currents, leading to erroneously low values of  $\Delta E_v$ .

We wish to acknowledge S. Nieh for providing us with important TEM data, and O. J. Marsh, T. K. Woodward, and M. B. Johnson for valuable discussions and assistance. This work was supported by the Defense Advanced Research Projects Agency under contract No. N00014-86-K-0841 and No. F49620-87-C-0021. One of us (DHC) received financial support from International Business Machines Corporation.

- <sup>1</sup>J. N. Schulman and T. C. McGill, *Appl. Phys. Lett.* **34**, 663 (1979).
- <sup>2</sup>C. E. Jones, T. N. Casselman, J. P. Faurie, S. Perkowitz, and J. N. Schulman, *Appl. Phys. Lett.* **47**, 140 (1985).
- <sup>3</sup>S. R. Hetzler, J. P. Bankus, A. T. Hunter, J. P. Faurie, P. P. Chow, and T. C. McGill, *Appl. Phys. Lett.* **47**, 260 (1985).
- <sup>4</sup>J. P. Faurie, J. Reno, and M. Boukerche, *J. Cryst. Growth* **72**, 111 (1985).
- <sup>5</sup>J. P. Bankus, A. T. Hunter, O. J. Marsh, C. E. Jones, G. Y. Wu, S. R. Hetzler, T. C. McGill, and J. P. Faurie, *J. Vac. Sci. Technol. A* **4**, 2110 (1986).
- <sup>6</sup>D. J. Leopold, M. L. Wroge, and J. G. Broerman, *Appl. Phys. Lett.* **50**, 924 (1987).
- <sup>7</sup>J. P. Bankus, A. T. Hunter, J. N. Schulman, and J. P. Faurie (unpublished).
- <sup>8</sup>J. N. Schulman and C. L. Anderson, *Appl. Phys. Lett.* **48**, 1684 (1986).
- <sup>9</sup>M. A. Reed, R. J. Koestner, and M. W. Goodwin, *Appl. Phys. Lett.* **49**, 1293 (1986).
- <sup>10</sup>D. H. Chow and T. C. McGill, *Appl. Phys. Lett.* **48**, 1485 (1986).
- <sup>11</sup>D. H. Chow, T. C. McGill, I. K. Sou, J. P. Faurie, and C. W. Nieh (unpublished).
- <sup>12</sup>J. O. McCaldin, T. C. McGill, and C. A. Mead, *Phys. Rev. Lett.* **36**, 56 (1976).
- <sup>13</sup>W. A. Harrison, *Electronic Structure and The Properties of Solids* (Freeman, San Francisco, 1980).
- <sup>14</sup>J. Tersoff, *J. Vac. Sci. Technol. B* **4**, 1066 (1986).
- <sup>15</sup>T. F. Kuech and J. O. McCaldin, *J. Appl. Phys.* **53**, 3121 (1982).
- <sup>16</sup>S. P. Kowalczyk, J. T. Cheung, E. A. Kraut, and R. W. Grant, *Phys. Rev. Lett.* **56**, 1605 (1986).
- <sup>17</sup>T. M. Duc, C. Hsu, and J. P. Faurie, *Phys. Rev. Lett.* **58**, 1127 (1987).
- <sup>18</sup>C. K. Shih and W. E. Spicer, *Phys. Rev. Lett.* **58**, 2594 (1987).
- <sup>19</sup>A. Zoryk and M. Jaros, *Appl. Phys. Lett.* **50**, 1191 (1987).
- <sup>20</sup>Y. Guldner, G. Bastard, J. P. Vieren, M. Voos, J. P. Faurie, and A. Milion, *Phys. Rev. Lett.* **51**, 907 (1983).
- <sup>21</sup>J. P. Faurie, C. Hsu, and T. M. Duc, *J. Vac. Sci. Technol. A* **5**, 3074 (1987).
- <sup>22</sup>A. R. Bonnefoi, D. H. Chow, and T. C. McGill, to be published in *J. Appl. Phys.*
- <sup>23</sup>R. Dornhaus, G. Nimtz, and B. Schlicht, *Narrow-Gap Semiconductors* (Springer, Berlin, 1983), pp. 158–160.
- <sup>24</sup>S. M. Sze, *Physics of Semiconductor Devices* (Wiley, New York, 1981), pp. 255–259.
- <sup>25</sup>E. O. Kane, *Physics of III-V Compounds* (Academic, New York, 1966), Vol. 1, Chap. 3, pp. 75–100.
- <sup>26</sup>J. Reno, R. Sporken, Y. J. Kim, C. Hsu, and J. P. Faurie (unpublished).

### VI-3-3 TEMPERATURE-DEPENDENT PHOTOEMISSION STUDY OF HgTe-CdTe VALENCE-BAND DISCONTINUITY ( $\Lambda$ )

Temperature-dependent experiments using x-ray photoelectron spectroscopy (XPS) and ultraviolet photoelectron spectroscopy (UPS) have been carried out in order to figure out if the discrepancy between optical data and photoemission experiments could be explained by a temperature-related variation of  $\Lambda$ . (see section VI-3-1)

The samples have been cooled at 110K for the XPS experiments and at 50K for UPS. At room temperature we confirmed that  $\Lambda$  is positive (i.e. HgTe VBM lies within the forbidden gap of CdTe in the heterostructure) and relatively large ( $\Lambda = 0.35 \pm 0.05\text{eV}$ ). Moreover we found that  $\Lambda$  changes by only a few millivolts between 300K and 50K, with an estimated uncertainty of  $\sim 60\text{meV}$ .

Therefore, the relatively large discrepancy reported before cannot be explained in terms of a temperature dependence of  $\Lambda$ . For more details see the attached paper.

#### ATTACHED PAPERS:

1. "Temperature-dependent photoemission study of HgTe-CdTe valence band discontinuity"

# Temperature-dependent photoemission study of HgTe–CdTe valence-band discontinuity

R. Sporken

*Physics Department, University of Illinois at Chicago, Chicago, Illinois 60680 and Facultés Universitaires Notre-Dame de la Paix, Laboratoire Interdisciplinaire de Spectroscopie Electronique, Namur, Belgium*

S. Sivananthan and J. P. Faurie

*Physics Department, University of Illinois at Chicago, Chicago, Illinois 60680*

D. H. Ehlers, J. Fraxedas, and L. Ley

*Max-Planck-Institut für Festkörperforschung, Stuttgart, Federal Republic of Germany*

J. J. Pireaux and R. Caudano

*Facultés Universitaires Notre-Dame de la Paix, Laboratoire Interdisciplinaire de Spectroscopie Electronique, Namur, Belgium*

(Received 11 October 1988; accepted 9 November 1988)

We have studied the temperature dependence of the CdTe–HgTe valence-band discontinuity with x-ray photoelectron spectroscopy (XPS) and ultraviolet photoelectron spectroscopy (UPS). The samples have been cooled at 110 K for the XPS experiments and at 50 K for UPS. At room temperature, we measure a valence-band discontinuity of  $0.35 \pm 0.05$  eV, in agreement with previous photoemission results. The valence-band discontinuity is found to change by only a few millivolts between room temperature and 50 K, with an estimated uncertainty of  $\sim 60$  meV.

## I. INTRODUCTION

HgTe–CdTe superlattices have received a great deal of interest over the past several years due to their potential use for infrared detectors.<sup>1</sup> One important parameter in determining the electronic properties of these superlattices is the valence-band discontinuity  $\Lambda$  between the HgTe and CdTe layers. The value of this valence-band discontinuity has been the subject of many theoretical and experimental investigations. Nevertheless, it is still a matter of considerable dispute.<sup>2</sup>

The first direct determination of  $\Lambda$  with x-ray photoemission spectroscopy was performed by Kowalczyk *et al.*<sup>3</sup> These measurements required a few minutes of air exposure of the sample. They found a positive valence-band discontinuity of  $\Lambda = 0.35 \pm 0.06$  eV; i.e., the valence-band maximum of HgTe lies within the CdTe band gap. A very similar value ( $\Lambda = 0.36 \pm 0.05$  eV) was obtained by Duc *et al.*<sup>4</sup> using x-ray photoelectron spectroscopy (XPS) without exposing the samples to air.

On the other hand, experimental data from resonant Raman scattering,<sup>5</sup> from infrared transmission and luminescence and from magneto-optical experiments<sup>6</sup> agree with a small valence-band discontinuity ( $\Lambda < 120$  meV). The reason for this discrepancy between the optical data and the photoemission measurements is still not understood at the present time. The XPS results were obtained at room temperature, whereas the optical experiments were carried out mainly at low temperature. It has therefore been suggested to perform temperature-dependent experiments in order to figure out if this discrepancy can be explained by a temperature-related variation of  $\Lambda$ .<sup>7</sup>

Direct electrical measurements of  $\Lambda$  on a single-barrier heterostructure  $\text{Hg}_{0.78}\text{Cd}_{0.22}\text{Te}$ –CdTe– $\text{Hg}_{0.78}\text{Cd}_{0.22}\text{Te}$  have been reported recently.<sup>8</sup> The interpretation of the re-

sults yields a direct determination of  $390 \pm 75$  meV for the HgTe–CdTe valence-band discontinuity at 300 K. The analysis of current–voltage data taken at 190–300 K seems to indicate that the valence-band offset decreases at low temperature in this heterojunction.

In this paper, we present the results of photoemission experiments. We will show that the large difference between results from photoemission and from optical experiments cannot be explained by a temperature dependence of  $\Lambda$ .

## II. EXPERIMENTAL

All the samples analyzed in this work were grown by molecular-beam epitaxy (MBE) in a Riber MBE 2300 machine. CdTe(111) $\bar{B}$  substrates were used. The substrate preparation and the MBE growth have been described elsewhere.<sup>9</sup> Three types of samples have been measured: 200-nm-thick layers of CdTe and HgTe and heterostructures of HgTe–CdTe. These latter samples were 200-nm-thick HgTe layers covered with 1–3 nm thick CdTe layers. The samples were then kept under argon until they were introduced into the spectrometer. The measurements were carried out first in a Hewlett–Packard 5950A electron spectrometer with a monochromatized Al  $K\alpha$  source. The sample temperature could be varied between 110 K and room temperature for these measurements. A second batch of samples was measured in an ADES-400 spectrometer with a He resonance lamp. In this latter case, gentle argon ion sputtering ( $E_p = 500$  eV) was required to clean the samples, due to the higher surface sensitivity of ultraviolet photoemission spectroscopy (UPS) as compared to XPS. In the ADES-400 spectrometer, the samples could be cooled with liquid helium. In practice, the lowest temperature we have used for the measurements was  $\sim 50$  K. At lower temperatures, severe sample charging occurs with the CdTe samples. As a result,

it becomes impossible to measure UPS spectra over a reasonable period of time below 50 K.

### III. RESULTS

#### A. X-ray photoemission spectroscopy

The determination of the valence-band discontinuity between HgTe and CdTe with XPS has been discussed in several papers.<sup>3,4,7</sup> The method is based on the measurements of three energy differences:  $\Delta E_{\text{Cl}}$  ( $\text{Cd } 4d_{5/2} - \text{Hg } 5d_{5/2}$ ),  $E_{\text{Hg } 5d_{5/2}}^{\text{HgTe}} - E_{\text{VBM}}^{\text{HgTe}}$ , and  $E_{\text{Cd } 4d_{5/2}}^{\text{CdTe}} - E_{\text{VBM}}^{\text{CdTe}}$ .  $\Delta E_{\text{Cl}}$  ( $\text{Cd } 4d_{5/2} - \text{Hg } 5d_{5/2}$ ) is the energy separation between the Cd  $4d_{5/2}$  and Hg  $5d_{5/2}$  core levels across a HgTe–CdTe heterojunction,  $E_{\text{Hg } 5d_{5/2}}^{\text{HgTe}} - E_{\text{VBM}}^{\text{HgTe}}$  is the binding energy of the Hg  $5d_{5/2}$  core level with respect to the valence-band maximum (VBM) in HgTe, and  $E_{\text{Cd } 4d_{5/2}}^{\text{CdTe}} - E_{\text{VBM}}^{\text{CdTe}}$  is the corresponding value for the Cd  $4d_{5/2}$  core level in CdTe. The valence-band discontinuity is finally obtained according to the relation:

$$\Lambda = (E_{\text{Hg } 5d_{5/2}}^{\text{HgTe}} - E_{\text{VBM}}^{\text{HgTe}}) - (E_{\text{Cd } 4d_{5/2}}^{\text{CdTe}} - E_{\text{VBM}}^{\text{CdTe}}) + \Delta E_{\text{Cl}} (\text{Cd } 4d_{5/2} - \text{Hg } 5d_{5/2}). \quad (1)$$

The position of the core levels involved in Eq. (1) is obtained from a least-squares curve-fitting procedure. The most critical part is therefore the localization of the valence-band maximum for each of the binary compounds. However, since the density of states close to the VBM is very similar in HgTe and CdTe, a linear extrapolation of the leading edge in the valence-band spectra can be used to locate the VBM, because any systematic error associated with this procedure will cancel in Eq. (1). At this stage, we do not intend to deduce a new value of the HgTe–CdTe valence-band discontinuity from the room-temperature XPS data. The reason is that we have been working on one single batch of samples that were exposed to air, whereas some of the earlier XPS results<sup>4,7</sup> were obtained from many different samples without taking them out of the ultrahigh vacuum environment. However, we note that for each of the three terms in Eq. (1), our results agree with those obtained in earlier experiments<sup>4,7</sup> to within the published uncertainty. This confirms the validity of our method and attests to a high quality of our samples.

We have checked the temperature dependence of the valence-band discontinuity by cooling the samples to 110 K. Figure 1 shows the core-level and valence-band spectra obtained from a CdTe–HgTe heterojunction at room temperature and at 110 K. The two spectra are remarkably similar, especially as far as the positions of the different features are concerned. This gives a feeling of how small the temperature-induced changes of the valence-band discontinuity are. We have also investigated the effect of cooling on the CdTe and HgTe spectra. In none of these cases did we see any significant effect. We therefore decided to use UPS which provides better energy resolution for this kind of experiment. Moreover, in the UPS spectrometer, the samples could be cleaned *in situ* and cooled with liquid helium. These results will be presented in the next part of this paper.

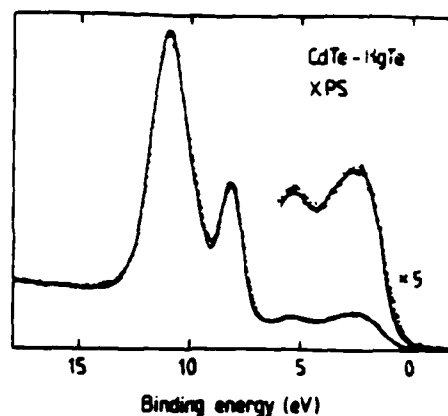


FIG. 1. Comparison between the XPS spectra of the Hg  $5d$  and Cd  $4d$  core levels and of the valence band measured on a CdTe–HgTe heterojunction at room temperature (solid line) and at 110 K (dots). The binding energy is measured with respect to the Fermi level.

#### B. Ultraviolet photoemission spectroscopy

UPS spectra were recorded using the He I ( $h\nu = 21.22$  eV) and He II ( $h\nu = 40.82$  eV) excitation lines. The samples were cleaned by gentle argon-ion sputtering, and the sample cleanliness was inferred directly from the UPS spectra. The geometry used for this experiment was grazing incidence and normal emission. However,  $k$  resolution is lost due to the surface roughening induced by the sputtering. Our spectra should thus be analyzed like conventional angle integrated UPS spectra.

Figure 2 shows typical UPS spectra obtained from CdTe, from HgTe, and from a CdTe–HgTe heterojunction. These spectra have been shifted on the energy scale in order to align the core levels (i.e., the Cd  $4d_{5/2}$  in CdTe with the Cd  $4d_{5/2}$  in the heterojunction, and the Hg  $5d_{5/2}$  in HgTe with the Hg  $5d_{5/2}$  in the heterojunction). The zero of the energy scale is arbitrarily chosen to coincide with the HgTe VBM which is located by a linear extrapolation of the leading edge in the valence-band spectrum. One can clearly see that the HgTe VBM lies within the forbidden gap of the CdTe in the heterojunction.

For the determination of  $\Lambda$ , we rewrite Eq. (1) in the following form:

$$\Lambda = (E_{\text{Hg } 5d_{5/2}}^{\text{HgTe}} - E_{\text{Cd } 4d_{5/2}}^{\text{CdTe}}) + \Delta E_{\text{Cl}} (\text{Cd } 4d_{5/2} - \text{Hg } 5d_{5/2}) - (E_{\text{VBM}}^{\text{HgTe}} - E_{\text{VBM}}^{\text{CdTe}}). \quad (2)$$

All the energies are measured with respect to an independent reference level, e.g., the spectrometer vacuum level. The core-level binding energies are then determined by a least-squares fit of mixed Gaussian–Lorentzian spin-orbit doublets to the data. The two first terms in Eq. (2) are thus known very accurately ( $\pm 15$  meV each). From our data obtained with the He II excitation, we deduce the following:

$$E_{\text{Hg } 5d_{5/2}}^{\text{HgTe}} - E_{\text{Cd } 4d_{5/2}}^{\text{CdTe}} = -2.876 \pm 0.015 \text{ eV}.$$

$$\Delta E_{\text{Cl}} (\text{Cd } 4d_{5/2} - \text{Hg } 5d_{5/2}) = 2.723 \pm 0.015 \text{ eV}$$

The results of these least-squares fits are shown in Fig. 3. The last term in Eq. (2) is obtained by measuring the shift which is needed to superpose the leading edge of the CdTe valence-band spectrum on the corresponding feature in

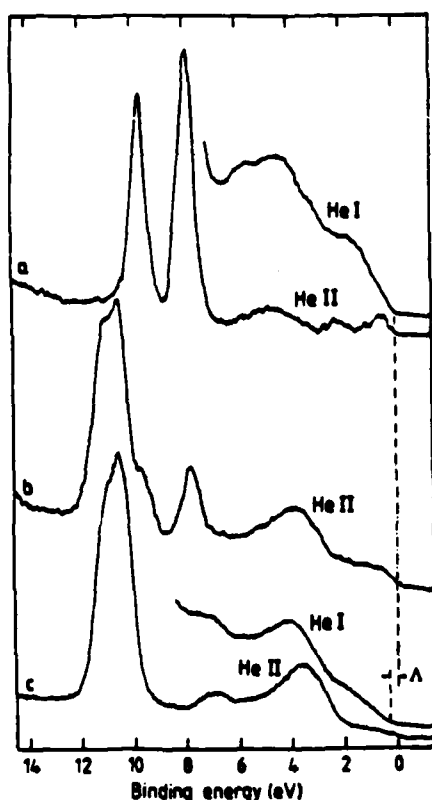


FIG. 2. UPS spectra from (a) HgTe, (b) a CdTe-HgTe heterojunction, and (c) from CdTe. These spectra have been shifted to align the core levels (the Cd  $4d_{5/2}$  in CdTe with the Cd  $4d_{5/2}$  in the heterojunction, and the Hg  $5d_{5/2}$  in HgTe with the Hg  $5d_{5/2}$  in the heterojunction). The binding-energy scale is referred to the HgTe VBM obtained by linear extrapolation of the leading edge in the HgTe valence-band spectra.

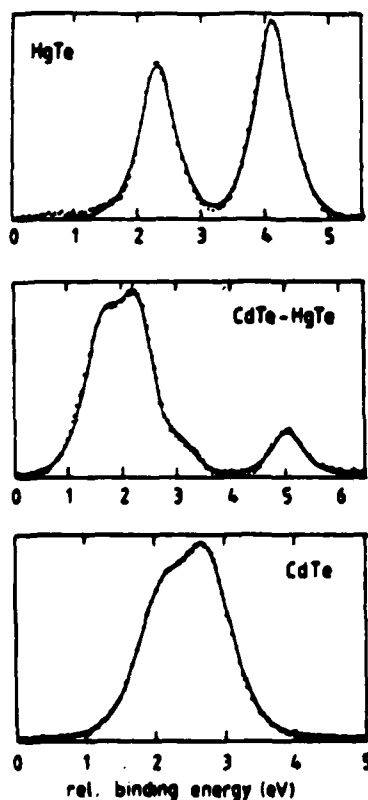


FIG. 3. Typical core-level spectra measured with the He II excitation ( $h\nu = 40.82$  eV) on HgTe, CdTe, and on a CdTe-HgTe heterojunction. The experimental data (dots) are shown together with representative results from least-squares fits (solid lines) of spin-orbit doublets.

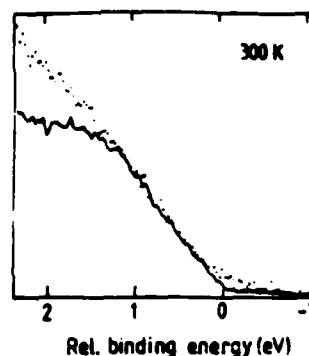


FIG. 4. Alignment of the VBM of CdTe (solid line) and HgTe (dots) at room temperature. The binding energies quoted here are measured with respect to the CdTe and HgTe VBM which are equal after alignment of the spectra.

HgTe valence-band spectrum (Fig. 4). Since the two binary compounds have a similar density of states close to the VBM, this shift can be measured to a very high accuracy. We find

$$E_{\text{VBM}}^{\text{HgTe}} - E_{\text{VBM}}^{\text{CdTe}} = -0.50 \pm 0.03 \text{ eV}.$$

This separation was measured on the He I excited valence-band spectra. However, in order to work under very stable conditions, the resonance lamp was operated at low He pressure to record both the He I and He II spectra. Finally, we obtain, according to Eq. (2):

$$\begin{aligned} \Lambda &= -2.876 + 2.723 + 0.50 \\ &= 0.35 \pm 0.05 \text{ eV}, \end{aligned}$$

in excellent agreement with previous XPS results.

The escape depth of the photoelectrons is much smaller in UPS than in XPS. For the data in Fig. 2, the thickness of the CdTe layer is thus very small, probably on the order of 1 nm. It is therefore remarkable that these data agree very nicely with previous XPS data,<sup>4,7</sup> obtained for CdTe layer thicknesses up to 4 nm. This gives us strong confidence in our UPS data and in the following temperature-dependent study.

The temperature dependence of the valence-band discontinuity can be determined very accurately, because a precise knowledge of the separation between the core levels and the valence-band maxima is not required anymore. In turn, all we need to measure now is the energy separation between same features in spectra measured under different conditions.

Figure 5 shows the UPS spectra for CdTe, HgTe, and the CdTe-HgTe heterojunction, obtained at room temperature and at 50 K. Again, these spectra have been shifted to align the core levels as was explained for Fig. 2. Below 50 K, it was impossible to achieve stable and reproducible results on CdTe due to severe sample charging. Even at 50 K, the CdTe sample charges positively, but a stable situation could be maintained for at least 1 or 2 h.

For each of the binary compounds, the temperature dependence of the core-level binding energies referred to the VBM is determined very accurately by alignment of these valence-band maxima measured at room temperature and at 50 K (Fig. 6). For clarity, we write these binding energies as

$$E_{\text{Cl}}^{\text{VBM}} = E_{\text{Cl}} - E^{\text{VBM}}, \quad (3)$$

and we define

$$\Delta E_{\text{Cl}} = E(\text{Cd } 4d_{5/2}) - E(\text{Hg } 5d_{5/2}) \quad (4)$$

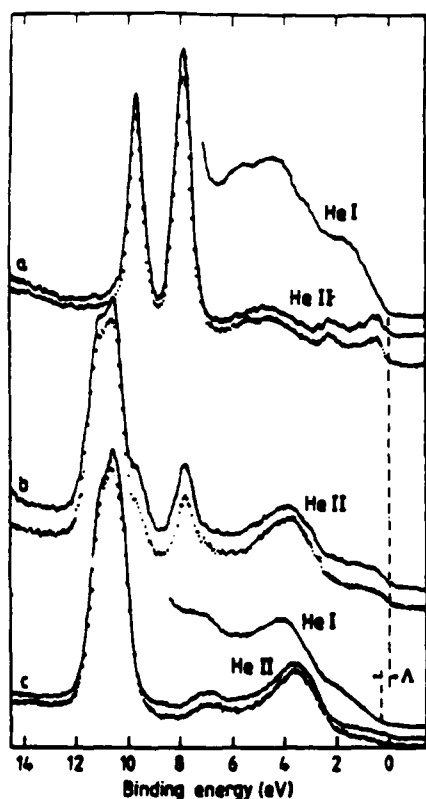


FIG. 5. Same as Fig. 2, but spectra obtained at 50 K are shown for comparison (dots).

across the heterojunction. We then obtain

$$E_{\text{Cl}}^{\text{VBM}}(\text{Hg } 5d_{5/2}, 300 \text{ K}) - E_{\text{Cl}}^{\text{VBM}}(\text{Hg } 5d_{5/2}, 50 \text{ K}) = -23 \text{ meV},$$

$$E_{\text{Cl}}^{\text{VBM}}(\text{Cd } 4d_{5/2}, 300 \text{ K}) - E_{\text{Cl}}^{\text{VBM}}(\text{Cd } 4d_{5/2}, 50 \text{ K}) = 10 \text{ meV},$$

$$\Delta E_{\text{Cl}}(300 \text{ K}) - \Delta E_{\text{Cl}}(50 \text{ K}) = 19 \text{ meV}.$$

The net result is that the valence-band discontinuity  $\Delta$  is found to decrease by only a few millivolts between room

temperature and 50 K, with an estimated uncertainty of  $\sim 60 \text{ meV}$ .

#### IV. CONCLUSIONS

In this paper, we have presented a photoemission study of the temperature dependence of the HgTe-CdTe valence-band discontinuity. This work was motivated by the large discrepancy between previous photoemission results obtained at room temperature and data from magneto-optical, resonant Raman scattering and infrared photoluminescence experiments mostly performed at low temperature. While the former experiments are consistent with a relatively large valence-band discontinuity of  $\sim 350 \text{ meV}$ , the latter agree with a smaller value of  $\Delta < 120 \text{ meV}$ .

The measurements presented here are x-ray and ultraviolet photoemission experiments. We confirm that, at room temperature,  $\Delta$  is positive (i.e., the HgTe VBM lies within the forbidden gap of CdTe in the heterostructure) and relatively large ( $\Delta = 0.35 \pm 0.05 \text{ eV}$ ). Moreover, we found that  $\Delta$  changes by only a few millivolts between room temperature and 50 K, with an estimated uncertainty of  $\sim 60 \text{ meV}$ . Therefore, the relatively large discrepancy reported above cannot be explained in terms of a temperature dependence of the valence-band discontinuity.

#### ACKNOWLEDGMENTS

We would like to thank I. K. Sou for the preparation of some of the samples used in this work and J. Riga and Th. Conard for assistance with the XPS measurements. The work at the University of Illinois at Chicago is supported by the U.S. Defense Advanced Research Projects Agency and monitored by the U.S. Air Force Office of Scientific Research under Contract No. F 4920-87-C-0021. The XPS work carried out at the Facultés Universitaires Notre-Dame de la Paix at Namur is supported by the Ministère de la Politique Scientifique (IRIS project). One of us (R.S.) is grateful to the Belgian National Foundation for Scientific Research [Fonds National de la Recherche Scientifique (F.N.R.S.)] for financial support.

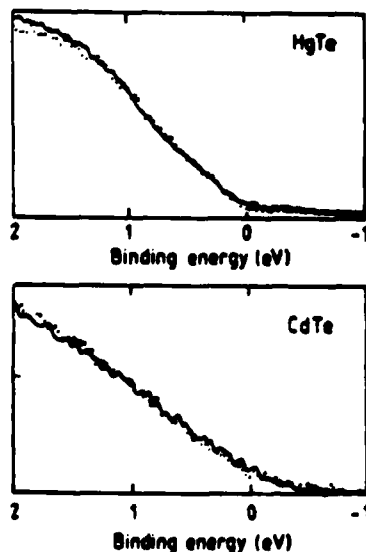


FIG. 6. Alignment of the valence-band maxima measured at room temperature (dots) and at 50 K (solid line) for CdTe and HgTe. These spectra have been obtained with He I excitation.

- <sup>1</sup>J. N. Schulman and T. C. McGill, *Appl. Phys. Lett.* **34**, 663 (1979).
- <sup>2</sup>J. P. Faurie, *Proceedings of the NATO Workshop on Band Structure Engineering in Semiconductor Microstructures*, II Ciocco, Italy, 1988, and references therein (to be published).
- <sup>3</sup>S. P. Kowalczyk, J. T. Cheung, E. A. Kraut, and R. W. Grant, *Phys. Rev. Lett.* **55**, 1605 (1986).
- <sup>4</sup>T. M. Duc, C. Hsu, and J. P. Faurie, *Phys. Rev. Lett.* **58**, 1127 (1987).
- <sup>5</sup>D. Olego, J. P. Faurie, and P. M. Roca, *Phys. Rev. Lett.* **55**, 328 (1985).
- <sup>6</sup>Y. Guldner, G. Bastard, J. P. Vieren, M. Voos, J. P. Faurie, and A. Million, *Phys. Rev. Lett.* **51**, 907 (1983).
- <sup>7</sup>J. P. Faurie, C. Hsu, and T. M. Duc, *J. Vac. Sci. Technol. A* **5**, 3074 (1987).
- <sup>8</sup>D. M. Chow, J. O. McCaldin, A. R. Bonnefoi, T. C. McGill, I. K. Sou, and J. P. Faurie, *Appl. Phys. Lett.* **51**, 2230 (1987).
- <sup>9</sup>J. P. Faurie, *IEEE J. Quantum Electron.* **22**, 1656 (1986).

## VII STIMULATED EMISSION FROM CdTe/HgCdTe HETEROSTRUCTURES GROWN BY MBE

Mercury based II-VI semiconductor heterostructures are one of the potential laser sources in the near and mid-infrared (IR) regions (1-5 $\mu$ m) for long distance data communications. Moreover, it has been recently theoretically predicted that these compounds are less than III-V compounds by the limiting Auger recombination process in the 1.5 $\mu$ m wavelength region.<sup>(1)</sup> Hence these compounds should be able to compete favorably with the current III-V semiconductor lasers.

Although MCT has been a very important material in the IR detector technology, its potential as a material for the development of IR lasers has not been fully explored. Our task in this program was related to the growth, characterization and device processing of IR laser sources in the 1-5 $\mu$ m wavelength range. This program was also supported by the Strategic Defense Initiative Organization/Innovative Science and Technology Office and monitored by the Naval Research Laboratory under contract No. N00014-87-C-2043.

This program has been very successful. We have reported the first observation of photoluminescence from CdTe/Hg<sub>1-y</sub>Cd<sub>y</sub>Te/Hg<sub>1-x</sub>Cd<sub>x</sub>Te ( $y > x$ ) separate confinement heterostructure. Fast progress has been obtained soon after since stimulated emission at 2.4 $\mu$ m from a Hg<sub>1-x</sub>Cd<sub>x</sub>Te(100) MBE epilayer, at 2.25 $\mu$ m from a CdTe/-Hg<sub>1-x</sub>Cd<sub>x</sub>Te/CdTe double heterostructures and at 2.4 $\mu$ m from a CdTe/Hg<sub>1-y</sub>Cd<sub>y</sub>Te/Hg<sub>1-x</sub>Cd<sub>x</sub>Te multi-quantum well separate confinement heterostructure (MQWSCH) have been observed.

Pulsed stimulated emission was observed from the MQWSCH up to 77K. Furthermore, the threshold for the lasing action in the MQWSCH is one order of magnitude lower than optically pumped GaAlAs semiconductor lasers operating at 0.9 $\mu$ m and about a factor of 3 lower than the AlGaSb/InAsSb lasers operating at 3.9 $\mu$ m. Although we cannot make a direct comparison of threshold powers due to the different wavelengths of operation of these lasers, this difference is an indication of the expected trend in Hg-based II-VI compound lasers<sup>(1)</sup> which is extremely promising for the use of Hg-based heterostructures as laser sources in the infrared. For more details see that attached papers.

### REFERENCES:

1. A. Haug, Semicond. Sci. Technol. 4, 803 (1989)

**ATTACHED PAPERS:**

1. "Photoluminescence from CdTe/Hg<sub>1-y</sub>Cd<sub>y</sub>Te/Hg<sub>1-x</sub>Cd<sub>x</sub>Te separate confinement heterostructures"
2. "Stimulated emission from a Hg<sub>1-x</sub>Cd<sub>x</sub>Te epilayer grown by molecular beam epitaxy"
3. "Stimulated emission from a Hg<sub>1-x</sub>Cd<sub>x</sub>Te epilayer and CdTe/Hg<sub>1-x</sub>Cd<sub>x</sub>Te heterostructures grown by molecular beam epitaxy"
4. "Stimulated emission from a CdTe/HgCdTe separate confinement heterostructure grown by molecular beam epitaxy"

# Photoluminescence from CdTe/Hg<sub>1-y</sub>Cd<sub>y</sub>Te/Hg<sub>1-x</sub>Cd<sub>x</sub>Te separate confinement heterostructures

K. K. Mahavadi, M. D. Lange, and J. P. Faurie

Physics Department, University of Illinois at Chicago, Chicago, Illinois 60680

J. Nagle

Laboratoire Central de Recherches, Thomson CSF, B.P. 10, Orsay F-91401, France

(Received 11 January 1989; accepted for publication 20 April 1989)

We report the first observation of photoluminescence from CdTe/Hg<sub>1-y</sub>Cd<sub>y</sub>Te/Hg<sub>1-x</sub>Cd<sub>x</sub>Te ( $y > x$ ) separate confinement heterostructures grown by molecular beam epitaxy. The spectral shape is determined by the band filling of electrons in the well which is due to a charge transfer effect. There is an appearance of high-energy transitions at high temperatures. The strong photoluminescence from the layer is highly promising for the observation of the laser action.

There is a considerable technological interest in the development of laser sources in the mid-infrared range (2–5  $\mu\text{m}$ ) for long distance data communications. Hg-based alloys and heterostructures are one of the potential laser sources in this region. Whereas Hg-based alloys are the most important materials for IR detection, surprisingly very little has been published on these II-VI semiconducting compound based lasers.<sup>1,2</sup> Quantum well (QW) lasers have well established advantages over the double-heterostructure (DH) lasers in III-V semiconducting alloys. Reduction of the threshold current density and improvement in modulation properties have been reported in GaAs/AlGaAs QW lasers.<sup>3</sup> Lasing action has been observed in many other material systems when the quantum wells are placed in a separate confinement optical cavity.<sup>4,5</sup> Recently, photoluminescence (PL) has been observed from a CdTe/Hg<sub>1-y</sub>Cd<sub>y</sub>Te superlattice placed in a double heterostructure.<sup>6</sup> We present in this letter the first observation of photoluminescence from a CdTe/Hg<sub>1-y</sub>Cd<sub>y</sub>Te/Hg<sub>1-x</sub>Cd<sub>x</sub>Te ( $y > x$ ) single quantum well separate confinement heterostructure (SCH) grown by molecular beam epitaxy (MBE). To the best of our knowledge, this is the first SCH grown in the CdTe/Hg<sub>1-y</sub>Cd<sub>y</sub>Te system.

A schematic of the single quantum well separate confinement heterostructure is shown in Fig. 1. The  $x$  value (0.36) of the active layer Hg<sub>0.45</sub>Cd<sub>0.55</sub>Te corresponds to a band gap of 340 meV ( $\sim 3.67 \mu\text{m}$ ) at 77 K. We choose the thickness of the confinement layer (7500 Å) that optimizes the optical confinement factor in a 500 Å well QW laser. The quantum well energy levels are calculated using the envelope function approximation.<sup>7</sup> We included the nonparabolicity of the conduction band and neglected any band mixing effects in the valence band in our calculations. We used<sup>8</sup> a value of 65 meV for the valence-band offset between Hg<sub>0.45</sub>Cd<sub>0.55</sub>Te and Hg<sub>0.64</sub>Cd<sub>0.36</sub>Te. The electron effective mass at the bottom of the conduction band is calculated using the expression

$$m_e^* = (3\pi^2/4P^2)E_g,$$

where  $P$  is the matrix element and  $E_g$  is the band gap. The band gap is determined using the expression given by Hansen *et al.*<sup>9</sup> For heavy hole effective mass, we used a value of  $0.3m_0$ .

The SCH was grown by MBE in a RIBER 2300 MBE

machine. The substrate is a semi-insulating CdTe (100). The growth temperature for the bottom CdTe layer was 300 °C and that for both Hg<sub>0.45</sub>Cd<sub>0.55</sub>Te and Hg<sub>0.64</sub>Cd<sub>0.36</sub>Te layers was 185 °C. Two CdTe effusion cells were used to grow the two mercury cadmium telluride layers with different  $x$  values. The 3000 Å top CdTe layer was grown at a substrate temperature of 185 °C to prevent any possible diffusion of mercury from the confinement layer into this layer. The individual layer thicknesses were determined from the growth rates of thick calibration layers grown under identical growth conditions. The detail of the growth of Hg-based alloys has been given elsewhere.<sup>10</sup>

Photoluminescence experiments were performed on this structure. A cw Nd:YAG laser ( $\lambda = 1.06 \mu\text{m}$ ) was used for photoexcitation. Samples were photoexcited from the front side through the 3000 Å CdTe layer. Since the excitation energy is below the band-gap energy of CdTe, carriers are mainly created in the wider gap Hg<sub>1-y</sub>Cd<sub>y</sub>Te confining layer. Samples were not in the form of optical cavities to observe stimulated emission. Samples were cooled in a Janis variable temperature closed-cycle helium cryostat. The luminescence was analyzed using a 0.75 m grating monochromator and lock-in detection technique. A cooled InSb detector was used to collect the luminescence.

Figure 2 shows the PL spectra of a SCH measured at four different temperatures. The sample was excited with an incident power of 125 W/cm<sup>2</sup>. The numbers along the horizontal axis show the calculated positions of  $\Delta n = 0$  confined particle transitions ( $nE-nHH$  and  $n'E-n'LH$ ) in the well. We observed that the emission from this structure is two to three times more intense than the emission from bulk or DH

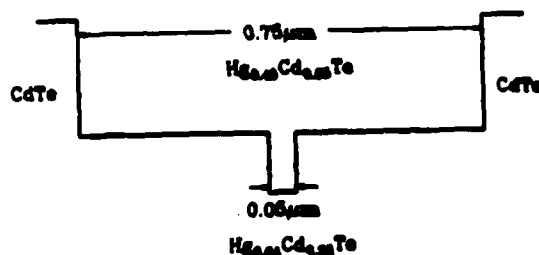


FIG. 1. Schematic cross section of CdTe/Hg<sub>1-y</sub>Cd<sub>y</sub>Te/Hg<sub>1-x</sub>Cd<sub>x</sub>Te separate confinement heterostructure.

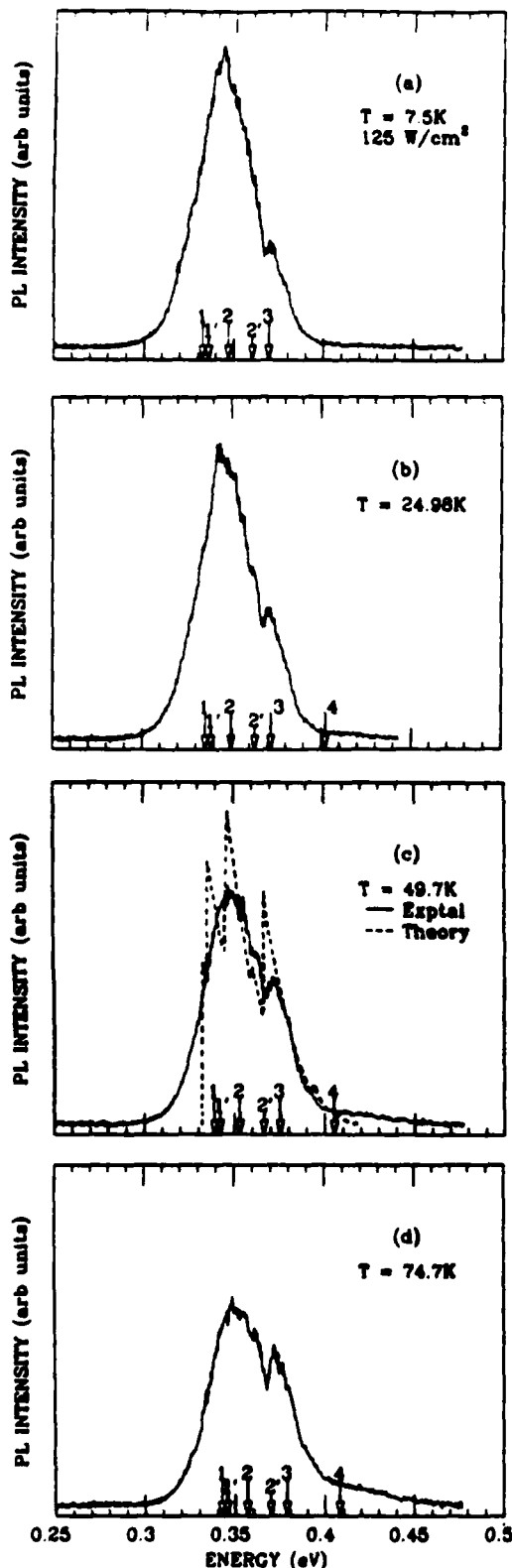


FIG. 2. PL spectra of a SCH structure at four different temperatures. The numbers in all four spectra indicate the energies of transitions between conduction and valence subbands. The dashed curve in (c) is the theoretical curve.

layers grown by MBE under identical conditions in our laboratory. This is particularly promising for the observation of the lasing action from this structure.

The spectra show that the electrons are occupying up to

the fourth electron subband to give the broad luminescence. The shift to higher energy of the spectra with temperature is due to the temperature variation of the band gap and the effective masses of electron and light hole. However, there is no significant change in the width of the luminescence peak with temperature. This could very well be explained if either the well layer or the confinement layers are *n* type with a carrier concentration of  $\sim 2 \times 10^{17}/\text{cm}^3$ . What we do see is the band filling of electrons in the well and this band filling in turn imposes the linewidth. The MBE-grown  $\text{Hg}_{1-x}\text{Cd}_x\text{Te}$  layers on (100) CdTe are typically *n* type with the electron concentrations in the range of  $(1-5) \times 10^{16}/\text{cm}^3$ . Charge transfer effects from the confinement layers might account for the high electron concentration in the well layer. Such a charge transfer has already been observed in the CdTe/ $\text{Hg}_{1-x}\text{Cd}_x\text{Te}$  heterostructures.<sup>11</sup>

Another interesting feature to be noted is that the strength of the 3HH transition is increasing and at the same time the strength of the lower subband transitions is decreasing when the temperature of the measurement is increased. There is an overall trend towards higher subband transitions with an increase in measurement temperature. Simulations have been made by assuming an injection of  $1 \times 10^{11}/\text{cm}^2$  holes, a real temperature of the lattice and carriers 10 K above the nominal temperature, and a Lorentzian broadening of 10 meV to analyze the experimental data. One of the simulated spectra is shown in Fig. 2(c). Comparison of the experimental and the simulated curves in Fig. 2(c) shows that the spectral width can very well be explained by the band filling of electrons in the well. Our simulations also reproduced very well the increase with temperature in luminescence due to higher lying subbands. The structure around 400 meV is probably due to the 4E-4HH transition for the following reason: The quasi-Fermi level for holes being close to the "bottom" of the valence band, the occupation probability of the 4HH band ( $E_{4hh} \sim 3$  meV with respect to the quasi-Fermi level) is higher than the occupation of the 3LH band ( $E_{3lh} \sim 33$  meV). The shape of the spectra varied only a little with the level of minority-carrier injection. More generally, we found that the ratio of the intensity between different transitions is mainly given by the ratio of the occupation factors of the holes. Finally, the dip around 360 meV in all the spectra might either be due to the reabsorption of luminescence by a defect in the upper layers or due to some experimental artifact.

In summary, we have performed photoluminescence experiments on the first CdTe-(HgCd)Te separate confinement heterostructures grown by molecular beam epitaxy. There is an evidence for the occupation of several electronic levels due to the charge transfer and this band filling determines the width of the PL peak. There is an appearance of high-energy transitions at high temperatures. The strong PL is a sign of the high quality of the structure and gives us hope to observe the lasing action.

The authors would like to thank Dr. C. Weisbuch for useful discussions. Thanks are also due to S. Farook and Z. Ali for their technical assistance. This work is supported by Strategic Defense Initiative Organization/Innovative Science and Technology Office, monitored by the Naval Re-

search Laboratory under contract No. N00014-87-C-2043 and by the Defense Advanced Research Projects Agency monitored by the Air Force Scientific Office for Research under contract No. F48620-87-C-0021.

<sup>1</sup>T. C. Harman, *J. Electron. Mater.* **8**, 191 (1979).

<sup>2</sup>P. Becla, *J. Vac. Sci. Technol. A* **6**, 2725 (1988).

<sup>3</sup>H. Z. Chen, A. Ghaifari, H. Morkoç, and A. Yariv, *Appl. Phys. Lett.* **51**, 2094 (1987).

<sup>4</sup>Y. Ohmori, Y. Suzuki, and H. Okamoto, *Jpn. J. Appl. Phys.* **24**, L657 (1985).

<sup>5</sup>M. Ikeda, A. Toda, K. Nakano, and Y. Mori, *Appl. Phys. Lett.* **50**, 1033 (1987).

<sup>6</sup>T. H. Myers, R. W. Yanka, K. A. Harris, A. R. Reisinger, J. Han, S. Hwang, Z. Yang, N. C. Giles, H. W. Cook, Jr., J. F. Schetzina, R. W. Green, and S. McDevitt, *J. Vac. Sci. Technol. A* **7**, 300 (1989).

<sup>7</sup>G. Bastard, *Phys. Rev. B* **24**, 5693 (1981).

<sup>8</sup>C. Hsu, T. N. Duc, and J. P. Faurie, *J. Phys. (Paris) Colloq.* **C5**, 48, 307 (1987).

<sup>9</sup>G. L. Hansen, J. L. Schmit, and T. N. Casselman, *J. Appl. Phys.* **53**, 7099 (1982).

<sup>10</sup>S. Sivananthan, M. D. Lange, G. Monfroy, and J. P. Faurie, *J. Vac. Sci. Technol. B* **6**, 788 (1988).

<sup>11</sup>Y. Guldner, G. S. Boebinger, J. P. Vieren, M. Voss, and J. P. Faurie, *Phys. Rev. B* **36**, 2958 (1987).

# Stimulated emission from a $\text{Hg}_{1-x}\text{Cd}_x\text{Te}$ epilayer grown by molecular beam epitaxy

K. K. Mahavadi, J. Bleuse, X. Chu, and J. P. Faurie

Department of Physics, University of Illinois at Chicago, Chicago, Illinois 60680

(Received 26 May 1989; accepted for publication 18 July 1989)

We report on the observation of stimulated emission from a (100) oriented  $\text{Hg}_{1-x}\text{Cd}_x\text{Te}$  epilayer grown by molecular beam epitaxy. The cleaved epilayers were cooled and optically pumped by a Nd:YAG laser and were found to lase continuously up to 40 K.

Mercury cadmium telluride ( $\text{HgCdTe}$ ) has been a very important semiconducting material in infrared (IR) detector technology. However, its potential for the development of infrared lasers has not been fully explored. Only a few isolated reports have been published on the mercury (Hg) based II-VI compound lasers.<sup>1-3</sup> Prior to our work, all published studies were performed on the liquid phase epitaxially grown and Bridgman-grown  $\text{Hg}_{1-x}\text{Cd}_x\text{Te}$  crystals. In this letter, we report the observation of stimulated emission from a  $\text{Hg}_{1-x}\text{Cd}_x\text{Te}$ (100) epilayer grown by molecular beam epitaxy (MBE).

The  $\text{Hg}_{0.34}\text{Cd}_{0.66}\text{Te}$ (100) layer was grown in a Riber 2300 MBE machine. The substrate was a semi-insulating (100) $\text{CdTe}$ . A  $\sim 1000\text{-\AA}$ -thick  $\text{CdTe}$  buffer layer was grown on the substrate to improve the surface smoothness. The  $0.6\text{-}\mu\text{m}$ -thick  $\text{Hg}_{1-x}\text{Cd}_x\text{Te}$  epilayer was grown at a substrate temperature of  $185^\circ\text{C}$ . The growth rate was  $1.74\text{ \AA/s}$ . Details of the growth of Hg-based alloys have been given elsewhere.<sup>4</sup>

The initial characterization of the layer showed that the layer is  $n$  type with a carrier concentration of  $2 \times 10^{16}/\text{cm}^3$  at 100 K. The carrier concentration was constant from room temperature down to 100 K. The minority-carrier lifetime was determined by the standard photoconductive technique and was found to be  $2.4\text{ }\mu\text{s}$  at 100 K. We also observed a strong photoluminescence from this layer at 10 K.

To prepare samples for the stimulated emission measurements, the  $\text{CdTe}$  substrate was first mechanically etched to a thickness of  $80\text{ }\mu\text{m}$ . Then it was further thinned to a thickness of  $\sim 20\text{ }\mu\text{m}$  by chemical etching in a 2% by volume solution of bromine methanol. Next, the  $\text{Hg}_{0.34}\text{Cd}_{0.66}\text{Te}$  layer was cleaved into small rectangular bars of  $200 \times 500\text{ }\mu\text{m}$ – $500 \times 1500\text{ }\mu\text{m}$  size using a sharp scalpel. Several of these cleaved samples were covered by a sapphire window and were pressed into indium mounted on a copper block for efficient heat sinking.<sup>5</sup> The mounted samples were cooled to 10 K using a variable temperature closed cycle cryostat. Using a cylindrical lens, the cw Nd:YAG laser beam was focused to a strip of  $50\text{ }\mu\text{m}$  width and  $500\text{ }\mu\text{m}$  length to cover the entire width of a selected sample. The emission was collected with a lens, dispersed by a  $0.75\text{ m}$  monochromator, and detected by a cooled InSb detector. Details of the experimental setup are given elsewhere.<sup>6</sup>

Figure 1 shows the typical cw emission spectra from one of the samples. These spectra are taken with wide slits to facilitate the observation of spontaneous emission below the

threshold. Curves taken at an input optical power density ( $P$ ) of less than  $2.8\text{ kW/cm}^2$  are below the threshold for the laser action to occur. For  $P = 2.8\text{ kW/cm}^2$  a slight glitch is emerging at a wavelength of  $2.42\text{ }\mu\text{m}$  from the broad luminescence background. This signals the onset of stimulated emission from this layer. Increasing the input power density to  $3.2\text{ kW/cm}^2$  has clearly increased the intensity of the multimode output by more than three times the intensity of the background. The increase in the output laser intensity as a function of incident power density is shown in Fig. 2. The laser action was observed up to an incident power density of  $5.2\text{ kW/cm}^2$ . However, the output intensity started to decrease above  $4.4\text{ kW/cm}^2$ . This might be due to excessive heating of the samples.

Figure 3 shows the spectrum taken with narrow slits. As can be seen from the figure, there are a few longitudinal modes in addition to the fundamental mode in the spectrum. However, we have not tried to determine the refractive index of the layer from the mode spacing for the following reason: The substrate was not rotated during the growth of the crystal and as a result we found that there is a band-gap variation of  $25\text{ meV/mm}$  along the length of the crystal. This crystal inhomogeneity might lead to uneven mode spacing due to

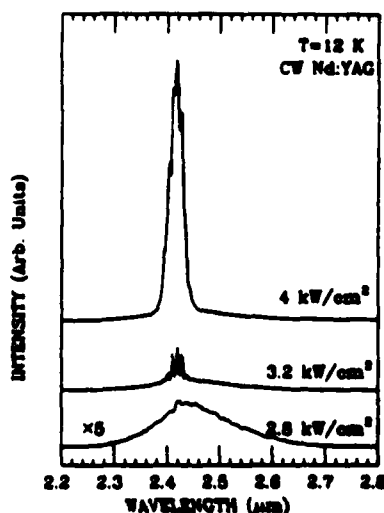


FIG. 1. cw emission spectra from a cleaved  $500 \times 1500\text{ }\mu\text{m}$   $\text{Hg}_{0.34}\text{Cd}_{0.66}\text{Te}$  MBE grown epilayer under different incident powers.

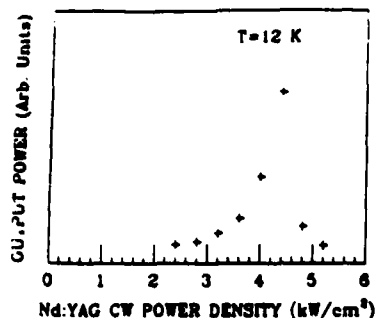


FIG. 2. Output intensity vs incident power density.

the variation of the refractive index. This might also explain the reason for observing the laser action on the higher energy side of the luminescence spectrum.

The samples were found to lase continuously up to 40 K.

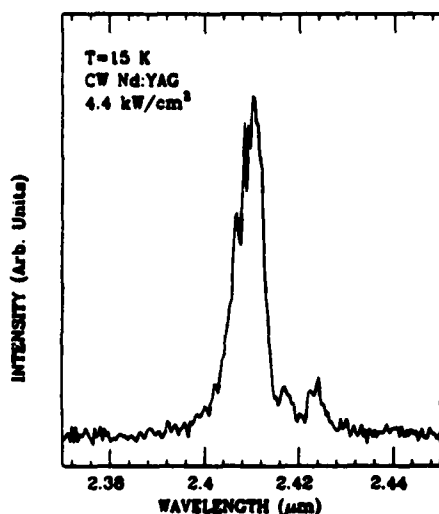


FIG. 3. cw laser spectrum taken with narrow slits. The spectrum shows a few longitudinal modes in addition to the fundamental mode.

Above this temperature no laser action was observed from any of the samples. We assume that above 40 K the stimulated emission from this layer can only be obtained under pulsed excitation. A similar observation has been made by Harman on liquid phase epitaxially grown  $\text{Hg}_{1-x}\text{Cd}_x\text{Te}$  epilayers.<sup>2</sup> Our work shows that the MBE-grown  $\text{Hg}_{1-x}\text{Cd}_x\text{Te}$  layers are of high quality and have a high potential for the development of IR laser sources. Since MBE facilitates the growth of novel artificially layered structures, the laser threshold can be lowered by designing suitable quantum well structures.

In conclusion, we have performed the stimulated emission experiments on  $\text{Hg}_{0.54}\text{Cd}_{0.46}\text{Te}$  layer grown by molecular beam epitaxy. The optically pumped cleaved samples were found to lase continuously up to 40 K.

The authors would like to thank P. S. Wijewarnasuriya and Mario de Souza for performing the Hall and lifetime measurements on the layer. Thanks are also due to S. Farook and Z. Ali for their technical assistance. This work is supported in part by Strategic Defense Initiative Organization/Innovative Science and Technology Office, monitored by Naval Research Laboratory under contract No. N00014-87-C-2043 and in part by Defense Advancement Research Project Agency, monitored by Air Force Scientific Office for Research under contract No. F48620-87-C-0021.

<sup>1</sup>I. Melngailis and A. J. Strauss, *Appl. Phys. Lett.* **8**, 179 (1966).

<sup>2</sup>T. C. Harman, *J. Electron. Mater.* **8**, 191 (1979).

<sup>3</sup>R. S. Putnam, M. M. Salour, and T. C. Harman, *Appl. Phys. Lett.* **43**, 408 (1983).

<sup>4</sup>S. Sivasubramanian, M. D. Lange, G. Monfroy, and J. P. Faurie, *J. Vac. Sci. Technol. B* **6**, 788 (1988).

<sup>5</sup>N. Holonyak, Jr. and D. R. Scifres, *Rev. Sci. Instrum.* **42**, 1885 (1971).

<sup>6</sup>K. K. Mahavadi, M. D. Lange, J. P. Faurie, and J. Nagle, *Appl. Phys. Lett.* **54**, 2580 (1989).

# Stimulated emission from a $\text{Hg}_{1-x}\text{Cd}_x\text{Te}$ epilayer and $\text{CdTe}/\text{Hg}_{1-x}\text{Cd}_x\text{Te}$ heterostructures grown by molecular beam epitaxy

K. K. Mahavadi, S. Sivananthan, M. D. Lange, X. Chu, J. Bleuse, and J. P. Faurie  
*Microphysics Laboratory, Department of Physics, University of Illinois at Chicago, Chicago, Illinois 60680*

(Received 15 October 1989; accepted 1 November 1989)

We present the results of stimulated emission experiments performed on a  $\text{Hg}_{0.54}\text{Cd}_{0.46}\text{Te}$  epilayer, a  $\text{CdTe}/\text{Hg}_{0.48}\text{Cd}_{0.52}\text{Te}/\text{CdTe}$  double heterostructure, and a  $\text{CdTe}/\text{Hg}_{0.45}\text{Cd}_{0.55}\text{Te}/\text{Hg}_{0.67}\text{Cd}_{0.33}\text{Te}$  multiquantum well separate confinement heterostructure grown by molecular beam epitaxy. The epilayer and the double heterostructure were found to lase continuously up to 40 K. Pulsed stimulated emission was observed from the multiquantum well separate confinement heterostructure up to 77 K.

## I. INTRODUCTION

There is a considerable technological interest in the development of laser sources in the mid infrared (IR) range (2–5  $\mu\text{m}$ ) for long distance data communications. Mercury-based alloys and heterostructures are one of the potential laser sources in this region. Moreover semiconductor lasers that operate around the 1.6  $\mu\text{m}$  wavelength region are limited by the dominant Auger recombination in the III–V semiconductor material systems of interest. Mercury based II–VI compounds are less affected by the Auger recombination in this wavelength region and hence should be able to compete favorably with the current III–V semiconductor lasers.<sup>1</sup> Though mercury cadmium telluride ( $\text{HgCdTe}$ ) has been a very important semiconducting material in IR detector technology, its potential for the development of IR lasers has not been fully explored. Only a few isolated reports have been published on the mercury (Hg)-based II–VI compound lasers.<sup>2–5</sup> Recently, photoluminescence (PL) has been observed from a  $\text{CdTe}/\text{Hg}_{1-x}\text{Cd}_x\text{Te}$  superlattice placed in a double heterostructure.<sup>6</sup> Previously we too have reported photoluminescence from a  $\text{CdTe}/\text{Hg}_{1-x}\text{Cd}_x\text{Te}/\text{Hg}_{1-x}\text{Cd}_x\text{Te}$  single quantum well separate confinement heterostructure<sup>7</sup> and stimulated emission from a  $\text{Hg}_{1-x}\text{Cd}_x\text{Te}$  epilayer.<sup>8</sup>

We present in this talk the preliminary results of stimulated emission experiments performed on a  $\text{Hg}_{0.54}\text{Cd}_{0.46}\text{Te}$  epilayer, a  $\text{CdTe}/\text{Hg}_{0.48}\text{Cd}_{0.52}\text{Te}/\text{CdTe}$  double heterostructure (DH) and a  $\text{CdTe}/\text{Hg}_{0.45}\text{Cd}_{0.55}\text{Te}/\text{Hg}_{0.67}\text{Cd}_{0.33}\text{Te}$  multiple quantum well separate confinement heterostructure (MQWSCH) grown by molecular beam epitaxy (MBE). Section II outlines the experimental details. The results and conclusions are presented in Secs. III and IV, respectively.

## II. EXPERIMENTS

The epilayer, the DH and the SCH structures were all grown in a RIBER 2300 MBE machine. The substrates were semiinsulating  $\text{CdTe}$  (100). The growth temperature for the buffer/bottom  $\text{CdTe}$  layer in both structures was 250 °C, and 185 °C for subsequent  $\text{HgCdTe}$  overlayers. For the

MQWSCH structure, two  $\text{CdTe}$  effusion cells were used to grow the mercury cadmium telluride layers with different cadmium compositions. For both DH and MQWSCH, the  $\text{CdTe}$  cap layer was grown at a substrate temperature of 250 °C, which was found suitable to grow high quality  $\text{CdTe}$  (100). The individual layer thicknesses were determined from the growth rates of thick calibration layers grown under identical conditions. Details of the growth of Hg-based alloys are given elsewhere.<sup>9</sup>

Low-temperature PL experiments were performed on these structures. A continuous wave (cw) Nd:YAG laser ( $\lambda = 1.06 \mu\text{m}$ ) was used for photoexcitation. Samples were cooled in a Janis variable temperature closed-cycle helium cryostat and were photoexcited from the front surface through the  $\text{CdTe}$  cap layer. The luminescence was analyzed using a 0.75 m grating monochromator and lock-in detection technique. A liquid nitrogen cooled InSb detector was used to detect the luminescence.

To prepare samples for the stimulated emission experiments, the  $\text{CdTe}$  substrates were first mechanically etched to a thickness of 80  $\mu\text{m}$ . Then the films were thinned to a thickness of 5 to 10 microns, by a fast chemical etching in a 2% by volume solution of bromine in methanol followed by a slow etching in a 0.04% by volume solution. Next, the samples were cleaved into small rectangular bars of  $100 \times 500 \mu\text{m}$  to  $1000 \times 1500 \mu\text{m}$  size using a sharp scalpel. Several of these cleaved samples were pressed into indium put on top of a copper block, and covered with a sapphire window for efficient heat sinking.<sup>10</sup> Using a cylindrical lens, the Nd:YAG laser beam was focused to a strip 50  $\mu\text{m}$  wide and of appropriate length to cover the entire width of a selected sample.

## III. RESULTS AND DISCUSSION

### A. $\text{Hg}_{0.54}\text{Cd}_{0.46}\text{Te}$ epilayer

The thickness of the epilayer is 0.6  $\mu\text{m}$ . The initial characterization of this layer showed that the layer is  $n$ -type with a carrier concentration of  $2 \times 10^{16}/\text{cm}^3$  down to 100 K. The minority carrier lifetime was determined by the standard photoconductive decay technique and was found to be 2.4  $\mu\text{s}$  at 100 K. Figure 1 shows the low-temperature photolumi-

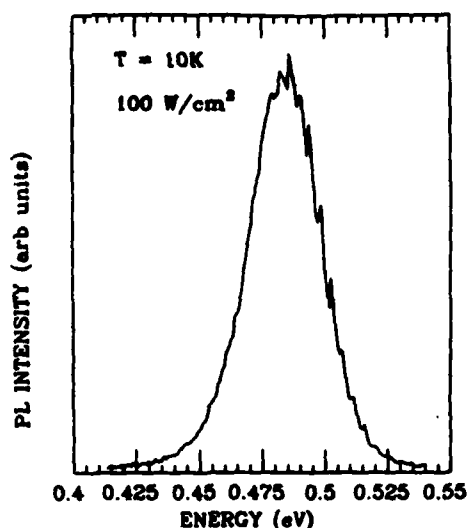


FIG. 1. Low-temperature PL spectrum from a Hg<sub>0.54</sub>Cd<sub>0.46</sub>Te epilayer.

nescence spectrum from the epilayer. The full width at half-maximum of the PL peak is 30 meV. The strong PL also indicates the high quality of this layer.

Figure 2 shows the typical CW stimulated emission spectra from one of the cleaved samples. The spectra were taken with wide slits to facilitate the observation of spontaneous emission below the threshold. At an input optical power density ( $P$ ) of 2.8 kW/cm<sup>2</sup> a slight glitch is emerging at a wavelength of 2.42  $\mu$ m from the broad luminescence background signaling the onset of stimulated emission from this sample. Increasing the input power density clearly increased the intensity of the multimode output at this wavelength. The integrated output intensity from this sample is plotted as a function of input optical power density in Fig. 3. The laser action

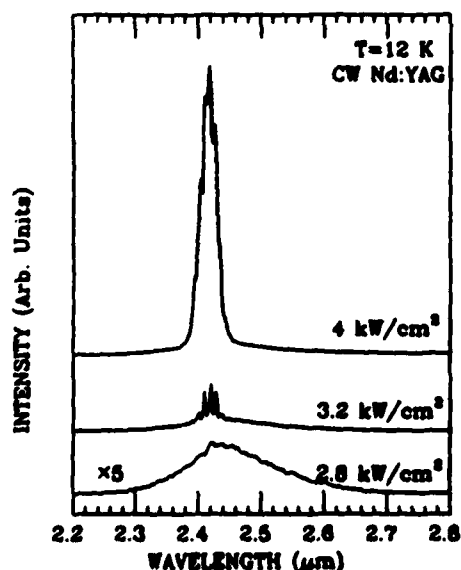


FIG. 2. Continuous wave stimulated emission spectra from a cleaved 500  $\times$  1500  $\mu$ m<sup>2</sup> Hg<sub>0.54</sub>Cd<sub>0.46</sub>Te epilayer under different incident powers.

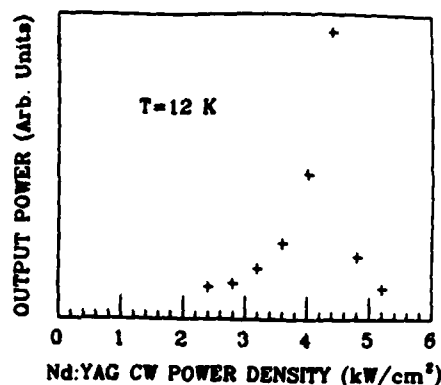


FIG. 3. Integrated output intensity vs incident power density from the same sample.

was observed up to an incident power density of 5.2 kW/cm<sup>2</sup>. However, as shown in Fig. 3, the output intensity started to decrease above 4.4 kW/cm<sup>2</sup>. This obviously is due to the heating of the samples. Though we have observed a few modes in addition to the fundamental mode, we have not tried to extract the refractive index of the layer from the mode spacing for the following reason: The substrate was not rotated during the growth of this layer and as a result we found that there is a bandgap variation of 25 meV/mm along the length of the crystal. This crystal inhomogeneity might have lead to the uneven mode spacing due to the variation of refractive index. The sample was found to lase continuously up to 40 K.

## B. Double heterostructure

A schematic of the double heterostructure is shown in Fig. 4. The bandgap of the Hg<sub>0.48</sub>Cd<sub>0.52</sub>Te corresponds to  $\sim$ 585 meV. Figure 5 shows the low temperature PL spectrum from one of the cleaved DH samples at 15 K. Under low excitation, the PL spectrum from the DH is very broad. This could be due to one or all of the following reasons. The increase in substrate temperature during the growth of the top cadmium telluride layer must have out-diffused<sup>11</sup> mercury from the active layer into this layer creating a graded  $x$ -value layer at this interface. Such a graded layer can give a broad luminescence spectrum. Second, the triangular well due to band bending at the CdTe/Hg<sub>0.48</sub>Cd<sub>0.52</sub>Te interface can also contribute to the width of the luminescence spectrum. Presently

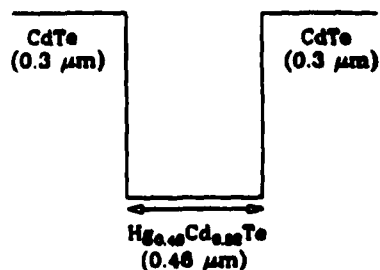


FIG. 4. A schematic of CdTe/Hg<sub>0.48</sub>Cd<sub>0.52</sub>Te double heterostructure.

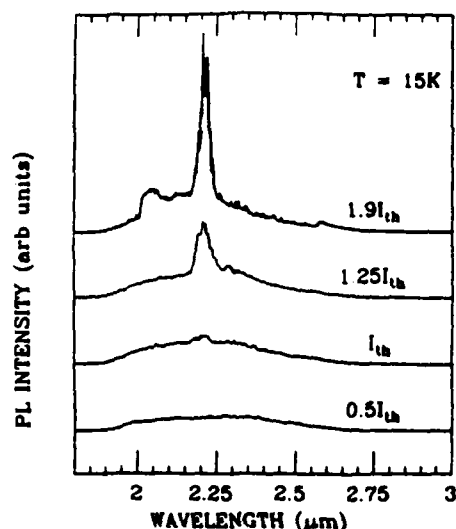


FIG. 5. Low-temperature PL spectra from a cleaved DH under different incident powers.

we are investigating these possibilities to understand the luminescence from this structure.

Above the pump intensity threshold  $I_{th} = 6.4 \text{ kW/cm}^2$ , a peak develops at  $\lambda = 2.2 \mu\text{m}$ , and narrows as the excitation power is increased. We were not able to go higher than  $12 \text{ kW/cm}^2$  because of our Nd:YAG laser power limit. Nevertheless, one can clearly see the building up of stimulated emission. The wide bump around  $\lambda = 2.05 \mu\text{m}$  which appears on the upper spectrum under high pump power is not yet fully understood.

Figure 6 shows the variation of the integrated output intensity with the input power density. Though there is some scatter, the output is a nonlinear function of input power. Figure 7 shows the spectrum taken with narrow slits. Once again, a few additional modes can be seen along with the fundamental mode. The mode spacing is calculated to be  $12.6 \text{ \AA}$  from the known values of cavity length ( $500 \mu\text{m}$ ), lasing wavelength ( $2.2 \mu\text{m}$ ) and refractive index (3.8).

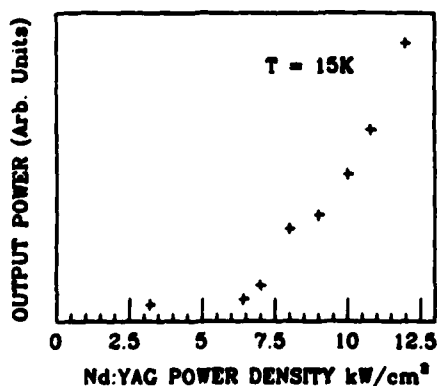


FIG. 6. Integrated output intensity vs incident power from the same DH.

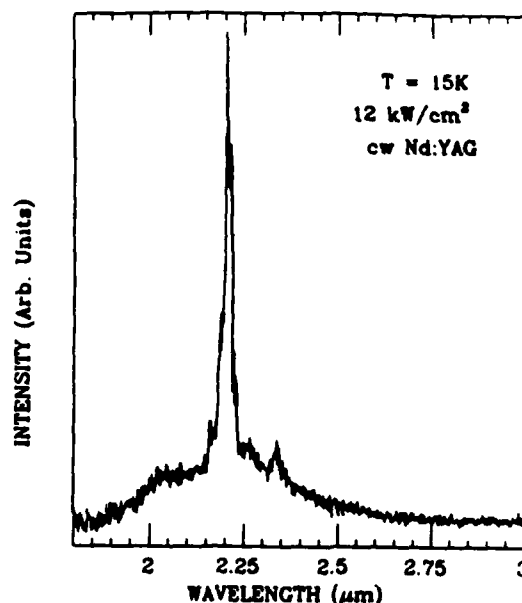


FIG. 7. Stimulated emission spectrum from the same DH taken with narrower slits.

However, these modes are not well resolved due to the relatively wide slit widths used. There are a couple of interesting observations to be made on this structure as compared to the epilayer results. (i) The threshold for the lasing for the DH is about 2.5 times that for the epilayer for the same cavity length. The reason for this might be the presence of a  $3000 \text{ \AA}$  CdTe cap layer. (ii) The DH seems to suffer less from the heating effects as lasing could be observed up to  $12 \text{ kW/cm}^2$ . This might in part be due to the difference in the sample thickness. The DH is found to lase continuously up to  $40 \text{ K}$ . We have tried pulsed excitation neither on the epilayer nor on the DH.

### C. MQW SCH laser

A schematic of the MQW SCH is shown in Fig. 8. The active layer is made of six  $100 \text{ \AA}$  quantum wells of  $\text{Hg}_{0.67}\text{Cd}_{0.33}\text{Te}$  separated by  $70 \text{ \AA}$  barriers of  $\text{Hg}_{0.45}\text{Cd}_{0.55}\text{Te}$ . The composition of the light confinement layer is the same as the barrier layers in the active layer. Details of the structure calculations are given elsewhere.<sup>12</sup>

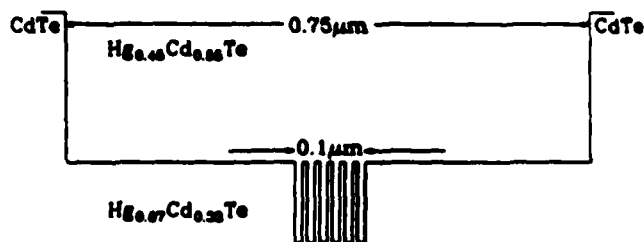


FIG. 8. A schematic of multiquantum well separate confinement heterostructure.

- <sup>1</sup>P. Becla, *J. Vac. Sci. Technol. A* 6, 2725 (1988).
- <sup>2</sup>T. H. Mayers, R. W. Yanka, K. A. Harris, A. R. Reisinger, J. Han, S. Hwang, Z. Yang, N. C. Giles, H. W. Cook, Jr., J. F. Schetzina, R. W. Green, and S. McDevitt, *J. Vac. Sci. Technol. A* 7, 300 (1989).
- <sup>3</sup>K. K. Mahavadi, M. D. Lange, J. P. Faurie, and J. Nagle, *Appl. Phys. Lett.* 54, 2580 (1989).
- <sup>4</sup>K. K. Mahavadi, J. Bleuse, X. Chu, and J. P. Faurie, *Appl. Phys. Lett.* 55, 1285 (1989).
- <sup>5</sup>S. Sivananthan, M. D. Lange, G. Monfroy, and J. P. Faurie, *J. Vac. Sci. Technol. B* 6, 788 (1988).
- <sup>6</sup>N. Holonyak, Jr. and D. R. Scifres, *Rev. Sci. Instrum.* 42, 1885 (1971).
- <sup>7</sup>Y. Kim, A. Ourmazd, M. Bode, and R. D. Feldman, *Phys. Rev. Lett.* 63, 636 (1989).
- <sup>8</sup>K. K. Mahavadi, S. Sivananthan, J. Bleuse, and J. P. Faurie (to be published).
- <sup>9</sup>N. Holonyak, Jr., H. Morkoç, T. J. Drummond, and K. Hess, *Appl. Phys. Lett.* 40, 658 (1982).
- <sup>10</sup>M. A. Tishler, N. G. Anderson, R. M. Colbas, and S. M. Bedair, *Appl. Phys. Lett.* 50, 1266 (1987).
- <sup>11</sup>B. A. Vojak and N. Holonyak, Jr., *Appl. Phys. Lett.* 54, 2518 (1989).

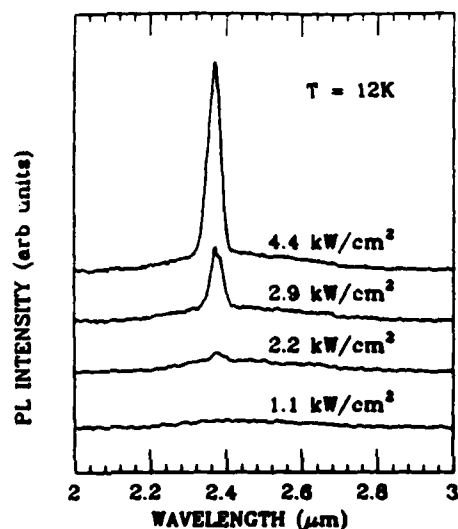


FIG. 9. Pulsed stimulated emission spectra from a cleaved  $1000 \times 1500 \mu\text{m}^2$  MQWSCH.

We used a Q-switched Nd:YAG laser for the stimulated emission experiments on this structure. One of the reasons for this is that this structure was only thinned down to  $20 \mu$  before cleavage, and as a result the heating by cw Nd:YAG laser should play a dominant role. The frequency of the laser was 30 kHz and the pulse width was  $10 \mu\text{s}$ . Figure 9 shows the stimulated emission spectra from a  $1000 \times 1500 \mu\text{m}^2$  cleaved sample. For an input peak power density of  $2.2 \text{ kW}/\text{cm}^2$ , a spike is emerging at a wavelength of  $2.36 \mu\text{m}$  from the broad spectrum. This signals the onset of stimulated emission from this structure. Further increase in the input power preferentially increased the intensity at this wavelength. Figure 10 shows the integrated output intensity as a function of input peak power. Above  $4.6 \text{ kW}/\text{cm}^2$  of incident peak power, the stimulated emission intensity started to decrease and finally no stimulated emission was observed above  $5.5 \text{ kW}/\text{cm}^2$ . This once again is due to the heating of the sample. Finally, Fig. 11 shows the stimulated emission spectrum taken at 77 K from this sample. The range of incident powers for which stimulated emission could be observed was even more

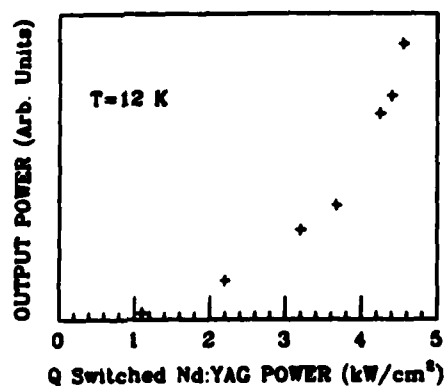


FIG. 10. Integrated output intensity vs input peak power from the same MQWSCH.

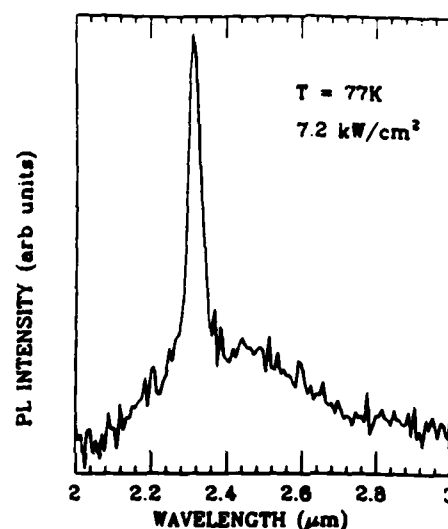


FIG. 11. Pulsed stimulated emission spectrum from the same MQWSCH at 77 K.

limited at 77 K. However, the observation of lasing action at 77 K itself is an important achievement in these mercury based II-VI compound microstructures.

#### IV. CONCLUSIONS

We performed stimulated emission experiments on a  $\text{Hg}_{0.54}\text{Cd}_{0.46}\text{Te}$  epilayer, a  $\text{CdTe}/\text{Hg}_{0.48}\text{Cd}_{0.52}\text{Te}/\text{CdTe}$  double heterostructure, and a  $\text{CdTe}/\text{Hg}_{0.45}\text{Cd}_{0.55}\text{Te}/\text{Hg}_{0.67}\text{Cd}_{0.33}\text{Te}$  multiquantum well separate confinement heterostructure grown by molecular beam epitaxy. The epilayer and the DH were found to lase continuously up to 40 K. Stimulated emission was observed from the MQWSCH under pulsed optical excitation up to 77 K. These preliminary results are highly promising for the development of injection lasers made of Hg-based microstructures. Finally, the threshold for the lasing action in the MQWSCH<sup>13-15</sup> is more than one order of magnitude lower than in optically pumped III-V semiconductor lasers.

#### ACKNOWLEDGMENTS

The authors would like to thank P. S. Wijewarnasuriya and Mario de Souza for performing the Hall and the lifetime measurements on the epilayer. Thanks are also due to S. Farook and Z. Ali for their technical assistance. This work is supported in part by Strategic Defense Initiative Organization/Innovative Science and Technology Office, monitored by Naval Research Laboratory under contract No. N00014-87-C-2043 and in part by Defense Advancement Research Project Agency, monitored by Air Force Scientific Office for Research under contract No. F48620-87-C-0021.

<sup>1</sup>A. Haug, *Semicond. Sci. Technol.* **4**, 803 (1989).

<sup>2</sup>I. Melngailis and A. J. Strauss, *Appl. Phys. Lett.* **8**, 171 (1979).

<sup>3</sup>T. C. Harman, *J. Elec. Mat.* **8**, 191 (1979).

<sup>4</sup>R. S. Putnam, M. M. Salour, and T. C. Harman, *Appl. Phys. Lett.* **43**, 408 (1983).

# Stimulated emission from a CdTe/HgCdTe separate confinement heterostructure grown by molecular beam epitaxy

K. K. Mahavadi, J. Bleuse, S. Sivananthan, and J. P. Faurie

Microphysics Laboratory, Department of Physics, University of Illinois at Chicago, Chicago, Illinois 60680

(Received 12 December 1989; accepted for publication 17 March 1990)

We present the results of low-temperature photoluminescence and stimulated emission experiments performed on a CdTe/Hg<sub>0.45</sub>Cd<sub>0.55</sub>Te/Hg<sub>0.67</sub>Cd<sub>0.33</sub>Te multi-quantum well separate confinement heterostructure grown by molecular beam epitaxy. The photoluminescence results suggest that because of the growth conditions, there is a strong interdiffusion in the multi-quantum well region. Pulsed stimulated emission was observed from this structure up to 77 K.

Mercury based II-VI semiconductor heterostructures are one of the potential laser sources in the near- and mid-infrared (IR) regions (1–5  $\mu\text{m}$ ) for long distance data communications. Moreover, these compounds are less affected by the limiting Auger recombination process in the 1.5  $\mu\text{m}$  wavelength region and hence should be able to compete favorably with the current III-V semiconductor lasers.<sup>1</sup> Although mercury cadmium telluride has been a very important semiconducting material in the IR detector technology, its potential as a material for the development of IR lasers has not been fully explored. Only a few reports have been published on mercury (Hg) based II-VI lasers.<sup>2–5</sup> Photoluminescence<sup>6</sup> (PL) and superradiance<sup>7</sup> have been reported from CdTe/Hg<sub>1–x</sub>Cd<sub>x</sub>Te superlattices placed in a double heterostructure. We have previously reported PL from a CdTe/Hg<sub>1–x</sub>Cd<sub>x</sub>Te/Hg<sub>1–x</sub>Cd<sub>x</sub>Te single quantum well separate confinement heterostructure<sup>8</sup> and stimulated emission (SE) both from a Hg<sub>1–x</sub>Cd<sub>x</sub>Te epilayer and from a CdTe/HgCdTe/CdTe double heterostructure.<sup>9</sup> In this letter, we present the preliminary results of low-temperature PL and SE experiments performed on a CdTe/Hg<sub>0.45</sub>Cd<sub>0.55</sub>Te/Hg<sub>0.67</sub>Cd<sub>0.33</sub>Te multi-quantum well separate confinement heterostructure (MQWSCH) grown by molecular beam epitaxy (MBE).

The MQWSCH was grown in a RIBER 2300 MBE machine. Details of the growth of Hg-based alloys are given elsewhere.<sup>10</sup> Briefly, the laser structure was deposited on a semi-insulating CdTe (100) substrate. The growth temperature for the buffer/bottom CdTe layer was 250 °C, and 185 °C for subsequent HgCdTe overlayers. The CdTe cap layer was grown for 20 min at a substrate temperature of 250 °C, which was found suitable to grow high quality CdTe (100). The individual layer thicknesses were determined from the growth rates of thick calibration layers grown under identical conditions.

The active layer was designed as six 100 Å quantum wells made of Hg<sub>0.67</sub>Cd<sub>0.33</sub>Te separated by 70 Å barriers made of Hg<sub>0.45</sub>Cd<sub>0.55</sub>Te. The carriers are confined in quantum wells formed by the Hg<sub>0.67</sub>Cd<sub>0.33</sub>Te layers. The thickness of the light confinement layer, made of Hg<sub>0.45</sub>Cd<sub>0.55</sub>Te, was chosen to be 7500 Å, in order to optimize the optical confinement factor for our design.

The quantum well energy levels were calculated in the envelope function approximation<sup>11</sup> using a transfer matrix

approach, with bulk electron and light hole dispersion relationships given by Kane's three-band model.<sup>12</sup> Bulk heavy hole dispersion relationships were assumed to be parabolic with a 0.3 $m_0$  effective mass for all  $x$  values. Parameters were the band gaps of the layers, determined using the expression given by Hansen *et al.*<sup>13</sup> and the Kane energies.<sup>14</sup> We used 350 meV for the valence-band offset between HgTe and CdTe,<sup>15</sup> and a linear interpolation for the valence-band offset between layers of different compositions.

The optical properties of this structure were initially investigated using low-temperature PL experiments. The experimental setup employed in these experiments is described elsewhere.<sup>8</sup> As seen in Fig. 1, the PL spectrum presents a main peak whose edge is at 440 meV and maximum at 478 meV, and a shoulder whose onset is at 500 meV. These features cannot be explained if the structure is exactly as designed (see above) because calculations give 355 meV for the energy of the fundamental interband transition between the first electron ( $E1$ ) and heavy hole (HH1) minibands, and 381 meV for a similar transition involving the light holes (LH1). Our calculations show that the energies of the transitions between the second minibands ( $E2$ -HH2) should be around 519 meV. The discrepancy between the experimental spectrum and our calculations could be explained either by well width inaccuracies or by interdiffusion of mercury in the multi-quantum well region. The former possibility is unlikely, since a well width of 200 Å would be required, and the growth rate control does not permit such a large error. Moreover, since the growth temperature was increased from 185 to 250 °C prior to deposition of the CdTe cap layer, interdiffusion is likely to have occurred in the multi-quantum well region. We thus simulated interdiffusion in the active layer and made a rough estimate of energy levels of the resulting potential profile. For a diffusion length of 45 Å the active layer is no longer a multi-quantum well, but rather a 1000-Å-wide well whose  $x$  value is around 42%. However, we cannot be certain of either the  $x$  value or the potential profile of the resulting structure due to the uncertainties in the thicknesses and the compositions of the original structure. According to these estimates, the main peak of the PL spectrum corresponds to transitions from the  $E1$  miniband and the high-energy shoulder corresponds to transitions

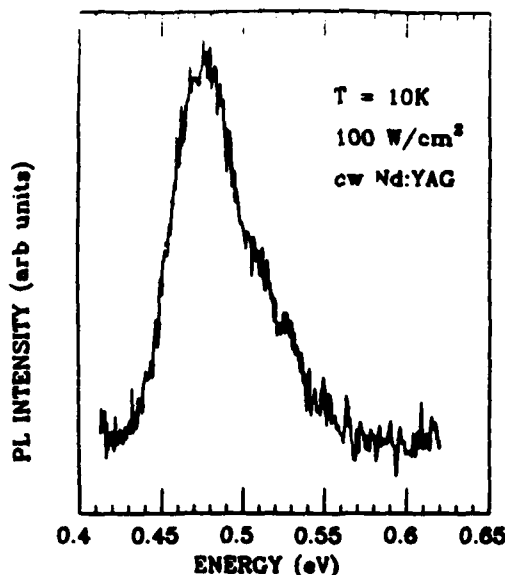


FIG. 1. Low-temperature photoluminescence spectrum from the MQWSCH taken at 10 K using a cw Nd:YAG laser.

from the bottom of the partially filled  $E2$  miniband. However, the Hall measurements give an electron concentration of only around  $10^{16}/\text{cm}^3$ , which is less than that required to fill the lowest conduction subband ( $8 \times 10^{16}/\text{cm}^3$ ). However, the inhomogeneous broadening due to the composition fluctuations in the wells can broaden the spectrum giving rise to the high-energy shoulder of the spectrum. Therefore, the high-energy shoulder might just be due to the  $E1$ - $LH1$  transition.

Sample preparation for the SE experiments is given elsewhere.<sup>9</sup> We used a Q-switched Nd:YAG laser as the excitation source. The frequency of the laser and the pulse width were 30 kHz and 10  $\mu\text{s}$ , respectively. Using a cylindrical lens, the Nd:YAG laser beam was focused to a stripe 50  $\mu\text{m}$  wide and long enough to cover the entire width of a selected sample.

Figure 2 shows the SE spectrum from a  $1000 \times 1500 \mu\text{m}^2$  cleaved sample. These spectra were taken with wide slits to facilitate the detection of the spontaneous emission below threshold. For an input peak power density of 2.2  $\text{kW}/\text{cm}^2$ , a spike is emerging from the broad spectrum at a wavelength of 2.36  $\mu\text{m}$ . This signals the onset of SE from this structure. Further increase in the input power preferentially increased the intensity at this wavelength. The integrated output intensity as a function of input peak power is shown in Fig. 3. Above 4.6  $\text{kW}/\text{cm}^2$  of incident peak power, the SE intensity started to decrease and finally no SE was observed above 5.5  $\text{kW}/\text{cm}^2$ . In our geometry, the SE was occurring from filaments  $\sim 50 \mu\text{m}$  wide and 1000  $\mu\text{m}$  long. The lasing threshold varied between 1.5 and 3  $\text{kW}/\text{cm}^2$  from sample to sample. This variation in the threshold could be due to uncertainties in the incident laser beam profile, the irradiated area, and the detection efficiency. A similar variation of the input power at which the lasing action ceased was also noted among different sam-

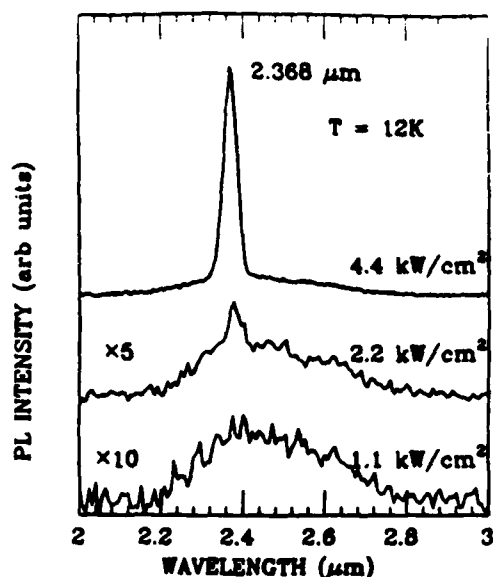


FIG. 2. Pulsed stimulated emission spectra from a cleaved  $1000 \times 1500 \mu\text{m}^2$  MQWSCH at 12 K using a Q-switched Nd:YAG laser. The threshold input power is 2.2  $\text{kW}/\text{cm}^2$ .

ples. We made no attempt to separate the various modes in the spectrum by reducing the slit widths.

A point to be noted from Figs. 1 and 2 is that the lasing wavelength is 2.36  $\mu\text{m}$  (525 meV), whereas the peak of the low-temperature PL is at 2.6  $\mu\text{m}$  (478 meV). This difference in peak position suggests either that the actual temperature of the structure is higher than the cryostat temperature or that the lasing is occurring on the high-energy shoulder of the PL spectrum. We believe that the former possibility is unlikely because sample heating should shift the luminescence spectrum to higher energies since the band gap of the  $\text{Hg}_{1-x}\text{Cd}_x\text{Te}$  ( $x < 0.5$ ) increases with increasing temperature, and we have not noticed any such change in either the linewidth or the spectral position up to the highest incident Nd:YAG powers used in the experiments. However, we did observe a faster growth of the

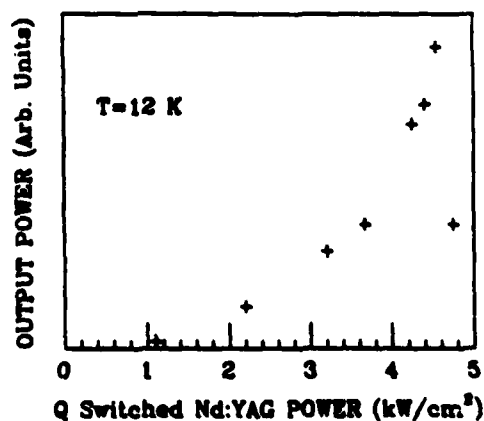


FIG. 3. Integrated output power vs input peak power from the MQWSCH of Fig. 2.

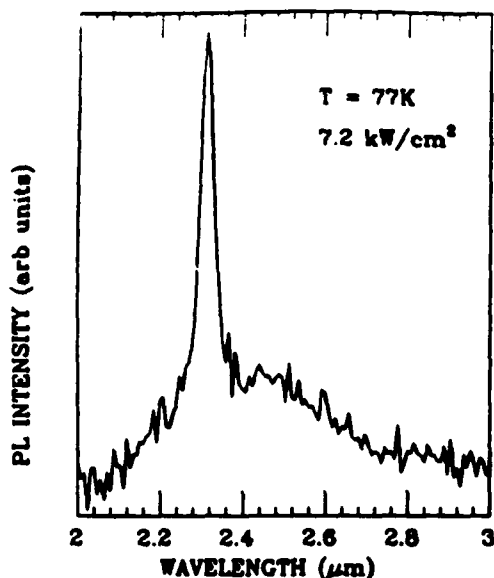


FIG. 4. Pulsed stimulated emission spectrum from the MQWSCH of Fig. 2 at 77 K.

high-energy structure with increasing incident power. This suggests that the laser action is occurring on the high-energy transition.

Finally, Fig. 4 shows the SE spectrum taken at 77 K. The range of incident powers for which SE could be observed was even more limited. However, the observation of SE at 77 K itself is an important achievement in these mercury-based II-VI compound microstructures. The lasing wavelength shifted to a shorter wavelength of  $2.32 \mu\text{m}$  at 77 K. This shift with temperature increase is in agreement with the expected shift of energy levels in the diffused multiquantum well structure. Further work is under way to improve the efficiency and the threshold of these optically pumped laser structures and to design suitable diode lasers.

In conclusion, we have performed low-temperature photoluminescence and stimulated emission experiments on a  $\text{CdTe}/\text{Hg}_{0.45}\text{Cd}_{0.55}\text{Te}/\text{Hg}_{0.67}\text{Cd}_{0.33}\text{Te}$  multiquantum well separate confinement heterostructure grown by molecular beam epitaxy. The actual active layer is likely to be a  $1000\text{-\AA}$ -wide quantum well because of interdiffusion in the multiquantum well region. As a consequence, any anneal-

ing at temperatures higher than  $200^\circ\text{C}$  is forbidden on such structures. This stresses the need for good *in situ* doping of HgCdTe compounds. Stimulated emission was observed from the MQWSCH under pulsed optical excitation up to 77 K. Finally, the threshold for the lasing action in the MQWSCH is one order of magnitude lower than optically pumped GaAlAs semiconductor lasers<sup>16</sup> operating at  $\sim 0.9 \mu\text{m}$  and about a factor of 3 lower than the AlGaSb/InAsSb lasers operating at  $3.9 \mu\text{m}$ .<sup>17</sup> Although we cannot make a direct comparison of threshold powers due to the different wavelengths of operation of these laser, this difference is an indication of the expected trend in Hg-based II-VI compound lasers.<sup>1</sup>

This work is supported in part by the Strategic Defense Initiative Organization/Innovative Science and Technology Office, monitored by the Naval Research Laboratory under contract No. N00014-87-C-2043, and in part by the Defense Advancement Research Project Agency, monitored by the Air Force Scientific Office for Research under contract No. F48620-87-C-0021.

<sup>1</sup> A. H. H. Semicond. Sci. Technol. 4, 803 (1989).

<sup>2</sup> I. Melngailis and A. J. Strauss, Appl. Phys. Lett. 8, 171 (1979).

<sup>3</sup> T. C. Harman, J. Electron. Mater. 8, 191 (1979).

<sup>4</sup> R. S. Putnam, M. M. Salour, and T. C. Harman, Appl. Phys. Lett. 43, 408 (1983).

<sup>5</sup> P. Becla, J. Vac. Sci. Technol. A 6, 2725 (1988).

<sup>6</sup> T. H. Mayers, R. W. Yanka, K. A. Harris, A. R. Reisinger, J. W. Han, S. Hwang, Z. Yang, N. C. Giles, J. W. Cook, Jr., J. F. Schetzina, R. W. Green, and S. McDevitt, J. Vac. Sci. Technol. A 7, 300 (1989).

<sup>7</sup> N. C. Giles, J. W. Han, J. W. Cook, Jr., and J. F. Schetzina, Appl. Phys. Lett. 55, 2026 (1989).

<sup>8</sup> K. K. Mahavadi, M. D. Lange, J. P. Faurie, and N. Nagle, Appl. Phys. Lett. 54, 2580 (1989).

<sup>9</sup> K. K. Mahavadi, J. Bleuse, X. Chu, and J. P. Faurie, Appl. Phys. Lett. 55, 1285 (1989); K. K. Mahavadi, S. Sivananthan, M. D. Lange, X. Chu, J. Bleuse, and J. P. Faurie, J. Vac. Sci. Technol. A 8, 1210 (1990).

<sup>10</sup> S. Sivananthan, M. D. Lange, G. Monfroy, and J. P. Faurie, J. Vac. Sci. Technol. B 6, 788 (1988).

<sup>11</sup> G. Bastard, Phys. Rev. B 24, 5693 (1981).

<sup>12</sup> E. O. Kane, J. Phys. Chem. Solids 1, 249 (1957).

<sup>13</sup> G. L. Hansen, J. L. Schmit, and T. N. Casselman, J. Appl. Phys. 53, 7099 (1982).

<sup>14</sup> S. E. Schacham and E. Finkman, J. Appl. Phys. 57, 2001 (1985).

<sup>15</sup> J. M. Berroir, Y. Guldner, J. P. Viere, M. Voca, X. Chu, and J. P. Faurie, Phys. Rev. Lett. 62, 2024 (1989), and references therein.

<sup>16</sup> N. Holonyak, Jr., R. M. Kolbas, R. D. Dupuis, and P. D. Dapkus, IEEE J. Quantum Electron. QE-16, 170 (1980).

<sup>17</sup> J. P. Van der Ziel, T. H. Chiu, and W. T. Tsang, Appl. Phys. Lett. 48, 315 (1986).

## **VIII ADVANCE MOLECULAR BEAM EPITAXY (MBE) PROTOTYPE FOR Hg BASED II-VI SEMICONDUCTING ALLOYS AND HETEROSTRUCTURES**

In July 1989 a new MBE machine called OPUS 45 was installed in the Micro-physics Laboratory. This machine was designed by the P.I. (Dr. J.P. Faurie) to be a prototype for an advanced production MBE system dedicated to the growth of mercury based II-VI compounds and has been built by ISA-RIBER.

OPUS 45 is a three ultra high vacuum chamber machine namely with a growth chamber, a preparation chamber, and a loading/unloading chamber. Up to three 2-inch or up to one 5-inch silicon wafer (platen-free) can be transferred and processed in a horizontal face-down position during all steps. This mode of transfer offers the opportunity to avoid particulate contamination as much as possible. It is achieved by a full motorized system that can move horizontally and vertically. The combination of these two motions allows to pick up a platen in the loading chamber and to bring it underneath the degassing station in the preparation chamber. Another identical system transports the platen from this position to the growth manipulator. Stepper motors have been chosen to operate the displacements and several optical fibers are used as interlocks to insure a precise control of the platen and cassette positions as well as manipulator position. Accuracy of  $\pm 0.5\text{mm}$  is currently obtained on each displacement. Gate valve and pressure sensors are also used for safety reasons.

Ten 5" molybdenum platens can be loaded at once in the introduction chamber and then transferred separately into the preparation chamber. This chamber is equipped with a cryopanel and a large oven identical to the growth manipulator oven heating samples up to  $800^{\circ}\text{C}$ .

The choice of a vertical configuration has been made for the growth chamber with great care addressed to the problem of contamination like cross-talking and flakes falling down into these cells and more specifically to the problem of mercury recuperation which has been one of the main concerns during the design of this machine.

Two cryopumps (CT8) with their own mercury recuperation system are connected together to the main growth chamber and are separated by their own gate valve (VTA 200). This configuration allows to outgass one cryopump while the other. In the growth chamber itself cryopanels (main and bottom) are designed to allow mercury to run down directly to the extreme bottom of the chamber where a mercury recuperation system has been also provided. In order to maintain an

ultrahigh vacuum environment and to keep the residual contaminants at a very low level, a permanent baking system has been designed for all the chambers. The pressure limit obtained in the system is  $5.10^{-11}$  Torr with liquid nitrogen in the cryopanel. In the same condition, the pressure limit is  $5.10^{-10}$  Torr when seven cells are heated at temperatures ranging from 150° to 800°C and the manipulator oven is at 600°C.

In the growth chamber, the cell implantation is defined as the following: the mercury cell occupies a central position and it is kept as close as possible to the wafers in order to lower the materials consumption. It is surrounded by its own conic cryopanel. All the 8 other cell ports face the wafers at the same angle and are regularly distributed around the vessel. The cell ports are wide enough to accommodate large capacity cell (100CC) and its individual cryopanel.

These cells have a specific design with a two heating filament stage which is very useful for tellurium compounds such as CdTe and ZnTe. In this case, the upper filament is only heated and regulated. For the other materials, both filaments are used and the current regulation is made on the bottom one. Temperature stabilities of the order of  $\pm 0.5^{\circ}\text{C}$  have been obtained respectively at 360°C (Te cell) and 550°C (CdTe cell) for more than three hours. The mercury cell has been designed to provide a constant Hg level and a small thermal time constant allowing rapid flux change. The cell is connected to a large reservoir. A sensor located in the effusion cell allows to adjust the level of mercury by means of the reservoir motion. Excellent flux stability has been obtained with this cell during a ten hour growth. Temperature stability is  $\pm 0.2^{\circ}$  at 150°C.

Great effort has been made on the design of the heating stage in order to achieve high temperature stability and uniformity. This parameter is one of the most important requirements for the growth of mercury based II-VI compounds. Recorded data on the temperature stability show  $\pm 0.5^{\circ}\text{C}$  at 300°C and 700°C. Temperature stability recorded at 600°C over a two-inch centered wafer is  $\pm 2.5^{\circ}\text{C}$  and  $\pm 4.0^{\circ}\text{C}$  over a three-inch wafer.

Finally, based on the latest computers and a digital PID controller designed for production, a process control uses a sophisticated software to simplify the operator work and improve the control accuracy. This machine therefore particularly adapted for the growth of HgCdTe on alternate substrates such as GaAs and Si for which the use of gallium is not suitable because of high temperature requirement for cleaning.

## **IX RESEARCH EFFORT ON A HIGH YIELD MULTIWAFFER MBE PROTOTYPE OF Hg BASED II-VI SEMICONDUCTING ALLOYS AND HETEROSTRUCTURES**

This second add-on on the current contract which has been accepted by DARPA has never been awarded to the Microphysics Laboratory. Nevertheless, preliminary experiments have been carried out on OPUS 45. First of all, this machine has been installed and the acceptance tests performed in August 1989. From September 1, 1989 through November 13, 1989 the first CdTe layers were grown on 2-inch GaAs and Si substrates.

### **CdTe/GaAs(100)**

Compared to what is obtained in the conventional MBE machine CdTe layers grown on GaAs appear to be more uniform and of much better quality. On a 0° off GaAs(100) substrate a 6 $\mu$ m thick CdTe film exhibiting a FWHM of 130 arc second has been grown compared to an average FWHM value of 220 arc second for CdTe films grown on GaAs(100) substrates in the conventional MBE machine.

Twin-free layers have been obtained on a slightly misoriented GaAs(100) substrates with an excellent surface morphology over the whole area as illustrated in Fig. 1. These layers yield strong PL spectra (Fig. 2) with a FWHM of the acceptor bound exciton peak at 1.59eV of only 0.7meV at 10K which confirms the high structural quality of these layers.

### **CdTe/Si(100)**

A FWHM of 800 arc sec has been obtained for a 6 $\mu$ m thick CdTe layer grown on Si(100). This compares very favorably to the typical results of about 1200 arc sec which were obtained in the RIBER 2300 machine several months ago. In addition the layers are very shiny and mirror-like over the whole surface.

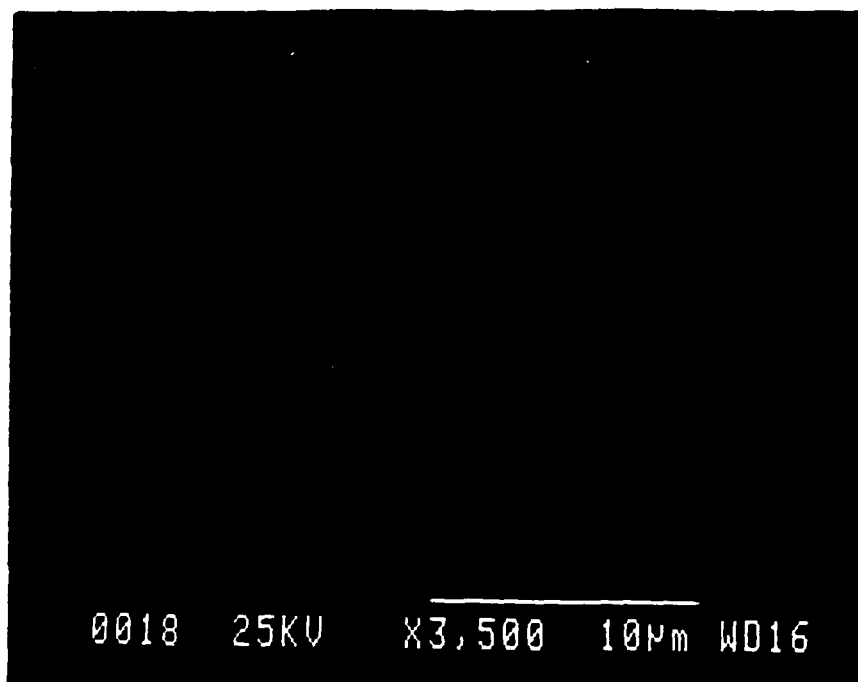
### **Thickness Uniformities**

Thickness uniformities measured in OPUS 45 are very impressive since a standard deviation of the layer thickness of only 0.24% has been measured on a 6 $\mu$ m thick CdTe film grown on a 2-inch GaAs(100). In the 2300 machine the best result was

0.6% for the same diameter.

FIGURE CAPTIONS:

- Fig. 1      10K photoluminescence spectrum of CdTe on GaAs(100) tilted  $2^\circ$  towards  $\langle 110 \rangle$ , excited with a 50mW Ar-Laser at  $514.5\mu\text{m}$  wavelength.
- Fig. 2      Scanning electron microscope image of the surface of two CdTe layers grown on Si (a)  $9204\text{m}$  thick CdTe on Si(100); (b)  $4\mu\text{m}$  thick CdTe on Si(100) tilted  $8^\circ$  towards  $\langle 110 \rangle$ .



Scanning electron micrograph of a 4.3µm thick layer of CdTe on GaAs(100) 2° off towards  $\langle 110 \rangle$ .

Photoluminescence spectrum for CdTe  
on GaAs(100) 2deg. off towards  $\langle 110 \rangle$ .  $T = 10\text{K}$

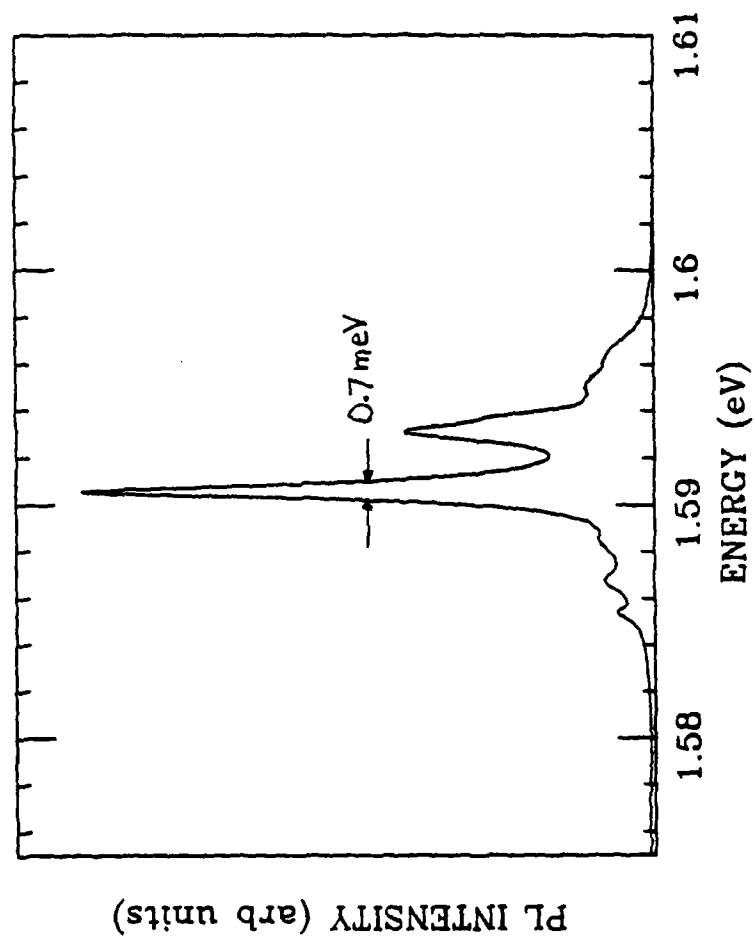


Fig. 2

## CONCLUSION

It is clear from this report that not only we have reached our goals but also that our achievements have gone beyond the scope of the contract program. The direct growth of CdTe and HgCdTe on Si(100) which was not planned is certainly a very important breakthrough in view of a monolithic approach of HgCdTe FPAs.

Stimulated emission observed in the 2-5 $\mu$ m wavelength range for Hg-based heterostructures is certainly also a very promising achievement since the threshold for the lasing action is much lower than in equivalent III-V compound laser structure.

The improvement of HgCdTe epilayers was certainly the driving force of this program. The formation of twins, particularly active, in the  $\langle 111 \rangle$  direction has been a major concern to the Microphysics Laboratory. Therefore we are very happy to have been able to identify the twinning to understand the complex twinning mechanisms and finally prevent the twin formation. It has been very hard to achieve it but the payoff is high since at the end of the contract the state-of-the-art in the laboratory is excellent as it can be seen from the results obtained for (211)B orientation.

Another source of satisfaction has been provided by our success in making photodiodes using the low energy ion technique developed in the Microphysics Laboratory. Not only the technique is inexpensive, fast and reliable giving the laboratory an excellent characterization tool, but in addition it might provide a technique to manufacture IR photodiodes.

At last the preliminary results obtained on OPUS 45 are extremely promising. However, there is one subject of disappointment. It concerns the p-type doping of HgCdTe. It is fair to say that neither in the MPLab nor elsewhere has a clean and elegant solution respecting a low temperature process, key parameter in MBE been yet found. Our scientific activity has been materialized by 59 papers published in refereed journals, 13 invited conferences and 62 contributed papers mostly presented at international meetings. The list is given in the annex.

## SUMMARY

1. Rotation twins are easily formed in CdTe(111) and HgCdTe(111) epilayers. In addition, reflection twins which are related to a change in the Hg pressure and/or the surface substrate temperature can be formed during the growth of HgCdTe.

A careful substrate preparation with a proper thermal cleaning can prevent the formation of double positioning twins. To avoid the formation of reflection twins a stringent control in the stability of Hg ( $\pm 2.5\%$ ), Te and CdTe fluxes, growth rate and surface substrate temperature ( $\pm 0.5\%$ ) is required, which is very difficult when the substrate is rotating. Such a control has been achieved in the Microphysics Laboratory and twin-free CdTe and HgCdTe(111)B layers have been grown.

A comparison between HgCdTe twinned layers and twin-free layers shows that electrically active acceptors along with high hole mobility are associated with the presence of reflection twins in HgCdTe. Etch pit density as low as  $8 \times 10^4 \text{ cm}^{-2}$  has been counted on twin-free HgCdTe layers which are two orders of magnitude lower than EPD's of twinned layers. From annealing experiments it has been found that a residual donor doping level of  $5 \times 10^{15} - 2 \times 10^{16} \text{ cm}^{-3}$  has been measured in both twinned and twin-free HgCdTe epilayers. It is currently, though, that this residual doping is due to antisite Te atoms.

The MBE growth of twin-free HgCdTe(111)B layers while the substrate is rotating represents a major accomplishment in the field. The progress achieved in the growth in the (111)B orientation has been used to control in better way the growth in different orientations. Layers grown in the (211)B orientation under the stringent growth control required for twin-free growth in (111)B exhibit outstanding properties.

2. The growth of high quality epitaxial layers of  $\text{Hg}_{1-x}\text{Cd}_x\text{Te}$  is limited by the substrate quality. CdTe and CdZnTe are the most widely used substrates for epitaxial growth of the  $\text{Hg}_{1-x}\text{Cd}_x\text{Te}$ . Unfortunately, it is difficult to produce good single crystals of these materials on a large area and these substrates are very expensive. GaAs and Silicon are attractive candidates as alternate substrates for  $\text{Hg}_{1-x}\text{Cd}_x\text{Te}$ . The Microphysics Laboratory has been the first to report in 1984 on the successful growth of  $\text{Hg}_{1-x}\text{Cd}_x\text{Te}$  on GaAs. Since then it has recently been demonstrated that it is possible to grow  $\text{Hg}_{1-x}\text{Cd}_x\text{Te}$  with excellent uniformity on a full 2-inch GaAs wafer. With a thickness uniformity  $\Delta t/t = 0.6\%$  and a

composition uniformity  $\Delta x/x = 0.7\%$  this is the best result ever reported by any growth technique. More recently it has been demonstrated that twin-free CdTe (111)B layers can be grown when using a misoriented substrate ( $2^\circ$  off). FWHM of 60 arcsecond has been obtained which is excellent compared to the 40 arcsecond exhibited by commercially available CdTe substrates. On a  $0^\circ$  off (100)GaAs the average FWHM is above 200 arcsecond.

Silicon is an even more attractive alternate substrate than GaAs because it is (i) available in larger area (ii) it is less expensive (iii) and above all it could eventually become possible to fabricate large area monolithic IR focal plane arrays taking advantage of the well-developed Si-integrated circuit technology. However, one severe problem with this heteroepitaxy is the very large (19%) lattice mismatch between CdTe and Si. We have successfully grown CdTe(111)B, CdTe(100) and HgCdTe(111)B on Si(100) which to the best of our knowledge has never been reported before. This result represents a major breakthrough in the field because it opens the door for the highly coveted monolithic FPA's technology.

3. One of the major achievements of the laboratory is related to understanding the role of the crystallographic orientation on the MBE growth process. In a first step we have observed that the sticking coefficient for Hg changes dramatically with the crystallographic orientation since a (111)A face requires almost 10 times more mercury than a (111)B face when the growth occurs at  $190^\circ\text{C}$ . We have found that such a difference has an influence on both the intrinsic and the extrinsic doping of the material.

Experiments carried out recently on the incorporation of indium during the growth of HgCdTe have shown that whereas in the (111)B orientation indium is incorporated in the metal site in the (100) orientation it appears that it is mostly incorporated interstitially.

4. The MPLab has devoted a great deal of time to understand and to control the intrinsic doping. Even though all the complex relationships between growth parameters and intrinsic doping are not fully understood, appreciable progress has been made. It is currently believed that the residual donor doping level found in MBE layers is due to the tellurium in antisite. This very important information has been proposed for the first time by the MPLab.

5. Impurities mostly substitute the metal site because HgCdTe MBE growth occurs under tellurium-rich conditions therefore Hg vacancies are easily formed. Indium which is a Group III element has been found to be an excellent donor whereas Li which is a Group I element has been found to be an acceptor but of no practical use because of its very high diffusion coefficient.

As and Sb were found to act as n-type dopants exhibiting a high self-compensation in HgCdTe grown by MBE. Photo-assistance during the growth using a Nd-YAG green laser pulsed at 10Khz did not change the electrical type of As doped HgCdTe. From these experiments and the results reported by other groups it is fair to conclude that no elegant solution has been found yet regarding the extrinsic p-type of MCT.

6. We have investigated the effect of low energy ions on HgCdTe and found that n-p junction is formed when a p-type material is bombarded. This approach which has been entirely developed in the Microphysics Laboratory is currently used to fabricate photodiodes on HgCdTe grown by MBE in the laboratory. We have found that this method is not only inexpensive but also fast and reliable. Photodiodes fabricated on the same HgCdTe epilayer either by ion implantation or by low energy ion shows the same performances between 300K and 77K. Stable photodiodes exhibiting excellent performances have been already fabricated.

7. The value of band discontinuities in HgTe-CdTe and related heterojunctions such as  $\text{Hg}_{1-x}\text{Cd}_x\text{Te}-\text{Hg}_{1-y}\text{Cd}_y\text{Te}$  has been the object of extensive research and discrepancies have been observed between magneto-optics and photoemission results. Valence band discontinuity value is of extreme importance in the bandgap engineering of electronic heterostructure devices. To explain these discrepancies it has been suggested that the band discontinuity can be temperature dependent. We have studied this temperature dependence by XPS and UPS and we have found that the valence band discontinuity  $\Delta E$  measured equal to 0.35 eV at 300K changes by only a few millivolts between 300K and 50K. Recently, Johnson et al<sup>(1)</sup> have shown that a HgTe-CdTe Type III superlattice while becoming semimetallic with increasing  $\Delta E_v$  reverts to semiconducting behavior as the offset is increased yet further. By coincidence, observed electron-cyclotron mass and bandgap can be either explained with  $\Delta E_v = 40 \text{ meV}$  or 350 meV. Cyclotron resonance experiments performed on a novel superlattice HgZnTe-CdTe have shown that calculations

using a small valence band offset can account for the in-plane cyclotron resonance, but not for the data obtained in tilted magnetic field.(2) Therefore, magneto-optics and photoluminescence are now consistent with a large valence band offset  $\Delta E_v$  of 0.35 eV.

It should be pointed out that regarding this very important issue the Microphysics Laboratory has played a major role since 1983 when the question was addressed for the first time.

8. We have investigated  $\text{Hg}_{1-x}\text{Cd}_x\text{Te}$  single layers,  $\text{Hg}_{1-x}\text{Cd}_x\text{Te}/\text{CdTe}$  double heterostructures (DH) and separate confinement heterostructures (MQWSCH) grown by MBE. All these structures have shown intense photoluminescence as well as stimulated emission. The epilayer and the DH were found to lase continuously up to 40K. Stimulated emission was observed from the MQWSCH under pulsed optical excitation up to 77K. In comparison with the optically pumped III-V semiconductor lasers, the threshold input optical power for the lasing action is lower in this structure.

9. In July 1989 a new MBE machine which is a mass-production MBE prototype was installed in the Microphysics Laboratory. This MBE machine exhibits new and important features such as the capability of handling a 5-inch diameter substrate or any other combination (3x2-inch, 11x1-inch), improved substrate temperature uniformity, improved Hg recovery facility and new cell assembly geometry.

This machine has been installed and the acceptance test performed. The first CdTe layers have been grown on 2-inch GaAs and Si substrates. Compared to what is obtained in the conventional MBE machine CdTe layers grown on GaAs appear to be more uniform and of much better crystal quality of 30-40%. A standard deviation of a layer thickness of only 0.24% has been measured for a 6 $\mu\text{m}$  CdTe epilayer grown on a 2-inch GaAs(100) substrate. This excellent result attests that OPUS 45 is a suitable MBE machine to grow uniform films on large area substrate.

#### REFERENCES:

1. N.F. Johnson, P.M. Hui and H. Ehrenreich, Phys. Rev. Lett. 61, 1993 (1988)
2. J.M. Berroir, Y. Guldner, J.P. Vieren, M. Voos, S. Chu and J.P. Faurie, Phys. Rev. Lett. 62, 2025 (1989)

# SCIENTIFIC ACTIVITY

## PUBLICATIONS:

1. Minority lifetime in p-type  $\text{Hg}_{1-x}\text{Cd}_x\text{Te}$  made by molecular beam epitaxy, M.E. DeSouza, M. Boukerche, and J.P. Faurie, J. Appl. Phys. (in press)
2. New development on the control of homoepitaxial and heteroepitaxial growth of CdTe and HgCdTe by MBE, J.P. Faurie, R. Sporken, S. Sivananthan, and M.D. Lange, J. Cryst. Growth (in press)
3. Evidence for semimetallic character in  $\text{Hg}_{1-x}\text{Zn}_x\text{Te}$  superlattices, J.M. Berroir, Y. Guldner, J. Manasses, J.P. Vieren, M.Voos, X. Chu and J.P. Faurie, Surface Science (in press)
4. Electron cyclotron resonance in type III HgZnTe-CdTe superlattices, M. Voos, J.M. Berroir, Y. Guldner, J.P. Vieren, X. Chu and J.P. Faurie, Surface Science 228, 37 (1990)
5. Stimulated emission from a CdTe/HgCdTe separate confinement heterostructure grown by molecular beam epitaxy, K.K. Mahavadi, J. Bleuse, S. Sivananthan and J.P. Faurie, Appl. Phys. Lett. 56 (21) 21 (1990)
6. Deep level photoluminescence spectroscopy of CdTe epitaxial layer surfaces, J.L. Shaw, L.J. Brillson, S. Sivananthan and J.P. Faurie, Appl. Phys. Lett. 56, 1267 (1990)
7. Subband structure of strained-layer CdTe/ZnTe superlattices: A reexamination, H. Mathieu, A. Chatt, J. Allegre and J.P. Faurie, Phys. Rev. B 41 9 6082 (1990)
8. The spreading resistance technique applied to MCT heterojunctions, M. Boukerche and J.P. Faurie, J. Vac. Sci. Technol. A 8 (2) 1233 (1990)
9. Stimulated emission from  $\text{Hg}_{1-x}\text{Cd}_x\text{Te}$  epilayers and CdTe/ $\text{Hg}_{1-x}\text{Cd}_x\text{Te}$  double heterostructures grown by MBE, K.K. Mahavadi, J. Bleuse, X. Chu, M.D. Lange, S. Sivananthan and J.P. Faurie, J. Vac. Sci. Technol. A8 (2) 1210 (1990)
10. High quality p-type HgCdTe grown by molecular beam epitaxy, P.S. Wijewarasuriya, M. Boukerche and J.P. Faurie, J. Appl. Phys. 67 (2) 859 (1990)
11. Structural properties of HgZnTe/CdTe strained layer superlattices grown by molecular beam epitaxy, J. Petruzello, D. Olego and J.P. Faurie, Appl. Phys. Lett. (?)
12. Electronic structure of cadmium telluride-zinc telluride strained-layer superlattices under pressure, B. Gil, D.J. Dunstan, J. Calatayud, H. Mathieu and J.P. Faurie, Phys. Rev. B. 40, 5522 (1989)

13. Molecular beam epitaxial growth of CdTe and HgCdTe on Si(100), R. Sporken, S. Sivananthan, K.K. Mahavadi, G. Monfroy, M. Boukerche, and J.P. Faurie, *Appl. Phys. Lett.* 55, 1879 (1989)
14. Stimulated emission from  $\text{Hg}_{1-x}\text{Cd}_x\text{Te}$  epilayer grown by molecular beam epitaxy, K.K. Mahavadi, J. Bleuse, X. Chu and J.P. Faurie, *Appl. Phys. Lett.* 55 (13) 1285 (1989)
15. Raman scattering determination of strain in CdTe/ZnTe superlattices, M.K. Jackson, R.H. Miles, T.C. McGill and J.P. Faurie, *Appl. Phys. Lett.* 55 (8) 21 (1989)
16. Magneto-absorption in a HgMnTe-CdTe superlattice: evidence of the exchange interaction in a semimagnetic semiconducting superlattice, G.S. Boebinger, Y. Guldner, J.M. Berroir, M. Voos, J.P. Vieren and J.P. Faurie, *NATO ASI Series Volume: Spectroscopy of Semiconducting Microstructures*. (in press)
17. Role of the crystallographic orientation on the incorporation of Indium in HgCdTe epilayers grown by MBE, I.K. Sou, P.S. Wijewarnasuriya, M. Boukerche and J. P. Faurie, *Appl. Phys. Lett.* 55 (10) 954 (1989)
18. Planar heterojunctions made on MBE grown mercury cadmium telluride using low energy ion sputtering, S.S. Yoo, M. Boukerche, M.DeSouza and J.P. Faurie, *SPIE Proceedings* 1106 (1989)
19. Photoluminescence from CdTe/ $\text{Hg}_{1-y}\text{Cd}_y\text{Te}$ / $\text{Hg}_{1-x}\text{Cd}_x\text{Te}$  separate confinement heterostructures, K.K. Mahavadi, M.D. Lange and J.P. Faurie, *Appl. Phys. Lett.* 54, 2580 (1989)
20. Valence band discontinuities in HgTe-CdTe-ZnTe heterojunction systems, J.P. Faurie, *Proceedings - NATO workshop on Band Structure Engineering in Semiconductor Microstructures*, Plenum Publishing Corporation p.81 (1989).
21. The intrinsic and extrinsic doping of mercury cadmium telluride grown by molecular beam epitaxy, M. Boukerche and J.P. Faurie, *Proceedings of the 3rd International Conference on Shallow Impurities in Semiconductors*, Vol. 95 of the Institute of Physics Conference Series.
22. Electron mass anisotropy in type-III HgZnTe-CdTe superlattices, J.M. Berroir, Y. Guldner, J.P. Vieren, M. Voos, X. Chu and J.P. Faurie, *Phys. Rev. Lett.* 62, 2024 (1989)
23. Study of CdTe layers grown on (111)B CdTe surfaces by molecular beam epitaxy, G. Monfroy, S. Sivananthan, and J.P. Faurie, *J. Vac. Sci. Technol.* A7, 326 (1989)

34. Ultrahigh electron and hole mobilities in zero-gap Hg-based superlattices, J.R. Meyer, C.A. Hoffman, and F.J. Bartoli; J.W. Han, J.W. Cook, Jr., and J. F. Schetzina; X. Chu and J.P. Faurie; J.N. Schulman, *Physical Review B* 38, 2204 (1988).
35. The investigation of Type III - Type I strained-layer superlattice system:  $\text{Hg}_{1-x}\text{Zn}_x\text{Te}-\text{CdTe}$ , X. Chu, S. Sivananthan and J.P. Faurie, *SPIE Vol. 878*, 42 (1988).
36. Characteristics of p-n junctions fabricated on  $\text{Hg}_{1-x}\text{Cd}_x\text{Te}$  epilayers grown by molecular beam epitaxy, J.P. Faurie, S. Sivananthan, M. Lange, R.E. Dewames, A.M.B. Vandewyck, G.M. Williams, D. Yamani and E. Tao, *Applied Physics Letters* 52 (25), 2151 (1988).
37. X-ray photoemission study of Hg clusters on  $\text{Hg}_{1-x}\text{Cd}_x\text{Te}$  surfaces, R. Sporken, S. Sivananthan, J. Reno and J. P. Faurie, *Journal of Vacuum Science and Technology B6*, 1204 (1988).
38. Electrical studies of single-barrier  $\text{Hg}_{1-x}\text{Cd}_x\text{Te}$  heterostructures, D.H. Chow, J.O. McCaldin, A.R. Bonnefoi, T.C. McGill, I.K. Sou, J.P. Faurie, F.A. Shirland, and O.K. Wu, *Journal of Vacuum Science and Technology A6*, (4) 2614 (1988).
39. The doping of mercury cadmium telluride grown by molecular beam epitaxy, M. Boukerche, P.S. Wijewarnasuriya, S. Sivananthan, I.K. Sou, Y.J. Kim, K.K. Mahavadi and J.P. Faurie, *Journal of Vacuum Science and Technology A6* (4) 2830 (1988).
40. X-ray photoemission from small mercury clusters on II-VI semiconductor surfaces, R. Sporken, S. Sivananthan, J. Reno and J.P. Faurie, *Physical Review B* 38, 1351 (1988).
41. Valence band discontinuities at the heterojunctions between CdTe, ZnTe, and HgTe in the (100) orientation - X-ray photoelectron spectroscopy study, by C. Hsu and J.P. Faurie, *Journal of Vacuum Science and Technology B6*, 773 (1988).
42. New achievements in  $\text{Hg}_{1-x}\text{Cd}_x\text{Te}$  grown by Molecular Beam Epitaxy, S. Sivananthan, M.D. Lange, G. Monfroy and J.P. Faurie, *Journal of Vacuum Science and Technology B6*, 788 (1988).
43. Electrochemical and electrooptical study of the strained-layer superlattice system  $\text{CdTe}-\text{ZnTe}$  - P. Lemasson, C. N. Van Huong, X. Chu, S. Sivananthan and J. P. Faurie - *Journal of Electrochemical Society* 135, 1282 (1988).
44. Transmission electron microscope investigation of (001) ZnTe on (001) GaAs

24. Electrical properties of intrinsic p-type shallow levels in HgCdTe grown by molecular beam epitaxy in the (111)B orientation, M. Boukerche, S. Sivananthan, P.S. Wijewarnasuriya, I.K. Sou, and J.P. Faurie, *J. Vac. Sci. Technol.* A7, 311 (1989)
25. Temperature dependent photoemission study of the HgTe-CdTe of the HgTe-CdTe valence-band discontinuity. R. Sporken, S. Sivananthan, D.H. Ehlers, J. Fraxedas, J.J. Pireaux, L. Ley, R. Caudano, and J.P. Faurie, *J. Vac. Sci. Technol.* A7 (2), 427 (1989)
26. Nonlinear optical coefficients of Hg-based superlattices, E.R. Youngdale, C.A. Hoffman, J.R. Meyer, and F.J. Bartoli; X. Chu and J.P. Faurie; J.W. Han, J.W. Cook and J.F. Schetzina, *J. Vac. Sci. Technol.* A7, 365 (1989)
27. Mechanism of interdiffusion in  $\text{Hg}_{1-x}\text{X}_x\text{Te}/\text{CdTe}$  superlattices ( $X = \text{Cd}, \text{Mn},$  and  $\text{Zn}$ ), J. L. Staudenman, R. D. Knox and J. P. Faurie, *Proceedings of the 1987 MRS Spring Conference.*
28. Hg-based superlattices as nonlinear optical materials, E.R. Youngdale, C.A. Hoffman, J. R. Meyer, F.J. Bartoli, X. Chu, J.P. Faurie, J.W. Han, J.W. Cook, Jr. and J.F. Schetzina, *Proceedings from IRIS Specialty Group on Infrared Materials* (1988)
29. Band offsets and lattice-mismatch effects in strained-layer CdTe/ZnTe superlattices, H. Mathieu, J. Allegre, A. Chatt, and P. Lefebvre and J.P. Faurie, *Physical Review B* 38, 7740 (1988)
30. Electro-optical and non-linear optical characterization of narrow gap superlattices, C.A. Hoffman, J.R. Meyer, R. Lindle, E.R. Youngdale, F.J. Bartoli, X. Chu and J.P. Faurie, *SPIE Vol.* 878, 47 (1988)
31. Photoluminescence of HgTe-CdTe superlattices: Comparison of theory and experiment, J.P. Baukus, A.T. Hunter, J.N. Schulman and J.P. Faurie, *Journal of Applied Physics* 64(1) (1988).
32. Effects of substrate misorientation on the structural properties of CdTe(111) grown by molecular beam epitaxy on GaAs(100), J.L. Reno, P.L. Gourley, G. Monfroy and J.P. Faurie, *Applied Physics Letters* 53(18) (1988).
33. Electron transport and cyclotron resonance in [211]-oriented HgTe-CdTe superlattices, C.A. Hoffman, J.R. Meyer, R.J. Wagner, and F.J. Bartoli, X. Chu, J.P. Faurie, L.R. Ram-Mohan and H. Xie, *J. Vac. Sci. Technol.* (In press)

- grown by molecular beam epitaxy, J. Petruzzello, D. Olego and J.P. Faurie, *Journal of Applied Physics* 63, 1783 (1988).
45. Electronic properties of HgTe/HgCdTe heterojunction, K.C. Woo, S. Rafol and J.P. Faurie, *Surface Science* 196, 665 (1988).
  46. Molecular beam epitaxial growth and characterization of two-inch diameter  $\text{Hg}_{1-x}\text{Cd}_x\text{Te}$  films on GaAs(100) substrates, M.D. Lange, S. Sivananthan, X. Chu and J.P. Faurie, *Applied Physics Letters* 52, 978 (1988).
  47. Two-dimensional electron gas in HgCdTe/CdTe heterostructures, G. S. Boebinger, Y. Guldner, J. P. Vieren, M. Voos and J. P. Faurie, *Surface Science* 196, 669 (1988).
  48. Observation of negative differential resistance from a single barrier heterostructure, D.H. Chow, T.C. McGill, I.K. Sou, J.P. Faurie and C.W. Nich, *Applied Physics Letters*, 52, 54 (1988).
  49. Mercury cadmium telluride junction grown in-situ by molecular beam epitaxy, M. Boukerche, S. Yoo, I.K. Sou, M. DeSouza, J.P. Faurie, *Journal of Vacuum Science and Technology A6*, 2623 (1988).
  50. Molecular beam epitaxial growth and properties of Hg-based microstructures, J.P. Faurie, *Physics and Application of Quantum Wells and Superlattices*, Plenum Publishing p.71, (1987).
  51. Electron transfer in  $\text{Hg}_{1-x}\text{Cd}_x\text{Te}$ -CdTe heterostructures, G. S. Boebinger, J. P. Vieren, Y. Guldner, M. Voos and J. P. Faurie, *Journal de Physique* 48, C5 337, (1987).
  52. Magneto-optical study of a HgMnTe-CdTe superlattice, G. S. Boebinger, Y. Guldner, J. M. Berroir, M. Voos, J. P. Vieren and J. P. Faurie, *Journal de Physique* 48, C5 301, (1987).
  53. Valence band discontinuities in the  $\text{Hg}_{1-x}\text{Cd}_x\text{Te}$  -  $\text{Hg}_{1-y}\text{Cd}_y\text{Te}$  (111)B system - XPS study, C. Hsu, Tran Minh Duc and J. P. Faurie, *Journal de Physique* 48, C5 307, (1987).
  54. Magneto-optical evidence of the exchange interaction in a  $\text{Hg}_{1-x}\text{Mn}_x\text{Te}$ -CdTe superlattice, G. S. Boebinger, Y. Guldner, J. M. Berroir, M. Voos, J. . J.P. Vieren and J. P. Faurie, *Physical Review B*, 36, 7930 (1987).
  55. Charge transfer in  $\text{Hg}_{1-x}\text{Cd}_x\text{Te}$ -CdTe heterostructures, Y. Guldner, G. S. Boebinger, M. Voos, J. P. Vieren and J. P. Faurie, *Physical Review B*, 36, 2958 (1987).
  56. Electrical determination of the valence band discontinuity in HgTe-CdTe

- heterojunctions, D.H. Chow, J.O. McCaldin, A.R. Bonnefoi, T.C. McGill, I.K. Sou and J.P. Faurie, *Applied Physics Letters* 51, 2230 (1987).
57. Hg incorporation in CdTe during the growth of HgTe-CdTe superlattices by Molecular Beam Epitaxy, J. Reno, R. Sporken, Y. J. Kim, C. Hsu and J. P. Faurie, *Applied Physics Letters* 51, 1545 (1987).
  58. Electrical properties of Li doped  $\text{Hg}_{1-x}\text{Cd}_x\text{Te}(100)$  by Molecular Beam Epitaxy, P. S. Wijewarnasuriya, I. K. Sou, Y. J. Kim, K. K. Mahavadi, S. Sivananthan, Boukerche and J. P. Faurie, *Applied Physics Letters* 51, 2025 (1987).
  59. "Strain and the Interpretation on Band Lineup Measurements" - a reply of Tran Minh Duc, C. Hsu and J. P. Faurie, *Physical Review Letters* 59, 947 (1987).

## CONFERENCES AND PROFESSIONAL MEETINGS

### INVITED SPEAKER:

1. Molecular Beam Epitaxy of Hg-based II-VI compounds, The Ninth International Conference on Crystal Growth, Sendai, Japan (August 1989)
2. Magneto-absorption in a HgMnTe-CdTe superlattice: evidence of the exchange interaction in a semimagnetic semiconducting superlattice, with G.S. Boebinger, Y. Guldner, J.M. Berroir, M. Voos and J.P. Vieren, NATO Meeting on Spectroscopy, Venice, Italy (May 1989)
3. IR Focal Plane Array Material and Processing Review - DARPA - DSO, Washington D.C. (April 4-5, 1989)
4. Recent progress towards in situ HgCdTe infrared device technology using the MBE approach - SPIE Conference - Monitoring and Control of Plasma-Enhanced Processing of Semiconductors - Santa Clara, California (Nov. 1-3, 1988).
5. Molecular beam epitaxial growth of mercury-based alloys - NATO Advanced Research Workshop - The Future of Small-Gap II-VI Semiconductors - Liege, Belgium (Sept. 5-9, 1988).
6. The intrinsic and extrinsic doping of mercury cadmium telluride grown by molecular beam epitaxy, M. Boukerche and J.P. Faurie, Third International Conference on Shallow Impurities in Semiconductors, Linkoping, Sweden (August 10-12, 1988).
7. Valence band discontinuities in HgTe-CdTe-ZnTe heterojunction systems- NATO Advanced Research Workshop - Band Structure Engineering in Semiconductor Microstructures - Pisa (April 88).
8. MBE growth and Hg-based Alloys and Superlattices - DARPA IR Focal Plane

Array Materials and Processing Review - Washington (April 88).

9. New achievements on the growth of  $\text{Hg}_{1-x}\text{Cd}_x\text{Te}$  by Molecular Beam Epitaxy-MRS 1987 Fall Meeting - Boston (Dec.87).
10. Molecular Beam Epitaxy of Hg bond II-VI semiconducting alloys - Workshop on MBE of  $\text{HgCdTe}$  - DARPA - CNVEO - Washington (Nov. 87).
11. Materials Science - Science and Engineering conference - University of Illinois - Chicago (Nov. 87).
12. New achievements on the growth of  $\text{Hg}_{1-x}\text{Cd}_x\text{Te}$  by Molecular Beam Epitaxy, American Vacuum Society Illinois Chapter - 5th Annual Fall Symposium Chicago (Sept. 87).
13. Molecular Beam Epitaxial growth and properties of Hg-based microstructures. Three lectures at the International School on the Physics of Solid State Devices - Erice (April 87).

#### CONTRIBUTED TALKS:

1. Two-dimensional excitons in a strongly localized regime in  $\text{CdTe/ZnTe}$  superlattices - with Y. Hefetz, D. Lee, A. V. Nurmikko, S. Sivananthan and X. Chu - 1986 MRS Fall Meeting - Boston (Dec. 1986).
2. Valence band discontinuities at heterojunction between  $\text{HgTe}$ ,  $\text{CdTe}$  and  $\text{ZnTe}$  - C. Hsu, T. M. Duc and J. P. Faurie - PCSI - Salt Lake City (Jan. 1987).
3. Structure of  $\text{CdTe/ZnTe}$  superlattices - R. H. Miles, T. C. McGill, S. Sivananthan, X. Chu and J. P. Faurie - PCSI - Salt Lake City (Jan. 1987).
4. Evidences for Interdiffusion during the Growth of  $\text{HgTe/CdTe}$  Superlattices-with J. L. Staudenmann, J. Reno and R. D. Knox - March Meeting of the American Physical Society, New York (March 1987).
5. Mercury Cadmium Telluride Heterojunctions Grown in-situ by MBE - with M. Boukerche, I. K. Sou, M. DeSouza and S. Yoo - March Meeting of the American Physical Society, New York (March 1987).
6. MBE Growth and Characterization of  $\text{HgTe-Hg}_{1-x}\text{Cd}_x\text{Te}$  and  $\text{HgTe-Hg}_{1-y}\text{Zn}_y\text{Te}$  Heterojunctions - I. K. Sou, J. Reno, S. Sivananthan, P. S. Wijewarnasuriya, M. Boukerche and J. P. Faurie - March Meeting of the American Physical Society, New York (March 1987).
7. Quantized Hall Effect in the  $\text{HgTe-HgCdTe}$  Heterojunctions - with K. C. Woo, S. Rafol and I. K. Sou - March Meeting of the American Physical

Society, New York (March 1987).

8. The Experimental Dependence of the Cutoff Wavelength on the Layer Thicknesses in a HgTe-CdTe Superlattice - with J. Reno - March Meeting of the American Physical Society, New York (March 1987).
9. Charge Transfer in CdTe-HgCdTe Heterostructures - with G. S. Boebinger, J. M. Berroir, Y. Guldner, J. P. Vieren and M. Voos - March Meeting of the American Physical Society, New York (March 1987).
10. Investigations of the Strains Between Layers in the CdTe/ZnTe Strained Layer-Superlattice System - with G. Monfroy, J. L. Staudenmann and R. D. Knox - March Meeting of the American Physical Society, New York (March 1987).
11. Resonance Tunnelling on HgTe-CdTe Double Barrier - with S. Rafol, S. Sivananthan, Y. J. Kim, M. Boukerche and K. C. Woo - March Meeting of the American Physical Society, New York (March 1987).
12. Molecular Beam Epitaxial Growth and Characteristics of a Strained-Layer Superlattice System: HgZnTe-CdTe - X. Chu, S. Sivananthan, P. S. Wijewarnasuriya and J. P. Faurie - March Meeting of the American Physical Society, New York (March 1987).
13. Magnetotransport of  $\text{Hg}_{1-x}\text{Zn}_x\text{Te}$ -CdTe Strained-Layer Superlattices - S. Rafol, X. Chu, K. C. Woo and J. P. Faurie - March Meeting of the American Physical Society, New York (March 1987).
14. Linearity of valence band discontinuity in Te based II-VI heterojunctions: CdTe, HgTe and ZnTe, Tran Minh Duc, C. Hsu and J. P. Faurie - Euro MBE 87 - Les Diablerets (April 1987).
15. II-VI compound superlattices as new infrared materials, Y. Guldner, M. Voos, G. S. Boebinger, J. P. Vieren and J. P. Faurie, NATO Workshop on HgCdTe -Freiburg (March 1987).
16. Mechanism of Interdiffusion in  $\text{Hg}_{1-x}\text{X}_x\text{Te}$ /CdTe superlattices (X = Cd, Mn and Zn), J. L. Staudenman, R. D. Knox and J. P. Faurie, MRS Spring Conference - Anaheim (April 87).
17. Valence band discontinuities in the HgTe-CdTe system - XPS study, C. Hsu, Tran Minh Duc and J. P. Faurie - 3rd International Conference on Modulated Semiconductor Structures, Montpellier (July 87).
18. Magneto-optical study of a HgMnTe-CdTe superlattice, G. S. Boebinger, Y. Guldner, J. M. Berroir, M. Voos, J. P. Vieren and J. P. Faurie - 3rd International Conference on Modulated Semiconductor Structures, Montpellier (July 87).

19. Electron transfer in  $\text{Hg}_{1-x}\text{Cd}_x\text{Te}$ -CdTe heterostructures, G. S. Boebinger, J. P. Vieren, Y. Guldner, M. Voos and J. P. Faurie - 3rd International Conference on Modulated Semiconductor Structures, Montpellier (July 87).
20. Magneto-transport properties of Hg-based lattice matched heterojunctions and strained-layer superlattices, K. C. Woo, S. Rafor and J. P. Faurie - 7th International Conference on Electronic Properties of Two-dimensional Systems - Santa Fe (July 87).
21. Two-dimensional gas in HgCdTe-CdTe heterostructures, G. S. Boebinger, Y. Guldner, J. P. Vieren, M. Voos and J. P. Faurie - 7th International Conference on Electronic Properties of Two-dimensional Systems - Santa Fe (July 87).
22. Type III - Type I transition and strain effect in  $\text{Hg}_{1-x}\text{Cd}_x\text{Te}$  - CdTe and  $\text{Hg}_{1-x}\text{Zn}_x\text{Te}$  - CdTe superlattices - X. Chu, S. Sivananthan and J.P. Faurie - 3rd International Conference on Superlattices, Microstructures and Microdevices - Chicago (August 1987).
23. Improvements in narrow bandgap MCT heterojunctions made by MBE - M. Boukerche, I.K. Sou, S. Yoo and J.P. Faurie - 3rd International Conference on Superlattices, Microstructures and Microdevices - Chicago (August 1987).
24. Observations of structural deviations in MBE grown II-VI superlattices with single periods - R.D. Knox, J.L. Staudenmann, G. Monfroy and J.P. Faurie - 3rd International Conference on Superlattices, Microstructures and Microdevices - Chicago (August 1987).
25. II-VI heterojunctions and band structures: A magneto-transport study - K.C. Woo, S. Rafor and J.P. Faurie - 3rd International Conference on Superlattices, Microstructures and Microdevices - Chicago (August 1987).
26. Valence Band discontinuities at the heterojunctions between CdTe, ZnTe, and HgTe in the (100) orientation - XPS study - C. Hsu, R. Sporken and J.P. Faurie - 8th MBE Workshop, Los Angeles (Sept. 1987).
27. New achievements on the growth of  $\text{Hg}_{1-x}\text{Cd}_x\text{Te}$  by Molecular Beam Epitaxy - S. Sivananthan, M.D. Lange and J.P. Faurie - 8th MBE Workshop, Los Angeles (Sept. 1987).
28. Abrupt isotype MCT heterojunctions made in-situ by MBE - M. Boukerche, I.K. Sou, M. DeSouza, S. Yoo and J.P. Faurie - The 1987 U.S. Workshop on the Physics and Chemistry of HgCdTe, New Orleans (Oct. 1987).
29. Electrical properties of n-type and p-type doped HgCdTe epitaxial layers grown by MBE - P.S. Wijewarnauriya, I.K. Sou, Y.J. Kim, K. Mahavadi, M. Boukerche

- and J.P. Faurie - The 1987 U.S. Workshop on the Physics and Chemistry of HgCdTe, New Orleans (Oct. 1987).
30. New achievements on the growth of  $\text{Hg}_{1-x}\text{Cd}_x\text{Te}$  by MBE - S. Sivananthan, M.D. Lange, X. Chu and J.P. Faurie - The 1987 U.S. Workshop on the Physics and Chemistry of HgCdTe, New Orleans (Oct. 1987).
  31. Systematic study by EER of thick MBE-grown epilayers of MCT covering the entire spectral range of 3-5 microns - P.M. Raccach, D. Yang, Z. Zhang, J.W. Garland, S. Sivananthan, M. Lange, P.S. Wijewarnasuriya and J.P. Faurie - The 1987 U.S. Workshop on the Physics and Chemistry of HgCdTe, New Orleans (Oct. 1987).
  32. Electrical measurements of the HgTe - CdTe valence band offset - D.H. Chow, J.O. McColdin, A.R. Bonnefol, T.C. McGill, I.K. Sou and J.P. Faurie - The 1987 U.S. Workshop on the Physics and Chemistry of HgCdTe, New Orleans (Oct. 1987).
  33. The investigation of Type III - Type I transition in a novel strained layer superlattice system:  $\text{Hg}_{1-x}\text{Zn}_x\text{Te}$  - CdTe - X. Chu, S. Sivananthan and J.P. Faurie - Symposium on Innovative Science and Technology, Los Angeles (Jan. 1988).
  34. Electrical and optical characterization of mercury based superlattices, C. Hoffman, J. Meyer, R. Lindle, E. Youngdale, F. Bartoli, X. Chu and J.P. Faurie, Symposium on Innovative Science and Technology, Los Angeles (Jan. 1988).
  35. X-ray photoemission study of Hg clusters on  $\text{Hg}_{1-x}\text{Cd}_x\text{Te}$  surfaces - R. Sporken, S. Sivananthan, J. Reno and J.P. Faurie - 15th Annual Conference on the Physics and Chemistry of Semiconductor Interface - Asilomar (Feb. 1988).
  36. Metal-Insulator-Semiconductor of  $\text{Hg}_{1-x}\text{Cd}_x\text{Te}$  Grown by Molecular Beam Epitaxy, S.S. Yoo, M. Boukerche and J.P. Faurie, Meeting of American Physical Society, New Orleans, Louisiana (March 1988).
  37. Magnetic Field Induced Metal-Insulator Transitions in n-Type HgZnTe-CdTe Superlattices, S. Rafol, K.C. Woo and J.P. Faurie, Meeting of American Physical Society, New Orleans, Louisiana (March 1988).
  38. Magnetoresistance and Field Dependence of the Hall Coefficient in MBE Grown  $\text{Hg}_{1-x}\text{Cd}_x\text{Te}$ , P.S. Wijewarnasuriya, M. Boukerche and J.P. Faurie, Meeting of American Physical Society, New Orleans, Louisiana (March 1988).

39. Incorporation of Sb and As as Electrically Active Impurities in  $\text{Hg}_{1-x}\text{Cd}_x\text{Te}$  Grown by MBE, S. Sivananthan, K. Mahavadi, I.K. Sou, P.S. Wijewarnasuriya, Y.-J. Kim and J.P. Faurie, Meeting of American Physical Society, New Orleans, Louisiana (March 1988).
40. Direct measurement of the valence band discontinuity at the  $\text{HgTe-CdTe}$  heterojunction, C. Hsu and J.P. Faurie, Meeting of American Physical Society, New Orleans, Louisiana (March 1988).
41. Magneto-optical Evidence of the Exchange Interaction in a  $\text{HgMnTe-CdTe}$  Superlattice, G.S. Boebinger, Y. Guldner, J.M. Berroir, M. Voos, J.P. Vieren and J.P. Faurie, Meeting of American Physical Society, New Orleans, Louisiana (March 1988).
42. Hg-based superlattices as nonlinear optical materials, E.R. Youngdale, C.A. Hoffman, J.R. Meyer, F.J. Bartoli, X. Chu, J.P. Faurie, J.W. Han, J.W. Cook, Jr. and J. F. Schetzina, IRIS - Specialty Group on Infrared Materials, Menlo Park, California (June 1988).
43. Magneto- and photo-transport investigation of  $\text{Hg}_{1-x}\text{Zn}_x\text{Te-CdTe}$ ,  $\text{HgTe-ZnTe}$  and  $\text{HgTe-CdTe}$  superlattices, C.A. Hoffman, J.R. Meyer, F. Bartoli, X. Chu and J.P. Faurie, 19th International Conference on the Physics of Semiconductors, Warsaw (Aug. 1988).
44. Minority-carrier lifetime in p-type  $\text{Cd}_x\text{Hg}_{1-x}\text{Te}$  layers grown by MBE, M.E. DeSouza, M. Boukerche and J.P. Faurie, The 1988 U.S. Workshop on the Physics and Chemistry of  $\text{HgCdTe}$ , Orlando, Florida (October 1988).
45. Improvements in the doping of MCT films grown by MBE, M. Boukerche, S. Sivananthan, M. Lange, P.S. Wijewarnasuriya, I.K. Sou and J.P. Faurie, The 1988 U.S. Workshop on the Physics and Chemistry of  $\text{HgCdTe}$ , Orlando, Florida (October 1988).
46. Nonlinear optical coefficients of Hg-based superlattices, E.R. Youngdale, C.A. Hoffman, J.R. Meyer, F.J. Bartoli, X. Chu, J.P. Faurie, J.W. Han, J.W. Cook, Jr. and J. F. Schetzina, The 1988 U.S. Workshop on the Physics and Chemistry of  $\text{HgCdTe}$ , Orlando, Florida (October 1988).
47. Temperature-dependent photoemission study of the  $\text{HgTe-CdTe}$  valence-band offset, R. Sporken, S. Sivananthan, J.P. Faurie, J.J. Pireaux, R. Caudano, D. Ethlers, J. Fraxedas and L. Ley, The 1988 U.S. Workshop on the Physics and Chemistry of  $\text{HgCdTe}$ , Orlando, Florida (October 1988).
48. Study of  $\text{CdTe}$  layers grown on (111)B  $\text{CdTe}$  surfaces by MBE, G. Monfroy,

- S. Sivananthan, S. Burns and J.P. Faurie, The 1988 U.S. Workshop on the Physics and Chemistry of HgCdTe, Orlando, Florida (October 1988).
49. Role of the crystallographic orientation on the incorporation and the diffusion of indium in HgCdTe epilayers grown by MBE, I.K. Sou and J.P. Faurie, American Physical Society Meeting, St. Louis, Missouri (March 1989)
  50. Photoluminescence from CdTe/Hg<sub>1-y</sub>Cd<sub>y</sub>Te/Hg<sub>1-x</sub>Cd<sub>x</sub>Te separate confinement heterostructures, K.K. Mahavadi, M.D. Lange and J.P. Faurie, American Physical Society Meeting, St. Louis, Missouri (March 1989)
  51. Structural properties of HgZnTe/CdTe strained layer superlattices on CdTe buffer layers grown by MBE, J. Petruzello, D. Olego, X. Chu and J. P. Faurie, American Physical Society Meeting, St. Louis, Missouri (March 1989)
  52. P-n junctions fabricated on Hg<sub>1-x</sub>Cd<sub>x</sub>Te epilayers grown by molecular beam epitaxy, S.S. Yoo, M. Boukerche and J.P. Faurie, SPIE's 1989 Technical Symposia on Aerospace Sensing, Orlando, Florida (March 1989)
  53. Growth of CdTe and HgCdTe on Si(100) by MBE, R. Sporken, S. Sivananthan, G. Monfroy, M. Boukerche and J.P. Faurie, The 10th MBE Workshop, Raleigh, NC (September 1989)
  54. Role of the crystallographic orientation on the incorporation and diffusion of indium in HgCdTe epilayers grown by MBE, I.K. Sou, M. Boukerche and J.P. Faurie, The 1989 Workshop on the Physics and Chemistry of Mercury Cadmium Telluride and Related II-VI Compounds, San Diego, CA (October 1989)
  55. Effect of twinning in (111)B Hg<sub>1-x</sub>Cd<sub>x</sub>Te grown by MBE. S. Sivananthan, S.S. Yoo, M. Boukerche, R. Sporken, G. Monfroy, P.S. Wijewarnasuriya, M. Lange and J.P. Faurie, The 1989 Workshop on the Physics and Chemistry of Mercury Cadmium Telluride and Related II-VI Compounds, San Diego, CA (October 1989)
  56. Electron transport and cyclotron resonance in (211)-oriented HgTe-CdTe superlattices, C.A. Hoffman, J.R. Meyer, R.J. Wagner, F.J. Bartoli, X. Chu, J.P. Faurie, L.R. Ram-Mohan and H. Xie, The 1989 Workshop on the Physics and Chemistry of Mercury Cadmium Telluride and Related II-VI Compounds, San Diego, CA (October 1989)
  57. Stimulated emission from Hg<sub>1-x</sub>Cd<sub>x</sub>Te epilayers and CdTe/Hg<sub>1-x</sub>Cd<sub>x</sub>Te double heterostructures grown by MBE, K.K. Mahavadi, J. Bleuse, X. Chu, M.D. Lange, S. Sivananthan and J.P. Faurie, The 1989 Workshop on the Physics and Chemistry of Mercury Cadmium Telluride and Related II-VI Compounds,

San Diego, CA (October 1989)

58. The spreading resistance technique applied to MCT heterojunctions, M. Boukerche and J.P. Faurie, The 1989 Workshop on the Physics and Chemistry of Mercury Cadmium Telluride and Related II-VI Compounds, San Diego, CA (October 1989)
59. Electron cyclotron resonance in type III HgZnTe-CdTe superlattices, M. Voos, J. Manasses, J.M. Berroir, Y. Guldner, J.P. Vieren, X. Chu and J.P. Faurie, The 4th International Conference on Modulated Semiconductor Structures (MSS4), Ann Arbor, Michigan (July 1989)
60. Photoluminescence study of  $\text{Hg}_{1-x}\text{Cd}_x\text{Te}/\text{Hg}_{1-y}\text{Cd}_y\text{Te}$  separate confinement heterostructures, K.K. Mahavadi, J. Bleuse, X. Chu and J.P. Faurie, The 4th International Conference on Modulated Semiconductor Structures (MSS4), Ann Arbor, Michigan (July 1989)
61. Evidence for semimetallic character in  $\text{Hg}_{1-x}\text{Cd}_x\text{Te}-\text{CdTe}$  superlattices, J.M. Berroir, Y. Guldner, J. Manasses, J.P. Vieren, M. Voos, X. Chu and J.P. Faurie, The EP2D58 Conference, Grenoble, France (September 1989)
62. CdTe/ZnTe strained layer superlattices under high pressure, A.D. Prins, B. Gil, D.J. Dunstan and J.P. Faurie, The 27th EHPRG Conference (1989)